LÉKAŘSKÁ FAKULTA V PLZNI

UNIVERZITA KARLOVA

ŠIKLŮV ÚSTAV PATOLOGIE

DOKTORSKÁ DIZERTAČNÍ PRÁCE

VYUŽITÍ IMUNOHISTOCHEMICKÝCH A MOLEKULÁRNĚ GENETICKÝCH METOD V PATOLOGII HLAVY A KRKU

MUDr. MARTINA BANĚČKOVÁ

Plzeň 2020
Obor: Patologie
Školitelka: prof. MUDr. Alena Skálová, CSc.

PŘEDMLUVA

Nádory hlavy a krku jsou morfologicky různorodou skupinou, kterou lze rozdělit podle lokality na nádory dutiny nosní, paranazálních sinusů a báze lební, nádory nazofaryngu, hypofaryngu, laryngu, trachey a parafaryngeálních prostorů, nádory dutiny ústní a mobilní části jazyka, nádory orofaryngu, nádory a nádorům podobné léze krku a lymfatických uzlin, nádory slinných žláz, odontogenní a maxilofaciální kostní nádory, nádory ucha a paraganglionové tumory. I přes dobrou dostupnost většiny oblastí hlavy a krku aspekcí a otorhinolaryngologickým vyšetřením, představuje velká část onemocnění pokročilé léze. Manipulační prostor pro chirurga zde nemusí být vždy dostatečně příznivý, jako je tomu v jiných místech. Důvodem může být například přítomnost skeletu, blízkost nervově-cévních svazků a dalších životně důležitých orgánů. Snaha odstranit nádor kompletně tak může mít mutilující následky.

Morfologická heterogenita a překryvný imunohistochemický profil nádorů hlavy a krku komplikuje cestu ke konečné diagnóze. Rozvojem molekulárně genetických metod došlo v nedávné době k výraznému pokroku v definování jednotlivých nádorů a nádorům podobných lézí v oblasti hlavy a krku. Je zřejmé, že genetické alterace mají vliv na fenotyp a biologické chování nádorů.

Doktorská dizertační práce se zabývá morfologií, molekulární genetikou a klinickým chováním vybraných nádorů hlavy a krku. Největší pozornost je věnována vzácným nádorům a nově definovaným nádorovým jednotkám. Podkladem dizertační práce jsou 4 prvoautorské články, z nichž se všechny týkají nádorů hlavy a krku s bližším zaměřením především na patologii slinných žláz a sinonazálního traktu. Dizertační práce je vypracována formou souhrnu 9 komentovaných publikací, všechny práce jsou samostatně krátce představeny.

První část se týká sekrečního karcinomu (mammárního typu), druhá část popisuje ostatní vybrané nádory a nádorům podobné léze hlavy a krku. Práce jsou řazeny chronologicky, přičemž prvoautorské práce jsou předřazeny spoluautorským.

PROHLÁŠENÍ

Prohlašuji, že jsem dizertační práci zpracovala samostatně a řádně uvedla a citovala všechny použité zdroje. Souhlasím s trvalým uložením elektronické verze své práce v databázi UK LF Plzeň.

V Plzni, dne 20.7. 2020
Martina Baněčková

PODĚKOVÁNÍ

Prof. MUDr. Aleně Skálové, CSc.,
svojí mentorce, za ve mě vloženou důvěru, trpělivost, přátelský přístup a profesionální rady

Prof. MUDr. Michalovi Michalovi
za podporu, cenné rady a poskytnuté zázemí

Univerzitě Karlově, Lékařské fakultě v Plzni
Svým spolupracovníkům Šiklova ústavu patologie a Bioptické laboratoře, s.r.o. v Plzni

Své rodině a nejbližším
za trpělivost a lásku

ABSTRAKT

Doktorská dizertační práce se zabývá morfologií, imunohistochemií, molekulární genetikou a biologickým chováním nádorů hlavy a krku se zvláštním zaměřením na nádory slinných žláz a sinonazálního traktu, které byly základem doktorského studia MUDr. Martiny Baněčkové na Lékařské fakultě Univerzity Karlovy v Plzni, v období let 2017–2020. Autorka se ve své publikační činnosti zaměřila na problematiku vzácných nádorů hlavy a krku. Výsledky tříletého výzkumu jsou prezentovány ve formě komentovaného souhrnu celkem 9 publikací. Čtyři práce vypracovala autorka jako hlavní autor a ve stručnosti je zde představuje.

První publikovaná prvoautorská práce má název „Sekreční karcinom mammárního typu nosní dutiny: Charakteristika 2 případů a jejich odlišení od low-grade sinonazálních adenokarcinomů. V této práci se autorka zabývala vztahem nově popsané jednotky – sekrečního karcinomu (SC) v nosní dutině s *ETV6*-rearanžovaným low-grade sinonazálním adenokarcinomem (LG SNAC). Tyto jednotky je nutné od sebe oddělit zejména kvůli odlišnému biologickému chování. Low-grade non-intestinální adenokarcinomy včetně *ETV6*-rearanžovaného LG SNAC se chovají klinicky příznivě, zatímco SC je většinou nízce maligní nádor, ale recidivující, invazivní a potenciálně agresivní. SC může být přítomen i v oblasti sinonazálního traktu, a proto může napodobovat nejenom nově definovaný *ETV6*-rearanžovaný LG SNAC, ale také musí být diferenciálně diagnosticky odlišen od agresivních intestinálních adenokarcinomů (ITAC)a high-grade non-intestinálních adenokarcinomů (non-ITAC) nosní a paranazálních dutin.

Ve druhé práci nazvané „Imunohistochemická a genetická analýza respiračních epiteliálních adenomatoidních hamartomů a seromucinózních hamartomů: jsou tyto jednotky prekurzorem pro sinonazální low-grade tubulopapilární adenokarcinomy?“ autorka hodnotí morfologický, imunohistochemický a genetický profil respiračního epiteliálního adenomatoidního hamartomu (REAH) a seromucinózního hamartomu (SH). Získané poznatky jsou pak porovnány s vyšetřením low-grade tubulopapilárního adenokarcinomu (LGTA). Bylo zjištěno, že serózní komponenta REAH a SH je pozitivní s CK7, MUC1 a SOX10 obdobně jako je tomu u LGTA. Navíc v jednom případě SH byla geneticky potvrzená klonalita a v jednom případě SH byla zjištěna genová fúze *EGFR-ZNF267* metodou sekvenování nové generace (NGS). SH a REAH jsou samostatné jednotky nesoucí překryvný morfologický a imunohistochemický profil s LGTA. Nejde o zcela indolentní léze, jak naznačuje slovo „hamartom“ v jejich názvu, dle výsledků naší studie se jedná o potenciální prekurzory jiných nádorů.

Ve třetí práci pojmenované „Revize solitárních fibrózních tumorů hlavy a krku: Zkušenosti jedné instituce s 20 případy a přehled literatury“ se autoři zabývali diferenciální diagnostikou a molekulárně genetickou detekcí exonů genů *NAB2* a *STAT6* u 20 případů solitárních fibrózních tumorů (SFT). Bylo zjištěno, že SFT mohou být napodobovány širokou škálou primárních i sekundárních novotvarů, které imitují oba základní růstové vzory hypocelulární i hypercelulární (hemangiopericytom-napodobující). Na základě revize literatury autoři shrnuli poznatky z 579 případů SFT z různých lokalit (200 případů bylo z oblasti hlavy a krku), které obsahovaly molekulárně genetická data popisující exony genů participujících v translokaci *NAB2-STAT6*. Výsledky studie shrnují, že metastatický potenciál mají jen ty SFT, jejichž fúze obsahuje DNA vazebnou doménu, tzv. STAT6-full varianty.

Čtvrtá práce nazvaná „SATB2 je často exprimovaný v osifikujících a neosifikujících periferních orálních fibromech v oblasti dásně, ale nikoliv v reaktivních fibromatózních lézích jiných struktur dutiny ústní“ pojednává o periferních orálních fibromech (POF) gingivální oblasti, což jsou nodulárně utvářené fibrózní léze, pravděpodobně vznikající na podkladě chronické traumatizace. Centrálně může POF obsahovat metaplastickou vláknitou kost, která je definující pro osifikující variantu. Osifikující POF bývají nejčastěji lokalizované v gingivální

oblasti, což je v ostrém kontrastu s ne-osifikujícími lézemi. V osifikujících POF a v polovině neosifikujících POF gingiválním oblasti jsme popsali silnou jadernou pozitivitu markeru SATB2, zatímco v lézích z non-gingiválních míst SATB2 exprimovaný nebyl. Zmíněná exprese SATB2 v gingiválních osifikujících POF je v souladu s domněnkou, že tyto léze pochází z periostálních vazů a tím se vysvětluje i jejich tendence k osifikaci. Výsledky studie je nutné brát v úvahu při hodnocení SATB2 pozitivních novotvarů pocházejících z dutiny ústní, tak aby nebyly tyto léze nadhodnoceny jako maligní.

SUMMARY

Current doctoral thesis is dealing with morphology, immunohistochemistry, molecular genetics and biological behavior of head and neck tumors with a particular emphasis on salivary gland and sinonasal lesions. Dr. Martina Baneckova has focused on this topic during her postgraduate studies at Charles University, Medical Faculty in Pilsen, in the years 2017 – 2020. In her publication activity, the author focused on rare tumors of the head and neck. A total of 9 publications were published over a span of three years are presented in a form of a commentary. Four of them are first-author papers and these are introduced briefly below.

The first study entitled "Mammary analog secretory carcinoma of the nasal cavity: Characterization of 2 cases and their distinction from other low-grade sinonasal adenocarcinomas" deals with the relationship of newly described entities, secretory carcinoma (SC) of the nasal cavity and *ETV6*-rearranged low-grade sinonasal adenocarcinoma (LG SNAC). It is important to distinguish these 2 entities because of different clinical behaviors. Low-grade non-ITAC, including *ETV6*-rearranged LG SNAC mostly behave in an indolent manner, whereas SC is a malignancy with metastatic potential. It is important to be aware of the possible occurrence of SC in the sinonasal region, as in this area SC represents a potential mimicker of non-intestinal-type adenocarcinomas (non-ITAC) and the more aggressive intestinal-type adenocarcinomas (ITAC).

In the second paper entitled "Immunohistochemical and genetic analysis of respiratory epithelial adenomatoid hamartomas and seromucinous hamartomas: are they precursor lesions to sinonasal low-grade tubulopapillary adenocarcinomas?" the authors evaluated the morphological, immunohistochemical and genetic profile of respiratory epithelial adenomatoid hamartoma (REAH) and seromucinous hamartoma (SH), and they compared these findings with the morphological and immunohistochemical features of low-grade tubulopapillary adenocarcinoma (LGTA). The serous component of REAH or SH was positively stained with CK7, MUC1 and SOX10 similarly to LGTA. In addition, one case of SH showed *EGFR-ZNF267* gene fusion detected by next generation sequencing, and one case of SH proved to be clonal using HUMARA assay. Our findings suggest that SH and REAH represent the variants of the same lesion. Moreover, SH and serous component of REAH might be precursor lesions of LGTA.

The third paper was entitled "Solitary fibrous tumors of the head and neck region revisited: A single-institution study of 20 cases and review of the literature." The authors dealt with molecular genetic background of solitary fibrous tumor (SFT), particularly the exact participation of the exons included in the *NAB2-STAT6* gene fusion in 20 cases. SFT might be included in the differential diagnosis of a wide spectrum of spindle shape and epithelioid-cell derived lesions, both primary and secondary malignancies. The literature review summarizes data from 579 cases of SFT from different location of the body (200 of them were from the head and neck). Based on the described exons participating in the *NAB2-STAT6* gene fusion, we concluded that the fusion containing a DNA-binding domain (STAT6-full variant) has metastatic potential.

The fourth study entitled "SATB2 is frequently expressed in ossifying and non-ossifying peripheral oral fibroma of the gingival region but not in reactive fibromatous lesions from other intraoral sites" discusses the problem of peripheral oral fibromas (POF) of the gingival region. POF are fibrous nodular lesions likely resulting from persistent localized injury. The presence of centrally located metaplastic woven bone defines the ossifying variant. Ossifying POF and half of non-ossifying POF of the gingival region featured strong and diffuse nuclear SATB2 immunoreactivity. SATB2 was not expressed in other non-gingival locations of the oral cavity. The described SATB2 positivity is consistent with proposed origin of gingival POFs from periosteal ligaments and explains their tendency for ossification. This finding must be taken

into consideration when evaluating SATB2 positive lesions of the oral cavity in order to avoid misdiagnosis of malignancy.

OBSAH

SEZNAM POUŽITÝCH ZKRATEK

AR	Androgenní Receptory
DBD	DNA Binding Domain (DNA vázající doména)
ETV6	ETS Variant Transcription Factor 6 (ETS transkripční faktor 6)
FISH	Fluorescenční In Situ Hybridizace
FNAC	Fine Needle Aspiration Cytology (Tenkojehlová aspirační cytologie)
HPC	Hemangiopericytom
HPV	Human papillomavirus (Lidský papilomavirus)
IC	Intraductal Carcinoma (Intraduktální karcinom)
ICC	Imunocytochemie, Imunocytochemický
IHC	Imunohistochemie, Imunohistochemický
ITAC	Intestinal Type Adenocarcinoma (Adenokarcinom intestinálního typu)
LG SNAC	Low-Grade Sinonasal Adenocarcinoma (Low-grade sinonazální adenokarcinom)
LGTA	Low-Grade Tubulopapilární Adenokarcinom
MS	Milánský Systém
MYB	MYB Proto-Oncogene, Transcription Factor (MYB protoonkogen, transkripční faktor)
NAB2	NGFI-A Binding Protein 2 (NHFI-A vázající protein 2)
NCOA4	Nuclear Receptor Coactivator 4 (Koaktivátor 4 jaderného receptoru)
NGS	Next Generation Sequencing (Sekvenování nové generace)
Non-ITAC	Non Intestinal Type Adenocarcinoma (Adenokarcinom non-intestinálního typu)
NOS	Not Otherwise Specified (Blíže nespecifikované)
NTRK3	Neurotrophic Receptor Tyrosine Kinase 3 (Neurotropní receptor pro tyrozinkinázu 3)
POF	Periferní Orální Fibrom
REAH	Respirační Epiteliální Adenomatoidní Hamartom
RET	Ret Proto-Oncogene (Ret protoonkogen)
RT-PCR	Reverse Transcription Polymerase Chain Reaction (Reverzní transkripční polymerázová řetězová reakce)
SC	Secretory Carcinoma (Sekreční karcinom)
SDC	Salivary Duct Carcinoma (Salivární duktální karcinom)
SFT	Solitární Fibrózní Tumor
SH	Seromucinózní Hamartom

SMR3B	Submaxillary Gland Androgen Regulated Protein 3B (Androgeny regulující protein 3B submaxilární žlázy)
STAT6	Signal Transducer And Activator Of Transcription 6 (přenašeč signálu a aktivátor transkripce 6)
TRIM27	Tripartite Motif Containing Protein 27 (Třístranný motiv nesoucí protein 27)
TrkC	Tyrosinkinase receptor C (Tyrozinkinázový receptor C)
VIM	Vimentin
WHO	World Health Organization (Světová zdravotnická organizace)

ÚVOD

1.1 Incidence nádorů hlavy a krku

Nádory hlavy a krku jsou v celosvětovém měřítku 9. nejčastějším maligním onemocněním a mají udávanou incidenci 650 tisíc nových případů a mortalitu 330 tisíc úmrtí za rok (1). V Evropě je ročně evidováno 250 tisíc nových případů a 63 500 úmrtí (2). Muži pak mají 4krát vyšší riziko onemocnění v porovnání se ženami. Výskyt nádorů hlavy a krku se zvyšuje směrem od severu k jihu. Nejnižší hodnoty jsou ve Švédsku a Anglii (9–10/ 100 000 obyvatel), zatímco nejvyšší výskyt je udáván ve Francii, kde jsou tyto nádory stejně častě jako nádory plic s incidencí kolem 50/100 000 obyvatel. Více než 90 % nádorů hlavy a krku je diagnostikováno jako dlaždicobuněčné karcinomy (3).

Nádory slinných žláz a sinonazálního traktu představují dvě morfologicky heterogenní podskupiny nádorů hlavy a krku s incidencí dosahující 0,59 a 1,5 nových případů ročně. Mortalita je u nádorů sinonazálního traktu v porovnání s novotvary slinných žláz vyšší a je udávána na 0,84 případů/100 000 obyvatel za rok, respektive pro slinné žlázy 0,24/100 000. V České republice je incidence nádorů slinných žláz 0,66 a nádorů sinonazálního traktu 0,16 na 100 000 obyvatel za rok. Mortalita je zde 0,24, respektive a 0,16/100 000 (4).

1.2 Klasifikace nádorů hlavy a krku

Světová zdravotnická organizace (WHO) byla vždy hybnou silou tvorby klasifikace nádorů, a to již od počátku první série Mezinárodní histologické klasifikace tumorů (International Histological Classification of Tumours) v roce 1967. První kniha věnovaná nádorům hlavy a krku byla publikovaná v roce 1971 a zabývala se histologickou typizací orofaryngeálních tumorů (5). Další edice WHO klasifikace nádorů hlavy a krku, publikovaná v roce 2005 integrovala do charakteristiky nádorových jednotek, nejenom jejich morfologii a imunoprofil, ale i některé molekulárně genetické vlastnosti (6). Tato klasifikace popisovala nádory různých lokalit hlavy a krku a použila při tom standardizovaný formát zahrnující definici, epidemiologii, etiologii, lokalizaci, klinické znaky, radiografický nález, šíření nádoru, staging, makroskopický nález, histopatologické znaky a pomocné vyšetřovací postupy, jimiž jsou histochemie, imunohistochemie, ultrastrukturální a molekulárně genetické metody.

Současně platná WHO klasifikace nádorů hlavy a krku pochází z roku 2017 (7). Hlavní změny se týkají zpřesnění klasifikace stávajících tumorů, popisu nových nádorových jednotek, a aktualizace biologického chování nádorů. WHO klasifikace zahrnuje nejen klasické klinicko-patologické informace, ale také imunoprofil a molekulárně genetické znaky nádorů. Velmi významnou novinkou je pak vyčlenění nádorů orofaryngu jako samostatné oblasti, a to zejména díky rozpoznání úlohy lidského papilomaviru (HPV) při vzniku podtypu dlaždicobuněčného karcinomu (8). Hlavním pokrokem je začlenění nových jednotek do kapitol definujících nádory sinonazálního traktu, slinných žláz a vytvoření nové kategorie nádorům podobných lézí.

1.3 Novinky ve WHO klasifikaci nádorů hlavy a krku

Jednou z diskutovaných oblastí ve 4. edici WHO klasifikace je oblast sinonazálního traktu, kam byly zařazeny 3 nové, dobře definované jednotky: seromucinózní hamartom, NUT karcinom a bifenotypický sinonazální sarkom (**Tabulka 1**) (9, 10). Navíc byla vytvořena skupina provizorních, nově vznikajících a dosud studovaných jednotek, jimiž jsou HPV-asociovaný karcinom s adenoidně cystickými rysy (11), SMARCB1 (INI-1) deficientní sinonazální karcinom (12, 13) a adenokarcinom napodobující renální karcinom (14), které jsou zmiňované v rámci diferenciální diagnózy jiných karcinomů. Jak NUT karcinom, tak SMARCB1 deficientní karcinom, byly před vydáním WHO klasifikace 2017 převážně

klasifikované jako špatně diferencované dlaždicobuněčné karcinomy či sinonazální nediferencované karcinomy (SNUC), které mají špatnou prognózu (12, 13, 15). Další novinkou je histopatologická a genetická klasifikace bifenotypického sinonazálního sarkomu jako samostatné jednotky, který byl původně řazen mezi maligní tumory z pochvy periferního nervu či fibrosarkomy (16).

V oblasti nádorů slinných žláz došlo též k aktualizaci klasifikace (**Tabulka 2**) (17). Jedinou nově zařazenou jednotkou v rámci nádorů slinných žláz je sekreční karcinom (mammárního typu), který byl vyčleněn z kategorie acinického karcinomu (18) na základě odlišné morfologie, imunoprofilu a přítomnosti rekurentní translokace *ETV6-NTRK3*. Genové fúze charakterizují i další nádory slinných žláz, jako je adenoidně cystický karcinom (*MYB-NFIB* nebo *MYBL1-NFIB*), mukoepidermoidní karcinom (*CRTC1-MAML2* nebo *CRTC3-MAML2*) či pleomorfní adenom (nejčastěji zlomy v *PLAG1* genu). Další novinky se týkají sklerózující polycystické adenózy a hyperplázie z vmezeřených duktů, které byly nově zařazeny do WHO klasifikace jako non-neoplastické procesy (19, 20). Dále došlo k přejmenování některých známých nádorových jednotek, například low-grade kribriformní cystadenokarcinom, též známý jako low-grade salivární duktální karcinom, byl přejmenován na intraduktální karcinom (21).

1.4 Molekulární genetika v diagnostice nádorů hlavy a krku

Pokroky ve vývoji molekulárně biologických metod a jejich využití při testování nádorů přispívají ke stále lepší a detailnější histopatologické i prognostické klasifikaci (**Tabulky 3 a 4**). Přestože chirurgická terapie je nepostradatelnou součástí léčby nádorů hlavy a krku, limitovaný prostor společně se snahou odstranit nádor kompletně mohou mít řadu nepříjemných vedlejších následků. Nutnost zachovat životně důležité struktury nedovoluje vždy nádor odstranit celý, proto zde na řadu přicházejí alternativní metody jako je cílená biologická léčba (targeted therapy). Tento typ terapie je součástí tzv. personalizované medicíny, kdy je komplexní genomová analýza nádorové DNA/RNApodkladem při výběru vhodného léčiva a léčba nemocných se zdánlivě stejným onemocněním se tak může lišit.

1.5 Sekreční karcinom slinných žláz

1.5.1 Sekreční karcinom, charakteristika a imunohistochemie

Sekreční karcinom (SC) slinných žláz byl poprvé popsaný kolektivem Skálové a spol. v roce 2010 pod názvem sekreční karcinom slinných žláz mammárního typu (mammary analogue secretory carcinoma, MASC) (18), na podkladě podobných histomorfologických a identických imunohistochemických a molekulárních znaků se SC prsu. Tato jednotka byla záhy nato potvrzena v dalších samostatných studiích a odbornou veřejností uznána jako distinktní, a proto byla posléze pod názvem „sekreční karcinom slinných žláz“ začleněna do WHO klasifikace 2017 (22).

Histologicky má SC blandní morfologii, lobulární růst a je složený z mikrocystických, tubulárních a solidních struktur s hojným, homogenním, eosinofilním až bublinovitým sekrečním materiálem, který je pozitivní v barvení PAS (periodic acid-shiff) bez i s diastázou. Imunohistochemicky vykazují nádorové buňky difúzní jadernou expresi s markery S100 protein, mammaglobin a SOX10. DOG1 marker je pozitivní v acinickém karcinomu, ale v SC je zcela negativní. Většina SC byla původně diagnostikovaná jako acinické karcinomy chudé na zymogenní granula, případně low-grade cystadenokarcinomy ne blíže specifikované (18).

Kromě zmíněné lokalizace SC v prsu a ve slinných žlázách byla popsána celá řada dalších míst výskytu, například štítná žláza (23, 24), kůže (25), nosní sliznice, ethmoidální sinusy (26), plíce (27) a vulva (28).

1.5.2 Genetický profil

SC je charakterizovaný chromozomální translokací t(12;15)(p13;q25) vedoucí ke genové fúzi *ETV6-NTRK3*. Identická fúze není specifická pouze pro SC. Byla též popsána v řadě jiných nádorů a to v inflamatorním fibrosarkomu, kongenitálním mezoblastickém nefromu (29), v některých hematologických malignitách (30), v podskupině ALK-negativního inflamatorního myofibroblastického tumoru (31), v podskupině gastrointestinálních stromálních tumorů (32), v papilárním karcinomu štítné žlázy (33), a dalších nádorech. V rámci salivární patologie však fúze *ETV6-NTRK3* nebyla popsána v žádném jiném nádoru, a proto je tato translokace v příslušném morfologickém a imunohistochemickém kontextu pro SC slinných žláz diagnostická. *ETV6-NTRK3* translokace je detekována v 95–97 % SC slinných žláz, zbylých 3–5 % případů se vyznačuje jinou genovou fúzí (nejčastěji *ETV6-RET*).

SC ve většině případů, ale ne vždy obsahuje *ETV6-NTRK3* translokaci (34, 35). Při použití metody reverzní transkripční polymerázové řetězové reakce (RT-PCR) nebylo možné v některých případech detekovat fúzního partnera *ETV6* genu a tyto nádory byly proto označeny jako *ETV6-X* translokované SC (35). V navazující studii byla, díky dostupnosti metody sekvenování nové generace (NGS), nalezena v těchto případech SC *ETV6-RET* fúze (36). V roce 2018 byl publikován další fúzní partner *ETV6* genu, a to *MET* gen (37). Jednalo se o SC postihující podčelistní slinnou žlázu, jenž byl léčený chirurgickou excizí a dále adjuvantní radioterapií a chemoterapií. Nádor několikrát recidivoval a metastazoval. Tento případ měl typickou morfologii a imunoprofil high-grade SC a obsahoval zlom *ETV6* genu. Metodou NGS byla stanovena translokace mezi intronem 4 *ETV6* genu a intronem 14 genu *MET*.

Dalším příspěvkem k rozšíření genetického pozadí SC byla práce Guilmette a spol., kteří poprvé představili 2 současné řídící (driver) mutace v SC (38). Jednalo se o zvláštní nádor s duální morfologií i imunoprofilem. Jedna komponenta vykazovala klasický profil SC a druhá komponenta byla kribriformně-papilární a imunohistochemicky byla negativní s S100 proteinem i mammaglobinem. Zde byla metodou NGS molekulárně geneticky zjištěna dvojitá fúze *ETV6-NTRK3* a *ETV6-MAML3* (38).

Nejnovější poznatky poukazují na to, že molekulární profil SC se bude v raritních případech dále rozšiřovat. Nově byly popsané fúze bez účasti genů z rodiny *ETV6*. V prvním případě se jednalo o publikaci Kastnerova a spol., kteří zaznamenali *NFIX-PKN1* fúzi v SC kůže, nikoliv ve slinných žlázách (39). Dále Sasaki a spol. recentně publikovali SC příušní žlázy s *CTNNA1-ALK* fúzí (40) a Skálová a spol. 2 případy SC, z nichž jeden obsahoval *VIM-RET* fúzi a druhý případ SC duální fúzi *ETV6-NTRK3* a *MYB-SMR3B* (41).

1.5.3 Prognóza a možnosti léčby

Prognóza SC je ve většině případů příznivá. SC má střední riziko lokální recidivy a nízké riziko vzdálených metastáz. V porovnání s acinickým karcinomem má SC mírně vyšší incidenci postižení lymfatických uzlin. SC je všeobecně považovaný za low-grade karcinom. Nicméně, kolektivem Skálová a spol. byly rovněž popsány high-grade SC (42). High-grade SC se chovají velice agresivně a prognóza pacientů s touto diagnózou je infaustní. Terapie high-grade SC byla v minulosti kvůli přítomnosti vzdálených metastáz paliativní. Avšak moderní léčebné postupy dovolují, díky znalosti genetického podkladu SC, i u těchto pacientů využít alternativní metody, např. biologickou léčbu.

Fúze *ETV6-NTRK3* je považována za klíčovou řídící fúzi v procesu tumorigeneze, jelikož SC má nízkou mutační zátěž. *ETV6-NTRK3* fúze vede k aktivaci signálních drah, jmenovitě Ras-MAP kináz a PI3K-AKT. Tyto dráhy jsou též aktivovány alteracemi dalších genů, jako jsou *RET, MET* a *ALK* geny. V souvislosti se znalostmi genetického pozadí lze následně využít tyrozinkinázové inhibitory (Rozlytrek, Vitrakvi) (43, 44), RET-inhibitory

(selpercatinib, Blue 667) (45) či multikinázové inhibitory (cabozantinib, crizotinib) (46, 47) v terapii pokročilých SC.

1.6 Intraduktální karcinom

1.6.1 Historie názvu

Intraduktální karcinom (IC) byl známý pod různými jmény, jako „low-grade salivární duktální karcinom“, „salivární duktální karcinom in situ“ (48), později v roce 2005 bylo přijato editory WHO klasifikace označení „low-grade kribriformní cystadenokarcinom“ (49). Tento termín odkazoval na cystické a solidní struktury tvořené intraduktálními epiteliálními proliferacemi připomínajícími buňky vmezeřených duktů a struktury napodobující atypickou duktální hyperplázii, mikropapilární a kribriformní duktální karcinom in situ prsu či borderline apokrinní léze prsu. Nová WHO klasifikace nádorů hlavy a krku (2017) navrhla název „Intraduktální karcinom“, který však stále není optimální, protože nově byly popsány případy „intraduktálního karcinomu“ s invazivním růstem (21, 50).

1.6.2 Histologický a imunohistochemický profil

IC je vzácný low-grade nádor s histomorfologickými znaky napodobujícími výše zmíněné prekurzorové léze prsu. Nádor je typicky tvořený intraduktálními a intracystickými proliferacemi luminálních duktálních buněk, které rostou solidně, kribriformně či papilárně. Intraduktální in situ komponenta je charakterizovaná zachovanou myoepiteliální vrstvou buněk, kterou lze prokázat markery p63, calponinem či cytokeratinem 14. Ve většině případů je IC neinvazivní low-grade karcinom, ale byly také popsány i případy invazivního IC (51).

Na základě imunoprofilu lze odlišit dva subtypy IC: typ z vmezeřených duktů a apokrinní typ. První varianta IC nesoucí fenotyp buněk z vmezeřených duktů, je tvořená malými eosinofilními buňkami s malými jádry bez jaderných atypií. Tento typ imunohistochemicky exprimuje S100 protein a mammaglobin. (49). Druhá, apokrinní varianta IC, roste spíše mikropapilárně, a je charakterizována apokrinními výběžky buněk, z nichž se odděluje sekreční materiál. Buňky apokrinního IC obsahují více cytoplazmy a často vykazují high-grade cytologické rysy včetně velkých jader a prominujících jadérek. V čistě apokrinní variantě IC jsou nádorové buňky obvykle negativní v průkazu S100 proteinu a SOX10 a mohou exprimovat androgenní receptory (AR). Část apokrinních IC je asociovaná s invazivním růstem (52). IC může vykazovat hybridní fenotyp mající znaky obou typů IC (50, 52, 53).

1.6.3 Genetický profil

Doposud byly publikovány pouze 3 práce zabývající se molekulárně genetickým pozadím IC (50-52). Kolektivem Weinreb a spol. byl popsán zlom v *RET* genu a translokace t(10;10)(q11.22;q11.21) s *NCOA4-RET* fúzí v podskupině IC s morfologií z vmezeřených vývodů (52). IC a SC mají shodný imunohistochemické profil a podobnou morfologii, ale v žádném případě IC nebyla zjištěna rearanže *ETV6* genu (50-52). V části případů IC s apokrinní morfologií byla nalezena translokace t(10;6)(p22.5;q11.21) s *TRIM27-RET* fúzí a ve dvou případech IC s invazivními rysy pak byly zastiženy další dvě fúze *TUT1-ETV5* a *KIAA1217-RET* (51).

1.6.4 Diferenciální diagnostika

Nejčastějšími mimikry IC jsou sekreční karcinom (SC) a salivární duktální karcinom (SDC). SC může napodobovat IC histologicky i imunohistochemicky. Oba mohou sdílet tytéž architektonické rysy, jako jsou kribriformní formace se sekrečními prostory, multicystické uspořádání a intracystický papilární růst. Dále mají shodný imunoprofil, s expresí SOX10, S100 proteinu a mammaglobinu. Na druhou stranu exprese AR není charakteristická pro SC.

Důležitým rozlišovacím znakem je i přítomnost zachované myoepiteliální vrstvy kolem hnízd a cyst IC, kterou lze potvrdit myoepiteliálními imunohistochemickými markery jako je p63, hladkosvalový aktin, CK14 či calponin (50, 51). Kontinuální myoepiteliální vrstva v SC přítomná není (18). Geneticky byla v obou jednotkách (SC i IC) zdokumentovaná rearanže *RET* genu. Zatímco v SC je popsaná asociace *RET* genu s *ETV6* genem (36), tak v IC byla Weinrebem a spol. popsána fúze *NCOA4-RET* (52) a Skálovou a spol. fúze *TRIM27-RET (50)*.

SDC je druhým nádorem, který lze zvažovat v diferenciální diagnostice IC. SDC je v porovnání s IC rozsáhle invazivní nádor s high-grade cytologickými i architektonickými rysy, které zahrnují výrazná jadérka, hrubý chromatin, nekrózy a vysokou mitotickou aktivitu včetně atypických mitóz. Buňky SDC mají obvykle apokrinní fenotyp a exprimují AR. SDC též může produkovat mammaglobin, avšak S100 protein je typicky negativní a je přítomna overexprese HER2 proteinu (54). SDC je charakterizovaný spektrem molekulárních alterací zahrnujících ERBB2 amplifikaci, mutace TP53 a MAP/PI3K cesty (55).

1.7 Respirační epiteliální léze

1.7.1 Respirační epiteliální adenomatoidní hamartom a seromucinózní hamartom

Skupinu respiračních epiteliálních lézí ve WHO klasifikaci tvoří dvě jednotky: respirační epiteliální adenomatoidní hamartom (REAH) a seromucinózní hamartom (SH) (56, 57). REAH a SH mají v části případů společné histologické znaky a zdá se, že spíše představují spektrum jedné léze než samostatné jednotky (58). Obě léze se častěji vyskytují u dospělých osob a vyrůstají převážně ze zadního nosního septa.

Je otázkou, zda tyto léze pojmenovat jako neoplastické či non-neoplastické, avšak přítomnost částečných alelických zlomů v REAH podporuje hypotézu, že se jedná o benigní tumory (59).

1.7.2 Histologický a imunohistochemický profil

Histologicky je REAH tvořený žlázovými strukturami vznikajícími kontinuálně z povrchového epitelu. Tyto struktury jsou kryté vrstevnatým řasinkovým epitelem respiračního typu často s příměsí mucinózních buněk. Struktury jsou obklopeny silnou vrstvou eozinofilní bazální membrány.

SH mikroskopicky sestává z lalůčků proliferujících malých žlázek a tubulů vystlaných jednovrstevným kubickým epitelem. Lalůčky bývají smíšené s normálními seromucinózními žlázkami nosní sliznice a často bývají v blízkosti do stromatu vtaženého povrchového respiračního epitelu. Bazální vrstva obvykle přítomná není, maximálně lze detekovat ojedinělé myoepitelie. Stroma obou lézí může být hutné a místy hyalinizované.

Imunohistochemicky exprimují respirační i seromucinózní žlázky CK7 a CK19, zatímco CK20 je negativní. Vysokomolekulární keratiny a p63 jsou vhodné pro zobrazení myoepiteliálních buněk. Žlázové struktury SH jsou imunoreaktivní s protilátkou S100 protein, která je současně negativní ve větších žlázkách respiračního typu u REAHu (58, 60).

1.7.3 SH a REAH jako možné prekurzorové léze?

V současné době neexistují definitivní rozlišovací kritéria mezi REAH s floridní seromucinózní žlázovou proliferací, SH a low-grade non-intestinálním sinonazálním adenokarcinomem (non-ITAC). Jo a spol. prezentovali sérii 29 low-grade non-ITAC, z nichž 6 bylo asociovaných s REAH (61). Obdobně pak SH prezentované Weinrebem a spol., měly obdobné histologické a imunohistochemické znaky, zahrnující ztrátu myoepiteliální vrstvy buněk kolem seromucinózních lalůčků (58).

Někteří autoři připodobňují žlázovou proliferaci SH k mikroglandulární adenóze prsu (62). Lze spekulovat, že termíny „adenóza“ či „adenom“ lépe vyjadřují podstatu těchto benigních žlázových proliferací než označení „hamartom“.

1.8 Solitární fibrózní tumor hlavy a krku

Solitární fibrózní tumor (SFT) patří mezi hraničně maligní měkkotkáňové nádory dříve označované jako hemangiopericytomy (HPC) či HPC napodobující léze (63). Poprvé byl SFT popsaný na pleuře (64) avšak 30 % jich roste extrathorakálně, oblast hlavy a krku nevyjímaje. V terénu hlavy a krku jsou sinonazální trakt a orbita nejčastějšími místy výskytu.

1.8.1 Histologický a imunohistochemický profil

Mikroskopicky je SFT představitelem spektra rozmanitých fenotypů a záleží, zda převažuje celulární či fibrózní komponenta. Typická architektura je kombinací hypocelulárních a hypercelulárních okrsků. Hypocelulární oblasti jsou vnořené do kolagenního stromatu s výraznou vaskulaturou definovanou parožnatě se větvícími cévami. Hypercelulární oblasti jsou tvořené kulatými až vřetenitými buňkami rostoucími v rohožkovitých a provazcovitých formacích či růstem napodobující epiteloidní léze nebo fibrosarkomy.

SFT jsou imunohistochemicky difúzně pozitivní s CD34. Exprese CD34 však klesá směrem k malignímu fenotypu. Navíc CD34 může být detekován i v řadě jiných mezenchymálních nádorů napodobujících SFT, například v epiteloidním hemangioendoteliomu či bifenotypickém sinonazálním sarkomu. SFT dále konzistentně exprimuje bcl2 a CD99. Žádný z těchto markerů však není zcela specifický a imunoreaktivita je typická i pro jiné mezenchymální léze. SFT je obvykle negativní s cytokeratiny, aktinem, desminem a S100 proteinem. V případě diferenciálně diagnostických rozpaků je nukleární exprese markeru STAT6 vysoce specifická a senzitivní a odráží pro SFT charakteristickou *NAB2-STAT6* genovou fúzi. Senzitivita STAT6 dosahuje až 95 % a pouze silná a difúzní jaderná exprese je považována za pozitivní. Pouze u 2 % jiných mezenchymálních tumorů (fibrózní histiocytom, desmoidní tumor či dediferencovaný liposarkom) byla zjištěna STAT6 exprese, a to převážně cytoplasmatická a slabě nukleární (65).

1.8.2 Genetický profil

Tři skupiny autorů nezávisle na sobě popsali translokaci *NAB2-STAT6* v SFT (66-68). Oba geny se nacházejí blízko sebe na chromozomu 12q13 a jsou přepisovány v opačných směrech. Fúzním produktem je chimérický onkoprotein, v němž je doména represoru NGFI-A vázajícího proteinu 2 (*NAB2)* vyměněna za transaktivační doménu karboxy-konce signálního transduktoru a aktivátoru transkripce 6 (*STAT6*). Vzniklý onkoprotein zvyšuje buněčnou proliferaci. Studie meningeálních SFT a hemangiopericytomů potvrdila, že meningeální hemangiopericytomy jsou ve skutečnosti hypercelulárními variantami SFT (69).

1.8.3 Prognostické faktory a chování

Neexistuje spojitost mezi morfologií a chováním SFT. Existují však kritéria malignity, která zahrnují: velikost léze více než 50 mm, rozsev nemoci v době diagnózy, infiltrativní okraje, hypercelulární růst, jaderná pleomorfie, přítomnost sarkomatoidních oblastí čili dediferenciace, nekrózy a mitotická aktivita (4 mitózy/10 zorných polí velkého zvětšení) (70). Se špatnou prognózou a klinickými výsledky jsou podle autorů Gold a spol. asociované ty extrathorakální SFT, které mají pozitivní chirurgické okraje, velikost převyšující 10 cm a maligní histologické znaky (popsané výše) (70).

1.8.4 Diferenciální diagnóza

Diferenciální diagnóza SFT čítá řadu primárních i sekundárních novotvarů zejména mezenchymálního původu (viz **Tabulka č. 5**). Žádný z diskutovaných nádorů však nevykazuje iunohistochemicky silnou jadernou expresi STAT6 a geneticky není definován *NAB2-STAT6* fúzí. Existuje však malé procento lézí, v nichž lze detekovat cytoplazmatickou a slabší jadernou pozitivitu STAT6. Nejdiskutovanější je STAT6 exprese v dediferencovaném liposarkomu, jejíž přítomnost lze vysvětlit sekvencí genů na 12 chromozomu. Zde se nachází *STAT6, MDM2* a *CDK4* v těsné blízkosti. *MDM2* a méně *CDK4* bývají amplifikované v dediferencovaném liposarkomu, zatímco *STAT6* nikoliv. Přítomnost *STAT6* je tak výsledkem společné amplifikace jednotlivých genů při doplňujících vyšetřeních.

1.9 Reaktivní hyperplastické léze dutiny ústní

1.9.1 Charakteristika a klasifikace reaktivních hyperplastických lézí dutiny ústní

Reaktivní hyperplastické léze jsou skupinou fibrózních změn pojivové tkáně dutiny ústní. Obvykle vznikají v ústní sliznici jako odpověď na zranění typu lokálního chronického dráždění v souvislosti se zubním kamenem, zubními výplněmi, drobnou traumatizací a iatrogenním poškozením. Sliznice reaguje na dráždění procesem lokální hyperplázie, která je mikroskopicky tvořená zralým kolagenem, fibroblasty, mineralizovanou tkání, endoteliemi a obrovskými vícejadernými buňkami. Nejčastěji jsou postiženy ženy ve druhé dekádě života (71).

Tyto léze sice nejsou považované za neoplázie, ale mohou být s nimi zaměněny. Klasifikace hyperplastických lézi sliznice dutiny ústní zahrnuje jednotky: fibrózní hyperplázie, pyogenní granulom, fibrózní epulis s osifikací nebo periferní osifikující fibromy a periferní obrovskobuněčné granulomy (72).

1.9.2 Periferní orální fibromy

Osifikující či neosifikující periferní orální fibromy (POF) jsou si navzájem velmi podobné léze až na přítomnost zralých metaplastických kostních ostrůvku v osifikující variantě. Neosifikující varianta je však na rozdíl od osifikujícího protějšku histologicky shodná s ostatními nodulárními fibrózními lézemi traumatického původu. Proč některé léze osifikují a jiné ne, je kontroverzní téma. Elanagai a spol. studovali expresi osteopontinu v normální gingivální tkáni a v různých fokálně reaktivních lézích včetně POF, aby ozřejmili příčinu osifikace (73). Zjistili, že osteopontin je exprimovaný ve všech osifikujících POF. Též se domnívali, že POF vzniká na podkladě stromálních buněk – osteoblastů (produkujících osteopontin), které jsou odvozené z periodontálních ligament.

SOUHRN KOMENTOVANÝCH PUBLIKACÍ

1.10 SEKREČNÍ KARCINOM SLINNÝCH ŽLÁZ A SINONAZÁLNÍHO TRAKTU

1.10.1 SEKREČNÍ KARCINOM MAMMÁRNÍHO TYPU DUTINY NOSNÍ: CHARAKTERISTIKA 2 PŘÍPADŮ A JEJICH ODLIŠENÍ OD LOW-GRADE SINONAZÁLNÍHO ADENOKARCINOMU

V přiložené publikaci jsme se blíže zabývali výskytem SC ve sliznici nosní dutiny. V prvním případě se jednalo o 51letou ženu bez předchozí historie karcinomu prsu. Pacientka pociťovala střídavé bolesti za pravým okem a příležitostně bolesti hlavy. Zobrazovací metody nalezly tumor v pravé straně nosního septa, který byl chirurgicky resekovaný. V odstupu 10 let od diagnózy byla pacientka naživu a bez obtíží. Ve druhém případě se jednalo o 65letou ženu, v osobní anamnéze pouze s pleomorfním adenomem dutiny ústní před 5 lety od aktuální diagnózy. Počítačová tomografie zachytila tumor pravé nosní dutiny prorůstající do nazofaryngu, který byl odstraněný rozsáhlou resekcí. V odstupu 4 let od diagnózy byla žena bez recidivy.

Histologicky byly oba případy obdobného vzhledu, neopouzdřené, nodulárně utvářené léze s tubulo-papilárním růstem a invazivními okraji. Nádorové buňky měly low-grade malá vezikulární jádra s jemně granulovaným chromatinem. Sekreční materiál pozitivní v barvení PAS (periodic acid-Shiff) byl též přítomen. Imunohistochemicky byly oba případy pozitivní v barvení CK7, S100 protein, mammaglobin, SOX10 a GATA3. Negativní markery byly CK20, SATB2, CDX2 a DOG1. V obou případech byla prokázaná translokace *ETV6-NTRK3* metodou sekvenování nové generace (NGS). V prvním případě byla zastižena atypická fúze mezi exony 5-13 a ve druhém případě typická fúze mezi exony 5-15.

V porovnání s patologií slinných žláz je diferenciální diagnostika SC v sinonazálním traktu obtížnější. Zde se do popředí diferenciální diagnostiky dostávají nádory typu low-grade sinonazálních adenokarcinomů (LG SNAC), které představují histologicky heterogenní skupinu nádorů zahrnující jak adenokarcinomy intestinálního typu (ITAC) tak non-intestinálního typu (non-ITAC). Skupina non-ITAC obsahuje nově popsanou kontroverzní jednotku, a to *ETV6*-rearanžovaný LG SNAC (74). Tento nádor byl popsán ve 3 případech doposud pouze v jediné publikaci (74). Diferenciálně diagnosticky by měl být *ETV6*-rearanžovaný LG SNAC odlišen od sinonasálního SC. Navzdory identickému genetickému pozadí obou jednotek byly popsány následující charakteristické rysy napomáhající v jejich diferenciaci: *ETV6*-rearanžovaný LG SNAC roste převážně tubulárně a je tvořený kubickými až cylindrickými buňkami s příležitostnými apokrinními rysy, místy lze zastihnout i trabekulární růst, nádorové buňky *ETV6*-rearanžovaného LG SNAC jsou nahloučené těsně k sobě s minimem vmezeřeného stromatu, s minimální či nulovou sekreční aktivitou. V porovnání s těmito znaky měly oba případy SC nosní dutiny hyalinizovaná septa a značnou produkci sekrečního materiálu. *ETV6*-rearanžovaný LG SNAC je pozitivní v barvení DOG1, negativní v mammaglobinu a pouze ojediněle byl detekovaný S100 protein. Hlavním důvodem pro odlišení obou jednotek je potenciální rozdíl v biologickém chování. Zatímco *ETV6*-rearanžovaný LG SNAC se chová příznivě, SC je low-grade maligní nádor, který v ojedinělých případech může podlehnout high-grade transformaci (42).

Mammary Analog Secretory Carcinoma of the Nasal Cavity

Characterization of 2 Cases and Their Distinction From Other Low-grade Sinonasal Adenocarcinomas

Martina Baneckova, MD,† Abbas Agaimy, MD,‡ Simon Andreasen, MD,§‖ Tomas Vanecek, PhD,¶ Petr Steiner, Mgr,*¶ David Slouka, MD, MBA, PhD,# Tomas Svoboda, MD, PhD,** Marketa Miesbauerova, MD,*† Michael Michal Jr, MD,*† and Alena Skálová, MD, PhD*†*

Abstract: Secretory carcinoma, originally described as mammary analog secretory carcinoma (MASC), is a low-grade salivary gland tumor characterized by a t(12;15)(p13;q25) translocation, resulting in an *ETV6-NTRK3* gene fusion. Most MASCs are localized to the parotid gland and intraoral minor salivary glands. Moreover, *ETV6*-rearranged carcinomas with secretory features have been reported recently in the thyroid (with and without a history of radiation exposure), skin, and in very rare instances in the sinonasal tract. Here, we describe 2 cases of primary MASC in the sinonasal tract and provide a detailed clinical and histopathologic characterization of their morphology, immunohistochemical profile, and genetic background and highlight features allowing for its separation from its recently described molecular mimicker, *ETV6*-rearranged low-grade sinonasal adenocarcinoma.

Key Words: nasal cavity, mammary analog secretory carcinoma, MASC, low-grade sinonasal adenocarcinoma, *ETV6-NTRK3*

(*Am J Surg Pathol* 2018;42:735–743)

Secretory carcinoma (SC), originally described as mammary analog secretory carcinoma (MASC), is a low-grade salivary gland tumor characterized by a t(12;15)(p13;q25) translocation, resulting in an *ETV6-NTRK3* gene fusion.[1] In addition to having identical genetics with SC, MASC expresses S100 and mammaglobin while being negative for DOG-1 and p63, thus highly resembling SC of the breast.[2] However, these features are unique among tumors of the salivary gland.

Most MASCs are localized in the parotid gland, submandibular gland, and minor salivary glands of the oral cavity, such as soft palate, lips, base of the tongue, and buccal mucosa. Since its description in the major and minor salivary glands,[1] MASC has been described in several other locations, such as skin,[3–5] thyroid,[6–8] and the sinonasal tract.[9,10] The first case of MASC of the sinonasal tract was reported by Lurquin et al,[9] and, very recently, another case with high-grade transformation was reported in the maxillary sinus.[10]

Primary sinonasal adenocarcinomas (SNACs) are uncommon and morphologically heterogenous.[11] These tumors are divided into nonsalivary and salivary types. Non–salivary-type SNACs are further classified into 2 broad categories: intestinal-type adenocarcinoma (ITAC) and the non–intestinal-type adenocarcinoma (non-ITAC).[12] The non–intestinal-type SNAC is of presumed surface epithelium/seromucinous gland origin and accounts for <1% of head and neck cancers.[11–13] It is morphologically a very diverse group, as it can show high-grade or low-grade features, as determined by the proliferative activity and pattern of growth.[14–17] An increasing number of distinct types of non-ITAC has been recognized recently, including a subset with rearrangement of the *ETV6* gene, the so-called *ETV6* gene–rearranged sinonasal low-grade SNAC.[18]

By screening a series of low-grade SNACs with fluorescence in situ hybridization (FISH) and/or reverse transcription polymerase chain reaction (RT-PCR), we identified 2 cases of primary MASC arising in the nasal cavity, and herein we provide a detailed clinical, histopathologic, and molecular characterization. Recognizing MASC in the sinonasal tract among other SNACs of the salivary type, as well as *ETV6*-rearranged low-grade SNAC, is important, as the correct diagnosis is prognostically relevant, and *ETV6*-related fusions serve as therapeutic targets.[19,20]

MATERIALS AND METHODS

Patient Material

Fifteen cases of low-grade non–intestinal-type SNAC with secretory features resembling MASC were identified in a review of the Salivary Gland Tumor Registry, at the

From the Departments of *Pathology; #Otorhinolaryngology; **Oncology and Radiotherapy, Oncological Clinic, Faculty of Medicine in Plzen, Charles University; †Bioptic Laboratory Ltd; ¶Department of Molecular Pathology, Bioptic Laboratory Ltd, Plzen, Czech Republic; ‡Institute of Pathology, Friedrich-Alexander-University, Erlangen, Germany; §Department of Otorhinolaryngology and Maxillofacial Surgery, Køge University Hospital; and ‖Department of Otolaryngology Head & Neck Surgery, Rigshospitalet, Denmark.

Conflicts of Interest and Source of Funding: Supported by the National Sustainability Program I (NPU I) Nr. LO1503 and by the grant SVV–2017 No. 260 391 provided by the Ministry of Education, Youth and Sports of the Czech Republic. The authors have disclosed that they have no significant relationships with, or financial interest in, any commercial companies pertaining to this article.

Correspondence: Alena Skálová, MD, PhD, Sikl's Department of Pathology, Medical Faculty of Charles University, Faculty Hospital, E. Benese 13, Plzen 305 99, Czech Republic (e-mail: skalova@fnplzen.cz).

TABLE 1. Antibodies Used for Immunohistochemical Study

Antibody Specificity	Clone	Dilution	Antigen Retrieval/Time (min)	Source
S100 protein	Polyclonal	RTU	CC1/20	Ventana Medical Systems
Mammaglobin	304-1A5	RTU	CC1/36	DakoCytomation
CK7	OV-TL 12/30	1:200	CC1/36	DakoCytomation
CK20	Ks20.8	1:100	CC1/36	DakoCytomation
CDX2	EPR2764Y	RTU	CC1/64	Cell Marque
GCDFP-15	EP1582y	RTU	CC1/64	Cell Marque
p63	4A4	RTU	CC1/64	Ventana Medical Systems
DOG-1	SP31	RTU	CC1/36	Cell Marque
GATA-3	L50-823	1:200	CC1/52	BioCareMedical
SOX10	Polyclonal	1:100	CC1/64	Cell Marque
Pan-TRK	A7H6R	1:20	CC1/64	Cell Signaling
SATB2	Polyclonal	1:100	CC2/68	Sigma Aldrich
STAT5a	Polyclonal	1:400	CC1/36	AssayDesigns Inc.
MIB1	30-9	RTU	CC1/64	Ventana Medical Systems

CC1 indicates EDTA buffer, pH 8.6; RTU, ready to use.

Department of Pathology, Faculty of Medicine in Plzen, and Biopticka Laboratory Ltd, Plzen, Czech Republic. Two additional cases with features mimicking MASC were retrieved from the files of the Institute of Pathology, Friedrich-Alexander University, Erlangen, Germany, thus amounting to a total of 17 cases. Clinical follow-up was obtained from the patients, their physicians, or from referring pathologists.

Histology and Immunohistochemistry

For conventional microscopy, tissues were fixed in formalin, routinely processed, embedded in paraffin (FFPE), cut, and stained with hematoxylin and eosin. In most cases, additional stains were also performed, including periodic acid-Schiff with and without diastase, mucicarmine, and alcian blue at pH 2.5.

For immunohistochemistry, 4-μm-thick sections were cut from paraffin blocks and mounted on positively charged slides (TOMO; Matsunami Glass Ind., Japan). Sections were processed on a BenchMark ULTRA (Ventana Medical Systems, Tucson, AZ), deparaffinized, and subjected to heat-induced epitope retrieval by immersion in a CC1 solution (pH 8.6) at 95°C. Following antigen retrieval, sections were stained with a pan-TRK antibody cocktail consisting of rabbit monoclonal antibodies, all obtained from Cell Signaling (Danvers, MA), targeting pan-TRK (clone A7H6R, active against TrkA, TrkB, and TrkC, 1:50 dilution), ROS1 (clone D4D6, 1:50), and ALK (clone D5F3, 1:50), as described elsewhere.[21]

All other primary antibodies used are summarized in Table 1. Visualization was performed using the ultraView Universal DAB Detection Kit (Roche Diagnostics, Mannheim, Germany) and ultraView Universal Alkaline Phosphatase Red Detection Kit (Roche Diagnostics). The slides were counterstained with Mayer hematoxylin. Appropriate positive and negative controls were used.

Molecular Genetic Study

Detection of *ETV6-NTRK3* Fusion Transcript by RT-PCR

RNA was extracted using the RecoverAll Total Nucleic Acid Isolation Kit (Ambion, Austin, TX). cDNA was synthesized using the Transcriptor First Strand cDNA Synthesis Kit (RNA input 500 ng) (Roche Diagnostics). All procedures were performed according to the manufacturer's protocols. Amplification of a 105 bp product and a 133 bp product of the β2-microglobulin gene, and a 247 bp product of the *PGK* gene was used to test the quality of the extracted RNA, as previously described.[22–24] This resulted in the detection of the classic fusion transcript of exon 5 of the *ETV6* gene and exon 15 of the *NTRK3* gene.[25]

For PCR, 2 μL of cDNA was added to the reaction, which consisted of 12.5 μL of HotStar Taq PCR Master Mix (Qiagen, Hilden, Germany), 10 pmol of each primer (Table 2), and distilled water up to 25 μL.[26,27] The amplification program comprised denaturation at 95°C for 14 minutes followed by 45 cycles of denaturation at 95°C for 1 minute; annealing at temperatures shown in Table 2 was carried out for 1 minute and extension at 72°C for 1 minute. The procedure was completed by incubation at 72°C for 7 minutes.

Successfully amplified PCR product was purified with magnetic particles using Agencourt AMPure (Agencourt

TABLE 2. Primers for Detection of *ETV6-NTRK3* Fusion Transcripts

Original Primer Name	Sequence	Annealing Tempearture (°C)	Localization
TEL971* (ETV6A†)	ACCACATCATGGTCTCTGTCTCCC	65	*ETV6* exon 5 outer
TRKC1059* (NTRK3A†)	CAGTTCTCGCTTCAGCACGATG	65	*NTRK3* exon 15 outer

*Bourgeois et al.[25]
†Ito et al,[26] Skalova et al.[27]

Bioscience Corporation, A Beckman Coulter Company, Beverly, MA). The product was then bidirectionally sequenced using Big Dye Terminator Sequencing Kit (PE/Applied Biosystems, Foster City, CA) and purified with magnetic particles using Agencourt CleanSEQ (Agencourt Bioscience Corporation); all this was carried out according to the manufacturer's protocols and run on an automated sequencer ABI Prism 3130xl (Applied Biosystems) at a constant voltage of 13.2 kV for 11 minutes.

Detection of *ETV6* and *NTRK3* by FISH Method

Four-μm-thick FFPE sections were placed onto positively charged slides. Hematoxylin and eosin–stained slides were examined for determination of areas for cell counting.

The unstained slides were routinely deparaffinized and incubated in the 1× Target Retrieval Solution Citrate pH 6 (Dako, Glostrup, Denmark) at 95°C/40 minutes and subsequently cooled for 20 minutes at room temperature in the same solution. The slides were washed in deionized water for 5 minutes and digested in protease solution with Pepsin (0.5 mg/mL) (Sigma Aldrich, St Louis, MO) in 0.01 M HCl at 37°C/25 to 60 minutes according to the sample conditions. The slides were then placed in deionized water for 5 minutes, dehydrated in a series of ethanol solution (70%, 85%, 96% for 2 min each), and air-dried.

For the detection of *ETV6* rearrangement, a commercial probe, Vysis *ETV6* Break Apart FISH Probe Kit (Vysis/Abbott Molecular, Illinois), was used. The *ETV6* probe was mixed with water and LSI/WCP (Locus-Specific Identifier/Whole Chromosome Painting) Hybridization buffer (Vysis/Abbott Molecular) in a 1:2:7 ratio, respectively.

The probe for the detection of the rearrangement of the *NTRK3* gene region was mixed from custom-designed SureFISH probes (Agilent Technologies Inc., Santa Clara, CA). Chromosomal regions for *NTRK3* break-apart probe oligos are chr15:87501469-88501628 and chr15:88701444-89700343. The probe mixture was prepared from corresponding probes (each color was delivered in a separated well), deionized water, and LSI Buffer (Vysis/Abbott Molecular) in a 1:1:1:7 ratio, respectively.

An appropriate amount of mixed probe was applied on specimens, covered with a glass coverslip, and sealed with rubber cement. The slides were incubated in the ThermoBrite instrument (StatSpin/Iris Sample Processing, Westwood, MA) with codenaturation at 85°C/8 minutes and hybridization at 37°C/16 hours. The rubber-cemented coverslip was then removed, and the slide was placed in posthybridization wash solution (2× SSC/0.3% NP-40) at 72°C/2 minutes. The slide was air-dried in the dark, counterstained with 4', 6'-diamidino-2-phenylindole (DAPI; Vysis/Abbott Molecular), coverslipped, and immediately examined.

FISH Interpretation

The sections were examined with an Olympus BX51 fluorescence microscope (Olympus Corporation, Tokyo, Japan) using a ×100 objective and filter sets Triple Band Pass (DAPI/SpectrumGreen/SpectrumOrange), Dual Band Pass (SpectrumGreen/SpectrumOrange), and Single Band Pass (SpectrumGreen or SpectrumOrange).

For each probe, 100 randomly selected non-overlapping tumor cell nuclei were examined for the presence of yellow or green and orange fluorescent signals. Yellow signals were considered negative, and separate orange and green signals were considered as positive.

Cutoff values were set to >10% of nuclei with chromosomal breakpoint signals (mean, +3 SD in normal non-neoplastic control tissues).

Sample Preparation for Next-generation Sequencing

For next-generation sequencing (NGS) studies, 2-3 FFPE sections (10 μm thick) were macrodissected to isolate tumor-rich regions. The samples were extracted for total nucleic acid using Agencourt FormaPure Kit (Beckman Coulter, Brea, CA), following the corresponding protocol with overnight digestion and an additional 80°C incubation, as described in the modification of the protocol by ArcherDX (ArcherDX Inc., Boulder, CO). Total nucleic acid was quantified using the Qubit Broad Range RNA Assay Kit (Thermo Fisher Scientific) and 2 μL of sample.

RNA Integrity Assessment and Library Preparation for NGS

Unless otherwise indicated, 250 ng of FFPE RNA was used as an input for NGS studies. To assess RNA quality, the PreSeq RNA QC Assay using iTaq Universal SYBR Green Supermix (Biorad, Hercules, CA) was performed on all samples during library preparation to generate a measure for the integrity of RNA (in the form of a cycle threshold value). Library preparation and RNA QC were performed following the Archer Fusion Plex Protocol for Illumina (ArcherDX Inc.). A custom primer set with 28 primers spanning regions on 3 specific genes of interest including *ETV6* was used. Final libraries were diluted 1:100,000 and quantified in a 10 μL reaction following the Library Quantification for Illumina Libraries protocol and assuming a 200 bp fragment length (KAPA, Wilmington, MA). The concentration of the final libraries was around 200 n. The threshold representing the minimum molar concentration for which sequencing can be robustly performed was set at 50 nM.

NGS and Analysis (Archer)

The libraries were sequenced on an MiSeq sequencer (Illumina, San Diego, CA). The libraries were diluted to 4 nM, and equal amounts of up to 16 libraries were pooled per run. The recommended number of raw reads per sample was set to 500,000. Library pools were diluted to 16 pM library stock with 10% 12.5 pM PhiX and loaded in the MiSeq cartridge. Analysis of sequencing results was performed using the Archer Analysis software (version 5; ArcherDX Inc.). Fusion parameters were set to a minimum of 5 valid fusion reads with a minimum of 3 unique start sites within the valid fusion reads.

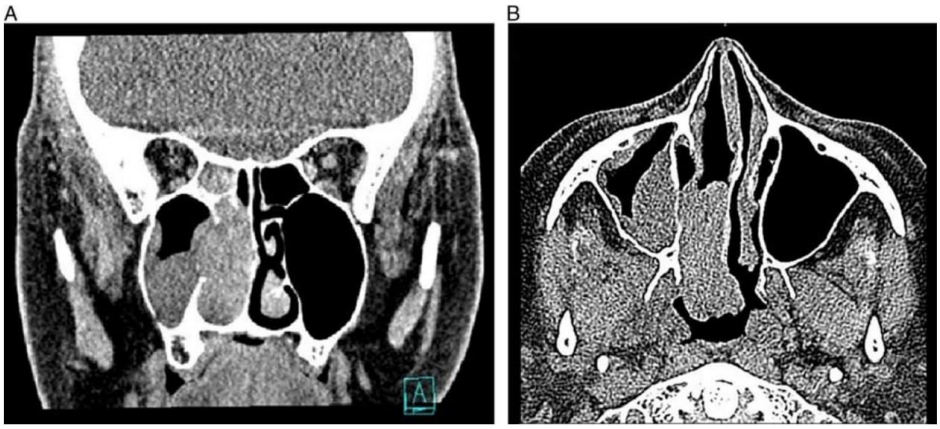

FIGURE 1. Representative imaging of case 2. A, Coronal computed tomography of case 2 demonstrating a right-sided nasal mass. B, The mass extends into the nasopharynx. There was no involvement of the maxillary sinus.

RESULTS

Case Histories

Case 1

A 51-year-old woman, nonsmoker without a prior history of breast cancer, presented with intermittent tenderness or pain behind the right eye and occasional forehead discomfort. A mass was identified on the right side of the nasal septum, and the patient was referred to surgical resection. The resected specimen measured 1.5×1.5×0.4 cm, and the patient was staged as T1N0M0. The patient was alive and showed no evidence of recurrent disease after >10 years of follow-up.

Case 2

A 65-year-old woman, nonsmoker without prior history of breast cancer, presented with right-sided nasal obstruction, nasopharyngeal secretion, and occasional retrobulbar pain. Past medical history was unremarkable except for a pleomorphic adenoma of the palate 5 years previously. Computed tomography identified a mass in the right nasal cavity extending into the nasopharynx. The patient underwent surgical excision of the mass including the middle turbinate along with maxillary sinus antrostomy, right ethmoidectomy, and partial resection of the nasal septum. The tumor measured 4×4×1.5 cm, and the patient was staged as T2NxM0. The patient received adjuvant radiotherapy and is alive with no evidence of disease after 4 years of follow-up (Figs. 1A, B).

Detailed clinicopathologic findings in these 2 patients are presented in Table 3.

Histopathology and Immunohistochemical Findings

Cases 1 and 2 had histologic features and immunoprofiles identical to salivary gland MASC. The tumors were unencapsulated and composed of tubular, papillary, and microcystic growth patterns with invasive margins (Fig. 2A). The tumor cells had low-grade vesicular and round to oval nuclei with fine, granular chromatin. Abundant eosinophilic homogenous extracellular periodic acid-Schiff with diastase–positive material (Fig. 2B) was present in both cases. The tumors were composed of solid microcystic growth patterns, in places divided by thick hyalinized fibrous septa (Fig. 2C). Focal necrotic areas were present in case 2 (Fig. 2D). In contrast to acinic cell carcinoma (AciCC), both tumors lacked cytoplasmic periodic acid-Schiff with diastase–positive zymogen granules. Mitoses were few, and there was no lymphovascular invasion or perineural growth.

In contrast, cases 3 to 17 displayed histologic features of low-grade tubulopapillary adenocarcinomas or

TABLE 3. Clinical Findings in 2 MASCs of the Nasal Cavity

Cases	Age (y)/Sex	Site	Size (cm)	Stage (TNM)	Local Recurrence	Duration of Symptoms (y)	Treatment	Follow-up (y)	Outcome
1	51/F	Right nasal septum	1.5×1.5×0.4	T1N0M0	No	1-2	Surgery	14	Alive NED
2	65/F	Right nasal cavity	4×4×1.5	pT2pNxM0	No	1	Surgery+RT	4	Alive NED

F indicates female; NED, no evidence of disease; RT, radiotherapy.

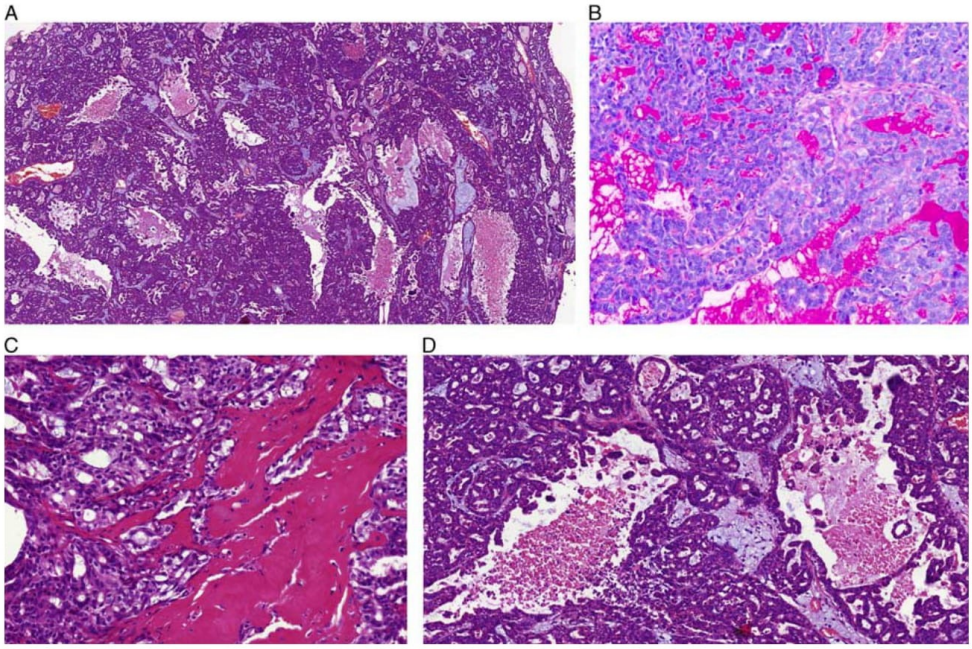

FIGURE 2. Histologic findings of sinonasal MASC. A, MASC shows admixed tubular, papillary, and microcystic growth patterns. B, Abundant periodic acid-Schiff with diastase–positive extracellular material within tubular and cystic spaces. C, The tumors were composed of solid, microcystic growth patterns, occasionally divided by thick hyalinized fibrous septa. D, Focal necrosis was present in case 2.

low-grade non–intestinal-type SNAC, not otherwise specified.[13,16,17]

The immunohistochemical findings are summarized in Tables 4 and 5. Both MASCs were positive for CK7, SOX10, GATA3, STAT5, and S100 (diffuse and strong staining in all tumor cells). Immunohistochemical staining for mammaglobin was diffusely positive in case 1 and focally positive in case 2 (Figs. 3A–D). Both cases were negative for p63 protein, CK20, CDX2, SATB2, and DOG-1 (Table 4). The remaining 15 cases, except for case 13, were negative for mammaglobin. Case 13 was S100 protein/SOX10/GATA3-positive with focal staining for mammaglobin in <5% of the tumor cells. Data from all 17 cases are summarized in Table 5.

TABLE 4. Immunohistochemical Results of 2 Cases of MASC in the Nasal Cavity

Antibody	Case 1	Case 2
CK7	+(D)	+(D)
S100	+(D)	+(F)
Mammaglobin	+(D)	+(F)
GATA3	+(D)	+(D)
SOX10	+(D)	+(D)
Pan-TRK	+	+
Stat5	+	+
p63	Neg	Neg
CK20	Neg	Neg
CDX2	Neg	Neg
DOG-1	Neg	Neg
GCDFP*	+(F)*	+(E)*
MIB1	5%	40%

*Immunochemistry performed at Department of Otorhinolaryngology and Maxillofacial Surgery, Køge University Hospital, and Department of Otolaryngology Head & Neck Surgery Rigshospitalet.

D indicates diffuse staining; E, staining of extracellular material; F, focal staining.

Genetic Findings

After histologic and immunohistochemical characterization, all 17 cases were characterized for the presence of the *ETV6-NTRK3* fusion transcript and/or rearrangement of *ETV6*. These findings are summarized in Table 6. Two cases, cases 1 and 2, showed *ETV6* gene rearrangement by FISH. Case 1 was negative with RT-PCR, but a product was identified with RT-PCR in case 2, and sequencing confirmed an exon 5 to 15 junction. In case 1, NGS identified an atypical exon 5-13 fusion. Cases 3 to 17 were negative or not analyzable with either RT-PCR or FISH, or were negative for both methods (Table 6 and Figs. 4A–C).

TABLE 5. Immunohistochemical Results of All 17 Cases

Case No.	Final Diagnosis	CK7	CK20	DOG-1	GATA3	SOX10	S100	MGA	p63	STAT5	MIB1	CDX2	SATB2
1	MASC	+	Neg	Neg	+	+	+	+	Neg	+	5%	Neg	Neg
2	MASC	+	Neg	Neg	+	+	+	+	Neg	+	40%	Neg	Neg
3	LG SNAC	+	Neg	Neg	+	+	+	Neg	Neg	ND	ND	Neg	ND
4	LG SNAC	Neg	Neg	Neg	+	+	+	Neg	Neg	ND	ND	Neg	ND
5	LG SNAC	+	Neg	Neg	Neg	Neg	Neg	Neg	Neg	ND	20%	Neg	Neg
6	LG SNAC	+	Neg	Neg	Neg	Neg	Neg	Neg	Neg	+	3%	Neg	Neg
7	LG SNAC	+	Neg	Neg	+	+	Neg	Neg	Neg	+	3%	Neg	Neg
8	LG SNAC	+	Neg	Neg	ND	+	+	Neg	Neg	ND	5%	Neg	ND
9	LG SNAC	+	Neg	Neg	Neg	+	+	Neg	Neg	+	3%	Neg	Neg
10	LG SNAC	+	Neg	NA	NA	NA	Neg	NA	NA	NA	NA	NA	Neg
11	LG SNAC	+	Neg	Neg	Neg	Neg	Neg	Neg	Neg	ND	90%	Neg	ND
12	LG SNAC	+	Neg	Neg	Neg	Neg	+	Neg	+	+	5%	Neg	ND
13	LG SNAC	+	Neg	Neg	+	+	+	+(F) 5%	Neg	+	10%	Neg	ND
14	LG SNAC	+	Neg	Neg	Neg	Neg	+(F)	Neg	+	+(F)	2%	Neg	Neg
15	LG SNAC	+	Neg	Neg	Neg	Neg	+	Neg	Neg	Neg	2%	Neg	Neg
16	LG SNAC	+	Neg	Neg	ND	+(F)	+	Neg	Neg	ND	2%	Neg	Neg
17	LG SNAC	+	Neg	Neg	Neg	+	Neg	Neg	Neg	ND	0%	ND	Neg

F indicates focally; LG, low grade; NA, not analyzable; ND, not done; Neg, negative.

DISCUSSION

In contrast to the sinonasal tract, diagnosing MASC in the major salivary glands as well as the oral minor glands is not difficult in most cases. MASC is well characterized not only by histologic and immunohistochemical features but also by the *ETV6-NTRK3* gene fusion.[1] However, if MASC is present in unexpected locations, the differential diagnosis is more challenging. MASC can be confused with other salivary gland tumors, including AciCC and adenocarcinoma not otherwise specified.[28] More than half of cases previously diagnosed as zymogen granule–poor AciCC were positive for *ETV6* translocation on rereview and therefore classified as MASC, and most tumors previously diagnosed as AciCC of the minor salivary glands also represent MASC.[29,30] In contrast to AciCC, MASC shows no basophilic granularity in the cytoplasm of any of the constituent cells, this being the hallmark of the serous acinar cells of AciCC. Moreover, MASC has a completely different immunohistochemical profile than AciCC, almost always strongly expressing

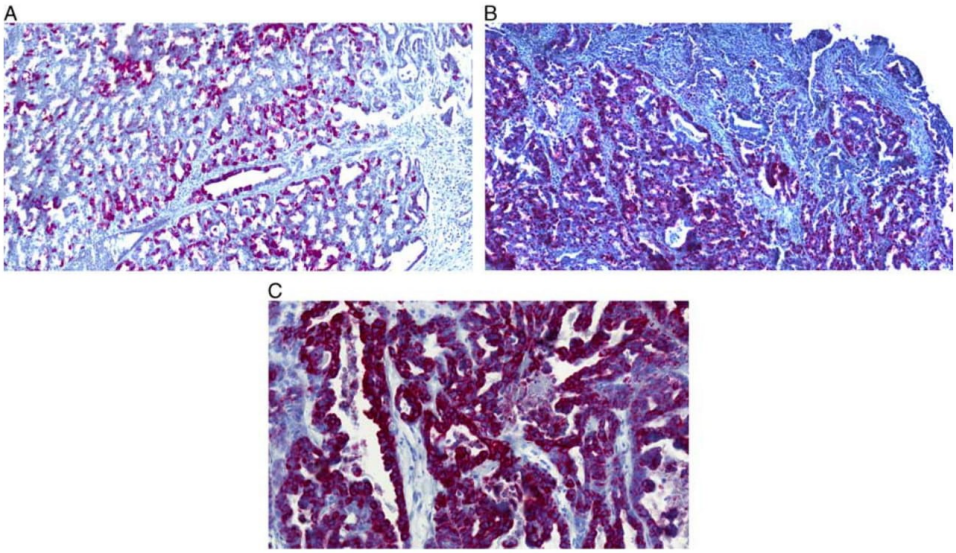

FIGURE 3. Immunohistochemical characteristics of MASC in the sinonasal tract. In both MASCs, tumor cells were intensely and diffusely positive for mammaglobin (A), S100 (B), and CK7 (C).

TABLE 6. Results of Molecular Analysis of 17 Cases of Sinonasal Carcinomas

		FISH		RT-PCR		
Cases	**Final Diagnosis**	***ETV6***	***NTRK3***	**Exons 5-15 Fusion Transcript**	**Archer NGS**	**Gene Status**
1	MASC	Break	NA	Neg	*ETV6-NTRK3* exons 5-13	*ETV6-NTRK3*
2	MASC	Break	Break	+	ND	*ETV6-NTRK3*
3	LG SNAC	NA	Intact	NA	ND	Neg
4	LG SNAC	Intact	Intact	Neg	ND	Neg
5	LG SNAC	Intact	ND	Neg	ND	Neg
6	LG SNAC	Intact	ND	Neg	ND	Neg
7	LG SNAC	Intact	ND	Neg	ND	Neg
8	LG SNAC	NA	ND	Neg	ND	Neg
9	LG SNAC	Intact	ND	ND	ND	Neg
10	LG SNAC	Intact	ND	ND	ND	Neg
11	LG SNAC	Intact	ND	Neg	ND	Neg
12	LG SNAC	NA	ND	NA	ND	NA
13	LG SNAC	NA	ND	Neg	ND	Neg
14	LG SNAC	Intact	ND	Neg	ND	Neg
15	LG SNAC	Intact	ND	Neg	ND	Neg
16	LG SNAC	NA	ND	NA	ND	NA
17	LG SNAC	Intact	ND	Neg	ND	Neg

LG indicates low grade; NA, not analyzable; ND, not done.

S100 protein and mammaglobin,[1,31,32] and lacking DOG-1 expression.[33]

Low-grade SNACs represent a histologically heterogenous group of tumors, including non-ITAC and ITAC subtypes.[13] In recent years, an increasing number of distinct types of SNACs have been recognized, including HPV-related multiphenotypic sinonasal carcinoma, SMARCB1-deficient sinonasal carcinoma, and tubulopapillary low-grade SNAC.[16,34–37] Recently, Andreasen et al[18] reviewed a series of low-grade SNACs of non-ITAC type with tubulopapillary growth pattern and found a subset of tumors harboring *ETV6* rearrangements and the *ETV6-NTRK3* fusion in 2 of 3 cases. From a strictly genetic perspective, *ETV6*-rearranged low-grade SNAC represents a pitfall for identifying true sinonasal MASC. However, despite the identical genetic features of sinonasal MASC and *ETV6*-rearranged low-grade SNAC, the following features allow for accurate separation. First, all 3 *ETV6*-rearranged low-grade SNACs reported were predominantly tubular, composed of cylindrical to cuboidal

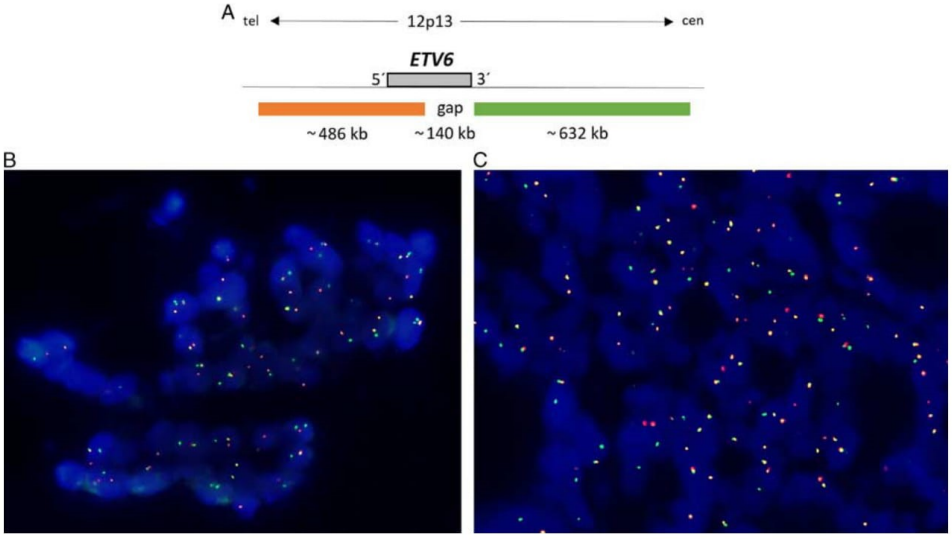

FIGURE 4. FISH. A, Design of the *ETV6* break-apart probe. B, Case 1 showing separate green and orange signals for *ETV6*. C, *NTRK3* indicating concomitant rearrangement of both genes.

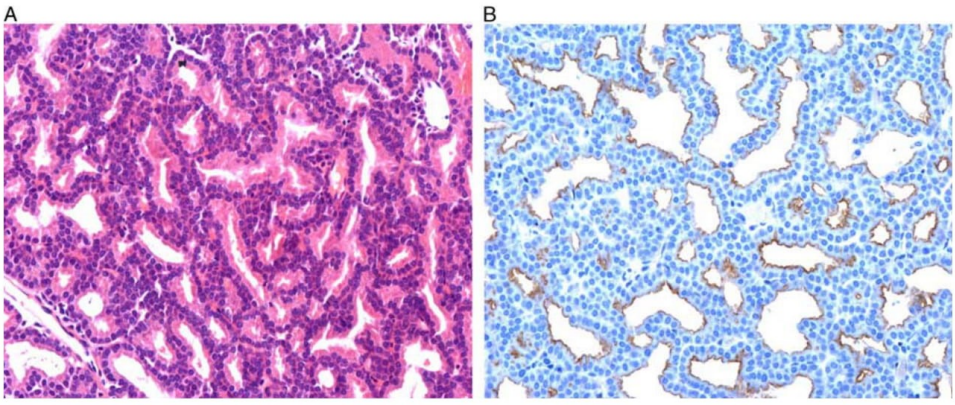

FIGURE 5. Histologic and immunohistochemical findings in *ETV6*-rearranged low-grade SNACs. A, *ETV6*-rearranged low-grade SNACs are composed of glands arranged back-to-back with little intervening stroma and minimal to absent secretory features. B, Tumors are focally DOG-1 positive.

tumor cells with occasional apocrine features and focal trabecular areas, which were not prominent features of sinonasal MASC. Second, tumor cells in *ETV6*-rearranged low-grade SNAC were arranged back-to-back with little intervening stroma with minimal or absent secretory features (Fig. 5A).[18] In contrast, both our MASCs showed abundant hyalinized septae and pronounced secretory features. Third, *ETV6*-rearranged low-grade SNAC is positive for DOG-1, negative for mammaglobin, and negative or patchy positive for S100, with the opposite being the case in MASC (Fig. 5B). Fourth, both MASCs presented here were invasive, whereas this was not seen in *ETV6*-rearranged low-grade SNAC.

The most important reason for separating these 2 entities is the difference in clinical behavior. While low-grade non-ITAC, including *ETV6*-rearranged low-grade SNAC, behaves in an essentially benign manner, MASC is a bona fide malignancy. Awareness of the existence of MASC within this anatomic region is important not only for separating these from the recently described *ETV6*-rearranged low-grade SNAC but also for separating MASC from more aggressive SNACs of non-ITAC and ITAC types.

In conclusion, we report 2 cases of sinonasal MASC and describe its unique features, which are valuable in its separation from *ETV6*-rearranged low-grade SNAC and other low-grade SNACs. Importantly, this separation is merited not only for academic reasons, as the more aggressive nature of MASC could necessitate treatment with TRK inhibitors.[19,20]

REFERENCES

1. Skalova A, Vanecek T, Sima R, et al. Mammary analogue secretory carcinoma of salivary glands, containing the *ETV6-NTRK3* fusion gene: a hitherto undescribed salivary gland tumor entity. *Am J Surg Pathol*. 2010;34:599–608.
2. Tognon C, Knezevich SR, Huntsman D, et al. Expression of the *ETV6-NTRK3* gene fusion as a primary event in human secretory breast carcinoma. *Cancer Cell*. 2002;2:367–376.
3. Amin SM, Beattie A, Ling X, et al. Primary cutaneous mammary analog secretory carcinoma with *ETV6-NTRK3* translocation. *Am J Dermatopathol*. 2016;38:842–845.
4. Bishop JA, Taube JM, Su A, et al. Secretory carcinoma of the skin harboring *ETV6* gene fusions: a cutaneous analogue to secretory carcinomas of the breast and salivary glands. *Am J Surg Pathol*. 2017;41:62–66.
5. Hyrcza MD, Ng T, Crawford RI. Detection of the *ETV6-NTRK3* translocation in cutaneous mammary-analogue secretory carcinoma. *Diagn Histopathol*. 2015;21:481–484.
6. Dogan S, Wang L, Ptashkin RN, et al. Mammary analog secretory carcinoma of the thyroid gland: a primary thyroid adenocarcinoma harboring *ETV6–NTRK3* fusion. *Modern Pathol*. 2016;29:985–995.
7. Dettloff J, Seethala RR, Stevens TM, et al. Mammary analog secretory carcinoma (MASC) involving the thyroid gland: a report of the first 3 cases. *Head Neck Pathol*. 2017;11:124–130.
8. Stevens TM, Kovalovsky AO, Velosa C, et al. Mammary analog secretory carcinoma, low-grade salivary duct carcinoma, and mimickers: a comparative study. *Mod Pathol*. 2015;28:1084–1100.
9. Lurquin E, Jorissen M, Debiec-Rychter M, et al. Mammary analogue secretory carcinoma of the sinus ethmoidalis. *Histopathology*. 2015; 67:749–751.
10. Xu B, Aryeequaye R, Wang L, et al. Sinonasal secretory carcinoma of salivary gland with high grade transformation: a case report of this under-recognized diagnostic entity with prognostic and therapeutic implications. *Head Neck Pathol*. 2017; DOI:10.1007/s12105-017-0855-5.
11. Slootweg PJ, Chan JKC, Stelow EB, et al. Tumours of the nasal cavity, paranasal sinuses and skull base. In: El-Naggar AK, Chan JKC, Grandis JR, Takata T, Slootweg PJ, eds. *WHO Classification of Head and Neck Tumours*, 4th ed. Lyon: IARC Press; 2017:11–76.
12. Leivo I. Sinonasal adenocarcinoma: update on classification, immunophenotype and molecular features. *Head Neck Pathol*. 2016;10:68–74.
13. Skalova A, Bell D, Bishop JA, et al. Secretory carcinoma. In: El-Naggar AK, Chan JKC, Grandis JR, Takata T, Slootweg PJ, eds. *WHO Classification of Head and Neck Tumours*, 4th ed. Lyon: IARC Press; 2017:177–178.
14. Heffner DK, Hyams VJ, Hauck KW, et al. Low-grade adenocarcinoma of the nasal cavity and paranasal sinuses. *Cancer*. 1982;50: 312–322.
15. Wenig B, Hyams VJ, Heffner DK. Nasopharyngeal papillary adenocarcinoma. A clinicopathologic study of a low-grade carcinoma. *Am J Surg Pathol*. 1988;12:946–953.

16. Skálová A, Cardesa A, Leivo I, et al. Sinonasal tubulopapillary low-grade adenocarcinoma. Histopathological, immunohistochemical and ultrastructural features of poorly recognised entity. *Virchows Arch*. 2003;443:152–158.
17. Luna MA. Sinonasal tubulopapillary low-grade adenocarcinoma. A specific diagnosis or just another seromucous adenocarcinoma? *Adv Anat Pathol*. 2015;12:109–115.
18. Andreasen S, Skálová A, Agaimy A, et al. *ETV6* Gene rearrangements characterize a morphologically distinct subset of sinonasal low-grade non–intestinal-type adenocarcinoma. A novel translocation-associated carcinoma restricted to the sinonasal tract. *Am J Surg Pathol*. 2017;41:1552–1560.
19. Drilon A, Li G, Dogan S, et al. What hides behind the MASC: clinical response and acquired resistance to entrectinib after ETV6-NTRK3 identification in a mammary analogue secretory carcinoma (MASC). *Ann Oncol*. 2016;27:920–926.
20. Skalova A, Stenman G, Simpson RHW, et al. The role of molecular testing in the differential diagnosis of salivary gland carcinomas. *Am J Surg Pathol*. 2018;42:e11–e27.
21. Murphy DA, Ely HA, Shoemaker R, et al. Detecting gene rearrangements in patient populations through a 2-step diagnostic test comprised of rapid ihc enrichment followed by sensitive next-generation sequencing. *Appl Immunohistochem Mol Morphol*. 2017;25:513–523.
22. Viswanatha DS, Foucar K, Berry BR, et al. Blastic mantle cell leukemia: an unusual presentation of blastic mantle cell lymphoma. *Mod Pathol*. 2000;13:825–833.
23. Gaffney R, Chakerian A, O'Connell JX, et al. Novel fluorescent ligase detection reaction and flow cytometric analysis of SYT-SSX fusions in synovial sarcoma. *J Mol Diagn*. 2003;5:127–135.
24. Antonescu CR, Kawai A, Leung DH, et al. Strong association of SYT-SSX fusion type and morphologic epithelial differentiation in synovial sarcoma. *Diagn Mol Pathol*. 2000;9:1–8.
25. Bourgeois JM, Knezevich SR, Mathers JA, et al. Molecular detection of the ETV6-NTRK3 gene fusion differentiates congenital fibrosarcoma from other childhood spindle cell tumors. *Am J Surg Pathol*. 2000;24:937–946.
26. Ito Y, Ishibashi K, Masaki A, et al. Mammary analogue secretory carcinoma of salivary glands: a clinicopathological and molecular study including 2 cases harboring *ETV6-X* fusion. *Am J Surg Pathol*. 2015;39:602–610.
27. Skalova A, Vanecek T, Simpson RHW, et al. Mammary Analogue Secretory Carcinoma of Salivary Glands. Molecular Analysis of 25 *ETV6* Gene Rearranged Tumors With Lack of Detection of Classical *ETV6-NTRK3* Fusion Transcript by Standard RT-PCR: Report of 4 Cases Harboring *ETV6-X* Gene Fusion. *Am J Surg Pathol*. 2016;40:3–13.
28. Chiosea SI, Griffith C, Assaad A, et al. Clinicopathological characterization of mammary analogue secretory carcinoma of salivary glands. *Histopathology*. 2012;61:387–394.
29. Chiosea SI, Griffith C, Assaad A, et al. The profile of acinic cell carcinoma after recognition of mammary analog secretory carcinoma. *Am J Surg Pathol*. 2012;36:343–350.
30. Bishop JA, Yonescu R, Batista D, et al. Most nonparotid "acinic cell carcinomas" represent mammary analog secretory carcinomas. *Am J Surg Pathol*. 2013;37:1053–1057.
31. Skálová A. Mammary analogue secretory carcinoma of salivary gland origin: an update and expanded morphologic and immunohistochemical spectrum of recently described entity. *Head Neck Pathol*. 2013;7:S30–S36.
32. Bishop JA. Unmasking MASC: bringing to light the unique morphologic, immunohistochemical and genetic features of the newly recognized mammary analogue secretory carcinoma of salivary glands. *Head Neck Pathol*. 2013;7:35–39.
33. Chenevert J, Duvvuri U, Chiosea S, et al. DOG1: a novel marker of salivary acinar and intercalated duct differentiation. *Mod Pathol*. 2012;25:919–929.
34. Bishop JA. Newly described tumor entities in sinonasal tract pathology. *Head Neck Pathol*. 2016;10:23–31.
35. Bishop JA, Andreasen S, Hang JF, et al. HPV-related multiphenotypic sinonasal carcinoma: an expanded series of 49 Cases of the tumor formerly known as HPV-related carcinoma with adenoid cystic carcinoma-like features. *Am J Surg Pathol*. 2017;41:1690–1701.
36. Andreasen S, Bishop JA, Hansen TV, et al. Human papillomavirus-related carcinoma with adenoid cystic-like features of the sinonasal tract: clinical and morphological characterization of six new cases. *Histopathology*. 2017;70:880–888.
37. Agaimy A, Hartmann A, Antonescu CR, et al. SMARCB1 (INI-1)-deficient sinonasal carcinoma: a series of 39 cases expanding the morphologic and clinicopathologic spectrum of a recently described entity. *Am J Surg Pathol*. 2017;41:458–471.

1.10.2 SEKREČNÍ KARCINOM MAMMÁRNÍHO TYPU SLINNÝCH ŽLÁZ: MOLEKULÁRNÍ ANALÝZA 25 PŘÍPADŮ *ETV6* REARANŽOVANÝH TUMORŮ, U KTERÝCH NEBYL DETEKOVÁN KLASICKÝ *ETV6-NTRK3* FÚZNÍ TRANSKRIPT STANDARDNÍ RT-PCR: 4 PŘÍPADY DEFINOVANÉ *ETV6-X* GENOVOU FÚZÍ

Práce se zabývá klinickou a molekulární analýzou 25 případů morfologicky a imunohistochemicky typických SC. Všechny případy obsahovaly zlom *ETV6* genu a v 16 případech byl zjištěný zlom genu *NTRK3* metodou FISH, avšak klasická *ETV6-NTRK3* fúze nebyla zjištěna standardní RT-PCR. Ve čtyřech případech byl klasický fúzní transkript detekovaný senzitivní „nested" RT-PCR. V pěti případech byla zastižena atypická fúze *ETV6-NTRK3* mezi exony 4-14 či 5-14. Pět případů bylo neanalyzovatelných. Zbývající 4 případy byly negativní na přítomnost zlomu *NTRK3* genu a pozitivní na zlom *ETV6* genu.

Fúzní partner *ETV6* genu nebyl identifikován a fúze byla označena jako *ETV6-X*. Při sledování morfologických a klinických údajů pacientů s atypickými fúzemi a fúzí *ETV6-X* se zjistilo, že tyto SC mají histologicky častěji přítomná silná fibrózní septa a výrazně hyalinizované stroma. Byla předložena hypotéza, že SC s atypickou fúzí a non *NTRK3* fúzním partnerem mohou růst více infiltrativně a mohou mít agresivnější biologické chování.

Mammary Analogue Secretory Carcinoma of Salivary Glands

Molecular Analysis of 25 ETV6 Gene Rearranged Tumors With Lack of Detection of Classical ETV6-NTRK3 Fusion Transcript by Standard RT-PCR: Report of 4 Cases Harboring ETV6-X Gene Fusion

Alena Skálová, MD, PhD,† Tomas Vanecek, PhD,*‡*
Roderick H.W. Simpson, MB, ChB, FRCPath,§ Jan Laco, MD, PhD,‖
Hanna Majewska, MD, PhD,¶ Martina Baneckova, MUC, Petr Steiner, MSc,*‡*
*and Michal Michal, MD**

Abstract: *ETV6* gene abnormalities are well described in tumor pathology. Many fusion partners of *ETV6* have been reported in a variety of epithelial and hematological malignancies. In salivary gland tumor pathology, however, the *ETV6-NTRK3* translocation is specific for mammary analogue secretory carcinoma (MASC), and has not been documented in any other salivary tumor type. The present study comprised a clinical and molecular analysis of 25 cases morphologically and immunohistochemically typical of MASC. They all also displayed the *ETV6* rearrangement as visualized by fluorescent in situ hybridization but lacked the classical *ETV6-NTRK3* fusion transcript by standard reverse-transcriptase-polymerase chain reaction. In 4 cases, the classical fusion transcript was found by more sensitive, nested reverse-transcription-polymerase chain reaction. Five other cases harbored atypical fusion transcripts as detected by both standard and nested reverse-transcription-polymerase chain reaction. In addition, fluorescent in situ hybridization with an *NTRK3* break-apart probe was also performed; rearrangement of *NTRK3* gene was detected in 16 of 25 cases. In 3 other cases, the tissue was not analyzable, and in 2 further cases analysis could not be performed because of a lack of appropriate tissue material. Finally, in the 4 remaining cases whose profile was *NTRK3* split-negative and *ETV6* split-positive, unknown (non-*NTRK*) genes appeared to fuse with *ETV6* (*ETV6-X* fusion). In looking for possible fusion partners, analysis of rearrangement of other kinase genes known to fuse with *ETV6* was also performed, but without positive results. Although numbers were small, correlating the clinico-pathologic features of the 4 *ETV6-X* fusion tumors and 5 MASC cases with atypical fusion transcripts raises the possibility of that they may behave more aggressively.

Key Words: mammary analogue secretory carcinoma, MASC, *ETV6-NTRK3*, *ETV6-X* fusion transcript, clinicopathologic analysis

(*Am J Surg Pathol* 2016;40:3–13)

Mammary analogue secretory carcinoma (MASC) of salivary gland origin is a recently described tumor that harbors a characteristic balanced chromosomal translocation, t(12;15) (p13;q25) resulting in an *ETV6-NTRK3* fusion[1] identical to that in secretory carcinoma of the breast.[2] Histologically, MASC is composed of uniform cells with bland-looking vesicular nuclei and eosinophilic vacuolated cytoplasm, arranged in tubular, microcystic and solid growth patterns with abundant periodic acid-Schiff –positive secretions. MASC may histologically resemble zymogen granule-poor acinic cell carcinoma, low-grade cribriform cystadenocarcinoma, and adenocarcinoma not otherwise specified.[1] However, the diagnosis of MASC in most cases is not difficult based on histologic, immunohistochemical, and molecular features. Detection of *ETV6* by fluorescent in situ hybridization (FISH) is technically feasible and more than 150 cases of MASC have been published in the last 4 years since its original description in 2010.[1]

There have been several studies extending the description of the clinical, histologic, and immunohistochemical features of MASC[3–12] and the number of

From the *Department of Pathology, Faculty of Medicine in Plzen, Charles University, Prague; †Bioptic Laboratory Ltd; ‡Bioptic Laboratory Ltd, Molecular Pathology Laboratory, Plzen; ‖The Fingerland Department of Pathology, Charles University in Prague, Faculty of Medicine and University Hospital, Hradec Kralove, Czech Republic; §Department of Anatomical Pathology, University of Calgary and Foothills Medical Centre, Calgary, AB, Canada; and ¶Department of Pathology, Medical University of Gdansk, Gdansk, Poland.

Supported by Grant no. NT13701-4/2012 of IGA MH CR (Internal Grant Agency of Health Ministry, Czech Republic) and SVV grant 2015, no. 260171.

Conflicts of Interest and Source of Funding: The authors have disclosed that they have no significant relationships with, or financial interest in, any commercial companies pertaining to this article.

Correspondence: Alena Skálová, MD, PhD, Sikl's Department of Pathology, Medical Faculty of Charles University, Faculty Hospital, E. Benese 13, 305 99 Plzen, Czech Republic (e-mail: skalova@fnplzen.cz).

reported MASCs has grown considerably.[13–15] However, the molecular genetic and epigenetic background of MASC has not been completely studied, except for the *ETV6-NTRK3* fusion. Therefore, a recent paper by Ito et al[16] describing 2 MASC cases with *ETV6* fused with an unknown gene partner immediately attracted our attention; the authors hypothesized that such tumors may have unique clinicopathologic features.

Up until then, in all cases of MASC where the fusion was known, this was *ETV6* with *NTRK3*, and no other fusion partners have been reported so far. Nevertheless, for several years, we have been aware of a number of MASC cases positive for the *ETV6* gene split as visualized by FISH, but in which the classical *ETV6-NTRK3* fusion transcript (exon 5-exon 15 junction) was not detected by standard reverse-transcriptase polymerase chain reaction (RT-PCR). Twenty-five such MASC cases were retrieved from our consultation files and further analyzed.

MATERIALS AND METHODS

Among more than 4300 cases of primary salivary gland tumors, 121 cases of the newly recognized entity MASCs were retrieved from the consultation files of the Salivary Gland Tumor Registry, at the Department of Pathology, Faculty of Medicine in Plzen, Czech Republic (AS). The histopathologic features of all tumors and the immunohistochemical stains when available were reviewed by 2 pathologists (A.S. and M.B.). A diagnosis of MASC was confirmed in cases that displayed, if at least focally, histologic features consistent with original description[1] in conjunction with appropriate immunohistochemical profile, that is coexpression of S-100 protein, cytokeratin CK7, and mammaglobin with absence of p63 and DOG1 staining. For the purpose of this particular study, we have included only unequivocal cases of MASC positive for *ETV6* rearrangement by FISH. Twenty-five tumors harboring *ETV6* gene rearrangement as visualized by FISH but without detection of the classical *ETV6-NTRK3* fusion transcript by standard RT-PCR were further analyzed.

For conventional microscopy, the excised tissues were fixed in formalin, routinely processed, embedded in paraffin, cut, and stained with hematoxylin-eosin. In most cases, additional stains were also performed, including periodic acid-Schiff with and without diastase, mucicarmin, and alcian blue at pH 2.5.

For immunohistochemical studies, 4-μm-thick sections were cut from paraffin blocks, mounted on slides coated with 3-aminopropyltriethoxy-silane (Sigma, St. Louis), deparaffinized in xylene, and rehydrated in descending grades (100% to 70%) of ethanol. Sections were then subjected to heat-induced epitope retrieval by immersion in a CC1 solution at pH 8, at 95°C. Endogenous peroxidase was blocked by a 5-minute treatment with 3% hydrogen peroxide in absolute methanol. The slides were then stained by immunostainer BenchMark ULTRA (Roche). The primary antibodies used are summarized in Table 1. The bound antibodies were visualized using the Histofine Simple Stain MAX PO (Multi) Universal Immuno-peroxidase Polymer, anti-mouse and rabbit (Nichirei Biosciences Inc., Tokyo, Japan), and 3-3′-diaminobenzidine (Sigma) as chromogen. The slides were counterstained with Mayer hematoxylin. Appropriate positive and negative controls were employed.

Clinical follow-up was obtained from the patients, their physicians, or from referring pathologists.

Molecular Genetic Study

Detection of *ETV6-NTRK3* Fusion Transcript by RT-PCR

RNA was extracted using the RecoverAll Total Nucleic Acid Isolation Kit (Ambion, Austin, TX). cDNA was synthesized using the Transcriptor First Strand cDNA Synthesis Kit (RNA input 500 ng) (Roche Diagnostics, Mannheim, Germany). All procedures were performed according to the manufacturer's protocols. Amplification of a 105 and 133 bp product of the β2-microglobulin gene and 247 bp product of *PGK* gene was used to test the quality of the extracted RNA as previously described.[17–19] A detection of classical, exon 5 of *ETV6* gene and exon 15 of *NTRK3* gene,[20] as well as atypical, exon 4 of the *ETV6* gene and exon 14 of the *NTRK3* gene (and their combinatorial variants), fusion transcript was performed by RT-PCR. In addition, more sensitive, nested RT-PCR was performed for detection classical[16] as well as selected atypical junction of transcripts.

For single-round PCR, 2 μL of cDNA was added to reaction consisted of 12.5 μL of HotStar Taq PCR Master Mix (Qiagen, Hilden, Germany), 10 pmol of each primer (Table 2) and distilled water up to 25 μL. The amplification program comprised denaturation at 95°C for 14 minutes and then 45 cycles of denaturation at 95°C for 1 minute, annealing at temperature seen in Table 2 for 1 minute, and extension at 72°C for 1 minute. The program was finished by incubation at 72°C for 7 minutes. For nested PCR, the same reaction conditions were set. One microliter of PCR product from the first round was used as a template.

Successfully amplified PCR products were purified with magnetic particles Agencourt AMPure (Agencourt Bioscience Corporation, A Beckman Coulter Company, Beverly, MA). Products were then bidirectionally sequenced using Big Dye Terminator Sequencing kit (PE/Applied Biosystems, Foster City, CA), purified with magnetic particules Agencourt CleanSEQ (Agencourt Bioscience Corporation), all according to the manufacturer's protocol and run on an automated sequencer ABI Prism 3130xl (Applied Biosystems) at a constant voltage of 13.2 kV for 11 minutes.

Detection of *ETV6*, *NTRK3*, and Other 13 Genes Break by FISH Method

From each tumor, 4-μm-thick sections were cut from formalin-fixed paraffin-embedded blocks and placed

TABLE 1. Antibodies Used for Immunohistochemical Study

Antibody Specificity	Clone	Dilution	Antigen Retrieval/Time	Source
S-100 protein	Polyclonal	1:2000	CC1/20 min	DakoCytomation
CK7	OV-TL 12/30	1:200	CC1/36 min	DakoCytomation
GCDFP-15	EP1582y	RTU	CC1/64 min	Cell Marque
Mammaglobin	304-1A5	RTU	CC1/36 min	DakoCytomation
STAT 5a	Polyclonal	1:400	CC1/36 min	Assay Designs Inc.
Ki-67	30-9	RTU	CC1/64 min	Ventana
P63	4A4	RTU	CC1/64 min	Ventana
DOG1	K9	RTU	CC1/36 min	Leica
GATA3	L50-823	1:250	CC1/52 min	BioCare Medical
SOX10	Polyclonal	1:50	CC1/64 min	Cell Marque

CC1 indicates EDTA buffer, pH 8.6; RTU, ready to use.

on positively charged slides. The slides were routinely deparaffinized in xylen 3 times for 5 minutes and then washed twice in 100% ethanol, once in 95% ethanol and once in deionized water for 5 minutes. Then, the slides were heated in the 1× Target Retrieval Solution (pH 6) (Dako, Glostrup, Denmark) for 40 minutes at 95°C and subsequently cooled for 20 minutes at room temperature in the same solution. The slides were washed in deionized water for 5 minutes and tissues were covered with the Proteinase K (20 mg/mL) (SERVA, Heidelberg, Germany) for 10 minutes at room temperature. The slides were then placed into deionized water for 5 minutes, dehydrated in a series of ethanol solution (70%, 85%, 96% for 2 min each) and air-dried.

An appropriate amount of mixed break-apart probe (Table 3) was applied on each specimen and was incubated in the ThermoBrite instrument (StatSpin/Iris Sample Processing, Westwood, MA) at 85°C for 8 minutes and then at 37°C for 16 hours. Subsequently, the slide was washed in 2 × SSC/0.3% NP-40 solution at 72°C for 2 minutes and counterstained with DAPI.

TABLE 2. Primers for Detection of *ETV6-NTRK3* Fusion Transcripts

Original Primer Name	Sequence	Localization
ETV6-ex4-F3	AGCCGGAGGTCATACTGCAT	ETV6 exon 4 inner
ETV6-ex4-F4	CATTCTTCCACCCTGGAAAC	ETV6 exon 4 outer
ETV6B*	ACATCATGGTCTCTGTCTCCCCGC	ETV6 exon 5 inner
TEL971† (ETV6A*)	ACCACATCATGGTCTCTGTCTCCC	ETV6 exon 5 outer
NTRK3-ex14-R1	GTGATGCCGTGGTTGATGT	NTRK3 exon 14 inner
NTRK3 ex14-R2	AGTCATGCCAATGACCACAG	NTRK3 exon 14 outer
NTRK3B*	TTCTCGCTTCAGCACGATGTCT	NTRK3 exon 15 inner
TRKC1059† (NTRK3A*)	CAGTTCTCGCTTCAGCACGATG	NTRK3 exon 15 outer

*Ito et al.[16]
†Bourgeois et al.[20]

FISH Interpretation

Each specimen was examined with an Olympus BX51 fluorescence microscope using a 100× objective and filter sets Triple Band Pass (DAPI/SpectrumGreen/SpectrumOrange), Dual Band Pass (FITC/Texas Red), and Single Band Pass (SpectrumGreen or SpectrumOrange). Scoring was performed by counting the number of fluorescent signals in 100 randomly selected non-overlapping tumor cell nuclei. The slides were independently enumerated by 2 observers (T.V. and P.S.). The cut-off value for gene break was set at 10%.[1]

RESULTS

Molecular Genetic Findings

After making the histologic diagnosis of MASC and confirming the *ETV6* split, 25 cases with the absence of classical, exon 5-exon 15, *ETV6-NTRK3* fusion transcript as detected by standard RT-PCR were analyzed in greater detail (Table 4). The classical fusion transcript was analyzed by potentially more sensitive nested RT-PCR.[14] In addition, atypical, exon 4-exon 14, *ETV6-NTRK3* fusion transcript, and also possible combinations of exons involved in classical and atypical junction were analyzed by nested RT-PCR and/or RT-PCR. In 4 cases, the classical fusion transcript was found by nested RT-PCR. Five other cases harbored atypical, exon 4-exon 14 or exon 5-exon 14, *ETV6-NTRK3* fusion transcript as detected by both, nested and/or standard RT-PCR (Fig. 1). The rest of the cases remained negative on RT-PCR. In addition to RT-PCR studies, FISH with *NTRK3* break-apart probe was performed. The *NTRK3* gene split was detected in 16 of 25 cases. In 3 cases, the tissue was not analyzable, and in 2 other cases analysis could not be performed because of lack of formalin-fixed paraffin-embedded tissue material.

TABLE 3. Probes Used in Study

Gene Name	BAC Clone/Localization of Probe	Producer	Reaction Mixture (Probe-Probe:Water:Buffer)
ETV6	Commercial	Abbott/Vysis	1:2:7^{+}
NTRK3	RP11-97O12 RP11-96B23	BlueGnome	1-1:1:7^{++}
NTRK1	chr1:156188056-156785595 chr1:156851496-157451790	Agilent	1-1:1:7^{++}
NTRK2	chr9:86361009-87360838 chr9:87560839-88561053	Agilent	1-1:1:7^{++}
ABL1	RP11-17L7 RP11-143H20	BlueGnome	1-1:1:7^{++}
ABL2	chr1:178664366-179063610 chr1:179203866-180203965	Agilent	1-1:1:7^{++}
FGFR3	RP11-386I15 RP11-262P20	BlueGnome	1-1:1:7^{++}
FLT3	RP11-438F9 RP11-502P18	BlueGnome	1-1:1:7^{++}
FRK	chr6:115762599-116262838 chr6:116381774-116882068	Agilent	1-1:1:7^{++}
JAK2	Commercial	KREATECH Diagnostics	Ready to use
LYN	chr8:56192225-56792519 chr8:56925305-57525154	Agilent	1-1:1:7^{++}
PDGFRA	RP11-367N1 RP11-116G9	BlueGnome	1-1:1:7^{++}
PDGFRB	Commercial	CYTOCELL Technologie	Ready to use
PER1	RP11-298H4 RP11-89A15	BlueGnome	1-1:1:7^{++}
SYK	RP11-61N16 RP11-367F23	BlueGnome	1-1:1:7^{++}

TABLE 4. Results of Molecular Genetic Analysis of *ETV6* and *NTRK3* Genes Rearrangement and *ETV6-NTRK3* Fusion Transcripts

	FISH		RT-PCR Classical	Nested RT-PCR	RT-PCR Atypical 4-14[1]	Nested RT-PCR Atypical	RT-PCR Control Genes
Case Number	*ETV6* Break	*NTRK3* Break	5-15	Classical 5-15	or 5-14[2]	4-14[1]	105/133/247
Case 1	+	NA	–	–	–	–	+/+/–
Case 2	+	+	–	–	–	–	+/+/–
Case 3	+	+	–	+	–	–	+/+/+
Case 4	+	NA	–	–	–	–	+/–/–
Case 5	+	NP	–	–	–	–	+/+/+
Case 6	+	–	–	–	–	–	+/+/+
Case 7	+	NP	–	–	–	–	+/–/–
Case 8	+	+	–	+	–	–	+/+/–
Case 9	+	+	–	–	–	+[1]	+/+/+
Case 10	+	+	–	–	–	–	+/+/+
Case 11	+	NA	–	–	–	–	+/+/+
Case 12	+	+	–	+	–	–	+/+/+
Case 13	+	+	–	–	+[2]	–*	+/+/+
Case 14	+	+	–	–	+[1]	+[1]	+/+/+
Case 15	+	–	–	–	–	–	+/+/+
Case 16	+	+	–	–	–	–	+/+/–
Case 17	+	–	–	–	–	–	+/+/+
Case 18	+	+	–	+	–	–	+/+/–
Case 19	+	+	–	–	+[1]	+[1]	+/–/–
Case 20	+	–	–	–	–	–	+/+/+
Case 21	+	+	–	–	–	–	+/+/–
Case 22	+	+	–	–	–	–	+/+/–
Case 23	+	+	–	–	–	–	+/+/+
Case 24	+	+	–	–	–	–	+/+/+
Case 25	+	+	–	–	+[1]	+[1]	+/+/+

4, 5—numbers of exons of *ETV6* gene; 14, 15—numbers of exons of *NTRK3* gene.
*Only 4-14 junction was analyzed by nested RT-PCR.
NA indicates not analyzable; NP, not performed.

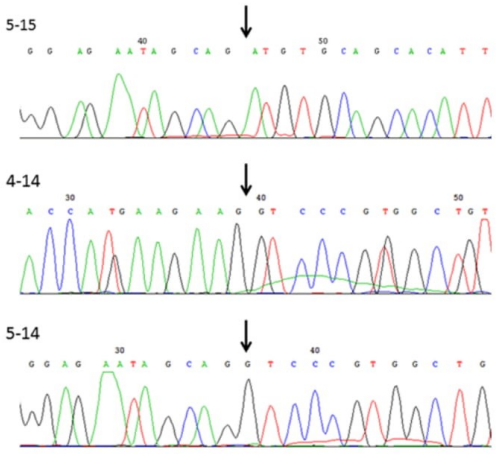

FIGURE 1. Sequence analysis of *ETV6-NTRK3* fusion transcripts. The most common exon 5-exon 15 (5-15) as well as 2 other atypical (4-14 and 5-14) fusions are shown. Arrows show point of fusion.

In the 4 remaining cases with the profile of *NTRK3* split-negative and *ETV6* split-positive, the fusion of *ETV6* gene to a non-*NTRK3* gene was suggested. To pursue possible fusion partners in these cases, we examined involvement of *NTRK1* and *NTRK2* genes, both members of the NTRK family. However, neither an *NTRK1* nor *NTRK2* gene split was detected (Fig. 2). Other kinase genes known to be possible partners of *ETV6*, such as *ABL1*, *ABL2*, *FGFR3*, *FLT3*, *FRK*, *JAK2*, *LYN*, *PDGFRA*, *PDGFRB*, *PER1*, and SYK were analyzed in cases, in which a sufficient formalin-fixed paraffin-embedded tissue was available (cases 17, 20). In case 17, no break of these genes was detected. In case 20, all genes except unanalyzable *FLT3*, *PDGFRA*, and *SYK* were negative, too.

Clinical and Histologic Characteristics of the Study Group

The clinical and follow-up data are summarized in Table 5. There were 9 female and 16 male patients. The median patient age was 47 years, with a range between 15 and 77 years. The most common anatomic site of involvement was the parotid gland, occurring in 12 patients (48%). Other sites of origin were the submandibular gland in 6 patients (24%), minor salivary gland of buccal mucosa, and retromolar gingiva in 2 patients each (8%) and 3 tumors arose in the upper lip (12%).

Follow-up Data

Clinical follow-up data were obtained from 22 patients, and ranged from 9 months to 19 years (mean 3 y and 11 mo), 3 patients were lost to follow-up. Detailed clinical, follow-up, and histologic findings in 25 patients with MASC are summarized in Table 6.

Five of the 22 patients experienced locally recurrent tumor 1 month to 19 years after the primary diagnosis (mean 55 mo). Cervical lymph node metastases developed in 6 patients, one of whom died of disseminated cancer 20 months after diagnosis with nodal (4 mo after diagnosis of primary tumor) and multiple distant metastases to lungs, liver, and bones at 10 months (case 9). Fourteen of 22 patients were alive with no evidence of recurrent or metastatic disease at last follow-up.

All tumors were treated by surgical excision; in 9 cases the excision was radical with clear surgical margins, but in 11 cases the surgical margins were positive and in 4 cases the tumor infiltration was close (< 0.5 mm) to the surgical margins. One patient underwent subtotal conservative parotidectomy in combination with radiotherapy (case 5). Recurrences were treated by radical reexcision with clear surgical margins in all 5 patients, radiotherapy was used in 4 of these 5 patients with recurrent disease.

Macroscopic Features

The median tumor size was 2.1 cm, with a range of 0.5 to 5.0 cm. Grossly, most tumors were variably invasive: 4 were entirely circumscribed, 6 had focally infiltrative edges, and 15 were predominantly infiltrative.

Microscopic and Immunohistochemical Features

On low-power magnification, 3 major growth patterns of MASC were identified in our material. Firstly, some tumors were well circumscribed and surrounded by a thick, focally uninterrupted, fibrous capsule enclosing predominantly papillary and macrocystic structures (Fig. 3). The second pattern was characterized by solid and lobular growth with a multilobular structure divided by thick hyalinized or thin fibrous septa (Fig. 4). These tumors either lacked a capsule or were only partially encapsulated with prominent infiltrative borders. These cases were predominantly composed of microcystic and slightly dilated glandular spaces filled with variable amount of eosinophilic homogenous secretory material. A prominent fibrosclerotic stroma with isolated tumor cells in small islands or trabeculae were seen in central part of the tumor in 12/25 (48%) cases (Fig. 5). The third pattern comprised a macrocystic growth pattern, in which larger cystic structures were lined mostly by a single, and focally a double layer of cells with prominent or focal apocrine differentiation including hobnail cells (Fig. 6). The cysts contained abundant proteinaceous eosinophilic material. However, most tumors demonstrated 2 or more architectural patterns with microcystic, tubular, solid, and papillary patterns often occurring together.

Regardless of the growth pattern of MASC, the tumor cells were often bland looking with abundant pale pink vacuolated and foamy cytoplasm and with vesicular oval nuclei with a single small but prominent nucleolus. The cytologic features were similar from cases to case. Range of nuclear atypia was assessed as grades 1 to 3. Mitotic figures were rare and necrosis was absent.

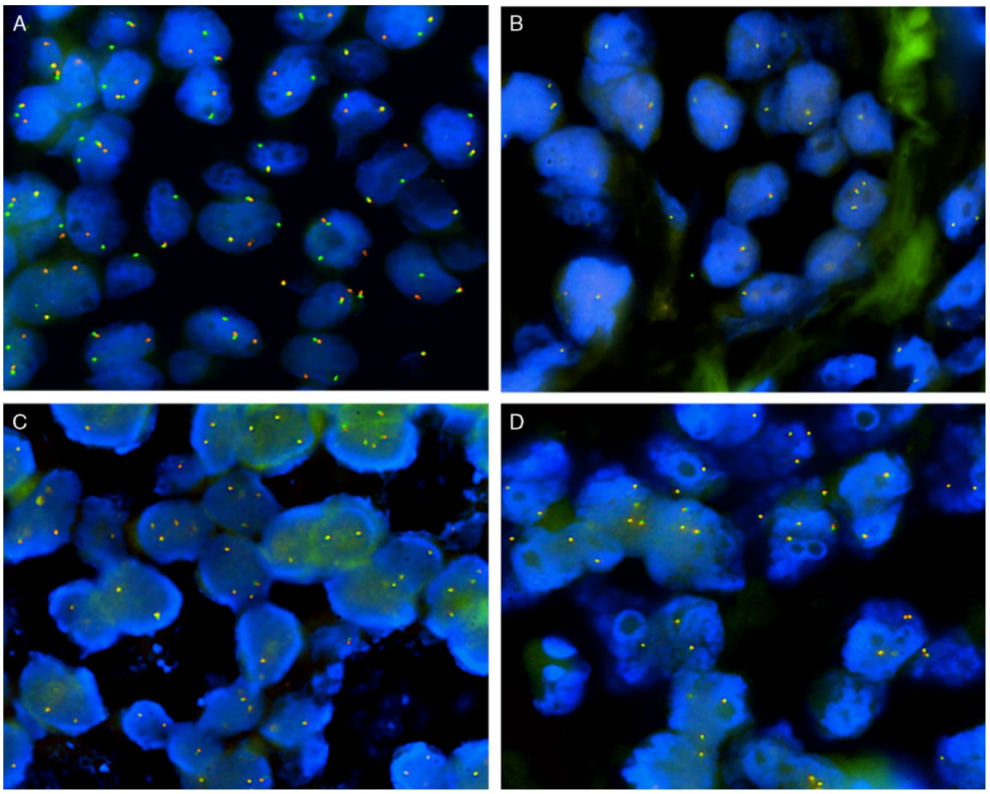

FIGURE 2. FISH analysis reveal rearranged *ETV6* gene (A), and intact genes *NTRK1* (B), *NTRK2* (C), and *NTRK3* (D) respectively, using break-apart probes. Yellow (red/green fusion) signal demonstrates intact chromosome, separated red and green signals mean gene break.

Lymphovascular invasion was present in 2 cases (8%), and perineural invasion was seen in 12 tumors (48%) (Table 5).

Histologic Findings in 4 MASC Cases *NTRK3* Split-negative *ETV6* Split-positive (*ETV6-X* Fusion)

Invasive growth into fibroadipose tissue adjacent to salivary glands was seen in 3 of the 4 (cases 15, 17, 20), and the remaining tumor was received as multiple fragments, and thus invasion could not be assessed (case 6). In detail: skeletal muscle was involved in 1 case (case 15), lymphovascular invasion in 1 (case 15), and perineural invasion seen in 2 (cases 17, 15). A capsule was not present in any of these tumors. The fibrosclerotic stroma and thick hyalinized fibrous septa were particularly prominent in 2 of 4 cases. Nuclei were assessed as grade 1 in 3 tumors, and nuclear grade 2 in the remaining 1 (case 20) (Tables 4 and 6).

Histologic Findings in 5 MASC Cases With Atypical Profile of *ETV6-NTRK3* Fusion Transcript

Except for 1 patient (case 25), all the other 4 tumors were invasive and nonencapsulated with infiltration of periglandular tissue and positive surgical margins. Perineural (2/5) and lymphovascular (1/5) invasion were observed. Four cases showed thick fibrous septa with focal hyalinization, and in each of 3 cases, trabeculae and nests of neoplastic cells were embedded in a completely hyalinized central part of the tumor (Fig. 7). Nuclei were assessed as grade 1 in 3 tumors (cases 14, 19, 25), and nuclear grade 3 in the remaining 1 (case 9) (Tables 4 and 6).

High-grade morphology was seen in 1 patient (case 9). The tumor was composed of 2 distinct carcinomatous components (Fig. 8). One component was a conventional MASC made of uniform neoplastic cells arranged in solid, tubular, and microcystic growth structures, divided by fibrous septa that were thick and partly hyalinized. The tumor cells had typical low-grade morphology;

TABLE 5. Clinical and Histologic Findings in 25 MASC Cases With *ETV6*-Split and Absence of *ETV6-NTRK3* Fusion Transcript by Standard RT-PCR

	N/Total (%)
Age	
Median age (y)	47
Range (y)	15-77
Sex	
Female	9/25 (36)
Male	16/25 (64)
Anatomic location	
Parotid gland	12/25 (48)
Submandibular gland	6/25 (24)
Minor gland	7/25 (28)
Size (cm)	
Median	2.1
Range	0.5-5.0
Follow-up data available	22/25 (88)
Median follow-up period	3 y 11 mo
Range	9-228 mo
Metastatic disease	
Cervical LN metastasis	6/22 (28)
Distant metastasis	1/22 (4)
Local recurrent disease	5/22 (23)
Histologic findings	
Invasive growth	15/25 (60)
Perineural invasion	12/25 (48)
LVI	2/25 (8)
Prominent hyalinized stroma	12/25 (48)

LN indicates lymph node; LVI, lymphovascular invasion.

vesicular round to oval nuclei with finely granular chromatin and distinct centrally located nucleoli. The other component was sharply delineated from the conventional MASC. It was composed of anaplastic cells with abundant cytoplasm and large pleomorphic nuclei. Solid tumor islands revealed areas of large geographical comedo-like necrosis and desmoplastic stroma indicated invasion. The tumor cells of the high-grade component had significantly increased mitotic activity and nuclear polymorphism and failed to produce secretory material, in contrast to the low-grade component.

Immunohistochemical Findings

By immunohistochemistry, all examined MASC cases were positive for S100 protein (25/25), mammaglobin (17/17), typically in strong and diffuse fashion (secretory material was also positive), and cytokeratin CK7 (17/17). GATA-3, SOX-10, and STAT5a staining was detected in most analyzed cases, respectively (17/17), (5/10), and (5/5). P63 protein was completely negative in most cases, with limited areas of positive peripheral myoepithelial cell staining suggestive of a focal intraductal component in 3 cases. DOG1 was negative in all cases (16/16). Proliferative activity was generally low, with mean MIB1 index 17% (range 5% to 40%).

DISCUSSION

MASC is a relatively newly described neoplasm of minor and major salivary glands characterized in most cases by a distinctive molecular alteration: a balanced t(12;15) (p13;q25) chromosomal rearrangement resulting in the fusion of the *ETV6* and *NTRK3* genes.[1] Interestingly, the same translocation, *ETV6-NTRK3*, can be seen not only in secretory carcinoma of breast,[2] but also in infantile fibrosarcoma,[21] congenital mesoblastic nephroma,[22] some hematopoietic malignancies,[23] ALK-negative inflammatory myofibroblastic tumors,[24] and in radiation-induced papillary thyroid carcinoma.[25]

The *ETV6-NTRK3* fusion gene encodes a chimeric oncoprotein tyrosine kinase that activates the Ras-MAP kinase and phosphatidylinositol-3-kinase–Akt pathways. An *ETV6* rearrangement may be detected from paraffin-embedded tissue by break-apart FISH or alternatively, the fusion transcript can be identified by RT-PCR. Detection of *ETV6* rearrangement from paraffin-embedded tissue is technically feasible, relatively widely available and is considered the gold standard for the diagnosis of MASC. However, in some of our MASC cases previously reported, RT-PCR failed to demonstrate the *ETV6-NTRK3* fusion transcript, even though they were FISH positive.[1,11,26]

Recently, Ito et al[16] reported 2 cases of MASC with the *ETV6* gene split detected by FISH but in which the *ETV6* gene appeared to be fused with a gene partner other than *NTRK3*. They further demonstrated that neither *NTRK1* nor *NTRK2* genes were involved.[16] In hematopoietic malignancies, >30 *ETV6* partner genes have been molecularly characterized,[27] but in MASC *ETV6* usually fuses with *NTRK3*, and no other fusion partners have been reported so far.[1,16] However, the 2 cases reported by Ito et al[16] plus several examples of MASC in our previous studies[1,11,26] that failed to demonstrate *ETV6-NTRK3* fusion transcript by classical RT-PCR together suggested that *ETV6* may on occasions fuse with an unknown non-*NTRK* gene partner (*ETV6-X* fusion). Therefore, we retrieved from our consultation files 25 such MASC cases all *ETV6* split by FISH but negative for *ETV6-NTRK3* fusion transcript as detected by standard RT-PCR.[20] This reaction analyzes the most common fusion in MASC, which is the junction of exon 5 of *ETV6* and exon 15 of *NTRK3* genes by single-round RT-PCR. In the present study, we used the more sensitive, nested RT-PCR,[16] and consequently we revealed the presence of the classical transcript in another 4 cases. In addition, we found 5 cases with atypical junctions. These junctions have not been described in MASC but are relatively common in radiation-induced papillary thyroid carcinoma.[25]

Simultaneously with the RT-PCR study, we performed FISH analysis of our tumors with various break-apart probes. Firstly, we investigated splits in the *NTRK3* gene. This analysis revealed, as in the study of Ito et al,[16] the presence of *ETV6*-positive/*NTRK3*-negative cases. On 2 available samples, we then performed analysis for rearrangement of *NTRK3* homologs *NTRK1* and *NTRK2* but these were negative, similar to the findings of Ito et al[16] In addition to these *NTRK* homologs, we analyzed several kinase genes commonly fused with *ETV6* in hematological malignancies,[27] but we were unable to

TABLE 6. Clinical and Histologic Findings of 25 MASC Cases

Case Number	Age/ Sex	Primary Site	Tumor Size (mm)	Capsule	Invasion (LVI, PN)	Septa	Hyalinized Sclerosis
1	31/F	Buccal mucosa	10	Complete	No	No	No
2	24/F	Buccal mucosa	10	Invasive	No	No	No
3	38/F	Parotid	30	Invasive	PN+	++	+
4	48/M	Upper lip	10	Invasive	No	++	+
5	28/M	Parotid, deep lobe	50×30×15	Invasive	PN+	++	++
6	50/M	Lip	15	Invasive	No	No	No
7	66/F	Parotid	8	Complete	No	No	No
8	17/M	Parotid	40×35×25	Invasive	No	No	No
9	60/M	Parotid	40×35×25	Invasive	PN+LVI+	++	+++
10	39/M	Parotid	14	Incomplete	PN+	+	+
11	69/F	Retromolar gingiva	6	Complete	No	No	No
12	35/F	Parotid	27×15×10	Incomplete	PN+	++	No
13	15/M	Submandibular	18	Invasive	PN+	++	+
14	44/M	Submandibular	15	Incomplete	PN+	++	+
15	29/M	Parotid	23	Invasive	PN+LVI+	+	++
16	74/M	Parotid	30×30×25	Invasive	PN+	+	No
17	31/M	Submandibular	30	Invasive	PN+	++	++
18	73/M	Retromolar gingiva	15×20×25	Invasive	No	+	No
19	35/M	Submandibular	25	Invasive	No	+	No
20	77/F	Submandibular	25	Invasive	No	++	++
21	62/F	Lip	10	Complete	PN+	+	+
22	25/M	Parotid	13	Incomplete	No	+	No
23	62/M	Parotid	23×20×20	Incomplete	No	+	No
24	52/M	Submandibular	20	Invasive	No	+	No
25	48/F	Parotid	10	Incomplete	PN+	++	+

*PE—subtotal conservative parotidectomy.
†Close margins means distance from tumor < 0,5 mm.
CHT indicates chemotherapy; LN, lymph node; LVI, lymphovascular invasion; NA, not available; NED, no evidence of disease; PN, perineural invasion; RD, residual disease; RT, radiotherapy; SP, superficial parotidectomy.

identify any possible *ETV6* fusion partner. The remainder of our cases fell either firstly into a group with a different exon junction to that tested, or secondly into a group with expression below the detection limit of the methods used, or thirdly into a group with low quality of RNA.

The novel finding in our study is the identification of 5 MASC cases with atypical junctions, exon 4 of *ETV6* with exon 14 of *NTRK3* and exon 5 of *ETV6* with exon 14 of *NTRK3* that have not been described in MASC so far. Moreover, we confirmed the observation of Ito et al[16] that a subset of MASC cases very likely harbors *ETV6* fused with non-*NTRK* genes (*ETV6-X* fusion).

What was a particularly interesting finding of our study is that in both these groups of MASC with atypical junctions and *ETV6-X* fusion, we observed a more aggressive invasive growth pattern in 6/9 (67%) together with more frequent perineural invasion in 5/9 (55%), and lymphovascular invasion in 2/9 (22%) than in the cases with classical *ETV6-NTRK3* fusion. In addition, lymph node metastases were seen in 2 patients, and 1 patient even died of disseminated disease with multiple distant metastases. This is in accordance with recent observation of Ito et al,[16] who published 2 cases of *ETV6-X* fusion MASC with invasive histologic features including perineural or vascular involvement—this is in contrast with the generally low-grade behavior of MASC. Nevertheless, in our series, even MASC cases with the classical *ETV6-NTRK3* fusion often displayed an invasive growth pattern (12/16) as well as perineural invasion (6/16) but lymphovascular invasion was not seen.

Ito et al[16] have also suggested that MASC cases with *ETV6-X* fusion may have distinctive histomorphology, in particular, thick fibrous septa and abundant hyalinized stroma. We have found extensive hyalinized stromal fibrosis in 4/16 cases of MASC with classical *ETV6-NTRK3* fusion transcript, remaining 12 cases were devoid of extensive central fibrosclerotic foci. Thick fibrous septa were observed in most cases of MASC with classical fusion (11/16). The MASC cases with atypical exon junctions *ETV6-NRTK3* and *ETV6-X* fusions displayed more often central hyalinized fibrosis in 6/9 (66%) and thick fibrous septa in 7/9 (77%) than MASC with classical *ETV6-NTRK3* fusion.

In conclusion, the present study indicates that *ETV6* may fuse with genes other than *NTRK3*, or a subset of MASC cases may display atypical exon junctions *ETV6-NTRK3*. Our preliminary results also suggest that these atypical molecular features may be associated with more infiltrative histologic features of MASC, and less favorable clinical outcomes in patients, though the

TABLE 6. (*Continued*)

Surgical Margins	TNM	Metastasis (y, mo)	Local Recurrence (y, mo)	Treatment	Follow-up (y,mo)	Outcome
Clear	T1N0M0	No	No	Excision	11 mo	NED
Positive	T1N1M0	LN 2 y	Multiple 2 y	Excision	2 y, 4 mo	RD
Positive	pT2/cN0/cM0		rpT3 (19 y)	Excision, RT	19 y	NED
Positive	T1N0M0	No	rpT2 (2 mo)	Excision, re-excision margins clear	9 mo	NED
Positive	T3N0M0	No	No	*PE, RT	11 mo	NED
Positive	NA	NA	NA	NA	NA	NA
Clear	T1N0M0	No	No	Excision, SP	1 y, 6 mo	NED
Clear	T2N0M0	No (0/0)	No	Excision	12 y	NED
Positive	T4aN2bM1	LN 4 mo lung, liver, bones 10 mo	4 mo excision	Excision, RT	1 y, 8 mo	DOD
Close†	T2N0M0	No	No	SP	3 y, 1 mo	NED
Clear	T1N0M0	No	No	Excision	2 y	NED
Clear	pT2NxMx	No	No	Excision	4 y	NED
Close†	T3N2bM0	LN +	No	Excision, RT	4 y	NED
Positive	T1N0M0	No	No	Resection	4 y, 11 mo	NED
Positive	T2N1M0	LN+	No	Local excision, RT no neck dissection	2 y, 10 mo	NED
Positive	T2N0M0	No	No	Excision RT, CHT	8 y	NED
Positive	pT3pN0M0	No	Residual tumor	Excision, radical resection (1 mo)	2 y	NED
Positive	T2N2M0	LN+	NA	NA	NA	NA
Clear	T2N2M0	LN+ (3/36)	No	Excision, RT	4 y, 2 mo	NED
Clear	T2N0M0	No	No	Excision	1 y, 6 mo	NED
Clear	T1N0M0	No	No	Wide local excision	3 y	NED
Clear	T1N0M0	No	No	Excision	1 y, 3 mo	NED
Close†	T3N1M0	No (0/2)	No	Excision	7 y, 6 mo	NED
	T1N0M0	NA	NA	Excision	NA	NA
Close†	pT1N0M0	No	No	Excision	1 y, 3 mo	NED

numbers of published cases are low so far. Currently, molecular confirmation is considered the gold standard for the diagnosis of MASC, but there is growing body of evidence that the majority of tumors (up to 95%) can be accurately classified as MASC based solely on morphology and immunohistochemistry.[28] Recognizing MASC and testing for *ETV6* rearrangement may be, however, of potential value in patient treatment, because the presence of the *ETV6-NTRK3* translocation may represent a therapeutic target in MASC. Recent studies suggested that the inhibition of *ETV6-NTRK3* activation could serve as a therapeutic target for the treatment of patients with this fusion at other sites.[29,30]

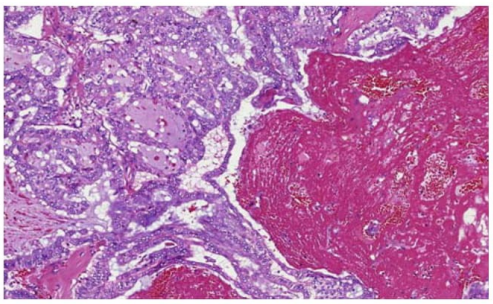

FIGURE 3. MASC (case 20, *ETV6-X* fusion) was composed of predominantly papillary and macrocystic structures.

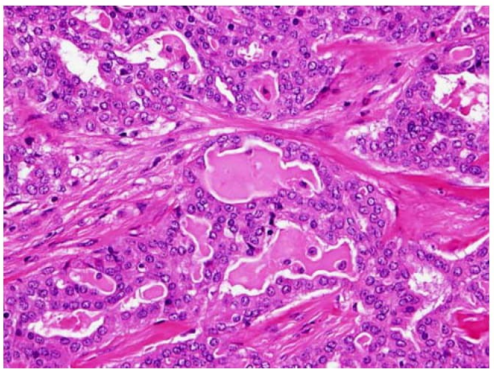

FIGURE 4. MASC composed of multilobular structure divided by thick hyalinized fibrous septa with microcystic and slightly dilated glandular spaces filled with variable amount of eosinophilic homogenous secretory material.

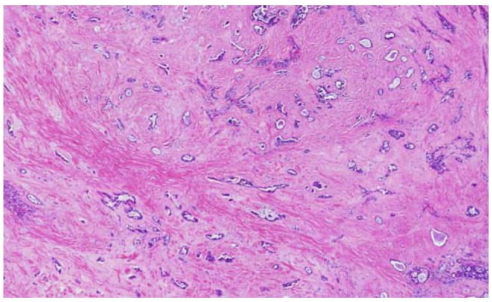

FIGURE 5. MASC (case 15, *ETV6-X* fusion) shows a prominent fibrosclerotic stroma with isolated tumor cells in small islands or trabeculae.

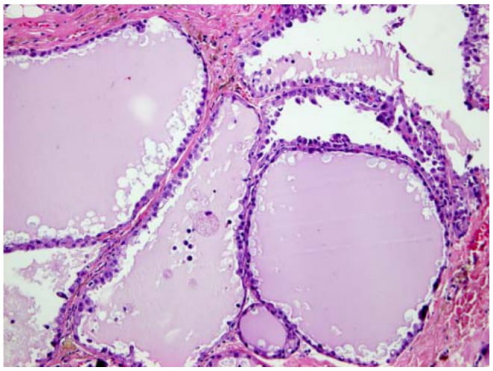

FIGURE 6. MASC with macrocystic growth pattern, in which larger cystic structures were lined mostly by a single, and focally a double layer of cells with prominent or focal apocrine differentiation including hobnail cells.

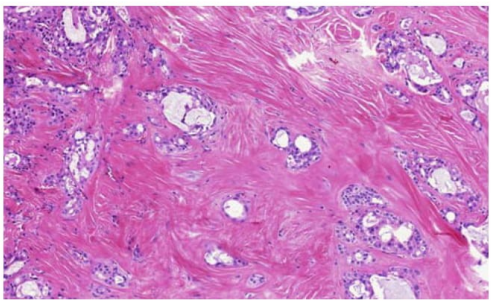

FIGURE 7. Thick fibrous septa with prominent hyalinization and trabeculae of neoplastic cells embedded in a completely hyalinized central part of the tumor were typical for *ETV6-X* fusion (case 17).

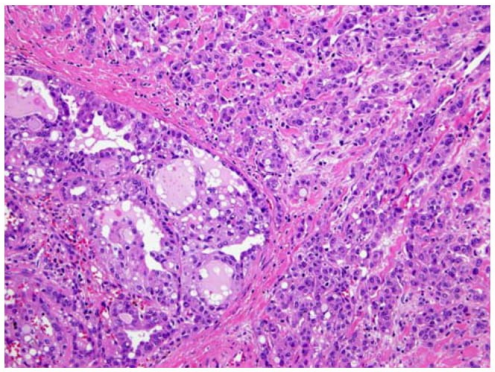

FIGURE 8. MASC with high-grade transformation was seen in 1 patient (case 9, atypical *ETV6/NTRK3* fusion). The tumor was composed of 2 distinct carcinomatous components.

ACKNOWLEDGMENTS

The authors thank the following physicians who contributed cases and kindly provided follow-up information where possible: Dr Takashi Saku, Niigata, Japan; Dr K. Sisson, Norfolk, UK; Dr Domingez-Malagon, Mexico City, Mexico; Prof. Dr Nina Gale, Ljubljana, Slovenia; Dr Svetlana Tafjord, Oslo, Norway; Dr Fred Petersson, Singapore; Dr AW Barrett, West Sussex, UK; Dr Llucia Alós, Barcelona, Spain; Dr Bruce Lyons, Plymouth, UK; Dr Susan Burroughs, Salisbury, UK; Dr Ioannis Venizelos, Thessaloniki, Greece; Dr Ann Sandison, Imperial College, London, UK; Dr Robert Jenkins, Truro, UK; Drs Vilo Gál and Boris Rychlý, Bratislava, Slovakia; and Drs Radim Žalud, Kolín, Jiří Kudela, Krnov, Petr Buzrla, Ostrava; Dana Cempírková, Jindřichův Hradec, Věra Fischerová, České Budějovice, all in Czech Republic.

REFERENCES

1. Skalova A, Vanecek T, Sima R, et al. Mammary analogue secretory carcinoma of salivary glands, containing the *ETV6-NTRK3* fusion gene: a hitherto undescribed salivary gland tumor entity. *Am J Surg Pathol*. 2010;34:599–608.
2. Tognon C, Knezevich SR, Huntsman D, et al. Expression of the *ETV6-NTRK3* gene fusion as a primary event in human secretory breast carcinoma. *Cancer Cell*. 2002;2:367–376.
3. Griffith C, Seethala R, Chiosea SI. Mammary analogue secretory carcinoma: a new twist to the diagnostic dilemma of zymogen granule poor acinic cell carcinoma. *Virchows Arch*. 2011;459:117–118.
4. Connor A, Perez-Ordoñez B, Shago M, et al. Mammary analog secretory carcinoma of salivary gland origin with the *ETV6* gene rearrangement by FISH: expanded morphologic and immunohistochemical spectrum of a recently described entity. *Am J Surg Pathol*. 2012;36:27–34.
5. Chiosea SI, Griffith C, Assad A, et al. The profile of acinic cell carcinoma after recognition of mammary analog secretory carcinoma. *Am J Surg Pathol*. 2012;36:343–350.
6. Chiosea SI, Griffith C, Assad A, et al. Clinicopathological characterization of mammary analogue carcinoma of salivary glands. *Histopathology*. 2012;61:387–394.
7. Laco J, Švajdler M Jr, Andrejs J, et al. Mammary analogue secretory carcinoma of salivary glands: a report of 2 cases with

expression of basal/myoepithelial markers (calponin, CD10 and p63 protein). *Pathol Res Pract*. 2013;209:167–172.
8. Bishop JA, Yonescu R, Batista D, et al. Utility of mammaglobin immunohistochemistry as a proxy marker for the ETV6-NTRK3 translocation in the diagnosis of salivary mammary analogue secretory carcinoma. *Hum Pathol*. 2013;44:1982–1988.
9. Bishop JA. Unmasking MASC: bringing to light the unique morphologic, immunohistochemical and genetic features of the newly recognized mammary analogue secretory carcinoma of salivary glands. *Head Neck Pathol*. 2013;7:35–39.
10. Patel KR, Solomon IH, El-Mofty SK, et al. Mammaglobin and S-100 immunoreactivity in salivary carcinomas other than mammary analogue secretory carcinoma. *Hum Pathol*. 2013;44:2501–2508.
11. Majewska H, Skálová A, Stodulski D, et al. Mammary analogue secretory carcinoma of salivary glands: first retrospective study of a new entity in Poland with special reference to *ETV6* gene rearrangement. *Virchows Arch*. 2015;466:245–254.
12. Urano M, Nagao T, Miyabe S, et al. Characterization of mammary analogue secretory carcinoma of salivary gland: discrimination from its mimics by the presence of the *ETV6-NTRK3* translocation and novel surrogate marker. *Hum Pathol*. 2015;46:94–103.
13. Bishop JA. Mammary analog secretory carcinoma of salivary glands: review of new entity with emphasis on differential diagnosis. *Pathol Case Rev*. 2015;20:7–12.
14. Bishop JA, Yonescu R, Batista D, et al. Most nonparotid "acinic cell carcinomas" represent mammary analog secretory carcinomas. *Am J Surg Pathol*. 2013;37:1053–1057.
15. Luo W, Lindley SW, Lindley PH, et al. Mammary analog secretory carcinoma of salivary gland with high-grade histology arising in palate, report of a case and review of literature. *Int J Clin Exp Pathol*. 2014;7:9008–9022.
16. Ito Y, Ishibashi K, Masaki A, et al. Mammary analogue secretory carcinoma of salivary glands: a clinicopathological and molecular study including 2 cases harboring *ETV6-X* fusion. *Am J Surg Pathol*. 2015;39:602–610.
17. Viswanatha DS, Foucar K, Berry BR, et al. Blastic mantle cell leukemia: an unusual presentation of blastic mantle cell lymphoma. *Mod Pathol*. 2000;13:825–833.
18. Gaffney R, Chakerian A, O'Connell JX, et al. Novel fluorescent ligase detection reaction and flow cytometric analysis of SYT-SSX fusions in synovial sarcoma. *J Mol Diagn*. 2003;5:127–135.
19. Antonescu CR, Kawai A, Leung DH, et al. Strong association of SYT-SSX fusion type and morphologic epithelial differentiation in synovial sarcoma. *Diagn Mol Pathol*. 2000;9:1–8.
20. Bourgeois JM, Knezevich SR, Mathers JA, et al. Molecular detection of the ETV6-NTRK3 gene fusion differentiates congenital fibrosarcoma from other childhood spindle cell tumors. *Am J Surg Pathol*. 2000;24:937–946.
21. Knezevich SR, McFadden DE, Tao W, et al. A novel ETV6-NTRK3 gene fusion in congenital fibrosarcoma. *Nat Genet*. 1998;18:184–187.
22. Rubin BP, Chen CJ, Morgan TW, et al. Congenital mesoblastic nephroma t(12;15) is associated with ETV6-NTRK3 gene fusion: cytogenetic and molecular relationship to congenital (infantile) fibrosarcoma. *Am J Pathol*. 1998;153:1451–1458.
23. Kralik JM, Kranewitter W, Boesmueller H, et al. Characterization of a newly identified ETV6 NTRK3 fusion transcript in acute myeloid leukemia. *Diagn Pathol*. 2011;6:19.
24. Alassiri A, Lum A, Goytain A, et al. *ETV6-NTRK3* is expressed in a subset of ALK-negative inflammatory myofibroblastic tumors: case series of 20 patients. *Mod Pathol*. 2015;28:36.
25. Leeman-Neill RJ, Kelly LM, Liu P, et al. *ETV6-NTRK3* is a common chromosomal rearrangement in radiation-associated thyroid cancer. *Cancer*. 2014;120:799–807.
26. Skálová A, Vanecek T, Majewska H, et al. Mammary analogue secretory carcinoma of salivary glands with high-grade transformation: report of 3 cases with the *ETV6-NTRK3* gene fusion and analysis of TP53, beta-catenin, EGFR, and CCND1 genes. *Am J Surg Pathol*. 2014;38:23–33.
27. De Braekeleer E, Douet-Guilbert N, Morel F, et al. ETV6 fusion genes in hematological malignancies: a review. *Leuk Res*. 2012; 36:945–961.
28. Shah AA, Wenig BM, LeGallo RD, et al. Morphology in conjunction with immunohistochemistry is sufficient for the diagnosis of mammary analogue secretory carcinoma. *Head Neck Pathol*. 2015;9:85–95.
29. Chi HT, Ly BT, Kano Y, et al. *ETV6-NTRK3* as a therapuetic target of small molecule inhibitor PKC412. *Biochem Biophys Res Commun*. 2012;429:87–92.
30. Tognon CE, Somasiri AM, Evdokimova VE, et al. *ETV6-NTRK3*-mediated breast epithelial cell transformation is blocked by targeting the IGF1R signaling pathway. *Cancer Res*. 2011;71:1060–1070.

1.10.3 MOLEKULÁRNÍ PROFILOVÁNÍ SEKREČNÍHO KARCINOMU MAMMÁRNÍHO TYPU ODHALILO SKUPINU NÁDORŮ DEFINOVANÝCH NOVOU *ETV6-RET* TRANSLOKACÍ

Metodické pokroky molekulární genetiky přinesly další diagnostický nástroj, a to metodu masivního paralelního sekvenování, tzv. next generation sequencing (NGS), jejíž použití umožnilo najít fúzního partnera SC s *ETV6-X* fúzí (34, 35). Metodou NGS byla otestovaná série nádorů obsahujících jednak 4 původní případy SC označené jako *ETV6-X* a jednak 26 případů SC s *ETV6* zlomem (detekovaným metodou FISH) či s morfologií a imunoprofilem odpovídajícími SC, které nebyly analyzovatelné metodou FISH pro nízkou kvalitu vstupního materiálu.

Tento postup odhalil v 10 případech novou a v SC doposud nepopsanou fúzi mezi exonem 6 genu *ETV6* a exonem 12 genu *RET*. Fúze byla potvrzena v 9 případech metodami RT-PCR či FISH a v 1 případě nebylo ke konfirmaci *ETV6-RET* fúze dostatečné množství materiálu.

Navazující klinické sledování bylo provedeno v 8 z 10 případů s potvrzenou *ETV6-RET* fúzí. Všechny tumory byly odstraněné chirurgickou excizí; 5 z nich bylo řešeno subtotální konzervativní parotidektomií a 4 případy prostou excizí, 1 případ byl bez informací o léčbě. Ve dvou případech následovala po chirurgické léčbě radioterapie. V jednom případě SC komplikovaného metastatickým rozsevem následovala po parciální parotidektomii konkomitantní chemoterapie s radioterapií.

Translokace *ETV6-RET* doposud nebyla popsána v žádném jiném nádoru slinných žláz než v SC.

Výstupem práce bylo popsání nové genové fúze *ETV6-RET* v 10 případech SC. Odlišení alternativní fúze s účastí *RET* onkogenu je důležité zejména u pacientů s pokročilým onemocněním, kde běžné terapeutické postupy selhávají. Obdobně jako tyrozinkinázový receptor C (TrkC lokus) *NTRK3* genu lze využít pro aplikaci tyrozinkinázových inhibitorů (43), tak i na pokročilé maligní onemocnění s *RET* fúzí lze cílit prostřednictvím RET-inhibitorů, jakými jsou například Blue 667 či LOXO 292 (45, 75, 76).

Molecular Profiling of Mammary Analog Secretory Carcinoma Revealed a Subset of Tumors Harboring a Novel *ETV6-RET* Translocation

Report of 10 Cases

Alena Skalova, MD, PhD,† Tomas Vanecek, PhD,‡ Petr Martinek, PhD,‡ Ilan Weinreb, MD,§ Todd M. Stevens, PhD,‖ Roderick H.W. Simpson, MD, MB, ChB, FRCPath,¶ Martin Hyrcza, MD, PhD,# Niels J. Rupp, MD,** Martina Baneckova, MD,*† Michael Michal, Jr, MD,*†† David Slouka, MD, MBA, PhD,‡‡ Tomas Svoboda, MD, PhD,§§ Alena Metelkova, MD, PhD,‖‖ Arghavan Etebarian, DDS, OMP,¶¶ Jaroslav Pavelka, PhD,‡## Steven J. Potts, PhD,*** Jason Christiansen, PhD,*** Petr Steiner, MSc,*‡ and Michal Michal, MD**

Abstract: *ETV6* gene abnormalities are well described in tumor pathology. Many fusion partners of *ETV6* have been reported in a variety of epithelial, mesenchymal, and hematological malignancies. In salivary gland tumor pathology, however, the *ETV6-NTRK3* translocation is specific for (mammary analog) secretory carcinoma, and has not been documented in any other salivary tumor type. The present study comprised a clinical, histologic, and molecular analysis of 10 cases of secretory carcinoma, with typical morphology and immunoprofile harboring a novel *ETV6-RET* translocation.

From the Departments of *Pathology; ‡‡Otorhinolaryngology; §§Oncology and Radiotherapy, Oncological Clinic; ‖‖Clinical Oncology, Oncological Clinic, Faculty of Medicine in Plzen; ††Biomedical Center, Faculty of Medicine in Pilsen, Charles University; †Bioptic Laboratory Ltd; ‡Bioptic Laboratory Ltd, Molecular Pathology Laboratory; ##Faculty of Education, University of West Bohemia, Plzen, Czech Republic; §Department of Pathology, University Health Network, Toronto, ON, Canada; ‖Department of Pathology, University of Alabama at Birmingham, Birmingham, AL; ¶Department of Anatomical Pathology, University of Calgary and Foothills Medical Centre, Calgary, AB; #Department of Pathology and Molecular Medicine, St. Joseph's Healthcare & Hamilton Health Sciences, McMaster University, Vancouver, BC, Canada; **Department of Pathology and Molecular Pathology, University Hospital Zurich, Zurich, Switzerland; ¶¶Department of Oral and Maxillofacial Pathology, School of Dentistry, Tehran University of Medical Sciences, Tehran, Iran; and ***Ignyta Inc. San Diego, California, United States.

Conflicts of Interest and Source of Funding: Supported in parts by the National Sustainability Program I (NPU I) Nr. LO1503 and by the grant SVV–2017 No. 260 391 provided by the Ministry of Education Youth and Sports of the Czech Republic. The NGS analysis was in part supported by Ignyta Inc., San Diego, CA. The authors have disclosed that they have no significant relationships with, or financial interest in, any commercial companies pertaining to this article.

Correspondence: Alena Skalova, MD, PhD, Sikl's Department of Pathology, Medical Faculty of Charles University, Faculty Hospital, E. Benese 13, Plzen 305 99, Czech Republic (e-mail: skalova@fnplzen.cz).

Key Words: salivary, mammary analog secretory carcinoma, MASC, *ETV6-NTRK3*, *ETV6-RET* fusion transcript

(*Am J Surg Pathol* 2018;42:234–246)

(Mammary analog) secretory carcinoma of salivary gland origin is a recently described tumor that harbors a characteristic balanced t(12;15)(p13;q25) chromosomal translocation resulting in an *ETV6-NTRK3* fusion[1] identical to that commonly found in secretory carcinoma (SC) of the breast.[2] The *ETV6-NTRK3* fusion gene encodes a chimeric tyrosine kinase with transforming activity in epithelial and myoepithelial cells in the mouse mammary gland.[3]

Over many years, Skalova et al[1] began to identify a distinctive, hitherto unrecognized neoplasm arising in the salivary glands characterized by morphologic and immunohistochemical features strongly reminiscent of those of SC of the breast. These salivary carcinomas are composed of microcystic and solid areas with abundant vacuolated colloid-like periodic acid-Schiff-positive secretory material within the microcystic spaces. These tumors had previously been categorized as either unusual variants of salivary acinic cell carcinoma (AciCC) or adenocarcinoma not otherwise specified.[1]

Salivary SC was initially recognized as an entity different from AciCC on the basis of 3 major findings.[1] First, SC showed no basophilia in the cytoplasm of any of the constituent cells, which is the hallmark of the serous acinar cells of AciCC resulting from the presence of cytoplasmic zymogen granules. Second, these neoplasms had a completely different immunohistochemical profile, almost always expressing S100 protein, mammaglobin, vimentin, STAT5, and MUC4, all of which are rarely expressed in AciCC. Finally, SCs were found to harbor an

TABLE 1. Antibodies Used for Immunohistochemical Study

Antibody Specificity	Clone	Dilution	Antigen Retrieval/Time (min)	Source
S100 protein	Polyclonal	RTU	CC1/20	Ventana
CK7	OV-TL 12/30	1:200	CC1/36	Dako Cytomation
GCDFP-15	EP1582y	RTU	CC1/64	Cell Marque
Mammaglobin	304-1A5	RTU	CC1/36	Dako Cytomation
STAT 5a	Polyclonal	1:400	CC1/36	Assay Designs Inc.
Ki-67	30-9	RTU	CC1/64	Ventana
P63	4A4	RTU	CC1/64	Ventana
DOG1	SP31	RTU	CC1/36	Cell Marque
GATA3	L50-823	1:200	CC1/52	BioCare Medical
SOX10	Polyclonal	1:100	CC1/64	Cell Marque

CC1 indicates EDTA buffer, pH 8.6; RTU, ready to use (prediluted).

ETV6-NTRK3 fusion gene due to a t(12; 15)(p13,q25) translocation, a finding identical to SC of the breast[2] and absent in AciCCs.[1] Because of the morphologic similarities and identical *ETV6-NTRK3* fusion transcripts, the designation "mammary analog secretory carcinoma of salivary gland" has been proposed,[1] and the name was widely accepted and used in the literature. The most recent version of the World Health Organization Classification of Head and Neck Tumors, however, utilizes the terminology "secretory carcinoma"[4] for consistency, and because SCs have been recently described at other extrasalivary and extramammary sites, such as thyroid gland,[5–8] skin,[9,10] and sinonasal mucosa.[11]

The presence of the *ETV6-NTRK3* fusion gene has not been demonstrated in any other salivary gland tumor, but the same translocation can be seen not only in SC of breast,[2] but also in infantile fibrosarcoma,[12] congenital mesoblastic nephroma,[13] certain hematopoietic malignancies,[14] ALK-negative inflammatory myofibroblastic tumors,[15] a small subset of gastrointestinal stromal tumors,[16] and in radiation-induced papillary thyroid carcinomas.[17] Moreover, *ETV6-NTRK3* translocated papillary thyroid cancers have been recently described in adult patients with no history of radiation exposure.[18]

The near 100% rate of *ETV6* gene rearrangement in SC has been subsequently confirmed by many other studies.[19–25] Detection of *ETV6* rearrangements by fluorescent in situ hybridization (FISH) or the *ETV6-NTRK3* fusion by reverse-transcriptase polymerase chain reaction (RT-PCR) in formalin-fixed paraffin-embedded (FFPE) material is technically relatively straightforward and > 300 cases of SC have been published since its original description.

Up until now, in all published cases of SC where the fusion partner is identified, *ETV6* is fused with *NTRK3*, and no other fusion partners have been reported so far. Nevertheless, for several years, we have been aware of several SC cases positive for the *ETV6* gene split as visualized by FISH, but in which the classic *ETV6-NTRK3* fusion transcript (exon 5-exon 15 junction) was not detected by standard RT-PCR. A subset of SCs showing *ETV6* rearrangements with so far unknown partners have been recently reported and provisionally called *ETV6-X* translocated SCs,[26] in agreement with a study of Ito et al,[27] who found 2 such cases. In the present study using the next-generation sequencing (NGS) as a diagnostic platform, we describe 10 cases morphologically and immunohistochemically typical of SC, harboring a novel *ETV6-RET* translocation.

MATERIALS AND METHODS

Among > 4500 cases of primary salivary gland tumors, 194 cases of SCs were retrieved from the consultation files of the Salivary Gland Tumor Registry, at

TABLE 2. Primers for Detection of *ETV6-NTRK3* Fusion Transcripts

Original Primer Name	Sequence	Annealing Temperature (°C)	Localization
ETV6-ex4-F3	AGCCGGAGGTCATACTGCAT	55	ETV6 exon 4 inner
ETV6-ex4-F4	CATTCTTCCACCCTGGAAAC	55	ETV6 exon 4 outer
ETV6B†	ACATCATGGTCTCTGTCTCCCCGC	55	ETV6 exon 5 inner
TEL971* (ETV6A†)	ACCACATCATGGTCTCTGTCTCCC	65	ETV6 exon 5 outer
NTRK3-ex14-R1	GTGATGCCGTGGTTGATGT	55	NTRK3 exon 14 inner
NTRK3 ex14-R2	AGTCATGCCAATGACCACAG	55	NTRK3 exon 14 outer
NTRK3B†	TTCTCGCTTCAGCACGATGTCT	55	NTRK3 exon 15 inner
TRKC1059* (NTRK3A†)	CAGTTCTCGCTTCAGCACGATG	65	NTRK3 exon 15 outer
ETV6-Archer1-F1	CGATGGGAGGACAAAGAATC	55	ETV6 exon 6
RET-Archer1-R1	AACCAAGTTCTTCCGAGGGA	55	RET exon 12
ETV6-Archer1-F2	CAACGGACTGGCTCGACTG	55	ETV6 exon 6
RET-Archer1-R2	GACCACTTTTCCAAATTCGCCT	55	RET exon 12

*Bourgeois et al[32]
†Ito et al,[27] Skalova et al[26].

FIGURE 1. A, The result of analysis by NGS with custom-designed ArcherDX Kit of case 3 (case 17 in Skalova et al[26]). Analysis revealed the presence of fusion transcript *ETV6-RET* joining exons 6 and 12, respectively. The red arrows represent position of primers. B, The confirmation of the presence of *ETV6-RET* fusion transcript by RT-PCR followed by Sanger sequencing. The black arrow indicates area of fusion.

the Department of Pathology, Faculty of Medicine in Plzen, and Biopticka Laborator Ltd, Plzen, Czech Republic (A.S. and M.M.).

The histopathologic features of all tumors and the immunohistochemical stains, when available, were reviewed by 2 pathologists (A.S. and M.B.). A diagnosis of SC was confirmed in cases that displayed, at least focally, histologic features consistent with original description[1] in conjunction with the appropriate immunohistochemical profile, that is, coexpression of S100 protein, cytokeratin CK7, and mammaglobin with the absence of p63 and DOG1 staining. For the purpose of this particular study, we have included 4 cases of SC with *ETV6-X* profile from study Skalova et al[26] and 26 cases of SC with *ETV6* gene break found by FISH or with morphologic and immunohistochemical pattern of SC but without analyzable *ETV6* gene break by FISH due to low quality or lack of material. Thus, a total of 30 SC cases were studied by NGS using ArcherDX Fusion Plex Kit.

For conventional microscopy, the excised tissues were fixed in formalin, routinely processed, embedded in paraffin (FFPE), cut, and stained with hematoxylin and eosin. In most cases, additional stains were also performed, including periodic acid-Schiff with and without diastase, mucicarmine, and alcian blue at pH 2.5.

For immunohistochemical studies, 4 µm thick sections were cut from paraffin blocks and mounted on positively charged slides (TOMO, Matsunami Glass Ind., Japan). Sections were processed on a BenchMark ULTRA (Ventana Medical System, Tucson, AZ), deparaffinized, and then subjected to heat-induced epitope retrieval by immersion in a CC1 solution at pH 8.6 at 95°C. After antigen retrieval, sections were stained with a pan-RTK antibody cocktail consisting of rabbit monoclonal antibodies, all obtained from Cell Signaling (Danvers, MA), targeting pan-Trk (A7H6R, active against TrkA, TrkB, and TrkC, 1:50 dilution), ROS1 (D4D6, 1:50), and ALK (D5F3, 1:50), as described previously.[28]

All other primary antibodies used are summarized in Table 1. The bound antibodies were visualized using the ultraView Universal DAB Detection Kit (Roche) and ultraView Universal Alkaline Phosphatase Red Detection Kit (Roche). The slides were counterstained with the Mayer hematoxylin. Appropriate positive and negative controls were used.

Clinical follow-up was obtained from the patients, their physicians, or from referring pathologists.

Molecular Genetic Study

Detection of ETV6-NTRK3 and ETV6-RET Fusion Transcripts by RT-PCR

RNA was extracted using the RecoverAll Total Nucleic Acid Isolation Kit (Ambion, Austin, TX). cDNA was synthesized using the Transcriptor First Strand cDNA Synthesis Kit (RNA input 500 ng; Roche Diagnostics, Mannheim, Germany). All procedures were performed according to the manufacturer's protocols. Amplification of a 105 and 133 bp product of the µ2-microglobulin gene and 247 bp product of the *PGK* gene was used to test the quality of the extracted RNA as previously described.[29–31] A detection of classic exon 5 of *ETV6* gene and exon 15 of *NTRK3* gene,[32] as well as atypical exon 4 of the *ETV6* gene and exon 14 of the *NTRK3* gene (and their combinatorial variants) fusion transcript was performed by RT-PCR. In addition, more sensitive, nested RT-PCR was performed for the detection of classic[26,27] as well as selected atypical junction of transcripts. Except that,

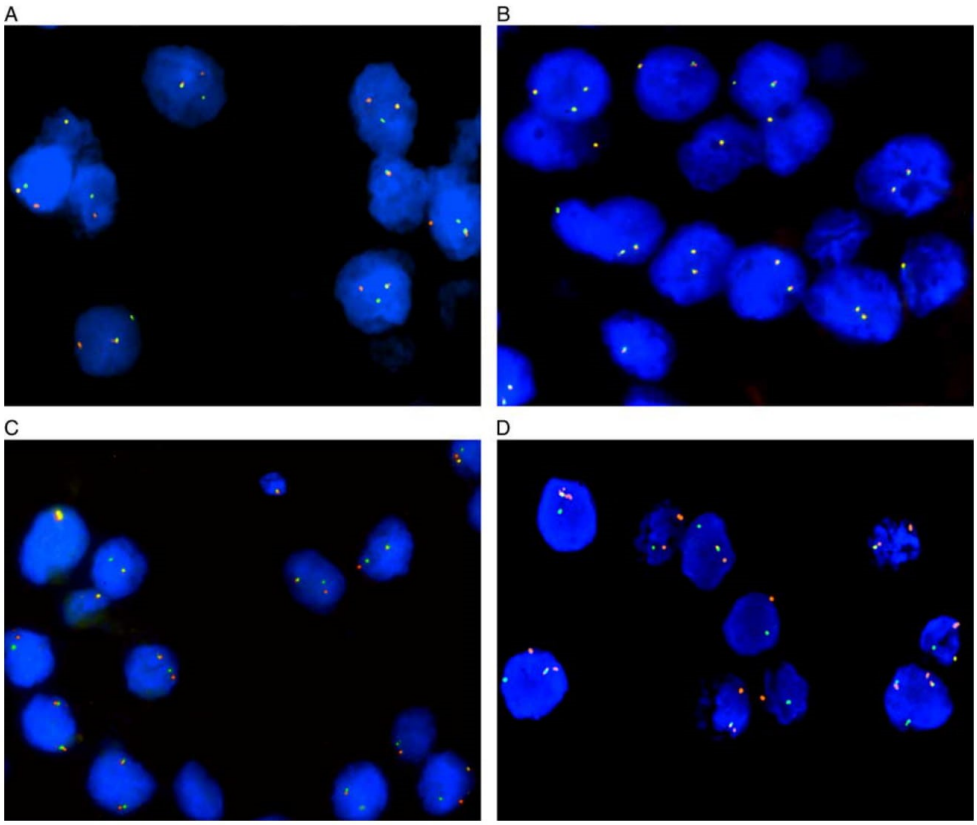

FIGURE 2. Interphase FISH analysis using break-apart probes (A–C) and dual-fusion probe (D). Positive cells with break-apart *ETV6* (A) and *RET* (C) probes contain nucleus with separate (split) orange and (or) green signals indicating a rearrangement (break) of 1 copy of the gene region and also 1 orange/green (yellow) fusion signal representing 1 normal (intact) copy of homolog locus. Negative cells with break-apart *NTRK3* (B) probe contain only normal (not split) yellow signal. Positive cells using fusion probe *ETV6-RET* (D) show orange/green (yellow) fusion signals representing translocation *ETV6-RET* and also separate orange and green signals showing the intact genes.

RT-PCR for *ETV6-RET* fusion transcript detection was also carried out after receiving of the NGS results.

For single-round PCR, 2 L of cDNA was added to reaction consisting of 12.5 μL of HotStar Taq PCR Master Mix (QIAgen, Hilden, Germany), 10 pmol of each primer (Table 2), and distilled water up to 25 μL. The amplification program comprised denaturation at 95°C for 14 minutes and then 45 cycles of denaturation at 95°C for 1 minute, annealing at temperature seen in Table 2 for 1 minute and extension at 72°C for 1 minute. The program was finished by incubation at 72°C for 7 minutes. For nested PCR, the same reaction conditions were utilized. One microliter of PCR product from the first round was used as a template.

Successfully amplified PCR products were purified with magnetic particles of Agencourt AMPure (Agencourt Bioscience Corporation, A Beckman Coulter Company, Beverly, MA). Products were then bidirectionally sequenced using Big Dye Terminator Sequencing Kit (Applied Biosystems, Foster City, CA), and purified with magnetic particles of Agencourt CleanSEQ (Agencourt Bioscience Corporation), all according to the manufacturer's protocol, and run on an automated sequencer ABI Prism 3130xl (Applied Biosystems) at a constant voltage of 13.2 kV for 11 minutes.

Detection of Alteration of ETV6, NTRK3, and RET Genes by FISH Method

Four-micrometer-thick FFPE sections were placed onto positively charged slides. Hematoxylin and eosin–stained slides were examined for determination of areas for cell counting.

TABLE 3. Molecular Genetics Findings in 10 Cases of SC With *ETV6-RET* Fusion

Case #	Case #	NGS Results	Fusion	FISH ETV6ba	FISH NTRK3ba	RT-PCR ETV6-NTRK3	FISH RETba	FISH ETV6-RET	RT-PCR ETV6-RET
1	6*	+	*ETV6-RET*	+	−	−	+	+	+
2	15*	+	*ETV6-RET*	+	−	−	+	ND	+
3	17*	+	*ETV6-RET*	+	−	−	+	+	+
4	20*	+	*ETV6-RET*	+	−	−	+	+	−
5		+	*ETV6-RET*	+	−	−	+	+	+
6		+	*ETV6-RET*	ND	ND	−	ND	+	+
7		+	*ETV6-RET*	+	−	−	+	+	+
8		+	*ETV6-RET*	NA	NA	−	NA	+	+
9		+	*ETV6-RET*	ND	ND	−	ND	ND	−
10	12†	+	*ETV6-RET*	+	−	−	+	+	+

*Skalova et al[26] (Table 6).
†Stevens et al[8] (Table 2).
NA indicates not analyzable; ND, not done due to lack of material.

The unstained slides were routinely deparaffinized and incubated in the ×1 Target Retrieval Solution Citrate pH 6 (Dako, Glostrup, Denmark) at 95°C for 40 minutes and subsequently cooled for 20 minutes at room temperature in the same solution. Slides were washed in deionized water for 5 minutes and digested in protease solution with Pepsin (0.5 mg/mL; Sigma Aldrich, St Louis, MO) in 0.01 M HCl at 37°C for 25 to 60 minutes, according to the sample conditions. Slides were then placed into deionized water for 5 minutes, dehydrated in a series of ethanol solutions (70%, 85%, 96% for 2 min each), and air dried.

Two commercial probes were used for the detection of rearrangement of *ETV6* and *RET* genes, Vysis ETV6 Break Apart FISH Probe Kit (Vysis/Abbott Molecular, IL) and ZytoLight SPEC RET Dual Color Break Apart Probe (ZytoVision GmbH, Bremerhaven, Germany). ETV6 probe was mixed with water and LSI/WCP (Locus-Specific Identifier/Whole Chromosome Painting) Hybridization buffer (Vysis/Abbott Molecular) in a 1:2:7 ratio, respectively. RET probe was factory premixed.

Probes for detection of rearrangement of *NTRK3* gene region and *ETV6-RET* genes fusion were mixed from custom designed SureFISH probes (Agilent Technologies Inc., Santa Clara, CA). Chromosomal regions for *NTRK3* break-apart probe oligos are chr15:87501469-88501628 and chr15:88701444-89700343; for *ETV6-RET* fusion probe, chr12:11675872-12175711 and chr10:43354893-43849282. Probe mixture was prepared from corresponding probes (each color was delivered in a separate well), deionized water, and LSI Buffer (Vysis/Abbott Molecular) in a 1:1:1:7 ratio, respectively.

An appropriate amount of mixed and premixed probes was applied on specimens, covered with a glass coverslip, and sealed with rubber cement. Slides were incubated in the ThermoBrite instrument (StatSpin/Iris Sample Processing, Westwood, MA) with codenaturation at 85°C for minutes and hybridization at 37°C for hours. Rubber cemented coverslip was then removed and the slide was placed in posthybridization wash solution (2×SSC/0.3% NP-40) at 72°C for 2 minutes. The slide was air dried in the dark, counterstained with 4′,6′-diamidino-2-phenylindole DAPI (Vysis/Abbott Molecular), coverslipped, and immediately examined.

FISH Interpretation

The sections were examined with an Olympus BX51 fluorescence microscope (Olympus Corporation, Tokyo, Japan) using a ×100 objective and filter sets Triple Band Pass (DAPI/SpectrumGreen/SpectrumOrange), Dual Band Pass (SpectrumGreen/SpectrumOrange), and Single Band Pass (SpectrumGreen or SpectrumOrange).

TABLE 4. Details of NGS Analysis by the Archer Platform in 10 Cases of SC With *ETV6-RET* Translocation

Case #	Case #	NGS Results	Fusion	Exons Included in Fusion	No. Valid Fusion Read	% of Reads Supporting Fusion	No. Unique Start Sites
1	Case 6*	+	ETV6-RET	6-12	51	100	17
2	Case 15*	+	ETV6-RET	6-12	84	20.1	33
3	Case 17*	+	ETV6-RET	6-12	1126	23.5	183
4	Case 20*	+	ETV6-RET	6-12	15	1.8	10
5		+	ETV6-RET	6-12	163	11.4	63
6		+	ETV6-RET	6-12	21	100	11
7		+	ETV6-RET	6-12	49	14	32
8		+	ETV6-RET	6-12	100	86.2	51
9		+	ETV6-RET	6-12	41	60.3	14
10	Case 12†	+	ETV6-RET	6-12	24	14.8	17

*Skalova et al[26] (Table 6).
†Stevens et al[8] (Table 2).

TABLE 5. Clinical Findings in 10 SCs With *ETV6-RET* Fusion Transcript

Case #	Age/ Sex	Case #	Stadium TNM	Local Recurrence	Length of Symptoms	Metastasis (y, mo)	Treatment	Follow-up	Outcome
1	50/M	Case 6*	NA	NA		NA	NA	NA	NA
2	29/M	Case 15*	pT2pN1M0	No	6 y	LN+	SP and RT, no neck dissection	4 y 6 mo	Alive NED
3	31/M	Case 17*	pT3pN0M0	Residual tumor	7 y	No	Excision radical resection (1 mo)	4 y	Alive NED
4	77/F	Case 20*	pT2N0M0	No	1 y	No	Excision, RT	3 y	DOC
5	51/M		pT3N0M0	Residual tumor	15 mo	No	Excision SP after 3 mo	8 mo	Alive NED
6	20/F		pT3N0M0	No	NA	No	PE	NA	NA
7	55/M		pT3N0M3	No	3 y	Multiple bone meta (pelvic, scapula) at 15 mo	PP, RT, and CHT	2 y	DOD
8	28/F		pT1N0M0	No	1 mo	No	Parotid resection and lymphadenectomy level II: 12 lymph nodes negative	2 y	Alive NED
9	33/M		pT1pN0 (0/2)	No	6 mo	No	PP	3 y 9 mo	Alive NED
10	34/M	Case 12†	pT2N0M0 (0/1)	No	Several months, very slow enlargement	No	SP	4 y 2 mo	Alive NED

*Skalova et al[26] (Table 6).
†Stevens et al[8] (Table 2).
CHT indicates chemotherapy; DOC, dead of other causes; DOD, dead of disease; LN, lymph nodes; NA, not available; NED, no evidence of disease; PE, parotidectomy; PP, partial parotidectomy; RT, radiotherapy; SP, superficial parotidectomy.

For each probe, 100 randomly selected nonoverlapping tumor cell nuclei were examined for the presence of yellow or green and orange fluorescent signals. Regarding break-apart probes, yellow signals were considered negative, and separate orange and green signals were considered positive; conversely, for fusion probe, yellow signals were considered positive, and separate orange and green signals were considered negative.

Cutoff values were set to >10% and 20% of nuclei (break-apart and fusion probes, respectively) with chromosomal breakpoint signals (mean, +3 SD rounded up in normal non-neoplastic control tissues).

Sample Preparation for NGS

For NGS studies, 2 to 3 FFPE sections (10 μm thick) were macrodissected to isolate tumor-rich regions. Samples were extracted for total nucleic acid using Agencourt FormaPure Kit (Beckman Coulter, Brea, CA) following the corresponding protocol with an overnight digest and an additional 80°C incubation as described in modification of the protocol by ArcherDX (ArcherDX Inc., Boulder, CO). Total nucleic acid was quantified using the Qubit Broad Range RNA Assay Kit (Thermo Fisher Scientific) and 2 μL of sample.

RNA Integrity Assessment and Library Preparation for NGS

Unless otherwise indicated, 250 ng of FFPE RNA was used as input for NGS studies. To assess RNA quality, the PreSeq RNA QC Assay using iTaq Universal SYBR Green Supermix (Biorad, Hercules, CA) was performed on all samples during library preparation to generate a measure of the integrity of RNA (in the form of a cycle threshold value). Library preparation and RNA QC were performed following the Archer Fusion Plex Protocol for Illumina (ArcherDX Inc.). A custom primer set with 28 primers spanning regions on 3 specific genes of interest, including all 8 exons of *ETV6* gene in 3′ direction, was designed and used. Final libraries were diluted 1:100,000 and quantified in a 10 μL reaction following the Library Quantification for Illumina Libraries protocol and assuming a 200 bp fragment length (KAPA, Wilmington, MA). The concentration of final libraries was around 200 nM. The threshold representing the minimum molar concentration for which sequencing can be robustly performed was set at 50 nM.

NGS and Analysis

Libraries were sequenced on a MiSeq sequencer (Illumina, San Diego, CA). They were diluted to 4 nM and equal amounts of up to 16 libraries were pooled per run. The optimal number of raw reads per sample was set to 500,000. Library pools were diluted to 16 pM library stock with 5% 12.5 pM PhiX and loaded into the MiSeq cartridge. Analysis of sequencing results was performed using the Archer Analysis software (v5; ArcherDX Inc.). Fusion parameters were set to a minimum of 5 valid fusion reads with a minimum of 3 unique start sites within the valid fusion reads.

RESULTS

Molecular Genetic Findings

Selected 30 cases of SC (as described earlier) were analyzed by NGS using the ArcherDX analysis platform.

TABLE 6. Clinical and Histologic Findings in 10 SCs With *ETV6-RET* Fusion Transcript

Case #	Age/ Sex	Case #	Location	Tumor Size (mm)	Capsule	Surgical Margins	Thick Fibrous Septa	Hyalinized Sclerosis	Invasion (LVI, PN)	Cystic Pattern	Necrosis	Comments
1	50/M	Case 6*	Lip	15	NA	2	No	No	NA	No	−	Fragmented tissue
2	29/M	Case 15*	Parotid	23	No	1	+	++	PN+, LVI +Extraglandular, muscle invasion	No	−	Hyalinized, multilobular, microcystic, and solid growth pattern
3	31/M	Case 17*	Submand	30	No	2	++	++	PN+	No	−	Hyalinized, multilobular, microcystic
4	77/F	Case 20*	Submand	70	Focal		+	+	No	+	−	Multicystic, papillary with apocrine cells
5	51/M		Parotid	10	No	1	++	++	PN+	No	+	Central hyalinized sclerosis, invasive growth pattern
6	20/F		Parotid	40	No	2	+	+	Extraglandular	No	−	Lobular, microcystic
7	55/M		Parotid	70	No	2	+	+	PN+, perivascular	+	+	High grade component
8	28/F		Parotid	12	No	1	+	+	Intraglandular	No	−	Predominantly solid and microcystic
9	33/M		Parotid	17	+	1	No	No	No	+	−	Predominantly cystic
10	34/M	Case 12†	Parotid	19	+	0	No	No	No	+	−	Multicystic with mural nodules

*Skalova et al[26] (Table 6).
†Stevens et al[8] (Table 2).
Surgical margins: free-0; close (means distance from the tumor <0.5 mm) -1; positive-2.
F indicates female; LVI, lymphovascular invasion; M, male; NA, not available; PN, perineural invasion.

This analysis detected a novel *ETV6-RET* fusion transcript joining exon 6 of *ETV6* gene and exon 12 of *RET* gene in 10 cases of salivary gland tumors displaying histologic and immunohistochemical features typical of SC (Fig. 1). All but 1 *ETV6-RET* positive SC case were then tested by at least 1 FISH probe for the presence of *ETV6-RET* rearrangements (Fig. 2). In case 9, there was no residual tissue material for confirmation of the NGS analysis by FISH tests. In addition, RT-PCR for the confirmation of the presence of *ETV6-RET* fusion transcript followed by Sanger sequencing on positive samples was performed in all 10 cases (Fig. 1). The results of the NGS tests, details of the analysis, and results of confirmatory genetic tests are summarized in Tables 3 and 4. In addition, NGS analysis resulted in detection of the *ETV6-NTRK3* fusion in 15 SC cases. In 4 cases, NGS revealed negative results, and 1 case was unanalyzable (detailed data not shown). No other fusion transcripts different from *ETV6-NTRK3* or *ETV6-RET* were found by NGS in any analyzable case of SC.

Clinical and Histologic Characteristics of the Study Group

The clinical and follow-up data of 10 patients with *ETV6-RET* translocated SC of salivary glands are summarized in Table 5. There were 3 female and 7 male patients. The median patient age was 40.8 years, with a range between 20 and 77 years. The most common anatomic site of involvement was the parotid gland, occurring in 7 patients. Other primary sites of the origin included the submandibular gland and minor salivary gland of the upper lip in 2 patients and 1 patient, respectively.

Follow-up Data

Clinical follow-up data were obtained from 8 patients, and ranged from 6 to 50 months (mean, 36 mo); 2 patients were lost to follow-up. Detailed clinical, follow-up, and histologic findings in 10 patients with *ETV6-RET* translocated SC are summarized in Table 5.

All tumors were treated by surgical excision; in 1 patient the excision was radical with clear surgical margins, in 4 cases the surgical margins were positive, and in 4 additional patients, the tumor infiltration was close (< 0.5 mm) to the surgical margins. Five patients underwent subtotal conservative parotidectomy, in 3 of them in combination with radiotherapy (cases 2, 4, and 7). Residual tumors were treated by radical reexcision with clear surgical margins in 2 patients. Concomitant chemotherapy and radiotherapy was used in 1 patient with high-grade transformed SC complicated by metastatic

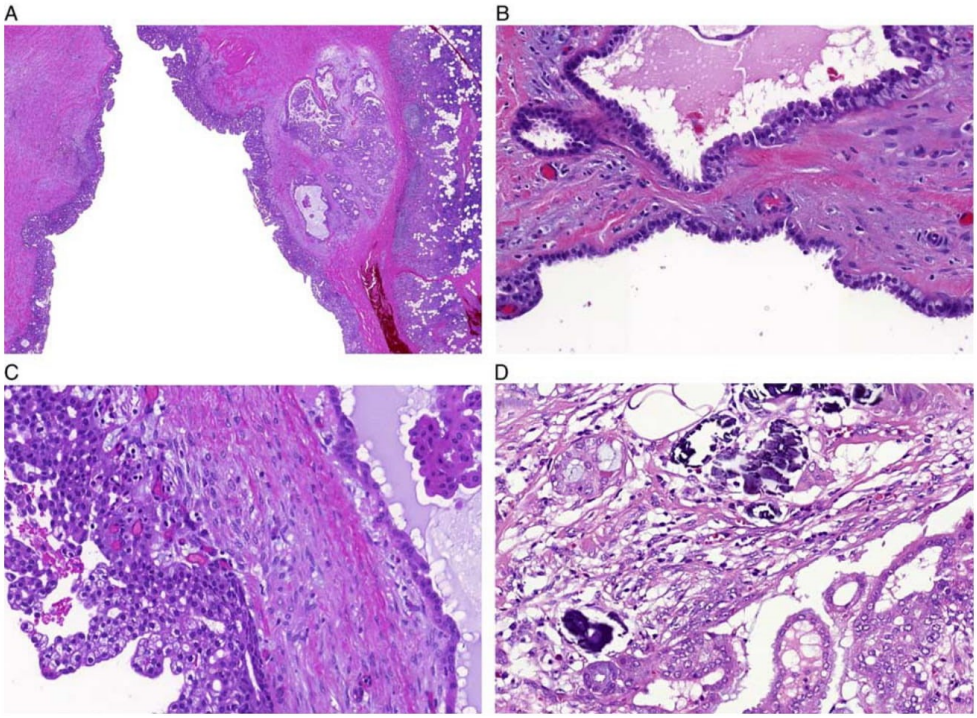

FIGURE 3. A, SC is well circumscribed and surrounded by a thick fibrous capsule enclosing predominantly multicystic growth pattern with multiple mural nodules. The cysts were lined mostly by a single or focally by a double layer of cells with prominent apocrine differentiation including hobnail (B) and vacuolated foamy cells (C). The fibrous capsule and septa comprised psammoma bodies in places (D).

disease at 15 months after surgery (case 7). Clinical and follow-up findings are summarized in Table 5.

Macroscopic Features

Detailed clinical and morphologic findings in 10 patients with *ETV6-RET* translocated SC are summarized in Table 6. The median tumor size was 3.6 cm, with a range of 1.0 to 7.0 cm. Grossly, most tumors were variably invasive: 2 were entirely circumscribed and encapsulated, 1 had focally infiltrative edges, and 7 were predominantly infiltrative.

Microscopic and Immunohistochemical Features

On low power magnification, 3 major growth patterns of SC were identified in our material. First, 3 tumors were well circumscribed and surrounded by a thick, focally uninterrupted, fibrous capsule enclosing a predominantly multicystic growth pattern with multiple mural nodules (Fig. 3A). The cysts were lined mostly by a single or focally by a double layer of cells with prominent apocrine differentiation including hobnail and vacuolated foamy cells (Figs. 3B, C), and contained abundant proteinaceous eosinophilic material. The fibrous capsule and septa comprised psammomatoid calcifications in some places (Fig. 3D). The second pattern was characterized by solid and microcystic growth with a multilobular structure divided by thin fibrous septa (Fig. 4A). The tumors either lacked a capsule or were only partially encapsulated with prominent infiltrative borders (Fig. 4B). These cases were predominantly composed of microcystic and slightly dilated glandular spaces filled with a variable amount of eosinophilic homogenous secretory material (Fig. 4C). The third pattern, prevailing in 3 cases, comprised a prominent fibrosclerotic stroma with isolated tumor cells in small islands or trabeculae, which were seen in the central part of the tumor (Fig. 5A). In case 7, 2 different growth patterns were seen, in particular low-grade components arranged in multiple macrocystic and microcystic lobules with comedo-like necroses, and high-grade components with limited secretory material and high proliferative activity (Fig. 5B).

However, most tumors demonstrated 2 or more architectural patterns, with microcystic, tubular, solid, and papillary patterns often occurring together. Regardless of

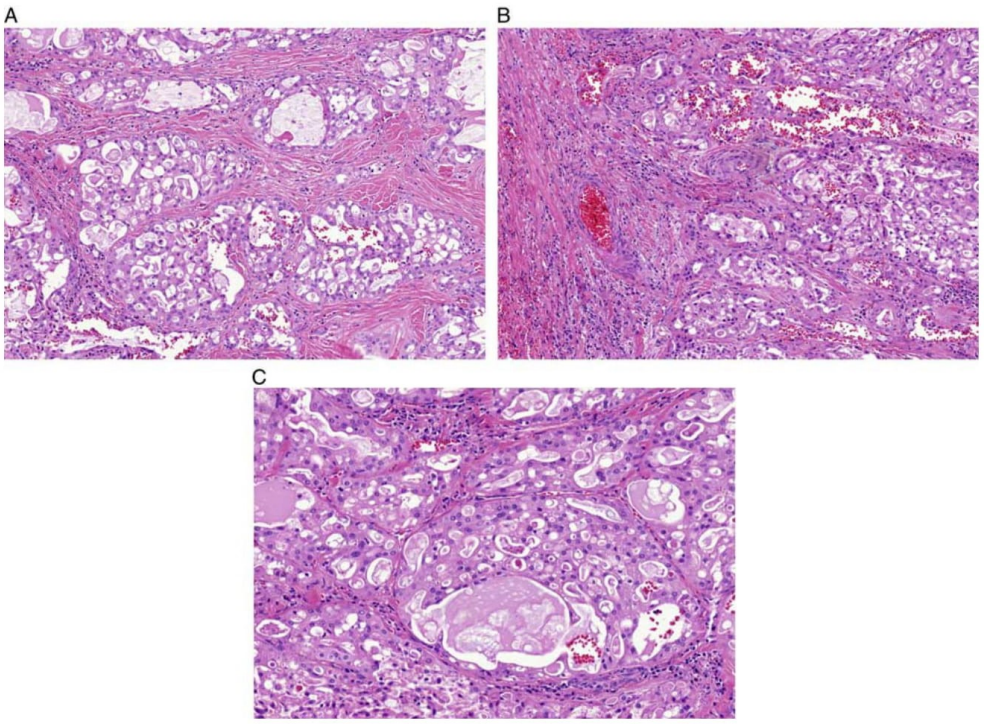

FIGURE 4. A, SC is characterized by solid and microcystic growth with a multilobular structure divided by thin fibrous septa. B, The tumor has a prominent infiltrative border. C, The tumor is predominantly composed of microcystic and slightly dilated glandular spaces filled with a variable amount of eosinophilic homogenous secretory material.

the growth pattern of SC, the tumor cells were often bland looking, with abundant pale pink vacuolated and foamy cytoplasm and with vesicular oval nuclei with a single small but prominent nucleolus. The cytologic features were similar from case to case. The range of nuclear atypia was assessed as grades 1 to 3. Mitotic figures were rare and necrosis was absent. Prominent perineural and intraneural invasion was seen in case 7 (Fig. 5C). Only 1 patient (case 2) presented with a single periparotideal lymph node metastasis at the time of diagnosis.

Immunohistochemical Findings

By immunohistochemistry, all examined SC cases were positive for S100 protein (Fig. 6A), mammaglobin (Fig. 6B), typically in strong and diffuse fashion (secretory material was also positive), and cytokeratin CK7 (Fig. 6C). GATA-3, SOX-10 (Fig. 6D), and STAT5a expression was detected in 3/6, 5/6, and 2/3 cases, respectively. P63 protein was completely negative in most cases, with limited areas of positive peripheral myoepithelial cell staining suggestive of a focal intraductal component in 3 cases. DOG1 was negative in all examined cases. Proliferative activity was generally low, with a mean MIB1 index of 15% (range, 5% to 40%).

DISCUSSION

Salivary gland tumors are increasingly being found to have characteristic chromosomal rearrangements. SC is a salivary gland tumor that recapitulates the histology and genetics of a rare malignancy of the breast SC. These tumors are defined by the t(12;15)(q13;q15) translocation, a fusion of the *ETV6* gene from chromosome 12 and the *NTRK3* gene from chromosome 15. The same translocation has been detected in most cases of the infantile fibrosarcomas, congenital mesoblastic nephromas,[13] chronic eosinophilic leukemias,[33] acute myeloid leukemia,[14] and some papillary carcinomas of the thyroid with and without previous irradiation.[18] These groups of tumors are the focus of interest, because tumors with *ETV6-NTRK3* fusion translocation respond well to treatment by entrectinib, which is a potent inhibitor of tyrosine kinases TRKA/B/C, ROS1, and ALK. The drug entrectinib is administered orally, is safe and well tolerated, and can cross the blood-brain barrier,

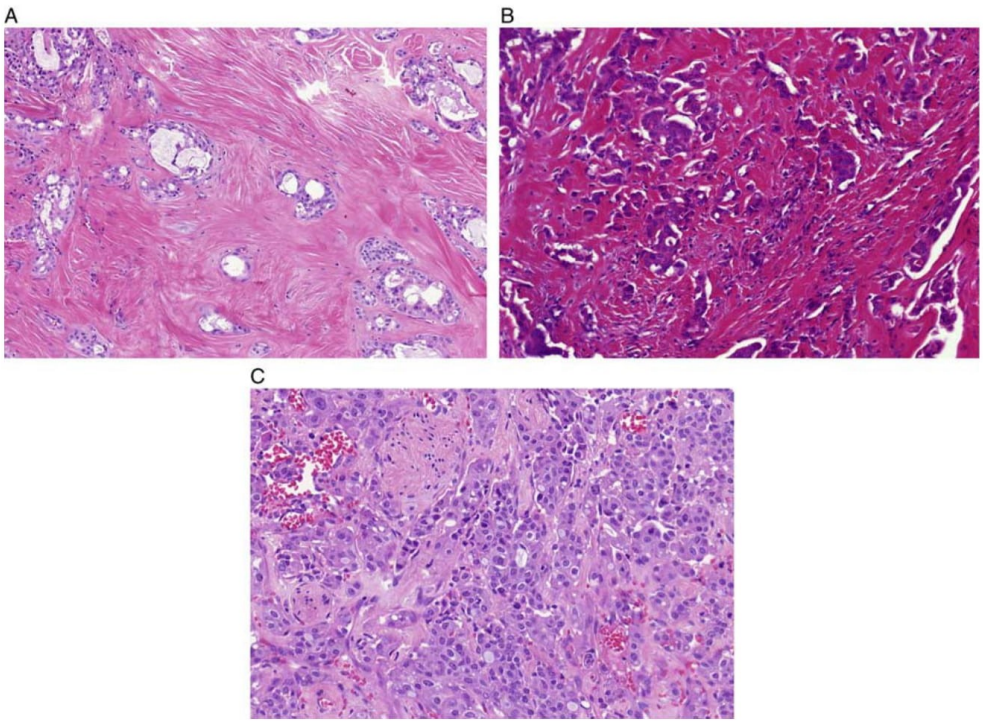

FIGURE 5. A, The third pattern of SC has a prominent fibrosclerotic stroma with isolated tumor cells in small islands or trabeculae were seen in the central part of the tumor. B, High-grade component of SC with limited secretory material and high proliferative activity. C, Prominent perineural and intraneural invasion was seen in 1 tumor.

so that it can be effective for treatment of brain metastases.[34,35]

Originally it appeared that all cases of SC share the same *ETV6-NTRK3* fusion translocation. However, in recent years Ito et al[27] and Skalova et al[26] described altogether 6 cases of SC with the *ETV6* gene split detected by FISH, but in which the *ETV6* gene appeared to be fused with a gene different to *NTRK3*. These cases were marked as SCs with *ETV6-X* fusion.

Herein, we describe a novel *ETV6-RET* fusion in 10 cases of salivary gland carcinomas with histologic features and IHC profile typical of SC, including the 4 *ETV6-X* SC cases published previously.[26] The presence of *ETV6-RET* fusion in SC was proven by at least 3 independent tests (NGS, FISH, RT-PCR), in all but 2 cases (Table 3, cases 4 and 9). In case 4, NGS and FISH confirmed *ETV6-RET* fusion but RT-PCR was negative, probably due to low or focal expression of fusion transcript (Table 4). Case 9 was the only sample unconfirmed by independent analysis. There was a lack of material for FISH analysis and RT-PCR for *ETV6-RET* fusion transcript detection was negative. In this case, low quality of RNA rather than low or focal expression is responsible for this result.

The alternative *ETV6-RET* transcription will be important for treatment of those SCs with uncontrolled regional growth or SCs with metastatic foci, as treatment with entrectinib and similar drugs with the same target specificity will probably be ineffective in these SCs with alternative fusion transcript different from *ETV6-NTRK3*. The alternative fusion partner different from *ETV6-NTRK3* in SC should not be of great surprise, because infantile fibrosarcoma with *ETV6-NTRK3* translocation may have alternative *EML4-NTRK3* translocation,[36] and there are descriptions of acute myeloid leukemias in which the *ETV6* gene fuses with many alternative fusion partners, including *ETV6-ABL1*,[37] *ETV6-LPXN*,[38] *ETV6-RUNX1*,[39] *ETV6-NCOA2*,[40] and many others.

To our knowledge, *ETV6-RET* fusions have not been reported in salivary gland tumors so far. Notably, however, recent studies using RNA sequencing have revealed that salivary duct carcinoma (SDC) may also be added to the growing list of gene fusion-positive salivary

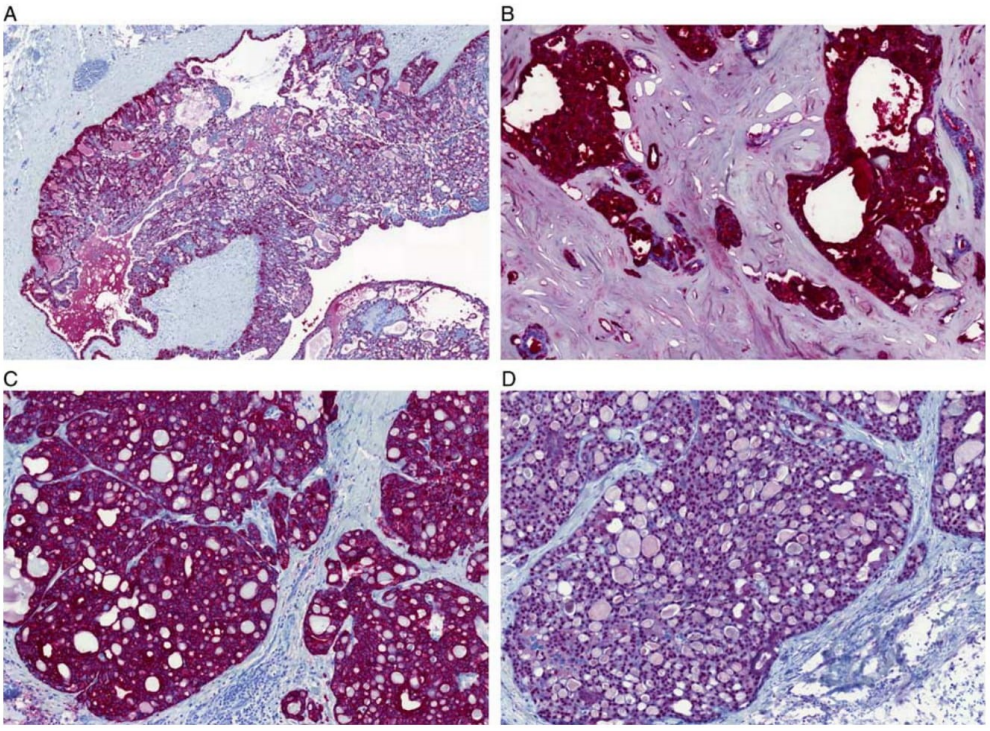

FIGURE 6. SC cases were all positive for S100 protein (A), mammaglobin (B), typically in strong and diffuse fashion (secretory material was also positive), and cytokeratin CK7 (C). SOX-10 positive nuclear expression is present (D).

carcinomas. *NCOA4-RET* fusions have been found in 2 SDCs.[41] Both *NCOA4-RET* translocated SDCs were positive for androgen receptors, and the tumors progressed in spite of undergoing concurrent chemoradiation, combination chemotherapy, and dual androgen deprivation therapy. Both patients with *NCOA4-RET* translocation, however, benefited from *RET*-targeted therapy.[41]

The treatment of SC has varied, ranging from simple excision to radical resection, neck dissection, adjuvant radiotherapy, and/or adjuvant systemic chemotherapy.[1,42,43] For patients presenting with a locally advanced, recurrent, or metastatic disease, the treatment options are currently limited and mainly palliative.[42,43] Therefore, SCs with *ETV6-RET* fusion translocation must be clearly distinguished from SCs with *ETV6-NTRK3* translocation, because the drugs RXDX105 and LOXO 292, effective with various tumors driven with *RET* gene alterations, are being tested for the treatment. SCs with *ETV6-RET* translocation might respond much better to these drugs, whereas entrectinib and similar inhibitors of tyrosine kinases TRKA/B/C will probably be ineffective.[44–47]

In summary, a novel finding in our study has been the discovery of a subset of SC patients with *ETV6-RET* fusions who may benefit from *RET*-targeted therapy. Many salivary gland malignancies are still included in the group of adenocarcinomas not otherwise specified. We believe that detailed genomic profiling and NGS of a large cohort of these unspecified neoplasms may lead to the identification of novel gene fusions and driver mutations characterizing new clinically relevant subgroups of salivary gland carcinomas. This study highlights that further molecular analyses of salivary gland tumors are warranted and deserve special attention to identify new tumor types with possible therapeutic implications.

ACKNOWLEDGMENTS

The authors thank Alos Lucia, MD (Barcelona, Spain), Rychlý B, MD, PhD (Bratislava, Slovac Republic), Vazmitel M, MD, PhD (USA), Dana Cempírková, MD (Jindřichův Hradec, Czech Republic), Ian Cook, MD (Salisbury, UK), and Tiziana Salviati, MD (Italy) for submitting the cases and clinical information about the patients.

REFERENCES

1. Skalova A, Vanecek T, Sima R, et al. Mammary analogue secretory carcinoma of salivary glands, containing the *ETV6-NTRK3* fusion gene: a hitherto undescribed salivary gland tumor entity. *Am J Surg Pathol*. 2010;34:599–608.
2. Tognon C, Knezevich SR, Huntsman D, et al. Expression of the *ETV6-NTRK3* gene fusion as a primary event in human secretory breast carcinoma. *Cancer Cell*. 2002;2:367–376.
3. Li Z, Tognon CE, Godinho FJ, et al. *ETV6-NTRK3* fusion oncogene initiates breast cancer from committed mammary progenitors via activation of AP1 complex. *Cancer Cell*. 2007;12:542–558.
4. Skálová A, Bell D, Bishop JA, et al. Secretory carcinoma. In: El-Naggar A, Chan JKC, Grandis JR, Takata T, Slootweg PJ, eds. *World Health Organization (WHO) Classification of Head and Neck Tumours*, 4th ed. Lyon, France: IARC Press; 2017:177–178.
5. Dogan S, Wang L, Ptashkin RN, et al. Mammary analog secretory carcinoma of the thyroid gland: a primary thyroid adenocarcinoma harboring *ETV6-NTRK3* fusion. *Mod Pathol*. 2016;29:985–995.
6. Reynolds S, Shaheen M, Olson G, et al. A case of primary mammary analog secretory carcinoma (MASC) of the thyroid masquerading as papillary thyroid carcinoma: potentially more than a one off. *Head Neck Pathol*. 2016;10:405–413.
7. Dettloff J, Seethala RR, Stevens TM, et al. Mammary analog secretory carcinoma (MASC) involving the thyroid gland: a report of the first 3 cases. *Head Neck Pathol*. 2007;11:266–267.
8. Stevens TM, Kovalovsky AO, Velosa C, et al. Mammary analog secretory carcinoma, low-grade salivary duct carcinoma, and mimickers: a comparative study. *Mod Pathol*. 2015;28:1084–1100.
9. Hyrcza MD, Ng T, Crawford RI. Detection of the *ETV6-NTRK3* translocation in cutaneous mammary-analogue secretory carcinoma. *Diagn Histopathol*. 2015;21:481–484.
10. Bishop JA, Taube JM, Su A, et al. Secretory carcinoma of the skin harboring *ETV6* gene fusions. A cutaneous analogue to secretory carcinomas of the breast and salivary glands. *Am J Surg Pathol*. 2017;41:62–66.
11. Lurquin E, Jorissen M, Debiec-Rychter M, et al. Mammary analogue secretory carcinoma of the sinus ethmoidalis. *Histopathology*. 2015;67:749–751.
12. Rubin BP, Chen CJ, Morgan TW, et al. Congenital mesoblastic nephroma t(12;15) is associated with ETV6-NTRK3 gene fusion: cytogenetic and molecular relationship to congenital (infantile) fibrosarcoma. *Am J Pathol*. 1998;153:1451–1458.
13. Knezevich SR, Garnett MJ, Pysher TJ, et al. *ETV6- NTRK3* gene fusions and trisomy 11 establish a histogenetic link between mesoblastic nephroma and congenital fibrosarcoma. *Cancer Res*. 1998;15:5046–5048.
14. Kralik JM, Kranewitter W, Boesmueller H, et al. Characterization of a newly identified ETV6-NTRK3 fusion transcript in acute myeloid leukemia. *Diagn Pathol*. 2011;6:19.
15. Alassiri AH, Ali RH, Shen Y, et al. *ETV6-NTRK3* is expressed in a subset of ALK-negative inflammatory myofibroblastic tumor. *Am J Surg Pathol*. 2016;40:1051–1061.
16. Brenca M, Rossi S, Polano M, et al. Transcriptome sequencing identifies *ETV6–NTRK3* as a gene fusion involved in GIST. *J Pathol*. 2016;238:543–549.
17. Leeman-Neill RJ, Kelly LM, Liu P, et al. *ETV6-NTRK3* is a common chromosomal rearrangement in radiation-associated thyroid cancer. *Cancer*. 2014;120:799–807.
18. Seethala RR, Chiosea SI, Liu CZ, et al. Clinical and morphological features of *ETV6-NTRK3* translocated papillary thyroid carcinoma in an adult population without radiation exposure. *Am J Surg Pathol*. 2017;41:446–457.
19. Griffith C, Seethala R, Chiosea SI. Mammary analogue secretory carcinoma: a new twist to the diagnostic dilemma of zymogen granule poor acinic cell carcinoma. *Virchows Arch*. 2011;459:117–118.
20. Fehr A, Loning T, Stenman G. Mammary analogue secretory carcinoma of the salivary glands with *ETV6-NTRK3* gene fusion. Letter to the editor. *Am J Surg Pathol*. 2011;35:1600–1602.
21. Connor A, Perez-Ordoñez B, Shago M, et al. Mammary analog secretory carcinoma of salivary gland origin with the *ETV6* gene rearrangement by FISH: expanded morphologic and immunohistochemical spectrum of a recently described entity. *Am J Surg Pathol*. 2012;36:27–34.
22. Chiosea SI, Griffith C, Assad A, et al. The profile of acinic cell carcinoma after recognition of mammary analog secretory carcinoma. *Am J Surg Pathol*. 2012;36:343–350.
23. Majewska H, Skálová A, Stodulski D, et al. Mammary analogue secretory carcinoma of salivary glands: first retrospective study of a new entity in Poland with special reference to *ETV6* gene rearrangement. *Virchows Arch*. 2015;466:245–254.
24. Pinto A, Nosé V, Rojas C, et al. Searching for mammary analogue secretory carcinoma among their mimicks. *Mod Pathol*. 2014;27:30–37.
25. Bishop JA. Unmasking MASC: bringing to light the unique morphologic, immunohistochemical and genetic features of the newly recognized mammary analogue secretory carcinoma of salivary glands. *Head Neck Pathol*. 2013;7:35–39.
26. Skalova A, Vanecek T, Simpson RHW, et al. Mammary analogue secretory carcinoma of salivary glands. Molecular analysis of 25 *ETV6* gene rearranged tumors with lack of detection of classical *ETV6-NTRK3* fusion transcript by standard rt-pcr: report of 4 cases harboring *ETV6-X* gene fusion. *Am J Surg Pathol*. 2016;40:3–13.
27. Ito Y, Ishibashi K, Masaki A, et al. Mammary analogue secretory carcinoma of salivary glands: a clinicopathological and molecular study including 2 cases harboring *ETV6-X* fusion. *Am J Surg Pathol*. 2015;39:602–610.
28. Murphy DA, Ely HA, Shoemaker R, et al. Detecting gene rearrangements in patient populations through a 2-step diagnostic test comprised of rapid IHC enrichment followed by sensitive next-generation sequencing. *Appl Immunohistochem Mol Morphol*. 2017;25:513–523.
29. Viswanatha DS, Foucar K, Berry BR, et al. Blastic mantle cell leukemia: an unusual presentation of blastic mantle cell lymphoma. *Mod Pathol*. 2000;13:825–833.
30. Gaffney R, Chakerian A, O'Connell JX, et al. Novel fluorescent ligase detection reaction and flow cytometric analysis of SYT-SSX fusions in synovial sarcoma. *J Mol Diagn*. 2003;5:127–135.
31. Antonescu CR, Kawai A, Leung DH, et al. Strong association of SYT-SSX fusion type and morphologic epithelial differentiation in synovial sarcoma. *Diagn Mol Pathol*. 2000;9:1–8.
32. Bourgeois JM, Knezevich SR, Mathers JA, et al. Molecular detection of the ETV6-NTRK3 gene fusion differentiates congenital fibrosarcoma from other childhood spindle cell tumors. *Am J Surg Pathol*. 2000;24:937–946.
33. Su RJ, Jonas BA, Welborn J, et al. Chronic eosinophilic leukemia, NOS with t(5;12)(q31;p13)/ETV6-ACSL6 gene fusion: a novel variant of myeloid proliferative neoplasm with eosinophilia. *Hum Pathol*. 2016;5:6–9.
34. Drilon A, Siena S, Ou SI, et al. Safety and antitumor activity of the multitargeted Pan-TRK, ROS1, and ALK inhibitor Entrectinib: Combined results from two phase I trials ALKA-372-001 and STARTRK-1. *Cancer Discov*. 2017;7:400–407.
35. Drilon A, Li G, Dogan S, et al. What hides behind the MASC: clinical response and acquired resistance to entrectinib after *ETV6-NTRK3* identification in a mammary analogue secretory carcinoma (MASC). *Ann Oncol*. 2016;27:920–926.
36. Tannenbaum-Dvir S, Glade Bender JL, Church AJ, et al. Characterization of a novel fusion gene *EML4-NTRK3* in a case of recurrent congenital fibrosarcoma. *Cold Spring Harb Mol Case Stud*. 2015;1:a000471.
37. Tirado CA, Siangchin K, Shabsovich DS, et al. A novel three-way rearrangement involving *ETV6* (12p13) and *ABL1* (9q34) with an unknown partner on 3p25 resulting in a possible *ETV6-ABL1* fusion in a patient with acute myeloid leukemia: a case report and a review of the literature. *Biomark Research*. 2016;4:16.
38. Abe A, Yamamoto Y, Iba S, et al. *ETV6-LPXN* fusion transcript generated by t(11;12)(q12.1;p13) in a patient with relapsing acute myeloid leukemia with NUP98-HOXA9. *Genes Chromosomes Cancer*. 2016;55:242–250.
39. Garcia DR, Arancibia AM, Ribeiro RC, et al. Intrachromosomal amplification of chromosome 21 (iAMP21) detected by *ETV6*/*RUNX1* FISH screening in childhood acute lymphoblastic leukemia: a case report. *Rev Bras Hematol Hemoter*. 2013;35:369–371.

40. Strehl S, Nebral K, König M, et al. *ETV6-NCOA2*: a novel fusion gene in acute leukemia associated with coexpression of T-lymphoid and myeloid markers and frequent NOTCH1 mutations. *Clin Cancer Res*. 2008;14:977–983.
41. Wang K, Russell JS, McDermott JD, et al. Profiling of 149 salivary duct carcinomas, carcinoma ex pleomorphic adenomas, and adenocarcinomas, not otherwise specified reveals actionable genomic alterations. *Clin Cancer Res*. 2016;22:6061–6068.
42. Skálová A, Vanecek T, Majewska H, et al. Mammary analogue secretory carcinoma of salivary glands with high-grade transformation: report of 3 cases with the *ETV6-NTRK3* gene fusion and analysis of TP53, beta-catenin, EGFR, and CCND1 genes. *Am J Surg Pathol*. 2014;38:23–33.
43. Luo W, Lindley SW, Lindley PH, et al. Mammary analog secretory carcinoma of salivary gland with high-grade histology arising in palate, report of a case and review of literature. *Int J Clin Exp Pathol*. 2014;7:9008–9022.
44. Li GG, Somwar R, Joseph J, et al. Antitumor activity of RXDX-105 in multiple cancer types with RET rearrangements or mutations. *Clin Cancer Res*. 2017;23:2981–2990.
45. Sabari JK, Siau ED, Drilon A. Targeting RET-rearranged lung cancers with multikinase inhibitors. *Oncoscience*. 2017;4:23–24.
46. Chi HT, Ly BT, Kano Y, et al. *ETV6-NTRK3* as a therapeutic target of small molecule inhibitor PKC412. *Biochem Biophys Res Commun*. 2012;429:87–92.
47. Tognon CE, Somasiri AM, Evdokimova VE, et al. *ETV6-NTRK3*-mediated breast epithelial cell transformation is blocked by targeting the IGF1R signaling pathway. *Cancer Res*. 2011;71:1060–1070.

1.10.4 ROZŠÍŘENÍ MOLEKULÁRNÍHO SPEKTRA SEKREČNÍHO KARCINOMU SLINNÝCH ŽLÁZ S NOVOU *VIM-RET* FÚZÍ

Přiložená studie hodnotí molekulárně genetický profil v souboru 49 SC. Ve 40 případech byla zjištěna klasická *ETV6-NTRK3* fúze, v 8 případech se jednalo o *ETV6-RET* a v jednom případě byla zjištěna fúze *VIM-RET*. Navíc byla v jednom případě SC metodou NGS zjištěna duální fúze *ETV6-NTRK3* a *MYB-SMR3B*.

Případ s *VIM-RET* fúzí byl představitelem klasického SC. Kromě případu SC příušní žlázy s *CTNNA1-ALK* reportovaného Sasakim a spol. (40) se jedná o druhý případ SC bez účasti 5´*ETV6* genu. I tento pacient by (obdobně jako pacienti z předchozích studií týkajících se *RET*-onkogenu) mohl profitovat z biologické léčby RET-inhibitory (45, 75, 76).

Druhý případ nádoru s duální fúzí byl naproti tomu variantou high-grade SC. Histologicky byl solidně rostoucí s hyalinizací až sklerotizací stromatu, místy se zastiženým desmoplastickým stromatem a komedo nekrózami. Tento pacient vyvinul v odstupu 48 a 62 měsíců lokální recidivy. Molekulárně geneticky byla zjištěna duální fúze sestavená z klasického fúzního transkriptu *ETV6-NTRK3* a enigmatické fúze *MYB-SMR3B*. *MYB* gen je známý z translokace *MYB-NFIB* adenoidně cystického karcinomu (77). V porovnání s pokročilými znalostmi o *MYB* genu je povědomí o *SMR3B* genu zatím nedostatečně prozkoumané a ví se pouze, že se funkčně uplatňuje výhradně ve slinných žlázách. Lze tudíž spekulovat, že společně s genem *MYB* může hrát roli v progresi nádorového onemocnění a v možné high-grade transformaci SC.

ORIGINAL ARTICLE

Expanding the Molecular Spectrum of Secretory Carcinoma of Salivary Glands With a Novel *VIM-RET* Fusion

Alena Skálová, MD, PhD,† Martina Banečkova, MD,*† Lester D.R. Thompson, MD,‡ Nikola Ptáková, MSc,§ Todd M. Stevens, MD,‖ Luka Brcic, MD, PhD,¶ Martin Hyrcza, MD, PhD,# Michael Michal Jr, MD, PhD,*†** Roderick H.W. Simpson, MD,# Thalita Santana, DDS, MSc,†† Michal Michal, MD,* Tomas Vaněček, PhD,§ and Ilmo Leivo, MD, PhD‡‡§§*

Background: Secretory carcinoma (SC), originally described as mammary analogue SC, is a predominantly low-grade salivary gland neoplasm characterized by a recurrent t(12;15)(p13;q25) translocation, resulting in *ETV6-NTRK3* gene fusion. Recently, alternative *ETV6-RET*, *ETV6-MAML3*, and *ETV6-MET* fusions have been found in a subset of SCs lacking the classic *ETV6-NTRK3* fusion transcript, but still harboring *ETV6* gene rearrangements.

Design: Forty-nine cases of SC revealing typical histomorphology and immunoprofile were analyzed by next-generation sequencing using the FusionPlex Solid Tumor kit (ArcherDX). All 49 cases of SC were also tested for *ETV6*, *RET*, and *NTRK3* break by fluorescence in situ hybridization and for the common *ETV6-NTRK3* fusions using reverse transcription polymerase chain reaction.

Results: Of the 49 cases studied, 37 (76%) occurred in the parotid gland, 7 (14%) in the submandibular gland, 2 (4%) in the minor salivary glands, and 1 (2%) each in the nasal mucosa, facial skin, and thyroid gland. SCswere diagnosed more frequently in males (27/49 cases; 55%). Patients' age at diagnosis varied from 15 to 80 years, with a mean age of 49.9 years. By molecular analysis, 40 cases (82%) presented the classic *ETV6-NTRK3* fusion, whereas 9 cases (18%) revealed an alternate fusion. Of the 9 cases negative for the *ETV6-NTRK3* fusion, 8 cases presented with *ETV6-RET* fusion. In the 1 remaining case in the parotid gland, next-generation sequencing analysis identified a novel *VIM-RET* fusion transcript. In addition, the analysis indicated that 1 recurrent high-grade case in the submandibular gland was positive for both *ETV6-NTRK3* and *MYB-SMR3B* fusion transcripts.

Conclusions: A novel finding in our study was the discovery of a *VIM-RET* fusion in 1 patient with SC of the parotid gland who could possibly benefit from *RET*-targeted therapy. In addition, 1 recurrent high-grade case was shown to harbor 2 different fusions, namely, *ETV6-NTRK3* and *MYB-SMR3B*. The expanded molecular spectrum provides a novel insight into SC oncogenesis and carries important implications for molecular diagnostics, as this is the first SC-associated translocation with a non-*ETV6* 5′ fusion partner. This finding further expands the definition of SC while carrying implications for selecting the appropriate targeted therapy.

Key Words: salivary glands, minor, mammary analogue secretory carcinoma, pathology, molecular, salivary gland neoplasms, carcinoma, gene rearrangement, gene fusion, *VIM-RET*, *ETV6-NTRK3*, *ETV6-RET*

(*Am J Surg Pathol* 2020;00:000–000)

Secretory carcinoma (SC), originally described as mammary analogue secretory carcinoma (MASC), is a predominantly low-grade salivary gland neoplasm characterized by a recurrent t(12;15)(p13;q25) translocation, resulting in *ETV6-NTRK3* gene fusion.[1] The same *ETV6-NTRK3* fusion gene has been recognized earlier in SC of the breast,[2] and several other rare malignancies, including infantile fibrosarcoma,[3] congenital mesoblastic nephroma,[4] papillary thyroid cancer,[5] and various hematological neoplasms.[6]

On the basis of overlapping morphologic, immunohistochemical (S100 protein and mammaglobin [MMG] positivity/p63 negativity), and molecular genetic features with SC of the breast,[2] we proposed the term "mammary analogue secretory carcinoma of salivary gland."[1] More recently, the World Health Organization (WHO) Classification of Tumors of the Head and Neck recommended a nomenclature change of MASC to SC.[7]

From the *Department of Pathology; **Biomedical Center, Faculty of Medicine in Plzen, Charles University; †Biopticka Laboratory Ltd; §Molecular Genetic Laboratory, Biopticka Laboratory Ltd, Plzen, Czech Republic; ‡Department of Pathology, Southern California Permanente Medical Group, Woodland Hills, CA; ‖Department of Pathology, University of Alabama at Birmingham, Birmingham, AL; ¶Diagnostic and Research Institute of Pathology, Medical University of Graz, Graz, Austria; #Department of Pathology and Laboratory Medicine, University of Calgary, Calgary Laboratory Services, Foothills Medical Centre, Calgary, AB, Canada; ††Department of Oral Pathology, Faculty of Dentistry, University of São Paulo, São Paulo, Brazil; ‡‡Institute of Biomedicine, University of Turku; and §§Department of Pathology, Turku University Hospital, Turku, Finland.

Preliminary results reported as a poster presentation at the United States and Canadian Academy of Pathology Annual Meeting in National Harbor, md, March 16-21, 2019 (Poster #411).

Conflicts of Interest and Source of Funding: The authors have disclosed that they have no significant relationships with, or financial interest in, any commercial companies pertaining to this article.

Correspondence: Alena Skálová, MD, PhD, Sikl's Department of Pathology, Charles University, Faculty of Medicine in Pilsen, E. Benese 13, Pilsen 305 99, Czech Republic (e-mail: skalova@fnplzen.cz).

Since its initial description, a number of published series have expanded and further defined the clinicopathologic characteristics of salivary SC.[8–15] Histomorphologically, most tumors have been described as infiltrative. Fibrous septae divide the tumors into multiple lobules that contain microcystic/cribriform, solid, tubular/glandular, follicular, or papillary-cystic structures with abundant intraluminal secretions. The neoplastic cells appear bland with round to oval and hyperchromatic to vesicular nuclei with inconspicuous small nucleoli. The cytoplasm has an eosinophilic, granular to vacuolated appearance.[1] The recent description of 15 cases of macrocystic SC[16] further expanded the morphologic spectrum of salivary SC. Moreover, since its initial description in the salivary glands, cases of SC have been reported in a multitude of new locations, such as the skin,[17–19] the sinonasal tract,[20–22] the thyroid,[23–25] and the lung,[26] further highlighting the anatomic spectrum of this entity.

The vast majority of SC cases harbor the canonical *ETV6-NTRK3* translocation.[1] Moreover, the current WHO Classification of Tumors of the Head and Neck of 2017 recognizes that the integration of molecular advances into clinical practice is inevitable and includes the *ETV6-NTRK3* gene fusion in the definition of SC.[7] However, a subset of SC cases have been described that harbor *ETV6* gene rearrangements, but lack the classic *NTRK3* fusion partner.[27,28] With the advent of targeted next-generation sequencing (NGS) assays, this was followed by the identification of novel alternative *ETV6* partners in a subset of SCs, such as *RET*,[29] *MET*,[30] and *MAML3*.[31]

To our knowledge, this is the first *VIM-RET* gene fusion reported in SC. This finding further expands the molecular definition of SC and carries implications for diagnostics and selection of appropriate targeted therapy.

MATERIALS AND METHODS

Case Selection and Clinicopathologic Review

The study was approved by the institutional review board. Forty-eight cases of SC of salivary glands and 1 SC of thyroid gland were retrieved from routine surgical pathology files and from tumors contributed by the co-authors to the consultation files of the Salivary Gland Tumor Registry, at the Department of Pathology, Faculty of Medicine in Plzen, and Biopticka Laboratory Ltd (Plzen, Czech Republic). The cases were submitted either for confirmation of the original diagnosis or because of possible targeted treatment of the patient. Clinical follow-up was obtained from the patients, their physicians, or from referring pathologists. The histopathologic features and the immunohistochemical stains of all tumors were reviewed (A.S., M.B.), and the diagnosis of SC was confirmed on the basis of morphologic and immunohistochemical features consistent with the original description.[1] The latter features comprised coexpression of S100 protein, SOX10, CK7, and MMG in the absence of DOG1 and p63 staining.

For immunohistochemical studies, 4-μm-thick sections were cut from paraffin blocks and mounted on positively charged slides (TOMO; Matsunami Glass Ind., Japan). Sections were processed on a BenchMark ULTRA (Ventana Medical SystemS, Tucson, AZ), deparaffinized, and then subjected to heat-induced epitope retrieval by immersion in a CC1 solution at pH 8.6 at 95°C. After antigen retrieval, sections were stained with a pan-TRK antibody cocktail consisting of rabbit monoclonal antibodies, all obtained from Cell Signaling (Danvers, MA), targeting pan-Trk (A7H6R, active against TrkA, TrkB, and TrkC, 1:50 dilution), ROS1 (D4D6, 1:50), and ALK (D5F3, 1:50), as described previously.[29] All the other primary antibodies used are summarized in Table 1. The bound antibodies were visualized using the ultraView Universal DAB Detection Kit (Roche) and the ultraView Universal Alkaline Phosphatase Red Detection Kit (Roche). The slides were counterstained with the Mayer hematoxylin. Appropriate positive and negative controls were used.

TABLE 1. Antibodies Used for Immunohistochemical Study

Antibody Specificity	Clone	Dilution	Antigen Retrieval/ Time (min)	Source
S100 protein	Polyclonal	RTU	CC1/20	Ventana
MMG	304-1A5	RTU	CC1/36	DakoCytomation
CK7	OV-TL 12/30	1:200	CC1/36	DakoCytomation
p63	4A4	RTU	CC1/64	Ventana
DOG1	SP31	RTU	CC1/36	Cell Marque
GATA-3	L50-823	1:200	CC1/52	BioCareMedical
SOX10	Polyclonal	1:100	CC1/64	Cell Marque
Pan-TRK	A7H6R	1:20	CC1/64	Cell Signaling
MIB1	30-9	RTU	CC1/64	Ventana
MYB	EP769Y	1:100	CC1/36	Abcam

CC1—EDTA buffer, pH 8.6.
RTU indicates ready to use.

All cases were analyzed by NGS using the FusionPlex Solid Tumor kit (ArcherDX). All 49 cases of SC were also tested for *ETV6*, *RET*, and *NTRK3* break by fluorescence in situ hybridization (FISH) and for the common *ETV6-NTRK3* fusion using reverse transcription polymerase chain reaction (RT-PCR).

Molecular Genetic Studies

Sample Preparation for NGS and RT-PCR

For NGS and RT-PCR analysis, 2 to 3 formalin-fixed, paraffin-embedded (FFPE) sections (10 μm thick) were macrodissected to isolate tumor-rich regions. Samples were extracted for total nucleic acid using the Agencourt FormaPure Kit (Beckman Coulter, Brea, CA). Both the RNA integrity assessment and detailed description of the analysis carried out using the Archer FusionPlex Solid Tumor Kit were reported previously by our group.[29]

RNA Integrity Assessment and Library Preparation for NGS

Unless otherwise indicated, 250 ng of FFPE RNA was used as an input for NGS library construction. To assess RNA quality, the PreSeq RNA QC Assay using iTaq Universal SYBR Green Supermix (Biorad, Hercules, CA) was performed on all samples during library preparation to generate a measure of the integrity of RNA (in the form of a

cycle threshold [C_t] value). Library preparation and RNA QC were performed following the Archer FusionPlex Protocol for Illumina (ArcherDX Inc.). The Archer FusionPlex Solid Tumor Kit was used. Final libraries were diluted 1:100,000 and quantified in a 10 μL reaction following the Library Quantification for Illumina Libraries protocol and assuming a 200 bp fragment length (KAPA, Wilmington, MA). The concentration of final libraries was around 200 nM. The threshold representing the minimum molar concentration for which sequencing can be robustly performed was set at 50 nM.

NGS Sequencing and Analysis

Libraries were diluted to 4 nM and sequenced on a NextSeq sequencer (Illumina, San Diego, CA). The optimal number of raw reads per sample was set to 3 million. Library pools were diluted to 1.6 pM library stock with 20% 1.8 pM PhiX and loaded in the NextSeq cartridge. The fusion and other rearrangement detection algorithm of Archer Analysis relies on the specificity of the gene-specific primers used in the amplification steps in the AMP process. The resulting FASTQ files were analyzed using the Archer Analysis software (version 5.1.7; ArcherDX Inc.).

Detection of Alterations of ETV6, NTRK3, and RET Genes by the FISH Method

Four-micron-thick FFPE sections were placed onto positively charged slides. Hematoxylin and eosin–stained slides were examined for determination of areas for cell counting. The unstained slides were routinely deparaffinized and incubated in the ×1 Target Retrieval Solution Citrate at pH 6 (Dako, Glostrup, Denmark) and at 95°C for 40 minutes and subsequently cooled for 20 minutes at room temperature in the same solution. Slides were washed in deionized water for 5 minutes and digested in protease solution with pepsin (0.5 mg/mL; Sigma Aldrich, St Louis, MO) in 0.01 M HCl at 37°C for 25 to 60 minutes, according to the sample conditions. Slides were then placed in deionized water for 5 minutes, dehydrated in a series of ethanol solutions (70%, 85%, and 96% for 2 min each), and air dried.

Two commercial probes were used for the detection of rearrangement of *ETV6* and *RET* genes, the Vysis ETV6 Break-Apart FISH Probe Kit (Vysis/Abbott Molecular, IL), and ZytoLight SPEC RET Dual Color Break-Apart Probe (ZytoVision GmbH, Bremerhaven, Germany). The *ETV6* probe was mixed with water and LSI/WCP (Locus-Specific Identifier/Whole Chromosome Painting) Hybridization buffer (Vysis/Abbott Molecular) in a 1:2:7 ratio, respectively. The *RET* probe was factory premixed. Probes for the detection of rearrangement of the *NTRK3* gene region were mixed from custom-designed SureFISH probes (Agilent Technologies Inc., Santa Clara, CA). Chromosomal regions for *NTRK3* break-apart probe oligos are chr15:87501469-88501628 and chr15:88701444-89700343. Probe mixture was prepared from the corresponding probes (each color was delivered in a separate well), deionized water, and LSI Buffer (Vysis/Abbott Molecular) in a 1:1:1:7 ratio, respectively.

An appropriate amount of mixed and premixed probes was applied on the specimens, covered with a glass coverslip, and sealed with rubber cement. Slides were incubated in the ThermoBrite instrument (StatSpin/Iris Sample Processing, Westwood, MA) with codenaturation at 85°C for 8 minutes and hybridization at 37°C for 16 hours. The rubber cemented coverslip was then removed and the slide was placed in a posthybridization wash solution (2×SSC/0.3% NP-40) at 72°C for 2 minutes. The slide was air dried in the dark, counterstained with 4′,6′-diamidino-2-phenylindole (DAPI; Vysis/Abbott Molecular), coverslipped, and examined immediately.

FISH Interpretation

The sections were examined with an Olympus BX51 fluorescence microscope (Olympus Corporation, Tokyo, Japan) using a ×100 objective and filter sets Triple Band Pass (DAPI/SpectrumGreen/SpectrumOrange), Dual Band Pass (SpectrumGreen/SpectrumOrange), and Single Band Pass (SpectrumGreen or SpectrumOrange). For each probe, 100 randomly selected nonoverlapping tumor cell nuclei were examined for the presence of yellow or green and orange fluorescent signals. For the break-apart probe, yellow signals were considered negative, and separate orange and green signals were considered positive. Cutoff values for the break-apart probes were set at > 10% of nuclei with chromosomal breakpoint signals (mean+3 SD in normal non-neoplastic control tissues).

RESULTS

Clinical Characteristics

Among the 49 studied cases, 37 (76%) occurred in the parotid gland, 7 (14%) in the submandibular gland, 2 (4%) in the minor salivary glands, and 1 (2%) each in the nasal mucosa, facial skin, and thyroid gland. The majority of cases were diagnosed in males (27; 55%). Patient age at diagnosis varied from 15 to 80 years, with a mean age of 49.9 years. Six SC cases were previously published.[13,29,32,33] The clinicopathologic, immunohistochemical, and molecular genetic findings of all 49 SC cases are summarized in Table 2.

Pathologic Features and Immunophenotype

The typical histologic features seen in most *ETV6-NTRK3* fused SC included solid and microcystic growth pattern with a multilobular architecture divided by thin fibrous septa (Fig. 1A). The tumors either lacked a capsule (42/48; 86%) or were only partially encapsulated (7/48; 14%), mostly showing prominent infiltrative borders (31/48; 65%). The tumor cells had vesicular low-grade nuclei with finely granular chromatin and distinctive centrally located nucleoli, surrounded by pale pink granular or vacuolated cytoplasm. Most SC cases were predominantly composed of solid and microcystic (30/49; 61%) and slightly dilated glandular spaces filled with a variable amount of eosinophilic homogenous secretory material (Fig. 1B). A less common growth pattern previously seen in SCs harboring the *ETV6-RET* gene fusion,[29] comprised a prominent fibrosclerotic stroma with isolated tumor cells in small islands or trabeculae, which were often seen in the central part of the tumor (Fig. 1C). Such a prominent sclerotic stroma was present in 5 of 8 (60%) *ETV6-RET* translocated SCs, but focal hyalinized stromal septa were seen in many other SCs including cases with *ETV6-NTRK3* fusion (Table 2).

AQ5

TABLE 2. Clinicopathologic, IHC, and Molecular Genetic Findings in 49 Cases of SC Analyzed by NGS[13,29,32,33]

Case No.	Age (y)	Sex	Site	Type of Growth	Fibrous Septa/ Hyalinization	Capsule/ Invasion	IHC S100	IHC MMG	NGS	FISH	RT-PCR
1	56	Female	Parotid	Solid, microcystic	Yes/yes	Invasion	3+	3+	*VIM-RET*	ND	*VIM-RET*
2	60	Male	Submandibular gland	Solid	Yes/yes	Invasion	3+	2+	*ETV6-NTRK3* *MYB-SMR3B*	ND	*ETV6-NTRK3*
3[32]	47	Female	Parotid left	Glandular, macrocystic	NA/NA	Invasion	3+	3+	*ETV6-NTRK3*	*ETV6-NTRK3*	*ETV6-NTRK3*
4[32]	37	Male	Submandibular gland right	Tubular, glandular	Yes/yes	Invasion	3+	3+	*ETV6-NTRK3*	*ETV6-NTRK3*	NA, neg
5	49	Male	Parotid left	Solid, microcystic	Yes/no	Circumscribed	3+	3+	*ETV6-NTRK3*	ND	ND
6	46	Female	Parotid	Solid, microcystic	Yes/yes*	Invasion	3+	3+	*ETV6-RET*	Neg	Neg
7	52	Male	Parotid	Solid, papillary	No/yes	Invasion	2+	3+	*ETV6-NTRK3*	*ETV6*	*ETV6-NTRK3*
8	67	Male	Submandibular gland	Cystic	No/no	Circumscribed	3+	2+	*ETV6-NTRK3*	*ETV6*	Neg
9	51	Female	Nasal mucosa	Tubular, microcystic, papillary	Yes/no	Invasion	1+	1+	*ETV6-NTRK3*	*ETV6*	Neg
10	52	Male	Parotid	Microcystic, lobular solid	Yes/no	Invasion	2+	3+	*ETV6-NTRK3*	*ETV6*	*ETV6-NTRK3*
11	36	Male	Parotid	Lobular solid, papillary, microcystic	Yes/yes	Invasion	2+	ND	*ETV6-NTRK3*	*ETV6*	*ETV6-NTRK3*
12	21	Male	Parotid	Nodular, cystic	Yes/no	Circumscribed	2+	ND	*ETV6-NTRK3*	*ETV6*	*ETV6-NTRK3*
13	74	Female	Parotid	Cystic, papillary, apocrine features	Yes/no	Circumscribed	2+	ND	*ETV6-NTRK3*	*ETV6*	*ETV6-NTRK3*
14	53	Female	Parotid right	Multilobular, papillary	Yes/yes	Circumscribed but invasion	2+	2+	*ETV6-NTRK3*	*ETV6*	*ETV6-NTRK3*
15	35	Female	Parotid right	Cystic, micropapillary, tubular	Yes/yes	Circumscribed	1+	1+	*ETV6-NTRK3*	*ETV6*	*ETV6-NTRK3*
16	15	Male	Parotid left	Multilobular solid	Yes/yes	Invasion	2+	3+	*ETV6-NTRK3*	*ETV6*	*ETV6-NTRK3*
17	26	Female	Submandibular gland left	Multicystic, solid, micropapillary	Yes/yes	Circumscribed but invasion	1+	3+	*ETV6-NTRK3*	*ETV6*	*ETV6-NTRK3*
18	47	Female	Parotid right	Macrocystic, solid, microcystic	No/no	Partially encapsulated	2+	3+	*ETV6-NTRK3*	NA	NA
19	59	Female	Lower lip mucosa	Nodular, solid, microcystic	No/no	Encapsulated	1+	3+	*ETV6-NTRK3*	*ETV6*	*ETV6-NTRK3*
20	52	Male	Parotid right	Lobular, solid, microcystic, macrocystic, papillary	Yes/yes	Circumscribed, partially encapsulated	1+	1+	*ETV6-NTRK3*	*ETV6*	*ETV6-NTRK3*
21	30	Female	Parotid left	Cystic, microcystic, papillary, apocrine	No/no	Circumscribed	1+	3+	*ETV6-NTRK3*	*ETV6*	*ETV6-NTRK3*
22	80	Female	Parotid right	Solid, microcystic	Yes/yes	Circumscribed partially encapsulated	2+	3+	*ETV6-NTRK3*	*ETV6*	*ETV6-NTRK3*
23	77	Female	Parotid right	Solid, microcystic	Yes/yes	Circumscribed	3+	2+	*ETV6-NTRK3*	*ETV6*	*ETV6-NTRK3*
24	60	Male	Parotid right	Multinodular, micropapillary, microcystic	Yes/yes	Circumscribed but invasion	3+	3+	*ETV6-NTRK3*	*ETV6*	*ETV6-NTRK3*
25	66	Male	Thyroid gland left	Solid microcystic, tubular, papillary, apocrine	Yes/yes	Circumscribed but invasion	1+	3+	*ETV6-NTRK3*	*ETV6-NTRK3*	ND
26[33]	34	Male	Parotid	Solid microcystic, papillary	No/yes	Circumscribed	2+	3+	*ETV6-RET*	*ETV6-RET*	ND
27	52	Female	Parotid	Solid microcystic	Yes/yes	Invasion	3+	1+	*ETV6-NTRK3*	*ETV6-NTRK3*	ND
28	60	Female	Parotid right	Solid microcystic, apocrine features	No/yes	Circumscribed but invasion	1+	3+	*ETV6-NTRK3*	*ETV6*	Neg
29	66	Male	Parotid right	Solid microcystic, tubular, papillary	Yes/yes	Invasion	3+	3+	*ETV6-NTRK3*	*ETV6-NTRK3*	Neg
30	20	Female	Submandibular gland	Solid microcystic	Yes/yes	Invasion	2+	3+	*ETV6-NTRK3*	NA	Neg
31	48	Female	Parotid right	Solid microcystic, tubular, papillary	Yes/yes	Invasion	1+	1+	*ETV6-NTRK3*	*ETV6*	ETV6-NTRK3
32	28	Female	Parotid right	Solid microcystic	Yes/yes*	Invasion	1+	3+	*ETV6-RET*	*ETV6-RET*	Neg
33	26	Female	Parotid	Micropapillary, microcystic, apocrine	Yes/no	Invasion	1+	2+	*ETV6-NTRK3*	*ETV6*	Neg
34	55	Male	Parotid	Microcystic micropapillary	Yes/yes*	Circumscribed but invasion	1+	2+	*ETV6-RET*	NA	Neg
35	58	Male	Parotid	Solid microcystic, multilobular	Yes/yes	Invasion	2+	3+	*ETV6-NTRK3*	NA	Neg
36	54	Female	Parotid	Solid microcystic, multilobular	Yes/yes	Invasion	3+	2+	*ETV6-NTRK3*	ND	Neg
37	74	Male	Parotid	Cystic, solid	Yes/yes	Circumscribed	2+	3+	*ETV6-NTRK3*	ND	Neg
38	43	Male	Parotid	Solid microcystic, papillary, apocrine	Yes/yes	Invasion	1+	3+	*ETV6-NTRK3*	ND	Neg

TABLE 2. (*continued*)

Case No.	Age (y)	Sex	Site	Type of Growth	Fibrous Septa/ Hyalinization	Capsule/ Invasion	IHC S100	IHC MMG	NGS	FISH	RT-PCR
39	51	Male	Parotid	Solid microcystic lobular	Yes/yes	Circumscribed but invasion	2+	3+	*ETV6-NTRK3*	ND	Neg
40	73	Male	Parotid	Cystic, solid	No/yes	Circumscribed encapsulated	2+	3+	*ETV6-NTRK3*	*ETV6*	Neg
41	66	Male	Parotid	Solid papillary	Yes/yes	Encapsulated	3+	ND	*ETV6-NTRK3*	*ETV6*	Neg
42[29]	77	Male	Submandibular gland	Cribriform, cystic papillary	Yes/yes	Circumscribed encapsulated	3+	1+	*ETV6-RET*	*ETV6-RET*	Neg
43	39	Female	Palate	Solid microcystic	NA	NA	3+	3+	*ETV6-NTRK3*	NA	Neg
44[29]	31	Male	Submandibular gland	Lobular, microcystic, solid	Yes/yes*	Invasion	3+	3+	*ETV6-RET*	*ETV6*	Neg
45[13]	73	Male	Parotid	Solid, microcystic	Yes/yes	Invasion	3+	3+	*ETV6-NTRK3*	*ETV6*	ETV6-NTRK3
46	41	Male	Parotid	Cystic papillary	No/no	Circumscribed encapsulated	1+	ND	*ETV6-NTRK3*	NA	Neg
47	20	Female	Parotid	Solid microcystic, tubular	Yes/no	Circumscribed but invasion	3+	ND	*ETV6-RET*	*RET*	Neg
48	78	Male	Facial skin	Cystic, cribriform, tubular	Yes/yes	Invasion	2+	Neg	*ETV6-NTRK3*	ND	ND
49	29	Male	Parotid left	Solid, microcystic	Yes/yes*	Circumscribed but invasion	3+	3+	*ETV6-RET*	*ETV6-RET*	Neg

Scoring system for assessment of IHC stainings for S100 protein and MMG: 1+, <50%; 2+, 50% to 75%; 3+, 75% to 100%.
*Prominent fibrosclerotic stroma.
IHC indicates immunohistochemistry; NA, not available; ND, not done; neg, negative.

SC with high-grade (HG) transformation consisted of 2 distinct sharply delineated carcinomatous components (Fig. 1D). One was a conventional SC composed of uniform neoplastic cells arranged in solid, tubular, and microcystic growth structures, divided by fibrous septa that were partly hyalinized. In contrast, the HG component appeared as a distinct population of anaplastic cells arranged in trabecular patterns, and with common perineurial invasion (Fig. 1D). Irregular-shaped tumor islands with large geographic comedo-like necrosis were often seen in the HG component of SC. The tumor cells herein showed nuclear pleomorphism, distinctive nucleoli and they lacked secretory activity (Fig. 1E).

Yet another growth pattern, seen in both *ETV6-NTRK3* and *ETV6-RET* fused SC cases, was a predominantly multicystic 1 (6/49; 12%). The cysts were lined mostly by a single or focally a double layer of cells with prominent apocrine differentiation; hobnail cells and vacuolated foamy cells were present as well (Fig. 1F). Very rare SCs were well circumscribed and surrounded by a thick, fibrous capsule, composed of 1 single cystic space that contained abundant proteinaceous eosinophilic material (3/49; 6%). Histologic findings are summarized in Table 2.

Immunohistochemical Findings

By immunohistochemistry, most examined cases were strongly and diffusely positive for S100 protein (Fig. 2A) and MMG (Fig. 2B). Both markers also stained the secretory material. In particular, immunostaining for S100 protein was seen in all cases of SC. Strong and diffuse nuclear-cytoplasmic expression in almost all neoplastic cells was seen in 19 (39%) cases, and intermediate positivity in 16 (33%) cases and mild in 14 (28%) cases. MMG was strongly expressed in 29 SCs (59%); intermediate and mild positivity was encountered in 7 (14%) and 6 (12%) cases, respectively. Immunohistochemical findings of S100 and MMG are presented in Table 2. Other expressed antibodies included CK7 (Fig. 2C), GATA-3, and SOX10 (Fig. 2D). The p63 protein was negative in most cases, but showed limited areas of positive peripheral myoepithelial cell staining suggestive of a focal intraductal component in 3 cases. DOG1 was negative in all examined cases. Proliferative activity was generally low, with a mean MIB-1 index of 15% (range: 5% to 40%).

Index Case 1: Salivary SC With a Novel VIM-RET Fusion

Histologically, this case featured a typical SC morphology, characterized by a predominantly solid and microcystic growth pattern with a multilobular architecture divided by thin fibrous septa (Fig. 3A). Perineurial growth was noted (Fig. 3B). Some areas showed macrocystic transformation. The cystic spaces were lined by a single layer of neoplastic cells and contained an eosinophilic material (Fig. 3C). Dense hyalinization with isolated tumor cell nests was present in some areas (Fig. 3D). Tumor cells were diffusely positive for MMG (Fig. 3E) and S100 protein (Fig. 3F).

Index Case 2: Salivary SC With Dual ETV6-NTRK3 and Novel MYB-SMR3B Fusions

SC of the submandibular gland showed a multifocal and widely invasive growth pattern in the submandibular gland (Fig. 4A). The tumor had a predominantly solid architecture; hyalinization and sclerotic areas were prominent. In some areas, the desmoplastic stroma surrounded isolated tumor cell nests. The neoplastic cells showed a nuclear pleomorphism and minimal residual secretory activity (Fig. 4B). Occasional comedo-like necrosis was present (Fig. 4C). A cytology specimen featured a pleomorphic cell population, with prominent nuclei and nuclear grooves (Fig. 4D). The cells had a high mitotic activity with an MIB-1 index of 40% (Fig. 4E). By immunohistochemistry, S100 protein, CK7, MMG, SOX10,

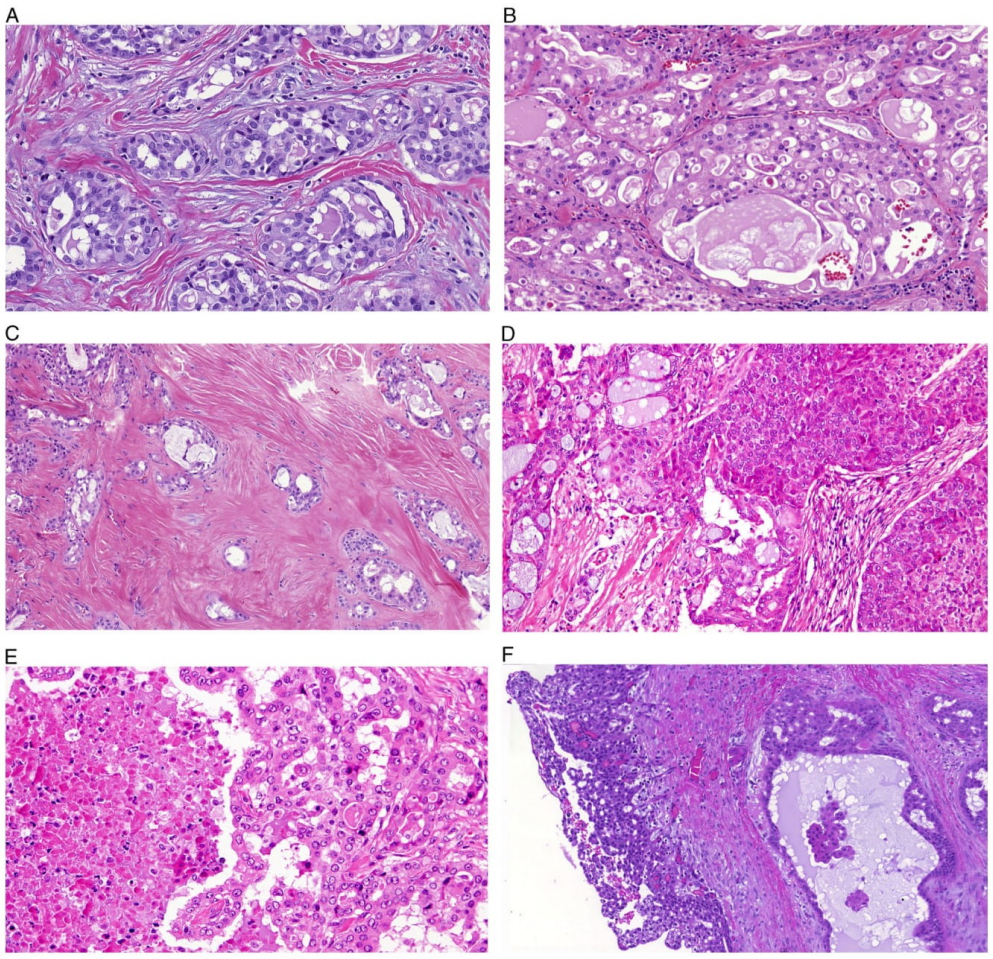

FIGURE 1. Major growth patterns in SC cases. A, Most *ETV6-NTRK3* fused SC showed a solid and microcystic growth pattern with a multilobular architecture divided by thin fibrous septa. B, SC composed of dilated glandular spaces filled with a variable amount of eosinophilic homogeneous secretory material. C, Usually centrally located prominent fibrosclerotic stroma permeated by isolated small islands or trabeculae of tumor cells. Overall, this pattern is rarely encountered in MASC, but is overrepresented in cases with *ETV6-RET* fusion. D, SC with HG transformation consisted of 2 distinct sharply delineated carcinomatous components. E, Irregular-shaped tumor islands with large geographic comedo-like necrosis are seen in the HG component of SC. Tumor cells in HG areas display apparent nuclear pleomorphism, prominent nucleoli and they lack any secretory activity. F, Predominantly multicystic growth pattern seen in both *ETV6-NTRK3* and *ETV6-RET* SC cases. The cysts were lined mostly by a single or focally a double layer of cells with prominent apocrine differentiation; hobnail and vacuolated foamy cells were present as well.

CK7, and pan-TRK were diffusely positive in all neoplastic cells. Nuclear staining for MYB was found in most neoplastic cells (Fig. 4F).

Index Case 3: SC of Thyroid Gland

This tumor was predominantly microcystic, with some areas showing fusion of the microcysts, thereby creating a cribriform pattern. Eosinophilic to basophilic secretions with scalloped edges were diffusely present within the microcysts. Focally dilated cysts containing variably thick and sometimes edematous fibrovascular cores were present. From these fibrovascular cores emanated nonhierarchically branched micropapillae, focally forming a "medusa head"-type appearance. The stroma was sclerotic to desmoplastic. The pushing type of

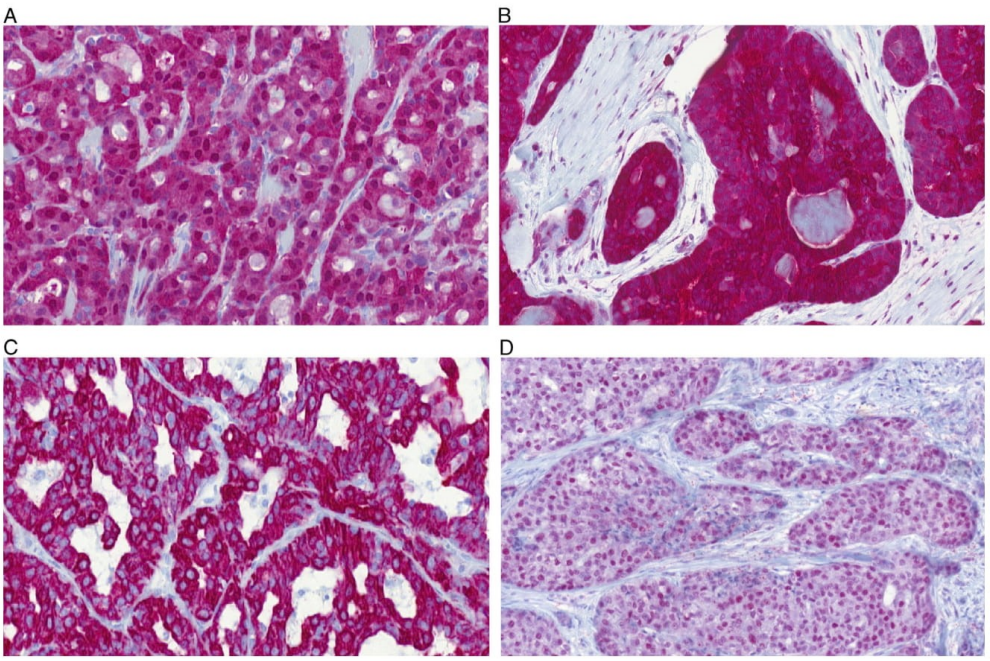

FIGURE 2. Immunohistochemical findings in the SC cohort. A–D, All studied cases showed typical immunohistochemical features of SC. The tumor cells showed membranous and nuclear S100 (A) and MMG (B) positivity, membranous CK7 (C) positivity, and nuclear SOX10 (D) positivity.

invasion predominated and extended into extrathyroidal tissue including skeletal muscle. Focally, small neoplastic tubular formations irregularly invaded into the surrounding tissues as well. Nuclei of the neoplastic cells were uniform, low grade, and oval, with a single inconspicuous to medium-sized nucleolus. Although nuclear grooves were present, no nuclear pseudoinclusions were seen and the chromatin patterns and nuclear size were distinct from conventional papillary thyroid carcinoma. Cytoplasm was amphophillic to eosinophilic. Focal apocrine snouts were noted. No necrosis or HG transformation was identified. MMG and S100 protein, and GATA-3, were diffusely expressed. TTF-1, thyroglobulin, PAX8, and NKX3.1 were all negative. A break-apart FISH study for *ETV6* was positive; NGS analysis revealed *ETV6-NTRK3* fusion confirmed by RT-PCR.

Molecular Findings and Clinicopathologic Correlates

Forty SC cases (82%) presented the classic *ETV6-NTRK3* fusion. Of the 9 *ETV6-NTRK3* fusion-negative cases, 8 presented with an *ETV6-RET* fusion. A novel *VIM-RET* fusion transcript was identified in 1 case of SC of the parotid gland (Fig. 5A) by NGS analysis. In addition, 1 recurrent HG SC of the submandibular gland was positive for both *ETV6-NTRK3* and *MYB-SMR3B* fusion transcripts (Fig. 5B). In the FISH analysis, *ETV6* splits were detected in 33/49 (67%), *NTRK3* splits in 5/49 (10%), and RET rearrangement in 5/49 (10%) (Table 2). The *ETV6-NTRK3* fusion was confirmed in 19 SCs (39%) by RT-PCR. The single SC harboring *VIM-RET* fusion was confirmed by RT-PCR as well. All results of molecular testing are summarized in detail in Table 2.

Clinical Outcome Highlighting the Potential for Local Recurrence and Distant Metastasis

Forty-three patients (88%) had clinical follow-up data available, with a median follow-up of 61.2 months (range: 7 to 192 mo). Nine patients developed local recurrence, with multiple recurrences in 2 of the patients between 12 and 36 months after initial surgery. Six patients in our cohort died, 3 of them at 24, 42, and 50 months after primary surgery due to metastatic disease with multiple distant metastases to lymph nodes, bones, and lungs, whereas the remaining 3 patients died of other unrelated causes with no evidence of tumor. Three patients are alive with recurrent or residual disease at 48, 60, and 187 months of follow-up. The remaining 34 patients were disease and recurrence free at the last contact, with a median follow-up of 45 months after primary diagnosis (range: 7 to 192 mo). Follow-up was unavailable in 6 cases. No patient has received treatment with TRK inhibitors so far.

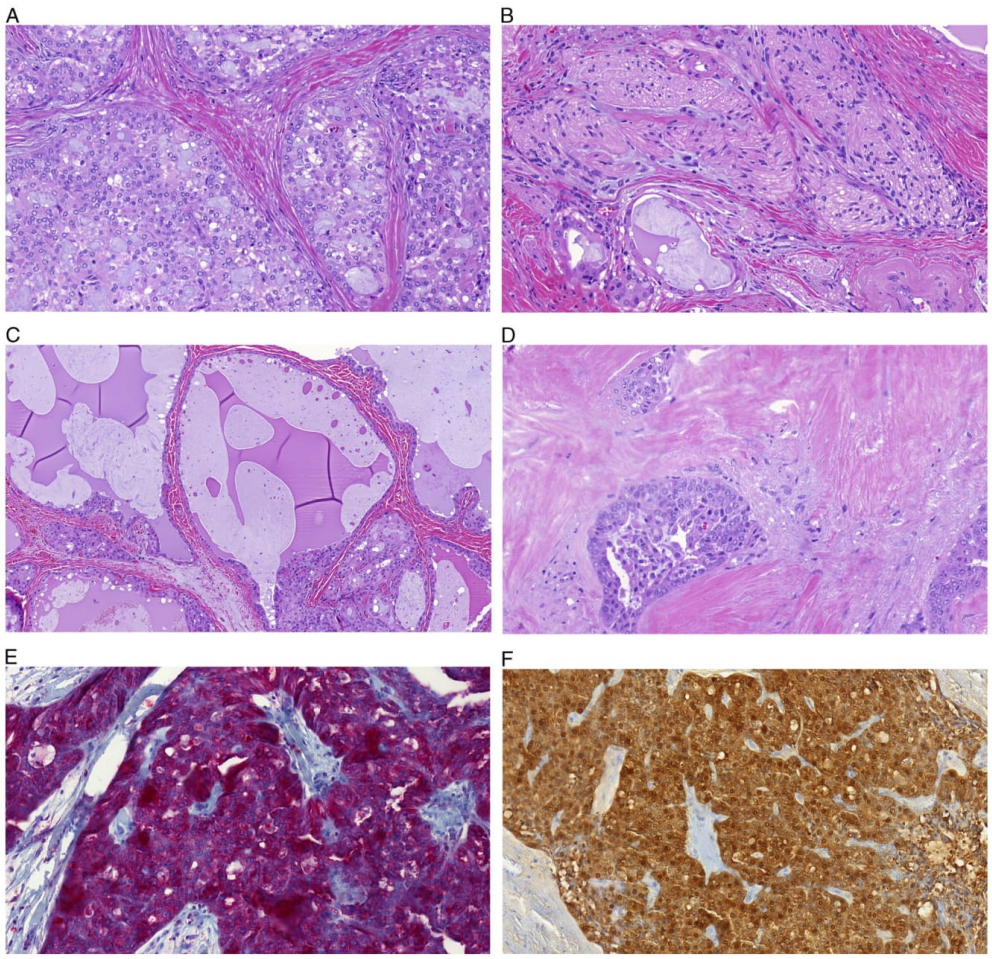

FIGURE 3. SC with *VIM-RET* fusion. A, SC of the parotid gland characterized by solid and microcystic growth. Thin fibrous septa separate the tumor into multiple nodules. B, Perineurial growth was noted. C, Some areas showed macrocystic transformation. The cystic spaces were lined by a single layer of neoplastic cells and contained an eosinophilic material. D, Dense hyalinization with isolated tumor cell nests was present in some areas. Tumor cells were diffusely positive for MMG (E) and S100 protein (F).

Index Case 1: Salivary SC With a Novel VIM-RET Fusion

A 56-year-old woman presented with a slowly growing mass in the parotid gland. Superficial parotidectomy was performed and the tumor was removed completely with free surgical margins. The patient refused any additional treatment. Twenty months after surgery, the patient is well, without clinical or radiologic signs of tumor recurrence.

Index Case 2: Salivary SC With Dual ETV6-NTRK3 and Novel MYB-SMR3B Fusions

A 61-year-old man presented with a recurrent tumor of the right submandibular gland measuring 1.9×1.5×1.0 cm. The affected salivary gland was resected and the patient underwent 35 rounds of radiotherapy. Four years later, the patient developed a tumor recurrence in the adjacent tissues in the right side of the neck. Lymph node dissection was performed and a single metastatic lymph

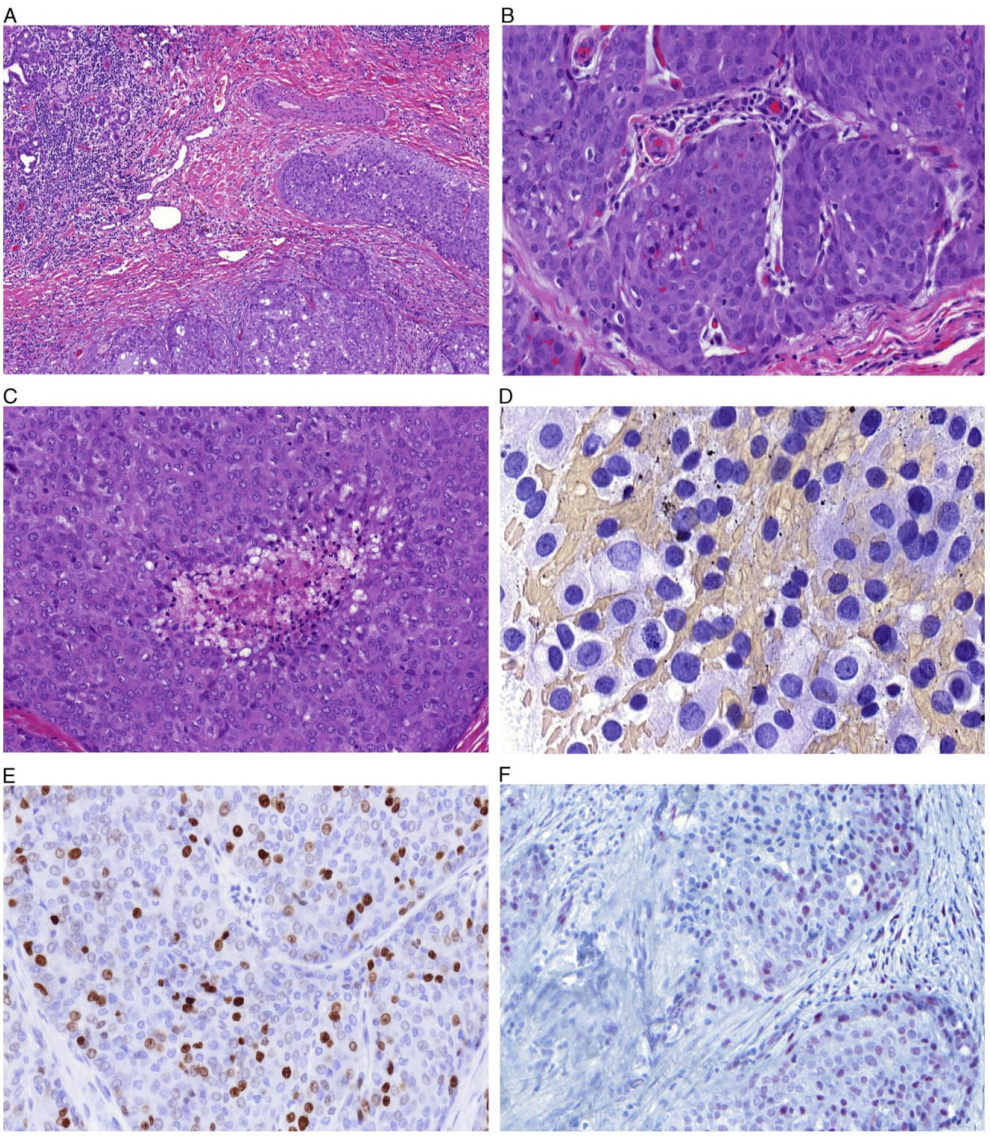

AQ6 **FIGURE 4.** SC with dual *ETV6-NTRK3* and *MYB-SMR3B*. A, SC of the submandibular gland showed multifocal and widely invasive growth into the residual normal glandular structures. B, Hyalinization and sclerotic areas were prominent and separated the areas of low-grade tumor cells (black star) with minimal residual secretory activity from HG areas (black arrowhead) composed of isolated tumor nests surrounded by a desmoplastic stroma. C, Comedo-like necrosis was present. D, Cytology preparation (PAP stain) featured a pleomorphic cell population with nuclear grooves, prominent nucleoli, and occasionally mitoses (red arrowhead). E, MIB 1 index (Ki-67) was 40%. F, Tumor cells were positive with the MYB antibody.

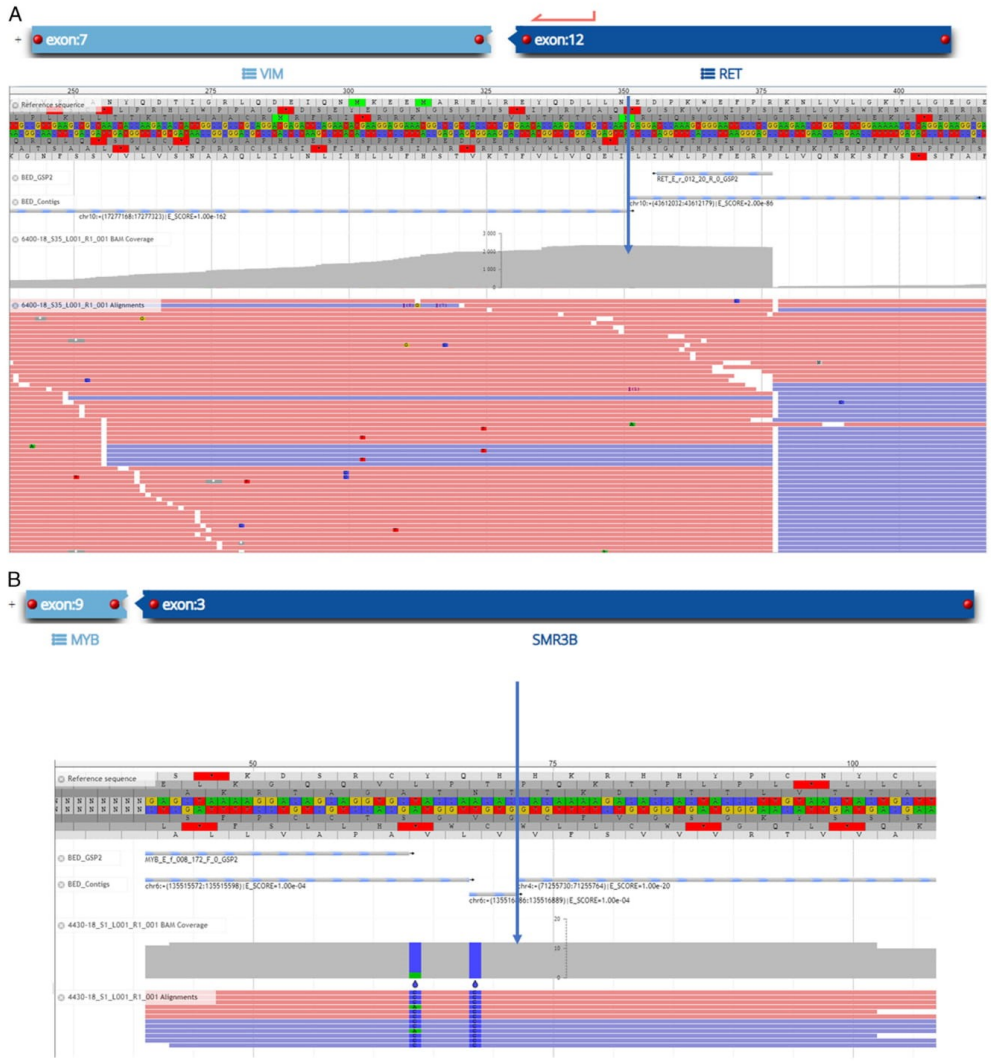

FIGURE 5. Schematic visualization of detected fusion transcripts identified by the ArcherDX assay. A, Fusion involving the VIM exon 7 with RET exon 12is illustrated along with detailed information about exons joining, coverage of studied region, and about the individual reads. The blue arrow shows the exact breakpoint. B, The fusion involving the *MYB* exon 9 with *SMR3B* exon 3 is illustrated along with detailed information about exons joining, coverage of studied region, and about the individual reads. The blue arrow shows the exact breakpoint.

node was found in 41 investigated lymph nodes of the neck. Postoperative positron emission tomography/computed tomography and lung computed tomography scans were negative. Fourteen months later, a new scar nodule was noted, which was confirmed to be recurrent carcinoma.

Index Case 3: SC of Thyroid Gland With ETV6-NTRK3 Fusion

Sections of a 3.0-cm right thyroid lobe mass in a 66-year-old man with a history of prostate adenocarcinoma showed a multilobulated tumor growing in microcystic and

papillocystic patterns within the thyroid. Although no lymphovascular space or perineural invasion was identified, metastatic SC histologically identical to the primary thyroid tumor was identified in 2 ipsilateral level 3 nodes. The metastatic deposits measured about 1.5 cm each, with one of them showing a focal limited extranodal extension about 1.0 mm from the node capsule. There were 25 and 5 separate negative lateral neck and level 6 lymph nodes, respectively. The patient underwent adjuvant radiotherapy, which was completed 3 months after thyroidectomy, and is currently alive, with no evidence of recurrence at 36 months of follow-up.

DISCUSSION

A specific chromosomal translocation t(12;15)(p13; q25) resulting in *ETV6-NTRK3* gene rearrangement was initially considered a distinct molecular signature of SC. However, more recent studies have raised the possibility of alternative *ETV6* partners, first published as SCs with *ETV6-X* gene fusions.[27,28] Subsequently, one such alternative rearrangement in a subset of SC was shown to be an *ETV6-RET* gene fusion.[29] The identification of this novel transcript further expanded the molecular diversity of SC and opened the possibility of integrating targeted *RET* inhibitors as a potential therapeutic strategy.

Although most SCs are slow-growing, low-grade malignancies that can be effectively managed by surgery alone, a small subset of SCs may transform into an aggressively growing HG carcinoma.[34] Moreover, even some SCs with low-grade morphology can present with more aggressive behavior that cannot be managed by surgery alone.[29] SCs with the classic *ETV6-NTRK3* gene fusion are well known to respond to new specific *TRK* tyrosine kinase inhibitors Vitrakvi (larotrectinib) and Rozlytrek (entrectinib) or to the second-generation tyrosine kinase inhibitors selitrectinib (LOXO-195)[35] and repotrectinib.[36] A small subset of SCs reveals, however, alternative fusion partners different from *ETV6-NTRK3*, such as *ETV6-ET*[29] and *VIM-RET* translocation.[37] These *RET*–fusion-positive tumors would obviously be unreactive to all first-generation and second-generation *TRK*-specific inhibitors. There are, however, specific *RET* inhibitors, such as selpercatinib (LOXO-292) and pralsetinib (Blu-667), under development, which are effective in the treatment of *RET*–fusion-positive tumors, and which are expected to be effective with these *RET*–fusion-positive SCs as well.[38]

The initial description of SC included only *ETV6-NTRK3* gene fusions, but since then, other alternative chimeric fusions have been reported such as *ETV6-RET*, *ETV6-MET*, dual *ETV6-NTRK3*, and *ETV6-MAML3*.[29–31] There is no consensus on whether molecular documentation is an absolute requirement to render the diagnosis of SC, especially in the setting of typical cytopathologic and/or light microscopic features in conjunction with diffuse MMG and S100 protein immunoreactivity.[39] Although the current WHO Classification includes *ETV6-NTRK3* fusion in the definition of SC, it does not, however, state that molecular testing is a requirement for a histopathologic diagnosis of salivary gland tumors.[7] Moreover, there are other salivary gland carcinomas characterized by recurrent translocations and gene rearrangements such as intraductal carcinoma (*NCOA4-RET* and *TRIM27-RET*),[40,41] the cribriform variant of polymorphous (low-grade) adenocarcinoma (*PRKD1-3* rearrangements),[42] clear cell carcinoma (*EWSR1-ATF1*),[43] mucoepidermoid carcinoma (*CRTC1-MAML2*),[44,45] and adenoid cystic carcinoma (*MYB-NFIB*),[46] which do not harbor their respective genetic abnormality in 100% of reported cases. However, the molecular confirmation of both fusion partners is a recommended requirement for aggressive cases where targeted therapies are considered.

Until recently, SC cases with an intact *ETV6* gene were viewed with skepticism. As the molecular profile of SC continues to expand, it would be expected that the *ETV6*-negative cases could result from an alternative genetic abnormality. Several *ETV6*-negative cases were reported in a cohort of macrocystic SCs[16] and also in a subset of SC cases with a more aggressive behavior.[47] Moreover, a novel *NFIX-PKN1* gene fusion was reported recently in 1 case of cutaneous SC.[48] From a routine pathology perspective, our present report of the first non-*ETV6* 5′ fusion partner in salivary SC also carries important implications for the choice of a molecular diagnostic technique. Although traditionally, many challenging diagnostic cases were confirmed molecularly using the *ETV6* FISH break-apart probe, our current finding of the *VIM-RET* fusion renders such a negative FISH result inconclusive. Therefore, along with the increasing clinical interest in the recognition of the particular 3′ fusion gene, it further supports the use of NGS sequencing for SCs where molecular confirmation is necessary for therapeutic choices.

The *VIM* gene, located at chromosome 10p13, encodes for vimentin, a ubiquitous intermediate filament protein of mesenchymal cells, which is, however, also present in some epithelia. Along with microtubules and actin microfilaments, intermediate filaments form part of the cytoskeleton of cells. Overexpression of vimentin has been suggested to signal the onset of epithelial-mesenchymal transformation during cancer progression.[49] The *RET* gene encodes for the well-known receptor tyrosine kinase protein. Although translocations involving the *RET* gene are relatively common in many malignancies,[50] its partnership with the *VIM* gene in gene fusions is infrequent. *VIM* fusions were described, however, in hemangioma[51] and prostate cancer.[52] Importantly, in our SC case, the *VIM* gene joins *RET* in a manner that preserves the tyrosine kinase domain, suggesting oncogenic potential for this fusion.

The second novel gene fusion, which is accompanied by the classic *ETV6-NTRK3* fusion, is *MYB-SMR3B*. The *MYB* gene is a transcription factor and, similar to the previously mentioned *RET*, has been implicated in tumorigenesis of many malignancies.[50] In terms of salivary gland tumors, it forms the well-known *MYB-NFIB* fusion in adenoid cystic carcinoma.[53] In contrast, translocations involving the *SMR3B* gene are rare, and, interestingly, the expression of this gene is nearly exclusive for salivary glands. We can speculate that its fusion with *MYB* may play a role in cancer progression and, perhaps, in acquisition of the HG features in this particular tumor case.

In conclusion, the main novel finding in our study is the discovery of a *VIM-RET* fusion in 1 patient with SC of

the parotid gland. Presumably, this patient might benefit from *RET*-targeted therapy. Furthermore, our finding indicates that a negative *ETV6* FISH result does not rule out SC as a diagnostic alternative. In addition, 1 recurrent HG SC was shown to harbor 2 different fusions: *ETV6-NTRK3* and *MYB-SMR3B*. These novel findings extend the molecular spectrum of SC, and provide a novel insight into its oncogenesis. *VIM-RET* fusion also carries important implications for molecular diagnostics as it represents the first SC-associated gene fusion with a non-*ETV6* 5′ fusion partner.

REFERENCES

1. Skalova A, Vanecek T, Sima R, et al. Mammary analogue secretory carcinoma of salivary glands, containing the *ETV6-NTRK3* fusion gene: a hitherto undescribed salivary gland tumor entity. *Am J Surg Pathol*. 2010;34:599–608.
2. Tognon C, Knezevich SR, Huntsman D, et al. Expression of the *ETV6-NTRK3* gene fusion as a primary event in human secretory breast carcinoma. *Cancer Cell*. 2002;2:367–376.
3. Knezevich SR, McFadden DE, Tao W, et al. A novel *ETV6-NTRK3* gene fusion in congenital fibrosarcoma. *Nat Genet*. 1998;18:184–187.
4. Knezevich SR, Garnett MJ, Pysher TJ, et al. ETV6-NTRK3 gene fusions and trisomy 11 establish a histogenetic link between mesoblastic nephroma and congenital fibrosarcoma. *Cancer Res*. 1998;15:5046–5048.
5. Leeman-Neill RJ, Kelly LM, Liu P, et al. *ETV6-NTRK3* is a common chromosomal rearrangement in radiation-associated thyroid cancer. *Cancer*. 2014;120:799–807.
6. Kralik JM, Kranewitter W, Boesmueller H, et al. Characterization of a newly identified *ETV6-NTRK3* fusion transcript in acute myeloid leukemia. *Diagn Pathol*. 2011;6:19.
7. Skalova A, Bell D, Bishop JA, et al. Secretory carcinoma. In: El-Naggar A, Chan JKC, Grandis JR, Takata T, Slootweg PJ, eds. *World Health Organization (WHO) Classification of Head and Neck Tumours*, 4th edition. IARC Press, Lyon, France. 2017:177–178.
8. Skalova A. Mammary analogue secretory carcinoma of salivary gland origin: an update and expanded morphologic and immunohistochemical spectrum of recently described entity. *Head Neck Pathol*. 2013;7:S30–S36.
9. Skalova A, Gnepp DR, Lewis JS Jr, et al. Newly described entities in salivary gland pathology. *Am J Surg Pathol*. 2017;41:e33–e47.
10. Griffith C, Seethala R, Chiosea SI. Mammary analogue secretory carcinoma: a new twist to the diagnostic dilemma of zymogen granule poor acinic cell carcinoma. *Virchows Arch*. 2011;459:117–118.
11. Fehr A, Loning T, Stenman G. Mammary analogue secretory carcinoma of the salivary glands with *ETV6-NTRK3* gene fusion. Letter to the editor. *Am J Surg Pathol*. 2011;35:1600–1602.
12. Connor A, Perez-Ordoñez B, Shago M, et al. Mammary analog secretory carcinoma of salivary gland origin with the *ETV6* gene rearrangement by FISH: expanded morphologic and immunohistochemical spectrum of a recently described entity. *Am J Surg Pathol*. 2012;36:27–34.
13. Majewska H, Skalova A, Stodulski D, et al. Mammary analogue secretory carcinoma of salivary glands: a new entity associated with *ETV6* gene rearrangement. *Virchows Arch*. 2015;466:245–254.
14. Bishop JA. Unmasking MASC: bringing to light the unique morphologic, immunohistochemical and genetic features of the newly recognized mammary analogue secretory carcinoma of salivary glands. *Head Neck Pathol*. 2013;7:35–39.
15. Bishop JA, Yonescu R, Batista D, et al. Most nonparotid "acinic cell carcinomas" represent mammary analog secretory carcinomas. *Am J Surg Pathol*. 2013;37:1053–1057.
16. Hernandez-Prera JC, Holmes BJ, Valentino A, et al. Macrocystic (mammary analogue) secretory carcinoma an unusual variant and a pitfall in the differential diagnosis of cystic lesions in the head and neck. *Am J Surg Pathol*. 2019;43:1483–1492.
17. Bishop JA, Taube JM, Su A, et al. Secretory carcinoma of the skin harboring *ETV6* gene fusions. A cutaneous analogue to secretory carcinomas of the breast and salivary glands. *Am J Surg Pathol*. 2017;41:62–66.
18. Kazakov DV, Hantschke M, Vanecek T, et al. Mammary-type secretory carcinoma of the skin. *Am J Surg Pathol*. 2010;34:1226–1227.
19. Hyrcza MD, Ng T, Crawford RI. Detection of the *ETV6-NTRK3* translocation in cutaneous mamary-analogue secretory carcinoma. *Diagn Histopathol*. 2015;21:481–484.
20. Lurquin E, Jorissen M, Debiec-Rychter M, et al. Mammary analogue secretory carcinoma of the sinus ethmoidalis. *Histopathology*. 2015;67:749–751.
21. Baneckova M, Agaimy A, Andreasen S, et al. Mammary analog secretory carcinoma of the nasal cavity: characterization of 2 cases and their distinction from other low-grade sinonasal adenocarcinomas. *Am J Surg Pathol*. 2018;42:735–743.
22. Xu B, Aryeequaye R, Wang L, et al. Sinonasal secretory carcinoma of salivary gland with high grade transformation: a case report of this under-recognized diagnostic entity with prognostic and therapeutic implications. *Head Neck Pathol*. 2018;12:274–278.
23. Reynolds S, Shaheen M, Olson G, et al. A case of primary mammary analog secretory carcinoma (MASC) of the thyroid masquerading as papillary thyroid carcinoma: potentially more than a one off. *Head Neck Pathol*. 2016;10:405–413.
24. Dettloff J, Seethala RR, Stevens TM, et al. Mammary analog secretory carcinoma (MASC) involving the thyroid gland: a report of the first 3 cases. *Head Neck Pathol*. 2017;11:124–130.
25. Dogan S, Wang L, Ptashkin RN, et al. Mammary analog secretory carcinoma of the thyroid gland: a primary thyroid adenocarcinoma harboring *ETV6-NTRK3* fusion. *Mod Pathol*. 2016;29:985–995.
26. Huang T, McHugh JB, Berry GJ, et al. Primary mammary analogue secretory carcinoma of the lung: a case report. *Hum Pathol*. 2018;74:109–113.
27. Ito Y, Ishibashi K, Masaki A, et al. Mammary analogue secretory carcinoma of salivary glands: a clinicopathological and molecular study including 2 cases harboring *ETV6-X* fusion. *Am J Surg Pathol*. 2015;39:602–610.
28. Skalova A, Vanecek T, Simpson RHW, et al. Mammary analogue secretory carcinoma of salivary glands. Molecular analysis of 25 *ETV6* gene rearranged tumors with lack of detection of classical *ETV6-NTRK3* fusion transcript by standard RT-PCR: report of 4 cases harboring *ETV6-X* gene fusion. *Am J Surg Pathol*. 2016;40:3–13.
29. Skalova A, Vanecek T, Martinek P, et al. Molecular profiling of mammary analogue secretory carcinoma revealed a subset of tumors harboring a novel *ETV6-RET* translocation: report of 10 cases. *Am J Surg Pathol*. 2018;42:234–246.
30. Rooper LM, Karantanos T, Ning Y, et al. Salivary secretory carcinoma with a novel *ETV6-MET* fusion: expanding the molecular spectrum of a recently described entity. *Am J Surg Pathol*. 2018;42:1121–1126.
31. Guilmette J, Dias-Santagata D, Nose V, et al. Novel gene fusions in secretory carcinoma of the salivary glands: enlarging the *ETV6* family. *Hum Pathol*. 2019;83:50–58.
32. Miesbauerová M, Tommola S, Šteiner P, et al. Cytopathological features of secretory carcinoma of salivary glands and ancillary techniques in its diagnostics: impact of new Milan system for reporting salivary gland cytopathology. *APMIS*. 2019;127:491–502.
33. Stevens TM, Kovalovsky AO, Velosa C, et al. Mammary analog secretory carcinoma, low-grade salivary duct carcinoma, and mimickers: a comparative study. *Mod Pathol*. 2015;28:1084–1100.
34. Skalova A, Vanecek T, Majewska H, et al. Mammary analogue secretory carcinoma of salivary glands with high grade transformation: report of three cases with the *ETV6-NTRK3* gene fusion and analysis of TP53, beta-catenin, EGFR and CCND1 genes. *Am J Surg Pathol*. 2017;38:23–33.
35. Kummar S, Lassen UN. TRK inhibition: a new tumor agnostic treatment strategy. *Targeted Oncology*. 2018;13:545–556.
36. Drilon A. TRK inhibitors in TRK fusion-positive cancers. *Ann Oncol*. 2019;30(suppl 8):viii23–viii30.
37. Skalova A, Santana Conceição T, Vanecek T, et al. Salivary secretory carcinoma with a novel *VIM-RET* fusion: NGS based molecular profiling of 49 cases revealed an expanding molecular spectrum of a recently described entity United State & Canadian Academy of Pathology Annual Meeting 2019/03/01. *Mod Pathol*. 2019;32:1–59.
38. Li AY, McCusker MG, Russo A, et al. *RET* fusions in solid tumors. *Cancer Treat Rev*. 2019;81:101911.

39. Shah AA, Wenig BM, LeGallo RD, et al. Morphology in conjunction with immunohistochemistry is sufficient for the diagnosis of mammary analogue secretory carcinoma. *Head Neck Pathol*. 2015;9:85–95.
40. Skálová A, Ptáková N, Santana T, et al. *NCOA4-RET* and *TRIM27-RET* are characteristic gene fusions in salivary intraductal carcinoma, including invasive and metastatic tumors. is "intraductal" correct? *Am J Surg Pathol*. 2019;43:1303–1313.
41. Skalova A, Vanecek T, Uro-Coste E, et al. Molecular profiling of salivary gland intraductal carcinoma revealed a subset of tumors harboring *NCOA4-RET* and novel *TRIM27-RET* fusions: a report of 17 cases. *Am J Surg Pathol*. 2018;42:1445–1455.
42. Weinreb I, Zhang L, Tirunagari LM, et al. Novel *PRKD* gene rearrangements and variant fusions in cribriform adenocarcinoma of salivary gland origin. *Genes Chromosomes Cancer*. 2014;53:845–856.
43. Antonescu CR, Katabi N, Zhang L, et al. *EWSR1-ATF1* fusion is a novel and consistent finding in hyalinizing clear-cell carcinoma of salivary gland. *Genes Chromosomes Cancer*. 2011;50:559–570.
44. Seethala RR, Dacic S, Cieply K, et al. A reappraisal of the *MECT1/MAML2* translocation in salivary mucoepidermoid carcinomas. *Am J Surg Pathol*. 2010;34:1106–1121.
45. Jee KJ, Persson M, Heikinheimo K, et al. Genomic profiles and *CRTC1-MAML2* fusion distinguish different subtypes of mucoepidermoid carcinoma. *Mod Pathol*. 2013;26:213–222.
46. Brill LB II, Kanner WA, Fehr A, et al. Analysis of *MYB* expression and *MYB-NFIB* gene fusions in adenoid cystic carcinoma and other salivary neoplasms. *Mod Pathol*. 2011;24:1169–1176.
47. Na K, Hernandez-Prera JC, Lim JY, et al. Characterization of novel genetic alterations in salivary gland secretory carcinoma. *Mod Pathol*. 2020;33:541–550.
48. Kastnerova L, Luzar B, Goto K, et al. Secretory carcinoma of the skin report of 6 cases, including a case with a novel *NFIX-PKN1* translocation. *Am J Surg Pathol*. 2019;43:1092–1098.
49. Satelli A, Li S. Vimentin in cancer and its potential as a molecular target for cancer therapy. *Cell Mol Life Sci*. 2011;68:3033–3046.
50. Kato S, Subbiah V, Marchlik E, et al. RET aberrations in diverse cancers: next-generation sequencing of 4871 patients. *Clin Cancer Res*. 2017;23:1988–1997.
51. Huang SC, Zhang L, Sung YS, et al. Frequent FOS gene rearrangements in epithelioid hemangioma: a molecular study of 58 cases with morphologic reappraisal. *Am J Surg Pathol*. 2015;39:1313–1321.
52. Ma Y, Miao Y, Peng Z, et al. Identification of mutations, gene expression changes and fusion transcripts by whole transcriptome RNAseq in docetaxel resistant prostate cancer cells [published correction appears in Springerplus. 2016 Dec 8;5(1):2084]. *Springerplus*. 2016;5:1861.
53. Stenman G, Andersson MK, Andren Y. New tricks from an old oncogene: gene fusion and copy number alterations of *MYB* in human cancer. *Cell Cycle*. 2010;9:2986–2995.

1.10.5 CYTOPATOLOGICKÉ ZNAKY SEKREČNÍHO KARCINOMU SLINNÝCH ŽLÁZ A POMOCNÉ TECHNIKY V DIAGNOSTICE: DOPAD NOVÉHO MILÁNSKÉHO SYSTÉMU NA REPORTOVÁNÍ CYTOPATOLOGIE SLINNÝCH ŽLÁZ

Poslední přiložená práce zabývající se problematikou SC se zaměřuje na jeho cytodiagnostiku s použitím nového Milánského klasifikačního systému reportování cytologií slinných žláz. Práce je zaměřená na roli cytologie v diagnostickém algoritmu pacientů s lézemi slinných žláz. Tenkojehlová aspirační cytologie (FNAC) je vnímána jako primární diagnostický test vhodný k předběžnému zhodnocení léze a následnému určení nejlepší možné terapie. V mnoha případech lze dobře rozlišit benigní nádory, jako je Warthinův tumor či pleomorfní (78). Dále lze s přijatelnou mírou specificity odlišit low-grade a high-grade karcinomy, které vyžadují elektivní řešení, kdy i s přispěním FNAC lze vybrat vhodnou operační techniku a v určitých případech rozhodnout i o míře radikality.

Studie se zabývá FNAC 6 případů SC, u kterých byla diagnóza SC posléze histologicky, imunocytochemicky (ICC) a molekulárně-geneticky potvrzena biopsií. Všechny aspiráty byly dostatečně celulární a buňky vytvářely více či méně kohezivní skupinky se středním stupněm jaderného polymorfismu. Cytoplazma byla eozinofilní, granulární a vakuolizovaná a to zejména v materiálu z cytobloku. Sekreční materiál byl pozitivní v barvení periodic acid-Shiff a jádra vykazovala pozitivní expresi S100 proteinu a mammaglobinu. Proliferační aktivita byla nízká.

Pro účely molekulární genetiky byl ve 4 případech dostupný cytoblok. Ve 3 případech metoda FISH prokázala zlom genu *ETV6* a v 1 případě byl materiál neanalyzovatelný pro nízkou vstupní kvalitu DNA. *NTRK3* fúzní partner byl potvrzený pouze ve 2 případech *ETV6* rearanžovaných SC. Ve zbylých případech, kde cytoblok nebyl dostupný nebo se jednalo o neanalyzovatelný materiál, byla zastižena translokace *ETV6-NTRK3* až ve finálním histologickém vzorku za použití metody NGS.

Kategorizace SC dle Milánského systému (MS) záleží na dostupnosti dalších vyšetření a na dostatečném množství materiálu. Pokud máme pouze nátěr na sklech, je téměř nemožné se snažit o přesnou cytologickou diagnózu a FNAC by měla být kategorizována jako „Salivární nádory s nejistým maligním potenciálem“ (79). Pokud však máme dostupný cytoblok či jiný materiál, lze doplnit cytologii o ICC. Pozitivita ICC markerů S100 proteinu, mammaglobinu a SOX10 a negativní exprese DOG1 (vylučující acinický karcinom) a p63 vytváří dohromady sadu optimálních ICC markerů, které lze aplikovat v případě suspektního SC. Máme-li k dispozici navíc ještě molekulárně genetické metody, můžeme ICC podpořit o detekci *ETV6* zlomu. Pokud však genetické metody nelze využít a jsou-li k dispozici pouze ICC výsledky, měly bychom tumor zařadit do kategorie dle MS „Suspektní z malignity“.

SC je cytologicky i histologicky obtížná jednotka pro překryv s jinými nádory slinných žláz. Klíčovým cytomorfologickým znakem, který by měl v cytologii vzbudit podezření na SC, je papilární uspořádání a jemně granulární cytoplasma buněk. Přesná cytologická diagnóza však vyžaduje další pomocná vyšetření, a to ICC či molekulárně genetické metody.

APMIS JOURNAL OF PATHOLOGY, MICROBIOLOGY AND IMMUNOLOGY

APMIS 127: 491–502

DOI 10.1111/apm.12950

Cytopathological features of secretory carcinoma of salivary glands and ancillary techniques in its diagnostics: impact of new Milan system for reporting salivary gland cytopathology

MARKÉTA MIESBAUEROVÁ,[1,2] SATU TOMMOLA,[3] PETR ŠTEINER,[4] MARTINA BANĚČKOVÁ,[1,2] ALENA SKÁLOVÁ[1,2] and IVANA KHOLOVÁ[3,5]

[1]Department of Pathology, Faculty of Medicine in Plzeň, Charles University, Plzeň; [2]Bioptic Laboratory, Ltd, Plzeň 2-Slovany, Czech Republic; [3]Department of Pathology, Fimlab Laboratories, Tampere, Finland; [4]Molecular Pathology Laboratory, Bioptic Laboratory, Ltd, Plzeň 2-Slovany, Czech Republic; and [5]Department of Pathology, Faculty of Medicine and Health Technology, Tampere University, Tampere, Finland

Miesbauerová M, Tommola S, Šteiner P, Baněčková M, Skálová A, Kholová I. Cytopathological features of secretory carcinoma of salivary glands and ancillary techniques in its diagnostics: impact of new Milan system for reporting salivary gland cytopathology. APMIS 2019; 127: 491–502.

Secretory carcinoma (SC) of salivary glands is a newly described low-grade malignancy characterized by the presence of *ETV6* rearrangement. Only a few cases and very small series with cytomorphology were reported so far. Six cases of fine-needle aspirations (FNAs) from afterward histologically, immunohistochemically and genetically confirmed SCs were retrieved from the archives of the authors. Ancillary immunocytochemistry (ICC) and translocation detection were performed on cell blocks (CBs). All aspirates were sufficiently cellular and cells were arranged in more or less cohesive groups with only mild nuclear polymorphism. The cytoplasm was eosinophilic, granulated and vacuolated, especially in CBs. Secretory material within the microcystic spaces was periodic acid-Schiff (PAS) positive. Triple positivity of immunomarkers S-100 protein, mammaglobin and vimentin was present. The proliferation index was low. Ancillary techniques suggested the possibility of SC in a few cytology cases; nevertheless, the final diagnosis was based on histomorphology, immunohistochemistry and genetics. The SC of salivary glands is detectable pre-operatively using ICC and genetics. The presence of the diagnostic *ETV6* rearrangement increases the accuracy of FNA to the maximum. According to the Milan system, cases genetically not confirmed should be categorized as Suspicious for Malignancy or Salivary Gland Neoplasm of Uncertain Malignant Potential (SUMP), both requiring surgery.

Key words: Salivary glands; secretory carcinoma; *ETV6*; FNA; Milan system; mammary analog secretory carcinoma.

Ivana Kholová, Department of Pathology, Fimlab Laboratories, PO Box 66, FIN 331 01 Tampere, Finland. e-mail: ivana.kholova@tuni.fi

The secretory carcinoma (SC) of salivary glands, originally described as mammary analog secretory carcinoma (MASC) by Skálová et al. in 2010 (1), is a low-grade malignancy included in the 4th edition of World Health Organization Classification of Head and Neck Tumours in 2017 under designation "secretory carcinoma" (2). As the original name implies, there is histomorphological, immunophenotypical and genetical resemblance to the secretory carcinoma of the breast, which also harbors the same genetic translocation t(12; 15)(p13;q25) resulting in *ETV6-NTRK3* gene fusion (1, 3). This specific fusion is confirmatory for SC and has not been reported in any other salivary gland tumors yet. New rearrangements *ETV6-RET* (4) and *ETV6-MET* (5) have been recently found in small subset of SCs, possibly associated with more aggressive behavior.

Most SCs occur in the parotid gland, followed by the submandibular gland and the minor salivary

Received 9 August 2018. Accepted 22 March 2019

Table 1. Summary of clinicopathological features of presented cases

Case	Age/sex	Clinical symptoms	Localization	Original cytopatho-logical diagnosis	Original histopatho-logical diagnosis	Histopathological features	Immunohis tochemistry
1	56/F	Mass 2.7 cm in max. diameter	Left parotid gland	PAP Class III – atypia, suspicious for malignancy	Secretory carcinoma	Infiltrative growth with hyalinization of the stroma. Tubular and cribriform structures with PAS-positive secretory material. Round to oval vesicular nuclei with prominent nucleoli. Pale abundant cytoplasm with vacuoles	CK7+, S100+, MGA+, p63−, CKPan+, vimentin+, EMA+, SMA−, AR−, calponin−, GCDFP15−, MIB1 6% PAS+ secretory material within the tubular spaces
2	72/F	Mass 3.4 cm in max. diameter	Right parotid gland	Neoplasm (cellular PA, myoep-ithelioma)	Secretory carcinoma	Encapsulated uninodular tumor with hyalinized thick capsule and multiple septa. Tubular structures with colloid-like secretory material. Eosinophilic abundant cytoplasm with vacuoles containing eosinophilic material	CK7+, S100+, MGA+, p63−, vimentin+, EMA+, SMA−, GCDFP15−, DOG1 focally+, MIB1 5–8% PAS+ secretory material within the tubular spaces
3	34/M	Mass 1 cm in max. diameter	Right sub-mandibular gland	PAP Class III – atypia, suspicious for malignancy (low-grade malignancy, PA, myoepithelioma, basal cell adenoma)	Polymorphous low-grade adeno-carcinoma or low-grade salivary duct carcinoma	Infiltrative multinodular growth with hyalinized septa. Tubular and pseudoglandular structures with PAS-positive secretory material. Vesicular nuclei. Pale abundant finely granulated cytoplasm with oncocytic features and focal vacuoles. Perineural invasion	CK7+, S100+, MGA+, p63−, CKPan+, vimentin+, EMA+, GCDFP15−, AR−, calponin−, MIB1 5% PAS+ secretory material within the microcystic spaces
4	47/M	Mass 1.9 cm in max. diameter	Left parotid gland	2 FNAs performed: (1) PAP Class II –	None – consultation	Infiltrative multinodular growth with septa containing	CK7+, S100+, MGA+, p63−, vimentin+, EMA+,

Table 1. *(continued)*

Case	Age/sex	Clinical symptoms	Localization	Original cytopathological diagnosis	Original histopathological diagnosis	Histopathological features	Immunohistochemistry
				adenoma, oncocytoma (2) PAP Class III – atypia, suspicious for malignancy		sparse lymphoid stroma. Pseudoglandular, macrocystic and focally tubular cell arrangement. Pale abundant finely granulated cytoplasm with oncocytic features and focal vacuoles. Perineural invasion	SMA−, AR−, MIB1 10% PAS+ secretory material within the cystic spaces
5	37/M	Mass 1.7 cm in max. diameter	Right parotid gland	PAP Class III – atypia, suspicious for malignancy (AciCC, SC)	Secretory carcinoma	Encapsulated uninodular tumor with capsule without septation. Microcystic to cystic structures with thyroid follicle-like arrangement with colloid-like material within. Foamy and vacuolated cytoplasm with clear cell appearance. Perineural invasion	CK7+, S100+, MGA+, p63 focally+, vimentin+, EMA+, GCDFP15−, DOG1−, MIB1 5–10% PAS+ secretory material within the cystic spaces
6	20/M	Mass 4 cm in max. diam., deficit of the facial nerve	Left parotid gland	Monomorphic adenoma	Low-grade cystadenocarcinoma with intranodal metastases	Cystic tumor with fibrous capsule and multiple small tumorous satellites beyond. The lining is composed of uniform, flattened and focally papillary formed cells	CK7+, S100+, MGA+, GATA3−, p63−, calponin−, CD31−, podoplanin−

F, female; M, male; PAP Class, Papanicolaou classification system; FNA, fine-needle aspiration; PA, pleomorphic adenoma; AciCC, acinic cell carcinoma; SC, secretory carcinoma; PAS-positive, periodic acid-Schiff-positive.

glands. Some extrasalivary tumors in the head and neck area contain *ETV6-NTRK3* translocation as well (6–8). Before the discovery of SC in 2010, these tumors were diagnosed as an unusual variant of acinic cell carcinoma (AciCC) poor of zymogen granules, mucoepidermoid carcinoma or as adenocarcinomas not otherwise specified (ADCs NOS) (1). Histologically, the SC consists of uniform eosinophilic cells with vacuolated cytoplasm arranged in cystic, tubular, solid or papillary patterns. The cystic spaces are characteristically filled by periodic acid-Schiff (PAS)-positive secretory

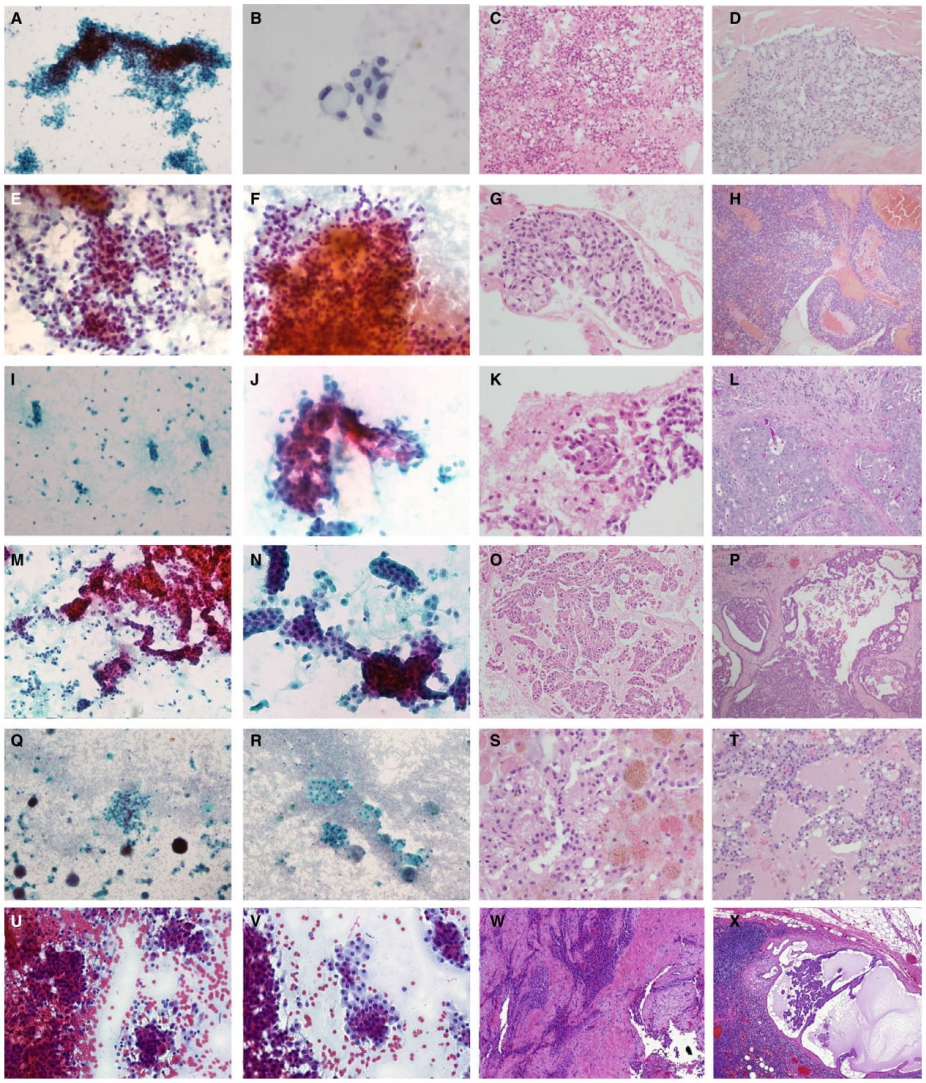

material. More than 200 articles on SC have been published so far, but very few are dedicated to the description of the cytomorphological features (9–23).

For decades, the reporting of salivary gland cytology has been full of confusions and diversity with the use of descriptive reports with no categories or with surgical pathology terminology. The development of a brand new uniform system for reporting salivary gland fine-needle aspirations (FNAs) has been highly required. The Milan

Fig. 1. Cytological and histological features of the series of secretory carcinoma (SC) (A–D Case 1, E–H Case 2, I–L Case 3, M–P Case 4, Q–T, Case 5, U–X Case 6). (A) Papillary arranged cohesive cluster of uniform cells (Papanicolaou, ×100). (B) Cell group with prominent signet-ring cell nuclei which are uniformly oval (Papanicolaou, ×400). (C) Cribriform and solid arrangement has been seen in the cell block (CB) of this case (hematoxylin-eosin, ×100). (D) Tubular to cribriform nest is surrounded by a hyalinized stroma. Homogeneous secretory material is visible within the tubular spaces (hematoxylin-eosin, ×100). (E) Peripherally loosely cohesive groups of uniform cells with mucinous-like material (Papanicolaou, ×200). (F) Peripherally loosely cohesive groups of uniform cells with hemorrhagic background (Papanicolaou, ×200). (G) Tubular and cribriform fragment composed of uniform cells with vacuolated cytoplasm and occasional signet-ring cells, within the tubular structures colloid-like secretory material is present in the CB (hematoxylin-eosin, ×200). (H) Tubular arrangement with colloid-like secretory material within the tubular and cystic spaces with the admixture of blood (hematoxylin-eosin, ×40). (I) Small cohesive clusters and singly dispersed cells in the scantly mucinous-like background (Papanicolaou, ×100). (J) Loosely cohesive, papillary arranged cell group with transgressing vessels (Papanicolaou, ×200). (K) Pseudoglandular fragments with striking squamoid-like appearance in CB. Nuclei are hyperchromatic and cytoplasm is finely granulated (hematoxylin-eosin, ×200). (L) Tubular and pseudoglandular structures with PAS-positive secretory material within the tubular and microcystic spaces, perineural invasion is seen (periodic acid-Schiff, ×100). (M) Papillary and trabecular cohesive clusters with dispersed cells on the mucinous-like background (Papanicolaou, ×100). (N) Cohesive papillary and trabecular structures with transgressing vessels (Papanicolaou, ×200). (O) Distinct papillae are covered by cylindric uniform cells with rich eosinophilic cytoplasm with focal vacuolization (hematoxylin-eosin, ×40). (P) Multinodular growth with pseudoglandular, macrocystic and focally tubular cell arrangement. The presence of secretory material within the cystic spaces is noted (hematoxylin-eosin, ×40). (Q) Loosely cohesive cell group with abundant cytoplasm, singly dispersed cells with macrophages and siderophages on the cystic background (Papanicolaou, ×100). (R) Loosely cohesive trabecular cell group with abundant cytoplasm, singly dispersed cells with macrophages on the cystic background (Papanicolaou, ×100). (S) Solid arrangement of uniform cells with eosinophilic, vacuolated and focally bubbled cytoplasm, siderophages are seen in the right side of the image (hematoxylin-eosin, × 200). (T) cystic structures with follicle-like arrangement and colloid-like material within. Note the foamy and vacuolated cytoplasm with clear cell appearance (hematoxylin-eosin, ×100). (U) Peripherally loosely cohesive clusters with hemorrhagic background (Papanicolaou, ×250). (V) Peripherally loosely cohesive clusters on the hemorrhagic background (Papanicolaou, ×180). (W) The histology of cystic tumor with fibrous capsule and mild hemorrhage. The cells are uniform, flattened and focally papillary arranged (hematoxylin-eosin, ×100). (X) Intraglandular lymph node with a cystic metastasis of SC (hematoxylin-eosin, ×50).

System for Reporting Salivary Gland Cytology (MSRSGC) follows the trend of thyroid cytopathology and cervical cytology Bethesda and urinary cytopathology Paris reporting systems where each category has a defined risk of malignancy (ROM) and suggested therapeutic approaches (24).

In our study, we present six cases of SCs of salivary glands that were pre-operatively examined by fine-needle aspiration (FNA), ancillary techniques, and retrospectively classified according to the MSRSGC. We suggest the appropriate approach to cytological diagnosis of SC using ancillary techniques. The MSRSGC categorization is important in order to improve the communication and understanding between the cytopathologists and clinicians and to stratify ROM.

MATERIALS AND METHODS

The series consists of six cases of histologically confirmed SCs with available FNA. Five cases were retrieved from the archive and consultation files of the Department of Pathology, Fimlab Laboratories, Tampere, Finland within a 5-year period (November 2011–December 2016) (IK, ST) and one case from the Salivary gland tumor registry of the Department of Pathology, Faculty of Medicine in Plzen and Biopticka Laboratory Ltd, Plzen, Czech Republic (AS). Clinical, cytomorphological, histomorphological and immunohistochemical (IHC) data were reviewed in all cases. The FNA has been performed with a 22G needle under ultrasound guidance by the clinician. The aspirated material has been routinely processed: alcohol fixed and Papanicolaou stained. Four-μm-thick sections were cut from CBs and stained with hematoxylin-eosin and PAS with and without diastase. Ancillary immunocytochemical (ICC) studies were performed on 2-μm-thick sections with the following primary antibodies: S-100 protein (polyclonal, dilution 1:5000, Ventana Medical System, Tucson, AZ, USA), mammaglobin (clone 31A5, ready-to-use , Ventana Medical System), vimentin (clone V9, ready-to-use, Ventana Medical System) and Ki-67 (clone 30-9, ready-to-use, Ventana Medical System). Appropriate positive controls were used. The same laboratory procedure has been performed also on formalin-fixed, paraffin-embedded surgically removed specimens. Cases with available residual CB material underwent genetic examination for the detection of *ETV6* and *NTRK3* rearrangements by fluorescent *in situ* hybridization (FISH) using break-apart probes. *ETV6-NTRK3* fusion transcript has been subsequently confirmed by reverse transcription polymerase chain reaction (RT-PCR) and Next Generation Sequencing (NGS) (1).

All procedures were performed in accordance with ethical standards of responsible Ethical Committee and with Declaration of Helsinki (1975, revised 1983). After approval by the Ethical Committee, informed consent of each individual was not requested.

RESULTS

The studied cohort consisted of four males and two females aged from 20 to 76 years (mean 44.3 years). All patients presented with a palpable

mass of various sizes (from 1 to 4 cm in diameter). Five tumors (83.3%) were localized in the parotid gland and one case (Case 3) in the submandibular gland. In all cases, FNA was followed by surgical removal of the lesion and histological and immunohistochemical examination. Clinical and demographic data are summarized in Table 1.

Cytomorphological features and ICC

Total of seven FNAs were taken from six cases, with FNA performed twice in Case 4. In four out of six cases, the Papanicolaou classification was used for the evaluation of FNA. PAP Class III category (atypia, suspicious for malignancy) was suggested in all four cases (Cases 1, 3, 4 and 5), where the Papanicolaou classification was applied and a wide spectrum of probable benign neoplasms was listed: pleomorphic adenoma, myoepithelioma and basal cell adenoma. Only once (Case 5), a suspicion for SC or AciCC was raised. The FNA in Case 4 was performed twice with two different conclusions: the first FNA was evaluated as PAP Class II category (adenoma or oncocytoma) and the second FNA was evaluated as PAP Class III category (atypia, suspicious for malignancy). Two cases, where no classification system was used (Cases 2 and 6), were evaluated as benign neoplasms with suggested diagnoses of pleomorphic adenoma or myoepithelioma (Case 2) and monomorphic adenoma (Case 6) (Table 1).

Despite the variable morphology of SC, all six cases had several common cytological features in FNA cytology. The cellularity of all smears was highly satisfactory. Cells were arranged in variably cohesive clusters or sheets of different sizes. Single dispersed cells were always present. Papillary structures with transgressing vessels were commonly seen. In Cases 1 and 2, a cribriform pattern was featured. The background was diverse, ranging from a clear background with mucinous material (Cases 1, 3, 4) to hemorrhagic (Cases 2, 6) and cystic (Case 5). The cytoplasm was variable in all cases. Except in Case 2, where the amount of cytoplasm was scant, the cytoplasm was abundant and finely granulated. In Cases 1, 4, 5 and 6, also vacuoles were present. Occasional signet-ring cells were found in Cases 1 and 4. Nuclei were either uniform, round to oval or mildly polymorphic. No mitoses were seen. In Case 5, the vacuolization of the nucleus was present. In Case 2, the nuclei were peripherally placed and gave the impression of myoepithelial differentiation. Furthermore, the nuclei were focally spindle shaped in Case 1. Chromatin was finely granulated and nucleoli were well discernible. Doubled nuclei were observed in Cases 3 and 4 (Fig. 1A,B,E,F,I,J,M,N,Q,R,U,V).

The CBs were available in five cases (Cases 1–5) and the morphological features of CB samples are summarized in Table 2. Compared to the cytotech specimens, the architecture of tissue fragments is better appreciated in CBs. It varied from cribriform, almost pseudoglandular arrangements to solid nests. The variability was visible, even within the single sample. Nuclear features were comparable to the findings in smears, but in the CBs the cytoplasmic features were easier to evaluate. Vacuolization with focal signet-ring cells was pronounced (Fig. 1G,S). In Case 2, the cytoplasmic vacuoles contained colloid-like substance (Fig. 1G). In Cases 3, 4 and 5, the cytoplasm was eosinophilic with oncocytic features. In Case 3, squamoid-like areas were seen (Fig. 1K). Only in Case 5, multiple siderophages and extracellular hemosiderin were present (Fig. 1S).

Ancillary techniques were performed on the CB material. The panel of PAS and four basic immunomarkers (S-100 protein, mammaglobin, vimentin and proliferation index) was positive in all cases except Case 5, where S100 could not be evaluated because of insufficient material in the CB (Fig. 2). PAS was positive in the secretory material within microcystic spaces and tubular or cribriform structures in all five cases (Fig. 1L). The proliferation index (MIB1/Ki-67) was low, less than 5% in all cases.

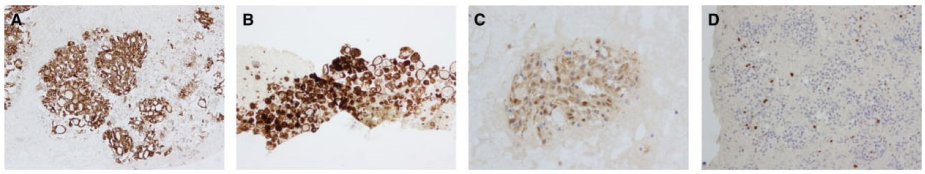

Fig. 2. Immunohistochemical panel demonstrating the triple positivity and proliferation index in secretory carcinomas (SCs). (A) Mammaglobin immunopositivity in cytoplasm (Case 1, ×100). (B) Vimentin nuclear immunopositivity (Case 5, ×100). (C) S-100 protein nuclear immunopositivity (Case 2, ×200). (D) Proliferation index is low, less than 5% (case 1, Ki-67, ×100).

Table 2. Cytomorphological features of presented cases in smears and in cell blocks

	Cellularity	Cell growth arrangement in smears	Background in smears	Nuclei in smears	Cytoplasm in smears	Cell growth arrangement in CBs	Nuclei in CBs	Cytoplasm in CBs	ICC in CBs
1	Rich	Cohesive clusters and cell groups of various sizes with papillary, trabecular and too less extent cribriform architecture. Singly dispersed cells.	Almost clear with very rare mucin-like secretory material	Mild polymorphism Irregularly placed Round to oval, rarely spindle shaped Variably rarely prominent nucleoli Finely granulated chromatin Occasionally binucleation	Abundant Finely granulated Focally vacuolated Occasional signet-ring cells	Solid, cribriform and occasionally pseudog-landular	Mild polymor-phism Irregularly placed Oval Focally vesicular with rare nucleation Focally prominent reddish nucleoli Finely granulated chromatin	Abundant, eosinophilic Finely granulated Small vacuoles Occasionally signet-ring cells	CK7+, S100+, MGA+, CKPan+, vimentin+, EMA+, SMA+ MIB1 3% PAS+
2	Moderate	Peripherally loosely cohesive sheets and large tissue fragments with papillary and occasionally cribriform structures with mucinous-like material intraluminally. Singly dispersed cells.	Hemorrhagic/ mucin-like secretory material	Uniform Peripherally placed (myoepithelial-like) Round to oval Hyperchromatic Inconspicuous nucleoli Finely granulated chromatin	Finely granulated Few	Tubular and cribriform	Mild polymor-phism Focally myoepithelial-like shaped Prominent nucleoli Finely granulated chromatin	Abundant, eosinophilic Vacuolated even grape-like and signet-ring cells, some containing colloid-like material	CK7+, S100+, p63−, EMA−, SMA+, AR−, CK5/6−, GFAP−, CEA+, DOG1+, CD117+ MIB1 low PAS+
3	Rich in both smears	Small cohesive mainly spherical clusters/loosely cohesive tubular and papillary structures with transgressing vessels. Singly dispersed cells	Clear/mucin-like secretory material	Uniform Centrally placed Round to oval bland Prominent nucleoli, focally doubled Hyperchromatic Occasionally binucleation	Polymor-phous Abundant Finely granular	Pseudog-landular	Uniform Centrally placed Round to oval Focally hyperchromatic, focally vesicular Prominent nucleoli	Abundant, eosinophilic Small multiple vacuoles Occasionally squamoid-like appearance	CK7+, S100+, MGA+, vimentin+ MIB1 < 5%
4	Rich	Small spherical cohesive clusters focally arranged in bigger papillary and trabecular structures with transgressing vessels and almost pseudoglandular structures. Singly dispersed cells	Mucin-like secretory material	Uniform Centrally placed Round Pinpoint nucleoli occasionally doubled Finely granulated chromatin	Abundant Finely granulated Occasional signet-ring cells	Pseudog-landular and tubular	Uniform Centrally placed Round Pinpoint nucleoli occasionally doubled Finely granulated chromatin Focally vesicular	Cylindric shaped Abundant Eosinophilic/ oncocytic Multiple small vacuoles Occasionally signet-ring cells	CK7+, S100+, MGA+, p63−, vimentin+, EMA+, SMA−, MIB1 low, PAS+
5	Rich	Loosely cohesive tissue fragments with trabecular and focally papillary structures with transgressing vessels. Singly dispersed cells	Cystic with plenty of macrophages and siderophages	Uniform Irregularly placed Round and focally vacuolated Inconspicuous nucleoli Finely granulated chromatin	Abundant Multiple small vacuoles Oncocytic-like	Solid	Uniform Irregularly placed Round to oval Prominent nucleoli	Abundant Eosinophilic/ oncocytic Multiple small vacuoles, focally bubble-like Intra- and extracyto-plasmic hemosiderin	CK7+, MGA+, CKPan+, vimentin+ MIB1 low PAS+
6	Rich	Huge clusters with some smaller, peripherally loosely cohesive clusters. Singly dispersed cells	Hemorrhagic	Mild polymorphism Irregularly placed Round Focally prominent nucleoli Fine chromatin	Abundant Focally cylindric shaped Foamy and focally vacuolated	ND	ND	ND	ND

ND, not determined; CB, cell block.

ETV6 gene rearrangement detection by FISH

Fluorescent in situ hybridization was performed in Cases 1–4, as the CB material in Cases 5 and 6 was not available anymore. The *ETV6* gene rearrangement was positive in three (Cases 1, 2 and 4) of the tested CBs (Fig. 3). The material for the remaining

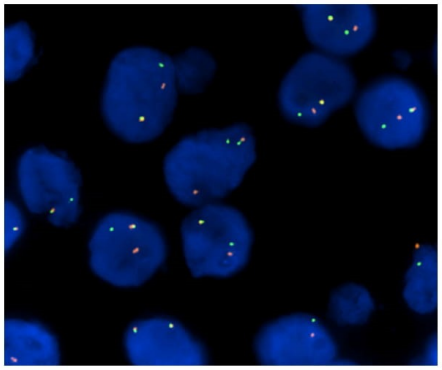

Fig. 3. FISH. FISH with ETV6 break-apart probe. Nuclei contain orange-yellow-green fusion signals from healthy alleles and separated orange and green signals from split alleles.

case (Case 3) was not analyzable due to the poor quality of DNA. The *NTRK3* gene was identified as a fusion partner in Cases 2 and 4, but was not confirmed in Case 1. For the remaining cases (Cases 3, 5 and 6), where CBs were not available or the material was insufficient, the translocation *ETV6-NTRK3* was confirmed in the final histological specimen and approved by the Next Generation Sequencing method.

Histological features

Three out of six resected tumors were diagnosed as SCs. The remaining three cases were sent as consultations, two cases with the diagnosis of suspicious low-grade malignancy and one with no specific diagnosis (Table 1). The presence of secretory material, uniform nuclei with variably prominent nucleoli and abundant cytoplasm were the common features in all cases. Contrary to the cellular uniformity, growth patterns, cell arrangements and the appearance of the cytoplasm varied from case to case. Case-specific features are listed in Table 1. Necrosis, angiolymphatic invasion, high mitotic activity and other signs of high-grade malignancy were not seen in any case. Results of IHC are listed in Table 1. The results of IHC in histology were identical to those in ICC in the CBs.

DISCUSSION

Secretaoty carcinoma of the salivary glands is recently described low-grade malignancy with a diagnostic rearrangement of *ETV6* gene on chromosome 12, which is unique in salivary tumors. There are three known fusion partners: *NTRK3* which is the most common and originally found (1), *RET* (4) and the very recently described *MET* (5). Since the publication of the first cases by Skálová et al. (1), the number of diagnosed SCs from resected tissue has increased rapidly. Therapeutically, there is also an increasing importance of pre-operative FNA diagnostics. Correct cytological diagnoses according to the new MSRSGC can guide the clinician to the appropriate management (24).

Small series and few cases on the cytology of SCs previously published in the literature are summarized in Table 3 (9–23). Our findings are in agreement with the cytological features presented in MSRSGC (24) and with previous descriptions (9–23). All the smears were sufficiently cellular. Background varied from clear, mucinous to cystic with degenerative changes. The most common architectural pattern of the cells was cohesive clusters arranged in papillary-like structures with occasional transgressing vessels. Cytoplasm was usually abundant, eosinophilic, with focal oncocytic features with fine granulation and vacuolization. Signet-ring cells were seldom present. In one case, the vacuoles contained colloid-like substances. Rarely myoepithelial-like cells were described both in our cohort and in the literature. Nuclei showed mild pleomorphism with focal binucleation, irregular placement and variably prominent nucleoli. Chromatin was finely granulated and no mitoses were seen. In a single case in our cohort, spindle-shaped nuclei and focal vacuolization of the nuclei were seen.

The described cytomorphology is non-specific for SC and is shared with multiple other tumors in salivary FNAs. In a pictures-based-survey of SC case among 109 cytopathologists, high diagnostic diversity was shown. In the mirror of relatively benign nuclear features and the malignant architectural appearance, the respondents answered both benign and low-grade malignancy depending if they stressed nuclear or architectural features (18). In the differential diagnosis, SC belongs to cystic and mucinous lesions with granulated or vacuolated eosinophilic cell cytoplasm. The SC is often misdiagnosed as AciCC, low-grade mucoepidermoid carcinoma (LG MEC), adenocarcinoma not otherwise specified (ADC NOS), neoplasia with myoepithelial differentiation, cellular pleomorphic adenoma (PA) or Warthin tumor (WT) (13). In cases with evident signs of high-grade malignancy with mitoses and necrosis, one should not forget SC in the differential diagnosis, as high-grade transformation of SC has been described (25). To exclude or confirm high-grade transformation, Ki-67 is useful on CBs.

It is evident that the salivary gland cytology is always challenging and rarely a final

Table 3. Summary of secretory carcinomas with cytomorphology presented in the literature

Reference	No. of cases	Original cytological diagnosis	Immunocytochemistry and special stains	Genetics
Petersson et al. (9)	1	Possible PA with oncocytic features	ND	*ETV6* rearrangement by FISH, translocation ETV6-NTRK3 confirmed by RT-PCR (histology material)
Pisharodi et al. (10)	1	Myoepithelial neoplasm or AciCC	Mucicarmine+, cytokeratins+, vimentin+, MGA+, GCDFP15+, S100+, calponin−, SMA−	*ETV6* rearrangement by FISH, translocation ETV6-NTRK3 confirmed by RT-PCR (histology material)
Lavine et al. (11)	1	Low-grade MEC	None	Not available in laboratory
Takeda et al. (12)	1	ND	ND	*ETV6* rearrangement by FISH, translocation ETV6-NTRK3 confirmed by RT-PCR (histology material)
Bajaj et al. (13)	1	Suspicious for low-grade MEC	Mucicarmine +	*ETV6* rearrangement by FISH (histology material)
Sethi et al. (14)	1	High-grade carcinoma (SDC, AciCC, MEC, ADC NOS)	S100+	*ETV6* rearrangement by FISH, translocation ETV6-NTRK3 confirmed by PCR (histology material)
Samulski et al. (15)	1	1st read: PA 2nd read: LG salivary gland neoplasm (AciCC, MEC)	ND	*ETV6* rearrangement (histology material)
Bellevicine et al. (16)	1	SC, AciCC-PCV	ND	ND
Inaba et al. (17)	1	AciCC mostly composed of intercalated duct cell type	ND	ETV6-NTRK3 by RT-PCR (histology material)
Kai et al. (18)	1	Atypia, suspicious for malignancy (Papanicolaou III)	ND	ETV6-NTRK3 by RT-PCR (histology material)
Oza et al. (19)	3	SC in all three cases	S100+, MGA+	ETV6-NTRK3 by RT-PCR (histology material)
Bishop et al. (20)	5	(1) Carcinoma (MEC) (2) Neoplasm (PA or MEC) (3) Neoplasm (AciCC, MEC) (4) Favor AciCC (5) Neoplasm (cellular PA)	ND	*ETV6* rearrangement by FISH (histology material)
Griffith et al. (21)	6	(1) Papillary neoplasm (2) Low-grade epithelial neoplasm (3) Benign salivary epithelium (4) Low-grade salivary gland neoplasm (5) Low-grade salivary gland neoplasm (6) SC	Only Cases 1, 2 and 6 (1) S100+, MGA+ (2) S100− (6) S100+	*ETV6* rearrangement by FISH in Cases 1 and 6. Case 2 was considered to be inadequate for analysis (cell block)
Higuchi et al. (22)	7	ND	ND	*ETV6* rearrangement by FISH, translocation ETV6-NTRK3 confirmed by RT-PCR (histology material)

specific diagnosis of malignancy is made without ancillary techniques (26, 27). Adequacy of the CBs depends primarily on the received material. The skills of the clinicians performing the FNA and of the laboratory technicians are both important (28).

Table 3. *(continued)*

Reference	No. of cases	Original cytological diagnosis	Immunocytochemistry and special stains	Genetics
Jung et al. (23)	9	(1) MEC (2) Favor AciCC (3) Suggestive of AciCC (4) PA (5) Suggestive of AciCC (6) Cellular PA (7) PA (8) Favor ADC (9) Mucin producing adenocarcinoma	ND	*ETV6* rearrangement by FISH (histology material)

PA, Pleomorphic adenoma; AciCC, acinic cell carcinoma; MEC, mucoepidermoid carcinoma; SDC, salivary dust carcinoma; ADC NOS, adenocarcinoma not otherwise specified; SC, secretory carcinoma; FISH, fluorescent *in situ* hybridization; RT-PCR, reverse transcription polymerase chain reaction; ND, not determined, ICC, immunocytochemistry; LG, low-grade; PCV, papillary cystic variant.

We have designed a basic staining panel to support and confirm the diagnosis of SC. This panel includes S-100 protein/mammaglobin A (MGA)/SOX10 positivity and DOG1/p63 negativity. Although vimentin is a non-specific marker, it can be used as an indicator of myoepithelial differentiation. Nevertheless, if DOG1 is available, negativity of DOG1 excludes the diagnosis of AciCC and supports the diagnosis of SC.

In cases, where the SC diagnosis is raised, molecular testing should follow. *ETV6* rearrangement is usually tested by FISH. If the result is positive, the diagnostic procedure is accomplished and the most accurate diagnosis is given to the clinician. If *NTRK3* or *RET* is detected as one of the fusion partners, SC is potentially treatable even in very advanced stages by the inhibitors of tyrosine-kinase activity that have been recently approved by the FDA. Targeted therapies are aimed for patients with advanced stages of the disease.

In previously reported series (Table 3), the performed ancillary studies were often limited. Only Pisharodi (10) performed sufficient ICC panel in her case report but the molecular detection was not done on CB. Genetic examinations were performed mainly on the final histological material. Only in one reported series, the FISH study was performed pre-operatively on CBs in three of six cases with positive conclusive results in two samples (20). Our study is the only one with a sufficient immunostaining panel for each case but also with an appropriate genetic control of the presence of ETV6 rearrangement in three out of six cases on CBs.

Categorization of SC according to MSRSGC depends on the availability of ancillary studies. If smears are available only, it is almost impossible to make a conclusive cytological diagnosis and the FNA should be classified as "Salivary gland Neoplasm of uncertain Malignant Potential (SUMP)." The ROM of this category is 35% according to MSRSGC, but a recent study by Liu et al. demonstrates a ROM of only 24% (29). If adequate CB or any other material is available, basic ICC according to the suggested staining panel should be performed, followed by genetic confirmation of the *ETV6* rearrangement, then the diagnosis of SC is certain and the FNA cytology should be concluded as "Malignant" according to MSRSGC. If genetic examination is not available in the laboratory and only ICC is confirmative for the diagnosis of SC, the MSRSGC category "Suspicious for malignancy" should be applied.

In summary, SC is a challenging tumor both in cytology and histology because of its non-specific overlapping morphological features. The key cytomorphological features to raise the suspicion for SC are papillary architecture and distinct granular cytoplasm. Its precise cytological diagnosis requires ancillary ICC and molecular testing on CB material. The availability of CB facilitates also the cytomorphological assessment. The ICC results are concordant with the IHC results. Nevertheless, the genetic testing is not always successful on CB material, often due to the lack of remnant material. We have suggested a diagnostic approach to SC cytology and presented the first SC cytology series in the context of MSRSGC.

The study was supported by VTR competitive grant (Ivana Kholová, MD, PhD) and by the grant SVV–2018 No. *260 391* provided by the Ministry of Education, Youth and Sports of the Czech Republic (Markéta Miesbauerová, MD, Martina Baněčková, MD and Alena Skálová, MD, PhD).

REFERENCES

1. Skalova A, Vanecek T, Sima R, Laco J, Weinreb I, Perez-Ordonez B, et al. Mammary analogue secretory carcinoma of salivary glands, containing the ETV6-NTRK3 fusion gene: a hitherto undescribed salivary gland tumor entity. Am J Surg Pathol 2010;34:599–608.
2. Skálová A, Bell D, Bishop JA, Inagaki H, Seethala R, Vielh P. Secretory carcinoma. In: El-Naggar AK, Chan JKC, Grandis JR, Takata T, Slootweg PJ, editors. WHO Classification of Head and Neck Tumours. Lyon: IARC, 2017:177–8.
3. Tognon C, Knezevich SR, Huntsman D, Roskelley CD, Melnyk N, Mathers JA, et al. Expression of the ETV6-NTRK3 gene fusion as a primary event in human secretory breast carcinoma. Cancer Cell 2002;2:367–76.
4. Skalova A, Vanecek T, Martinek P, Weinreb I, Stevens TM, Simpson RHW, et al. Molecular profiling of mammary analog secretory carcinoma revealed a subset of tumors harboring a novel ETV6-RET translocation: report of 10 cases. Am J Surg Pathol 2018;42:234–46.
5. Rooper LM, Karantanos T, Ning Y, Bishop JA, Gordon SW, Kang H. Salivary secretory carcinoma with a novel ETV6-MET fusion: expanding the molecular spectrum of a recently described entity. Am J Surg Pathol 2018;42:1121–6.
6. Baneckova M, Agaimy A, Andreasen S, Vanecek T, Steiner P, Slouka D, et al. Mammary analog secretory carcinoma of the nasal cavity: characterization of 2 cases and their distinction from other low-grade sinonasal adenocarcinomas. Am J Surg Pathol 2018;42:735–43.
7. Seethala RR, Chiosea SI, Liu CZ, Nikiforova M, Nikiforov YE. Clinical and morphologic features of ETV6-NTRK3 translocated papillary thyroid carcinoma in an adult population without radiation exposure. Am J Surg Pathol 2017;41:446–57.
8. Leeman-Neill RJ, Kelly LM, Liu P, Brenner AV, Little MP, Bogdanova TI, et al. ETV6-NTRK3 is a common chromosomal rearrangement in radiation-associated thyroid cancer. Cancer 2014;120:799–807.
9. Petersson F, Lian D, Chau YP, Yan B. Mammary analogue secretory carcinoma: the first submandibular case reported including findings on fine needle aspiration cytology. Head Neck Pathol 2012;6:135–9.
10. Pisharodi L. Mammary analog secretory carcinoma of salivary gland: cytologic diagnosis and differential diagnosis of an unreported entity. Diagn Cytopathol 2013;41:239–41.
11. Levine P, Fried K, Krevitt LD, Wang B, Wenig BM. Aspiration biopsy of mammary analogue secretory carcinoma of accessory parotid gland: another diagnostic dilemma in matrix-containing tumors of the salivary glands. Diagn Cytopathol 2014;42:49–53.
12. Takeda M, Kasai T, Morita K, Takeuchi M, Nishikawa T, Yamashita A, et al. Cytopathological features of mammary analogue secretory carcinoma-review of literature. Diagn Cytopathol 2015;43:131–7.
13. Bajaj J, Gimenez C, Slim F, Aziz M, Das K. Fine-needle aspiration cytology of mammary analog secretory carcinoma masquerading as low-grade mucoepidermoid carcinoma: case report with a review of the literature. Acta Cytol 2014;58:501–10.
14. Sethi R, Kozin E, Remenschneider A, Meier J, VanderLaan P, Faquin W, et al. Mammary analogue secretory carcinoma: update on a new diagnosis of salivary gland malignancy. Laryngoscope 2014;124:188–95.
15. Samulski TD, LiVolsi VA, Baloch Z. The cytopathologic features of mammary analog secretory carcinoma and its mimics. Cytojournal 2014;11:24.
16. Bellevicine C, Natella V, Somma A, De Rosa G, Troncone G. MASC is indistinguishable from acinic cell carcinoma, papillary-cystic variant on salivary gland FNA cytomorphology: case report with histological and immunohistochemical correlates. Cytopathology 2014;25:344–6.
17. Inaba T, Fukumura Y, Saito T, Yokoyama J, Ohba S, Arakawa A, et al. Cytological features of mammary analogue secretory carcinoma of the parotid gland in a 15-year-old girl: a case report with review of the literature. Case Rep Pathol 2015;2015:656107.
18. Kai K, Minesaki A, Suzuki K, Monji M, Nakamura M, Tsugitomi H, et al. Difficulty in the cytodiagnosis of mammary analogue secretory carcinoma: survey of 109 cytologists with a case originating from a minor salivary gland. Acta Cytol 2017;61:469–76.
19. Oza N, Sanghvi K, Shet T, Patil A, Menon S, Ramadwar M, et al. Mammary analogue secretory carcinoma of parotid: is preoperative cytological diagnosis possible? Diagn Cytopathol 2016;44:519–25.
20. Bishop JA, Yonescu R, Batista DA, Westra WH, Ali SZ. Cytopathologic features of mammary analogue secretory carcinoma. Cancer Cytopathol 2013;121:228–33.
21. Griffith CC, Stelow EB, Saqi A, Khalbuss WE, Schneider F, Chiosea SI, et al. The cytological features of mammary analogue secretory carcinoma: a series of 6 molecularly confirmed cases. Cancer Cytopathol 2013;121:234–41.
22. Higuchi K, Urano M, Takahashi RH, Oshiro H, Matsubayashi J, Nagai T, et al. Cytological features of mammary analogue secretory carcinoma of salivary gland: fine-needle aspiration of seven cases. Diagn Cytopathol 2014;42:846–55.
23. Jung MJ, Kim SY, Nam SY, Roh JL, Choi SH, Lee JH, et al. Aspiration cytology of mammary analogue secretory carcinoma of the salivary gland. Diagn Cytopathol 2015;43:287–93.
24. Faquin W, Rossi ED (Ed). The Milan System for reporting salivary gland Cytopathology. New York, NY: Springer, 2018: 182 p.
25. Skálová A, Vanecek T, Majewska H, Laco J, Grossmann P, Simpson RH, et al. Mammary analogue secretory carcinoma of salivary glands with high-grade transformation: report of 3 cases with the ETV6-NTRK3 gene fusion and analysis of TP53, β-catenin, EGFR, and CCND1 genes. Am J Surg Pathol 2014;38:23–33.
26. Lundberg M, Munsterhjelm B, Mäkitie A, Leivo I. Immunohistochemical staining of histological fragments derived from salivary gland tumour fine-needle biopsy aspirates. Acta Cytol 2017;61:17–20.

27. Pusztaszeri MP, Faquin WC. Update in salivary gland cytopathology: recent molecular advances and diagnostic applications. Semin Diagn Pathol 2015;32:264–74.
28. Krogerus L, Kholová I. Cell block in cytological diagnostics: review of preparatory techniques. Acta Cytol 2018;62:237–43.
29. Liu H, Ljungren C, Lin F, Zarka MA, Chen L. Analysis of histologic follow-up and risk of malignancy for salivary gland neoplasm of uncertain malignant potential proposed by the Milan system for reporting salivary gland cytopathology. Cancer Cytopathol 2018;126:490–7.

1.11 DALŠÍ BENIGNÍ A MALIGNÍ JEDNOTKY HLAVY A KRKU

1.11.1 MOLEKULÁRNÍ PROFILOVÁNÍ INTRADUKTÁLNÍHO KARCINOMU SLINNÝCH ŽLÁZ ODHALILO PODSKUPINU KARCINOMŮ CHARAKTERIZOVANÝCH *NCOA4-RET* FÚZÍ A NOVOU *TRIM27-RET* FÚZÍ

Intraduktální karcinom (IC) je recentně definovaná jednotka ve WHO klasifikaci (21). V rámci diferenciální diagnózy jsou nejčastěji zmiňované sekreční karcinom (SC) a salivární duktální karcinom (SDC). První z přiložených publikací se zabývá vztahem mezi IC a SC. IC má obdobný imunoprofil jako SC, tj. S100 protein/ mammaglobin pozitivní, DOG1 negativní a p63 zachovanou myoepiteliální vrstvu kolem intraduktální komponenty IC či velmi vzácně i SC.

Retrospektivně bylo vyšetřeno 17 případů IC, v nichž nebyl prokázaný zlom *ETV6* genu metodou FISH ani fúze *ETV6-NTRK3* metodou RT-PCR. Analýza metodou NGS prokázala fúzi exonů 7 či 8 genu *NCOA4* s exonem 12 genu *RET* v 6 případech IC s fenotypem z vmezeřených duktů. Dále byla zjištěna fúze *TRIM27-RET* nacházející se mezi exony 3 a 12 ve 2 případech IC s apokrinní morfologií. Celkově byl *RET* zlom potvrzený ve 47 % případů IC. Přibližně v 50 % případů nebyla zastižena žádná fúze v naší studii ani ve studii Weinreba a spol (52). Pravděpodobně budou tyto *RET*-negativní IC obsahovat jinou fúzi, zatím nedetekovanou našimi stávajícími NGS platformami, což vyžaduje další zkoumání.

Molecular Profiling of Salivary Gland Intraductal Carcinoma Revealed a Subset of Tumors Harboring *NCOA4-RET* and Novel *TRIM27-RET* Fusions

A Report of 17 cases

Alena Skálová, MD, PhD, Tomas Vanecek, PhD,*† Emmanuelle Uro-Coste, MD, PhD,‡§ Justin A. Bishop, MD, PhD,‖ Ilan Weinreb, MD,¶ Lester D.R. Thompson, MD,# Stefano de Sanctis, MD, PhD,** Marco Schiavo-Lena, MD,†† Jan Laco, MD, PhD,‡‡ Cécile Badoual, MD, PhD,§§ Thalita Santana Conceiçao, DDS, MSc, PhD,‖‖ Nikola Ptáková, MSc,† Martina Baněčkova, MD,* Marketa Miesbauerová, MD,* and Michal Michal, MD**

Abstract: Intraductal carcinoma (IC) is the new World Health Organization designation for tumors previously called "low-grade cribriform cystadenocarcinoma" and "low-grade salivary duct carcinoma." The relationship of IC to salivary duct carcinoma is controversial, but they now are considered to be distinct entities. IC is a rare low-grade malignant salivary gland neoplasm with features similar to mammary atypical ductal hyperplasia or ductal carcinoma in situ, that shows diffuse S100 protein and mammaglobin positivity and is only partially defined genetically. (Mammary analogue) secretory carcinoma harboring *ETV6-NTRK3*, and in rare cases *ETV6-RET* fusion, shares histomorphologic and immunophenotypical features with IC. Recently, *RET* rearrangements and *NCOA4-RET* have been described in IC, suggesting a partial genetic overlap with mammary analogue secretory carcinoma. Here, we genetically characterize the largest cohort of IC to date to further explore this relationship. Seventeen cases of IC were analyzed by next-generation sequencing using the FusionPlex Solid Tumor kit (ArcherDX). Identified fusions were confirmed using fluorescence in situ hybridization break apart and, in some cases, fusion probes, and a reverse transcription polymerase chain reaction designed specifically to the detected breakpoints. All analyzed cases were known to be negative for *ETV6* rearrangement by fluorescence in situ hybridization and for *ETV6-NTRK3* fusion by reverse transcription polymerase chain reaction. Next-generation sequencing analysis detected a *NCOA4-RET* fusion transcript joining exon 7 or 8 of *NCOA4* gene and exon 12 of *RET* gene in 6 cases of intercalated duct type IC; and a novel *TRIM27-RET* fusion transcript between exons 3 and 12 in 2 cases of salivary gland tumors displaying histologic and immunohistochemical features typical of apocrine IC. A total of 47% of IC harbored a fusion involving *RET*. In conclusion, we have confirmed the presence of *NCOA4-RET* as the dominant fusion in intercalated duct type IC. A novel finding in our study has been a discovery of a subset of IC patients with apocrine variant IC harboring a novel *TRIM27-RET*.

Key Words: salivary gland neoplasm, intraductal carcinoma, cystadenocarcinoma, mammary analogue secretory carcinoma, MASC, *NCOA4-RET*, *TRIM27-RET*, *RET*-targeted therapy

(*Am J Surg Pathol* 2018;42:1445–1455)

From the *Department of Pathology, Charles University, Faculty of Medicine in Plzen; †Molecular and Genetic Laboratory, Biopticka Laboratory Ltd, Plzen; ‡‡The Fingerland Department of Pathology, Charles University, Faculty of Medicine and University Hospital, Hradec Kralove, Czech Republic; ‡Department of Pathology, Toulouse University Hospital; §INSERM U1037, Cancer Research Center of Toulouse (CRCT), Toulouse; §§Department of Pathology, G. Pompidou Hospital, Paris, APHP, Paris Descartes University, Paris, France; ‖Department of Pathology, UT Southwestern Medical Center, Dallas, TX; ¶Department of Pathology, University Health Network, Toronto, ON, Canada; #Southern California Permanente Medical Group, Woodland Hills, CA; **Histopathology Department, Addenbrooke Hospital, Cambridge University Hospitals NHS Trust, Cambridge, UK; ††Department of Pathology, IRCCS San Raffaele Scientific Institute, Milan, Italy; and ‖‖Department of Oral Pathology, Faculty of Dentistry, University of São Paulo, São Paulo, Brazil.

The preliminary results of the study were presented as a platform presentation at USCAP Meeting 2018, Vancouver, Canada, March 17-22, 2018 (A.S.).

Conflicts of Interest and Source of Funding: Supported in parts by the grant SVV–2018 No. 260 391 provided by the Ministry of Education Youth and Sports of the Czech Republic. The authors have disclosed that they have no significant relationships with, or financial interest in, any commercial companies pertaining to this article.

Correspondence: Alena Skálová, MD, PhD, Sikl's Department of Pathology, Medical Faculty of Charles University, Faculty Hospital, E. Benese 13, Plzen 305 99, Czech Republic (e-mail: skalova@fnplzen.cz).

Secretory carcinoma of the salivary glands, also known as mammary analogue secretory carcinoma (MASC), was originally described by Skálová et al, in 2010.[1] Most of these tumors were previously categorized as acinic cell carcinoma,[2–4] adenocarcinoma not otherwise specified or low-grade cystadenocarcinoma, but were recognized as a

distinct entity based on their morphologic and molecular resemblance to secretory carcinoma of the breast,[1] and subsequently adopted by the World Health Organization (WHO) Classification of Head and Neck Tumours in 2017 as secretory carcinoma of salivary glands.[5] MASCs are characterized by abundant eosinophilic cytoplasm and secretions, consistent immunohistochemical positivity for S100 and mammaglobin, and recurrent *ETV6-NTRK3* gene fusions. Increasing experience with MASCs, however, has also highlighted a small subset of cases that demonstrate divergent molecular findings.[6,7] Most notably, Skálová et al,[8] recently characterized 10 cases with alternate *ETV6-RET* fusion.

Intraductal carcinoma (IC) is the new WHO designation for tumors previously called "low-grade cribriform cystadenocarcinoma" and "low-grade salivary duct carcinoma."[9] The relationship of IC to salivary duct carcinoma (SDC) has been controversial, but recently they are considered to be distinct entities. IC is a rare low-grade malignant salivary gland neoplasm with features similar to mammary atypical ductal hyperplasia or ductal carcinoma in situ, that shows diffuse S100 protein and mammaglobin positivity and an intact myoepithelial cell layer decorated by p63 protein, calponin, and cytokeratin 14.

MASC has many architectural and immunophenotypic features similar to, or identical with IC. Both tumors may share diffuse S100 protein and mammaglobin positivity and similar architectural features, such as cribriform-like secretory spaces, multicystic architecture and papillary growth pattern.[1] These 2 morphologically similar entities should be, however, strictly separated. Pure IC is an in situ lesion with no capacity for metastasizing while MASC does not have any significant intraductal component and may metastasize. Most importantly, the neoplastic nests and cysts of IC are completely surrounded by a rim of non-neoplastic myoepithelial cells, which are positive for p63 protein, and other myoepithelial cell-related markers such as smooth muscle actin, CK14, and calponin. Thus, immunohistochemistry is helpful in differential diagnosis between IC and MASC; with p63 protein expression providing evidence of intact myoepithelial layer in IC while virtually negative in MASC.

Weinreb et al,[10] recently demonstrated recurrent rearrangements involving *RET* in 47% of ICs with an intercalated duct phenotype and confirmed *NCOA4-RET* fusion in one such case using next-generation sequencing (NGS) and direct sequencing. Dogan et al,[11] presented, however, at the USCAP Annual Meeting on March 6th 2017 as a poster, *NCOA4-RET* fusion in one of 4 tumors morphologically and immunophenotypically compatible with MASC using the NGS assay. The proposed novel finding of *NCOA4-RET* fusion in MASC attracted our attention as it was in contrast with our experience. So far, we have tested > 300 cases of MASC and never found any other fusion than *ETV6-NTRK3* or *ETV6-RET*.[1,8]

There have been only limited genomic and immunohistochemical comparative studies of pure IC and MASC, so far. One case of "low-grade cribriform cystadenocarcinoma" tested as part of the control group in the original description of MASC was *ETV6* negative by fluorescence in situ hybridization (FISH).[1] A second study found one case of "low-grade cribriform cystadenocarcinoma" to be *ETV6* negative by FISH.[12] A recent third study also showed *ETV6* negativity by FISH in 5 cases of IC tested.[13] In the study by Shah et al,[14] there was a single case originally classified as MASC that was negative to *ETV6* break by FISH, and positive for S100 and mammaglobin by immunohistochemistry, re-classified as IC on review. The study by Weinreb et al,[10] also found no evidence of *ETV6* rearrangement in any of their IC cases tested, and did not confirm the partner gene for *RET* in the majority of the tumors. Therefore, we used a comprehensive genetic analysis to examine the largest cohort of IC to date, with the goal of defining the most common gene fusions and potentially identifying novel fusions.

MATERIALS AND METHODS

Among more than 6200 cases of primary salivary gland tumors, 16 cases of IC were retrieved from the consultation files of the Salivary Gland Tumor Registry, at the Department of Pathology, Faculty of Medicine in Plzen, and Biopticka Laboratory Ltd, Plzen, Czech Republic (A.S. and M.M.). Interestingly, 7 cases were originally diagnosed as MASCs by referring pathologists, and sent as consults for molecular confirmation. One additional case of predominantly apocrine IC was added which was originally reported as case no. 15 in Weinreb et al,[10] and tested by NGS.

The histopathologic features of all tumors and the immunohistochemical stains, when available, were reviewed by 2 pathologists (A.S. and M.B.). A diagnosis of IC was confirmed in cases that displayed histologic features consistent with original description in conjunction with the appropriate immunohistochemical profile, that is, co-expression of S100 protein, cytokeratin CK7, and mammaglobin in the absence of DOG1 staining. Moreover, an intact myoepithelial layer decorated by p63 and/or CK14 and calponin provided evidence of intraductal component. Widely invasive carcinomas were excluded. Tumors were classified further into 2 groups, according to criteria published recently[10]: those that showed an intercalated duct phenotype and those with an apocrine phenotype. This was determined both histologically and immunohistochemically. Thus, a total number of 17 IC cases were studied by NGS using ArcherDX FusionPlex kit.

For conventional microscopy, the excised tissues were fixed in formalin, routinely processed, embedded in paraffin (FFPE), cut, and stained with hematoxylin and eosin. In most cases, additional stains were also performed, including periodic acid-Schiff with and without diastase, mucicarmine, and Alcian blue at pH 2.5.

For immunohistochemical analysis, 4-μm-thick sections were cut from paraffin blocks and mounted on positively charged slides (TOMO, Matsunami Glass IND, Japan). Sections were processed on a BenchMark ULTRA (Ventana Medical System, Tucson, AZ), deparaffinized and then subjected to heat-induced epitope retrieval by immersion in a CC1 solution at pH 8.6 at 95°C. All

TABLE 1. Antibodies Used for Immunohistochemical Study

Antibody Specificity	Clone	Dilution	Antigen Retrieval/ Time (min)	Source
S100 protein	Polyclonal	RTU	CC1/20	Ventana
Mammaglobin	304-1A5	RTU	CC1/36	DakoCytomation
CK7	OV-TL 12/30	1:200	CC1/36	DakoCytomation
p63	4A4	RTU	CC1/64	Ventana
DOG1	SP31	RTU	CC1/36	Cell Marque
GATA-3	L50-823	1:200	CC1/52	BioCareMedical
SOX-10	Polyclonal	1:100	CC1/64	Cell Marque
MIB1	30-9	RTU	CC1/64	Ventana
Androgen receptor	SP107	RTU	CC1/64	Cell Marque
Calponin	EP798Y	RTU	CC1/36	Cell Marque
CK 14	SP53	RTU	CC1/64	Cell Marque

CC1—EDTA buffer, pH 8.6.
RTU indicates ready to use.

other primary antibodies used are summarized in Table 1. The bound antibodies were visualized using the ultraView Universal DAB Detection Kit (Roche) and ultraView Universal Alkaline Phosphatase Red Detection Kit (Roche). The slides were counterstained with Mayer's hematoxylin. Appropriate positive and negative controls were employed.

Where available, clinical follow-up was obtained from the patients, their physicians, or from referring pathologists.

Molecular Genetic Study

Sample Preparation for NGS and Reverse Transcriptase Polymerase Chain Reaction

For NGS and reverse transcriptase polymerase chain reaction (RT-PCR) analysis, 2 to 3 FFPE sections (10 μm thick) were macrodissected to isolate tumor-rich regions. Samples were extracted for total nucleic acid using Agencourt FormaPure Kit (Beckman Coulter, Brea, CA) following the corresponding protocol with an overnight digest and an additional 80°C incubation as described in modification of the protocol by ArcherDX (ArcherDX Inc., Boulder, CO). RNA component of the total nucleic acid was quantified using the Qubit Broad Range RNA Assay Kit (Thermo Fisher Scientific) and 2 μL of sample.

RNA Integrity Assessment and Library Preparation for NGS

Unless otherwise indicated, 250 ng of FFPE RNA was used as input for NGS library construction. To assess RNA quality, the PreSeq RNA QC Assay using iTaq Universal SYBR Green Supermix (Biorad, Hercules, CA) was performed on all samples during library preparation to generate a measure of the integrity of RNA (in the form of a cycle threshold [Ct] value). Library preparation and RNA QC were performed following the Archer FusionPlex Protocol for Illumina (ArcherDX Inc.). The Archer FusionPlex Solid Tumor Kit was used. Final libraries were diluted 1:100,000 and quantified in a 10 μL reaction following the Library Quantification for Illumina Libraries protocol and assuming a 200 bp fragment length (KAPA, Wilmington, MA). The concentration of final libraries was around 200 nM. Threshold representing the minimum molar concentration for which sequencing can be robustly performed was set at 50 nM.

NGS Sequencing and Analysis

Libraries were sequenced on a NextSeq. 500 sequencer (Illumina, San Diego, CA). They were diluted to 4 nM and equal amounts of up to 16 libraries were pooled per run. The optimal number of raw reads per sample was set to 3,000,000. Library pools were diluted to 1.8 pM library stock spiked with 20% PhiX and loaded in the NextSeq MID cartridge. Analysis of sequencing results was performed using the Archer Analysis software (v5; ArcherDX Inc.). Fusion parameters were set to a minimum of 5 valid fusion reads with a minimum of 3 unique start sites within the valid fusion reads.

FISH Analysis of RET Break and TRIM27-RET Fusion

Four micrometer thick FFPE sections were placed onto positively charged slides. Hematoxylin and eosin–stained slides were examined for determination of areas for cell counting.

The unstained slides were routinely deparaffinized and incubated in the ×1 Target Retrieval Solution Citrate pH 6 (Dako, Glostrup, Denmark) at 95°C for 40 minutes and subsequently cooled for 20 minutes at room temperature in the same solution. Slides were washed in deionized water for 5 minutes and digested in protease solution with Pepsin (0.5 mg/mL) (Sigma Aldrich, St. Louis, MO) in 0.01 M HCl at 37°C for 35 to 60 minutes according the sample conditions. Slides were then placed into deionized water for 5 minutes, dehydrated in a series of ethanol solution (70%, 85%, 96% for 2 min each) and air-dried.

For the detection of *RET* rearrangement, factory premixed commercial probe ZytoLight SPEC RET Dual Color Break Apart Probe (ZytoVision GmbH, Bremerhaven, Germany) have been used. For the *TRIM27-RET* dual-fusion detection custom designed SureFISH probe (Agilent Technologies Inc., Santa Clara with chromosomal regions chr6:28631476-29131075 and chr10:43354893-43849282 have been used. Probe-mixture for the fusion detection was prepared from corresponding probes (each color was delivered in separated well), deionized water and LSI Buffer (Vysis/Abbott Molecular) in a 1:1:1:7 ratio, respectively.

An appropriate amount of mixed and premixed probes was applied on specimens, covered with a glass coverslip and sealed with rubber cement. Slides were incubated in the ThermoBrite instrument (StatSpin/Iris Sample Processing, Westwood, MA) with codenaturation at 85°C/8 minutes and hybridization at 37°C/16 hours. Rubber cemented coverslip was then removed and the slide was placed in post-hybridization wash solution (2×SSC/0.3% NP-40) at 72°C/2 minutes. The slide was air-dried in the dark, counterstained with 4′, 6′-diamidino-2-phenylindole DAPI (Vysis/Abbott Molecular), cover slipped and immediately examined.

TABLE 2. Primers for RT-PCR Analysis

Primer Name	Sequence 5′-3′
NCOA4-RET-7-12-F	CCCTTCCTGGAGAAGAGAGG
NCOA4-RET-7-12-R	GTACCCTGCTCTGCCTTTCA
NCOA4-RET-8-12-F	TACCCAAAAGCAGACCTTGG
NCOA4-RET-8-12-R	CGCCTTCTCCTAGAGTTTTTCC
TRIM27-RET-3-12-F	TGATCGCTCAGCTAGAAGAGAA
TRIM27-RET-3-12-R	CCAAGTTCTTCCGAGGGAAT

FISH Interpretation

The sections were examined with an Olympus BX51 fluorescence microscope (Olympus Corporation, Tokyo, Japan) using a ×100 objective and filter sets Triple Band Pass (DAPI/SpectrumGreen/SpectrumOrange), Dual Band Pass (SpectrumGreen/SpectrumOrange) and Single Band Pass (SpectrumGreen or SpectrumOrange).

For each probe, 100 randomly selected nonoverlapping tumor cell nuclei were examined for the presence of yellow or green and orange fluorescent signals. Regarding break-apart probe, yellow signals were considered negative, separate orange and green signals were considered as positive; conversely for fusion probe, yellow signals were considered positive, separate orange and green signals were considered as negative. Cut-off values for break apart and fusion probes were set to <10% and 20% of nuclei with chromosomal breakpoint and fusion signals, respectively (mean+3 SD in normal non-neoplastic control tissues).

RT-PCR Analysis of NCOA4-RET and TRIM27-RET Fusion Transcripts

Two microliter of cDNA prepared by standard RT procedure using Transcriptor First Strand cDNA Synthesis Kit (RNA input 500 ng) (Roche Diagnostics, Mannheim, Germany) was added to reaction consisted of 12.5 µL of HotStar Taq PCR Master Mix (QIAgen, Hilden, Germany), 10 pmol of each fusion specific primer (Table 2) and distilled water up to 25 µL. The amplification program comprised denaturation at 95°C for 14 minutes and then 45 cycles of denaturation at 95°C for 1 minute, annealing at temperature 55°C for 1 minute and extension at 72°C for 1 minute. The program was finished by incubation at 72°C for 7 minutes.

TABLE 3. Detailed Molecular Findings of 17 Cases of Salivary Gland ICs

No.	Age/ Sex	Diagnosis	NGS	Exons Joining	FISH RET ba	FISH TRIM27-RET Fusion	RT-PCR Fusion Specific	FISH ETV6 ba	RT-PCR ETV6-NTRK3
1	38/M	Pure IC intercalated duct type, solid microcystic, rich lymphoid stroma	NCOA4-RET	8-12	Positive*	ND	Positive	Negative	Negative
2	47/M	Pure IC intercalated duct type, solid multicystic, "MASC-like"	NCOA4-RET	7-12	Positive*	ND	Positive	Negative	Negative
3	54/M	IC with apocrine features, micropapillary, minimal invasion	TRIM27-RET	3-12	Positive	Positive	Positive	Negative	Negative
4	50/M	Pure IC intercalated duct type, solid multicystic, "MASC-like"	NA	—	NA	ND	Negative	Negative	Negative
5	58/M	Pure IC intercalated duct type, solid microcystic, apocrine, papillary	NA	—	NA	ND	ND	NA	Negative
6	81/M	Pure IC intercalated duct type, "roman bridges" Invasive component of epithelial-myoepithelial carcinoma	NA	—	Negative	ND	Negative	Negative	Negative
7†	50/F	Pure IC intercalated duct type, unicystic	Negative	—	Negative	ND	ND	Negative	Negative
8	74/M	Pure IC intercalated duct type, papillary, multicystic	NCOA4-RET	8-12	Positive*	ND	Positive	Negative	Negative
9	36/F	Pure IC intercalated duct type, few apocrine cells	Negative	—	Negative	ND	ND	Negative	Negative
10	53/F	IC intercalated duct type, minimal invasion	Negative	—	Negative	ND	ND	Negative	Negative
11	75/F	IC with apocrine features, papillary, thick fibrous capsule	Negative	—	Negative	ND	ND	Negative	Negative
12	69/M	IC with apocrine features, unicystic	Negative	—	ND	ND	ND	ND	Negative
13	42/F	Pure IC intercalated duct type, unicystic	Negative	—	ND	ND	ND	Negative	Negative
14	61/F	Pure IC intercalated duct type, solid, microcystic, "MASC-like"	NCOA4-RET	7-12	Positive*	ND	Positive	Negative	Negative
15	36/M	Pure IC intercalated duct type, solid, microcystic, "MASC-like"	NCOA4-RET	8-12	Positive*	ND	Positive	NA	Negative
16	50/M	Pure IC intercalated duct type, solid, microcystic, "MASC-like"	NCOA4-RET	8-12	Positive	ND	Positive	ND	ND
17‡	66/M	IC with widespread apocrine features, and hybrid intercalated duct pattern	TRIM27-RET	3-12	Positive	Positive	Positive	ND	ND

*Cases 1 to 2, 8, and 14 to 16 showed a *RET* FISH signal pattern indicative of an inversion/rearrangement (in one allele a gap between orange and green signals was observed, hovewer this gap didnot reach internal cut-off (≥2 signal diameters apart).

†Published in Laco et al.[22]

‡Published as case no.15 in Weinreb et al.[10]

F indicates female; M, male; NA, not analyzable; ND, not done.

Successfully amplified PCR products were purified with magnetic particles Agencourt AMPure (Agencourt Bioscience Corporation, A Beckman Coulter Company, Beverly, MA). Products were then bi-directionally sequenced using Big Dye Terminator Sequencing kit (Applied Biosystems, Foster City, CA), purified with magnetic particles Agencourt CleanSEQ (Agencourt Bioscience Corporation), all according to manufacturer's protocol and run on an automated sequencer ABI Prism 3130×l (Applied Biosystems) at a constant voltage of 13.2 kV for 11 minutes.

RESULTS

Molecular Genetic Findings

The 17 cases of IC were analyzed by NGS using the ArcherDX analysis platform. This analysis detected a *NCOA4-RET* fusion transcript joining exon 7 or 8 of *NCOA4* gene and exon 12 of *RET* gene in 6 cases and a novel *TRIM27-RET* fusion transcript between exons 3 and 12 in 2 cases of salivary gland tumors displaying histologic and immunohistochemical features typical of apocrine IC (Table 3). The fusion transcripts were confirmed by RT-PCR and sequencing (Figs. 1A–C). FISH analysis using *RET* break-apart probe showed 2 different patterns, one "negative" when distance criteria was used according to the interpretation rules, but still showing small separation of signals (cases 1 to 2, 8, and 14 to 16) (Fig. 2A), and a regular break (classic positive pattern) with apparent separation of signals demonstrated in 2 cases (cases 3 and 17) (Fig. 2B). Confirmation using FISH *TRIM27-RET* fusion probe displayed fusion signals with amplification (Fig. 2C). Localization of *RET*, *NCOA4*, and *TRIM27* genes for an explanation of 2 different patterns of FISH break-apart results is shown in the figure (Fig. 2D).

All analyzed cases were negative for *ETV6-NTRK3* gene fusion by the FusionPlex kit, RT-PCR, and *ETV6* gene was found intact by FISH (Table 3). No other fusion transcripts different from *NCOA4-RET* or *TRIM27-RET* were found by NGS in any analyzable case of IC. A total of 47% of analyzed cases harbored a *RET* fusion by NGS, an identical finding to that found by Weinreb et al.[10] By RT-PCR, the fusions *NCOA4-RET* and *TRIM27-RET* were confirmed in all NGS positive cases. The *RET* FISH break-apart probe and

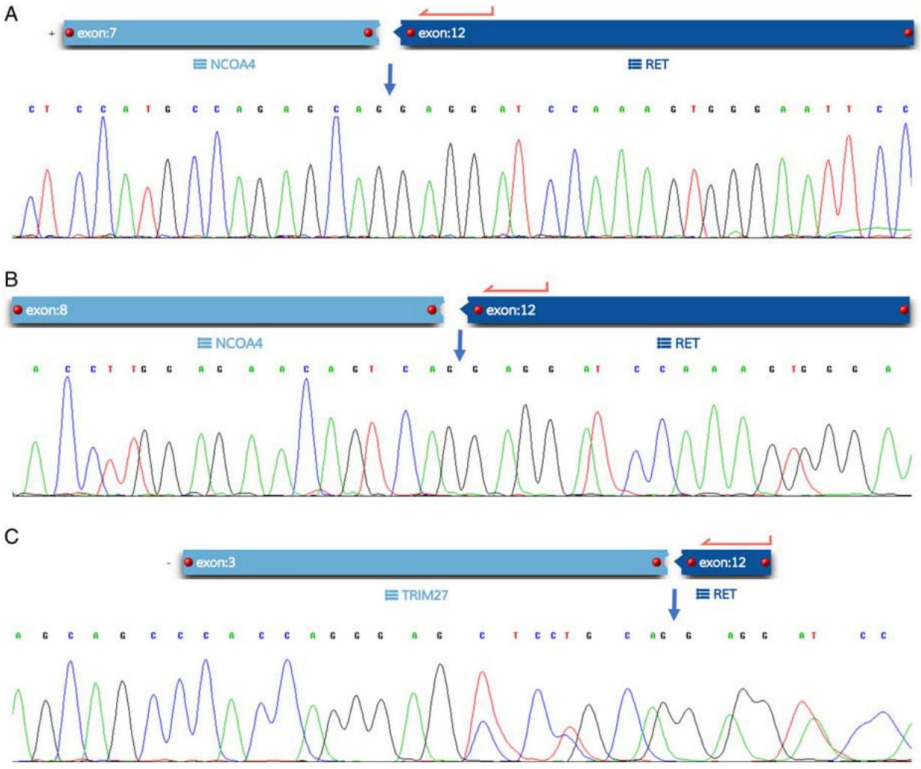

FIGURE 1. Schematic representation of the fusion transcripts with Sanger sequence of RT-PCR. *NCOA4-RET* exons 7 and 12 (A), *NCOA4-RET* exons 8 and 12 (B), *TRIM27-RET* exons 3 and 12 (C).

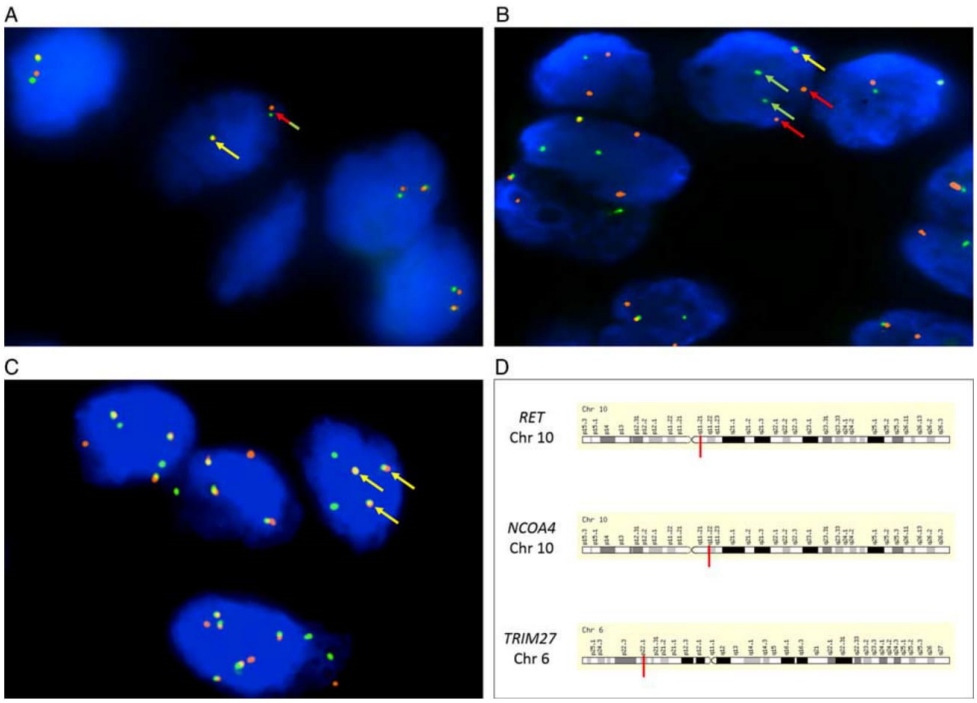

FIGURE 2. FISH analysis. A, Seemingly negative *RET* break-apart probe with small separation of signals (red-green arrow). B, Regular *RET* break-apart probe positivity (red and green arrows); yellow arrows show intact gene in both cases. C, *TRIM27-RET* fusion probe positivity with signal amplification (yellow arrows). D, Scheme of chromosomal localization of *RET*, *NCOA4*, and *TRIM27* genes.

TRIM27-RET fusion probe successfully detected the *RET* rearrangement in both cases with *TRIM27-RET*. "False" negative FISH results were obtained in all *NCOA4-RET* cases for *RET* rearrangement owing to this fusion being the result of an intrachromosomal rearrangement with inversion. Although a narrow separation of the FISH signals was noted in each case. The molecular findings are summarized in Table 3.

Clinical and Histologic Characteristics of the Study Group

The study cohort consisted of 15 pure ICs and 2 ICs with limited microinvasion. The patients with available clinical information included 11 males and 6 females, with a wide age-range at diagnosis of 36 to 81 years (mean, 55.3 y). The most common anatomic site of involvement was the parotid gland (no. = 16 patients), with one case in the buccal mucosa. The tumors ranged from 0.6 to 4.6 cm (mean, 1.64 cm). Detailed clinical, follow-up, and histologic findings in 17 patients with IC are summarized in Table 4.

Grossly, the tumors were entirely circumscribed and encapsulated in most cases, although infiltrative edges were seen in 2 cases. All tumors were treated by surgical excision with clear surgical margins. Five patients underwent subtotal conservative parotidectomy (cases 2, 8, 14 and 15), followed by radiation therapy (case 8), and cervical lymph node dissection (case 2), respectively. Clinical follow-up data were obtained from 15 patients, and ranged from 8 months to 15 years (mean, 5 y and 5 mo); 2 patients were lost to follow-up.

Microscopic and Immunohistochemical Features

Histologically, at low power magnification, most cases were well-circumscribed and encapsulated. Focal areas with microinvasion were seen in 2 cases of IC (case 3 and 10). In addition, in case 6 the tumor of parotid gland was a hybrid lesion composed of 2 separate components, one was invasive epithelial-myoepithelial carcinoma and the other pure IC without invasion. Lymphovascular and perineural invasion was absent in all cases. All tumors were characterized by luminal epithelial proliferations with ductal phenotype arranged mainly in multiple cystic patterns, besides solid and cribriform islands (Fig. 3A). Intracystic growth often formed micropapillary structures with anastomosing and filigreed epithelial tufts, comprising the so called Roman-bridges pattern (Fig. 3B). Eosinophilic proteinaceous secretion and hemorrhagic areas were occasionally observed in some cystic spaces, as well as

TABLE 4. Clinicopathologic Features of 16 Cases of Salivary Gland Intraductal Carcinomas

No.	Age/ Sex	Site	Size (cm)	Diagnosis	Nuclear Grade	S100 Protein/ MGA	AR	Treatment	Outcome (in months)
1	38/M	Parotid	4.0	Pure IC intercalated duct type, solid microcystic, rich lymphoid stroma	Low	+/+	−	Superficial parotidectomy	20 NED
2	47/M	Parotid	1.4	Pure IC intercalated duct type, solid multicystic, "MASC-like"	Low	+/+	−	Parotidectomy and neck dissection	36 NED
3	54/M	Parotid	2.2	IC with apocrine features, micropapillary, minimal invasion	High	+/+	+	Superficial parotidectomy	8 NED
4	50/M	Parotid	1.0	Pure IC intercalated duct type, solid multicystic, "MASC-like"	Low	+/+	−	Partial parotidectomy	57 NED
5	58/M	Parotid	1.5	Pure IC intercalated duct type, solid microcystic, apocrine, papillary	Low	+/+	+	Wide excision	144 NED
6	81/M	Parotid	NA	Pure IC intercalated duct type, "roman-bridges" Invasive component of epithelial-myoepithelial carcinoma*	Low	+/ND	−	NA	NA
7	50/F	Parotid	1.5	Pure IC intercalated duct type, unicystic	Low	+/+	−	Wide excision	72 NED
8	74/M	Parotid	1.5	Pure IC intercalated duct type, papillary, multicystic	Low	+/+	−	Parotidectomy and radiotherapy	62 NED
9	36/F	Buccal mucosa	0.6	Pure IC intercalated duct type, few apocrine cells	Low	+/+	ND	Wide excision	180 NED
10	53/F	Parotid	2.0	IC intercalated duct type, minimal invasion	Low	+/+	−	Parotidectomy	180 NED
11	75/F	Parotid	4.6	IC with apocrine features, papillary, thick fibrous capsule	Intermediate	+/+	ND	Parotidectomy	72 NED
12	69/M	Parotid	0.9	IC with apocrine features, unicystic	Low	+/ND	ND	Parotidectomy	60 NED
13	42/F	Parotid	0.7	Pure IC intercalated duct type, unicystic	Low	+/ND	ND	Parotidectomy	60 NED
14	61/F	Parotid	1.5	Pure IC intercalated duct type, solid, microcystic, "MASC-like" Focal necrosis	Low	+/+	−	Partial parotidectomy (deep lobe)	8 NED
15	36/M	Parotid	1.0	Pure IC intercalated duct type, solid, microcystic, "MASC-like"	Low	+/+	−	Partial parotidectomy	8 NED
16	50/M	Parotid	2.5	Pure IC intercalated duct type, solid, microcystic, "MASC-like"	Low	+/+	−	Partial parotidectomy	12 NED
17*	66/M	Parotid	1.3	IC with widespread apocrine features, and hybrid intercalated duct pattern	Intermediate	+/+	+	NA	NA

*Published as case no.15 in Weinreb et al.[10]
F indicates female; MGA, mammaglobin; M, male; NA, not available; ND, not done; NED, no evidence of disease.

cholesterol clefts and foamy histiocytes. Tumor stroma was densely collagenized in 3 cases, while in one case there was rich lymphoid stroma with a growth pattern similar to Warthin tumor (case 1) (Fig. 3C).

On high-power magnification, all cases showed bland cytology, with tumor cells ranging from small to medium size, with indistinct cell borders, showing round or ovoid nuclei with dark condensed or finely dispersed chromatin and large pale to eosinophilic cytoplasm. Mitoses were inconspicuous and only in one case there were focal comedo necrosis (case 14). Tumor cells showed lipofuscin-like brown pigment within cells intracytoplasmic vacuoles in most cases (Fig. 3D). Six cases showed focal (cases 5, 9) or extensive apocrine differentiation (cases 3, 11, 12, 17) (Fig. 4A).

In ICs with apocrine and mixed hybrid growth patterns (6/17), most tumor cells were positive for androgen receptor (AR) (Fig. 4B). All examined IC cases were positive for S100 protein (Fig. 5A), mammaglobin (Fig. 5B), and SOX-10 (Fig. 5C), typically in a strong and diffuse manner. An intact myoepithelial cell layer surrounding tumor islands was evidenced by p63 immunohistochemical expression (which was negative in other tumor cells) (Fig. 5D). Calponin, and CK 14 decorated an intact peripheral myoepithelial cell layer in all examined cases, as well. Staining for DOG1 was negative in most cases, with limited areas of positive cells in one case. Proliferative activity was generally low, with a mean MIB1 index <5% (range 1% to 10%).

DISCUSSION

The term "intraductal carcinoma" of the salivary gland was first introduced in 1983 by Chen[15] in a description of a single case arising in minor salivary gland of the oral cavity. Subsequently, several case reports and small series of the same tumor entity were published with various names, including "low-grade salivary duct carcinoma,"[16,17] and "low-grade cribriform cystadenocarcinoma."[18] These all referred to a combination of cystic and solid structures of varying size formed by intraductal epithelial proliferation composed of cells resembling intercalated ductal cells and structures similar to atypical ductal hyperplasia and ductal carcinoma in situ of breast. In the current WHO classification, this tumor is now again regarded as an IC.[9]

IC has been surrounded by controversy since its discovery not only because of variable terminologies, but mainly because of its uncertain relationship to SDC.[16–19]

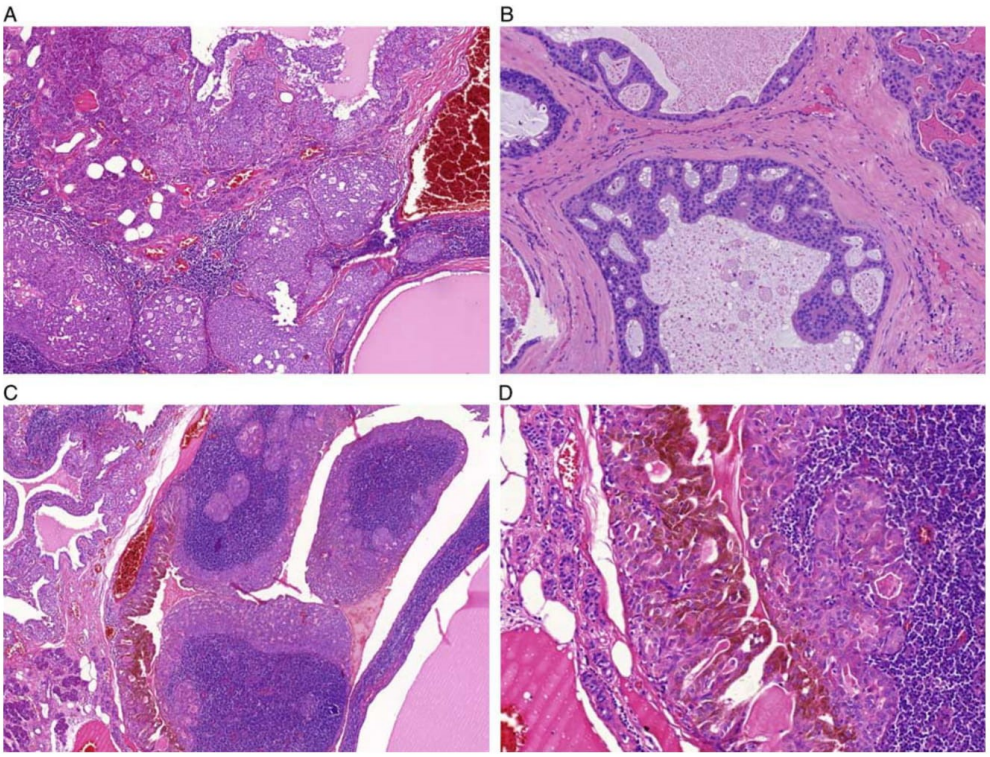

FIGURE 3. IC, intercalated duct type. A, All tumors were characterized by luminal epithelial proliferations with ductal phenotype arranged mainly in multiple cystic patterns, besides solid and cribriform islands. B, Intracystic growth often formed micropapillary structures with anastomosing and filigreed epithelial tufts, comprising the so called Roman-bridges pattern. C, There was rich lymphoid stroma with growth pattern similar to Warthin tumor in case 1. D, Tumor cells showed lipofuscin-like brown pigment within cells intracytoplasmic vacuoles in most cases.

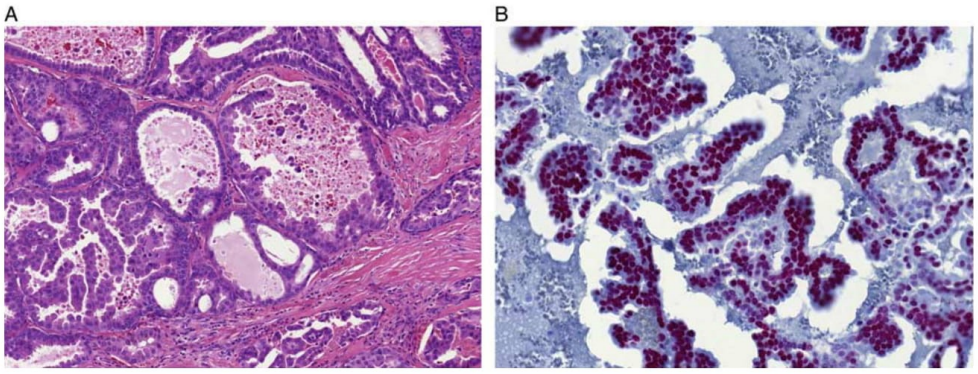

FIGURE 4. IC, apocrine variant. IC with widespread apocrine differentiation (A). Most tumor cells were positive for AR (B).

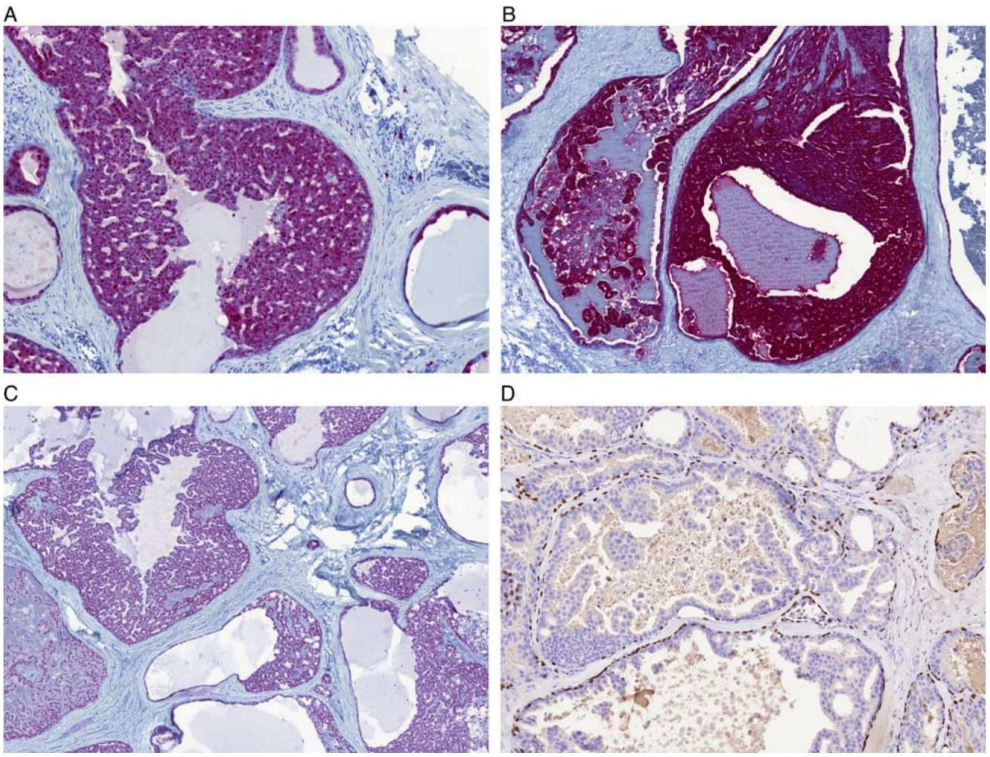

FIGURE 5. IC, immunoprofile. IC cases were positive for S100 protein (A), mammaglobin (B), and SOX-10 (C), typically in a strong and diffuse manner. An intact myoepithelial cell layer surrounding tumor islands was evidenced by p63 immunohistochemical expression (which was negative in other tumor cells) (D). Calponin, and CK 14 (D) decorated an intact peripheral myoepithelial cell layer.

In typical cases, IC is noninvasive low-grade carcinoma composed of bland neoplastic cells positive for S100, which is in sharp contrast to SDC. SDC is defined by the recent WHO classification as an aggressive epithelial malignancy resembling high-grade mammary ductal carcinoma; and it is composed of polymorphic cells with S100 negative and AR positive immunoprofile.[20] Therefore these 2 lesions are generally accepted as distinct and separate entities.[19,21,22] Despite this, there are, in the literature, occasional well documented low-grade ICs with subsequent widespread invasion.[10,23] Even more confusing are rare cases of true high-grade SDC reported as purely "in situ lesions."[24]

In recent years, many salivary gland low-grade carcinomas have been found to have pathognomonic translocations and characteristic chromosomal rearrangements. These include *ETV6-NTRK3* and *ETV6-RET* in MASC,[1,8] *MYB-NFIB* and *MYBL1-NFIB* in adenoid cystic carcinoma,[25] *EWSR1-ATF1* in (hyalinizing) clear cell carcinoma,[26] *CRTC1/CRTC3-MAML2* in mucoepidermoid carcinoma,[27] and *PRKD1-3* rearrangements in cribriform adenocarcinoma of tongue and other minor salivary glands.[28] These alterations are tumor-specific and are present in majority of the cases of the given tumor entity. Therefore they may serve as diagnostic markers useful for improvement of salivary gland tumor classification and taxonomy. There have been very few genomic studies to investigate the relationship of carcinomas with prevailing intraductal growth pattern and their morphologies and mimics. In particular, recently Weinreb et al,[10] reported a series of intraductal and invasive carcinomas of intercalated salivary duct origin. They categorized IC into intercalated duct and apocrine phenotype. IC with intercalated duct differentiation harbored a *NCOA4-RET* fusion in one index case and an inversion pattern of *RET* rearrangement by FISH in a subset of cases suggested this may represent a dominant fusion.[10] Only one case in this study showed a classic break-apart pattern with *RET* FISH, suggesting an alternate fusion.[10] In contrast, IC with apocrine phenotype were shown to be negative for *NCOA4-RET*.[10]

In the current study, which is the largest genomic study of IC to date, the *NCOA4-RET* was confirmed to be the dominant fusion in IC, and likely represented all the *RET* positive cases previously reported with an inversion pattern of rearrangement by FISH. A new finding in our study has been a discovery of a subset of IC patients with apocrine variant IC harboring a novel *TRIM27-RET*. The single case with a classic break-apart for *RET* reported by Weinreb et al,[10] was retested in this study and confirmed to harbor *TRIM27-RET*. To our knowledge, *TRIM27--RET* has not been recognized in any other salivary gland tumor so far. A total of 8 of 17 cases (47%) were confirmed to harbor a *RET* fusion. Interestingly, recent studies using RNA sequencing have revealed that SDC may also be added to the growing list of gene fusion-positive salivary carcinomas, with *NCOA4-RET* fusions having been found in 2 SDCs.[29] Both *NCOA4-RET* translocated SDC were positive for AR, and the tumors progressed in spite of undergoing concurrent chemoradiation, combination chemotherapy, and dual androgen deprivation therapy. Both patients with *NCOA4-RET* translocation, however, benefited from *RET*-targeted therapy.[29]

IC has a generally identical immunoprofile with MASC (S100 protein/mammaglobin positive and DOG1/p63 negative in tumor ductal cells with p63 protein immunostaining only in abluminal myoepithelial layer); interestingly MASC (particularly those with *ETV6-RET* gene fusions) seem to closely resemble *NCOA4-RET* translocated ICs by histomorphology as well. Therefore, it is possible that the *NCOA4-RET* gene fusion reported in one case of "MASC" actually represented a case of IC, possibly with invasion concealing its intraductal origin.[11]

In conclusion, NGS analysis of 17 cases of IC detected a *NCOA4-RET* fusion transcript joining exon 7 or 8 of *NCOA4* gene and exon 12 of *RET* gene in 6 cases of intercalated duct type IC; and a novel *TRIM27-RET* fusion transcript between exons 3 and 12 in 2 cases of salivary gland tumors displaying histologic and immunohistochemical features typical of apocrine IC for a total of 47% of IC cases. All analyzed cases were negative for *ETV6-NTRK3* gene fusion by the FusionPlex kit, RT-PCR, and *ETV6* gene was found intact by FISH. A novel finding in our study has been a discovery of a subset of IC patients with apocrine variant IC harboring a novel *TRIM27-RET*. The *RET* negative cases seen in this study and by Weinreb and colleagues, account for half of all ICs. There is likely a non-*RET* fusion or other finding that is not detectable using our current NGS platform and requires further study.

REFERENCES

1. Skálová A, Vanecek T, Sima R, et al. Mammary analogue secretory carcinoma of salivary glands, containing the *ETV6-NTRK3* fusion gene: a hitherto undescribed salivary gland tumor entity. *Am J Surg Pathol*. 2010;34:599–608.
2. Bishop JA, Yonescu R, Batista D, et al. Most nonparotid "acinic cell carcinomas" represent mammary analog secretory carcinomas. *Am J Surg Pathol*. 2013;37:1053–1057.
3. Chiosea SI, Griffith C, Assaad A, et al. Clinicopathological characterization of mammary analogue secretory carcinoma of salivary glands. *Histopathology*. 2012;61:387–394.
4. Chiosea SI, Griffith C, Assaad A, et al. The profile of acinic cell carcinoma after recognition of mammary analog secretory carcinoma. *Am J Surg Pathol*. 2012;36:343–350.
5. Skalova A, Bell D, Bishop JA, et al. Secretory carcinoma. In: El-Naggar A, Chan JKC, Grandis JR, Takata T, Slootweg PJ, eds. *World Health Organization (WHO) Classification of Head and Neck Tumours*, 4th ed. Lyon, France: IARC Press; 2017:177–178.
6. Ito Y, Ishibashi K, Masaki A, et al. Mammary analogue secretory carcinoma of salivary glands: a clinicopathologic and molecular study including 2 cases harboring *ETV6-X* fusion. *Am J Surg Pathol*. 2015;39:602–610.
7. Skalova A, Vanecek T, Simpson RH, et al. Mammary analogue secretory carcinoma of salivary glands: molecular analysis of 25 *ETV6* gene rearranged tumors with lack of detection of classical *ETV6-NTRK3* fusion transcript by standard RT-PCR: Report of 4 cases harboring *ETV6-X* gene fusion. *Am J Surg Pathol*. 2016;40:3–13.
8. Skálová A, Vanecek T, Martinek P, et al. Molecular profiling of mammary analog secretory carcinoma revealed a subset of tumors harboring a novel *ETV6-RET* translocation: report of 10 cases. *Am J Surg Pathol*. 2018;42:234–246.
9. Loening T, Leivo I, Simpson RHW, et al. Intraductal carcinoma. In: El-Naggar A, Chan JKC, Grandis JR, Takata T, Slootweg PJ, eds. *World Health Organization (WHO) Classification of Head and Neck Tumours*, 4th ed. Lyon, France: IARC Press; 2017:170–171.
10. Weinreb I, Bishop JA, Chiosea SI, et al. Recurrent *RET* gene rearrangements in intraductal carcinomas of salivary gland. *Am J Surg Pathol*. 2018;42:442–452.
11. Dogan S, Benayed R, Chen H, et al. Genomic profiling of the two related "cousins" acinic cell carcinoma and mammary analog secretory carcinoma of salivary glands reveals novel *NCOA4-RET* fusion in mammary analog secretory carcinoma. Abstract USCAP 2017. *Mod Pathol*. 2017;Suppl 30:323A.
12. Bishop JA, Yonescu R, Batista D, et al. Utility of mammaglobin immunohistochemistry as a proxy marker for the *ETV6-NTRK3* translocation in the diagnosis of salivary mammary analogue secretory carcinoma. *Hum Pathol*. 2013;44:1982–1988.
13. Stevens TM, Kovalovsky AO, Velosa C, et al. Mammary analog secretory carcinoma, low grade salivary duct carcinoma, and mimickers: a comparative study. *Mod Pathol*. 2015;28:1084–1100.
14. Shah AA, Wenig BM, LeGallo RD, et al. Morphology in conjunction with immunohistochemistry is sufficient for the diagnosis of mammary analogue secretory carcinoma. *Head and Neck Pathol*. 2015;9:85–95.
15. Chen KT. Intraductal carcinoma of the minor salivary gland. *J Laryngol Otol*. 1983;97:189–191.
16. Delgado R, Klimstra D, Albores-Saavedra J. Low grade salivary duct carcinoma. A distinctive variant with a low grade histology and a predominant intraductal growth pattern. *Cancer*. 1996;78:956–967.
17. Brandwein-Gensler M, Hille J, Wang LJ, et al. Low-grade salivary duct carcinoma: description of 16 cases. *Am J Surg Pathol*. 2004;28:1040–1044.
18. Brandwein-Gensler MS, Gnepp DR. WHO classification of tumours. Low-grade cribriform cystadenocarcinoma. In: Barnes L, Eveson JW, Reichert P, Sidransky D, eds. *Pathology and Genetics of Head and Neck Tumours*. Lyon: IARC Press; 2005:233.
19. Simpson RHW. Salivary duct carcinoma: new developments—morphological variants including pure in situ high grade lesions; proposed molecular classification. *Head Neck Pathol*. 2013;7:S48–S58.
20. Nagao T, Licitra L, Loening T, et al. Salivary duct carcinoma. In: El-Naggar A, Chan JKC, Grandis JR, Takata T, Slootweg PJ, eds. *World Health Organization (WHO) Classification of Head and Neck Tumours*, 4th ed. Lyon, France: IARC Press; 2017:173–174.
21. Cheuk W, Miliauskas JR, Chan JKC. Intraductal carcinoma of the oral cavity. A case report and a reappraisal of the concept of pure ductal carcinoma in situ in salivary gland carcinoma. *Am J Surg Pathol*. 2004;28:266–270.
22. Laco J, Podhola M, Doležalova H. Low-grade cribriform cystadenocarcinoma of the partoid gland: a neoplasm with favourable prognosis, distinct from salivary duct carcinoma. *Int J Surg Pathol*. 2010;18:369–373.
23. Weinreb I, Tabanda-Lichauco R, Van der Kwast T, et al. Low-grade intraductal carcinoma of salivary gland: report of 3 cases

with marked apocrine differentiation. *Am J Surg Pathol*. 2006;30:1014–1021.
24. Simpson RH, Desai S, Di Palma S. Salivary duct carcinoma in situ of the parotid gland. *Histopathology*. 2008;53:416–425.
25. Persson M, Andrén Y, Mark J, et al. Recurrent fusion of MYB and NFIB transcription factor genes in carcinomas of the breast and head and neck. *Proc Natl Acad Sci USA*. 2009;106:18740–18744.
26. Antonescu CR, Katabi N, Zhang L, et al. *EWSR1-ATF1* fusion is a novel and consistent finding in hyalinizing clear-cell carcinoma of salivary gland. *Genes Chromosomes Cancer*. 2011;50:559–570.
27. Tonon G, Modi S, Wu L, et al. t(11;19)(q21;p13) translocation in mucoepidermoid carcinoma creates a novel fusion product that disrupts a Notch signaling pathway. *Nat Genet*. 2003;33:208–213.
28. Weinreb I, Zhang L, Tirunagari LM, et al. Novel *PRKD* gene rearrangements and variant fusions in cribriform adenocarcinoma of salivary gland origin. *Genes Chromosomes Cancer*. 2014;53:845–856.
29. Wang K, Russell JS, McDermott JD, et al. Profiling of 149 salivary duct carcinomas, carcinoma ex pleomorphic adenomas, and adenocarcinomas, not otherwise specified reveals actionable genomic alterations. *Clin Cancer Res*. 2016;22:6061–6068.

1.11.2 *NCOA4-RET* A *TRIM27-RET* JSOU CHARAKTERISTICKÉ GENOVÉ FÚZE SALIVÁRNÍHO INTRADUKTÁLNÍHO KARCINOMU ZAHRNUJÍCÍ INVAZIVNÍ I METASTATICKÉ TUMORY: JE TERMÍN „INTRADUKTÁLNÍ“ SPRÁVNĚ?

Druhá studie zabývající se problematikou IC, analyzuje 33 nových případů IC a porovnává je se sérií 20 salivárních duktálních karcinomů (SDC). Těchto 33 případů IC bylo IHC a molekulárně geneticky vyšetřeno a identifikované fúze byly konfirmované metodami FISH a RT-PCR.

Soubor 33 IC tvořilo 24 případů s fenotypem z vmezeřených duktů, 6 případů s čistě apokrinními rysy a 4 případy hybridní morfologie. Všechny IC exprimovaly p63 či p40, v intaktní myoepiteliální abluminální vrstvě. Celkem 24 případů IC exprimovalo S100 protein a SOX10. Většina IC s apokrinním a hybridním fenotypem byly jaderně AR pozitivní. Čisté apokrinní IC navíc byly pozitivní na AR a negativní na S100 protein/SOX10, vyjma jednoho případu se všemi pozitivními markery.

V 11 případech IC z vmezeřených duktů byla zjištěna fúze *NCOA4-RET,* přičemž ve 2 případech byl přítomen invazivní růst a v 1 byla zastižena rozsáhlá invaze s metastázou do lymfatické uzliny. Ve 2 případech IC s apokrinními rysy byla identifikována fúze mezi exonem 3 genu *TRIM27* a exonem 12 genu *RET*, jeden z těchto 2 případů byl invazivního růstu. Dále byly zastiženy 2 případy s nově identifikovanými fúzními transkripty *TUT1-ETV5* (fenotyp z vmezeřených duktů) a *KIAA1217-RET* (hybridní fenotyp), oba měly invazivní charakter. Zbylé 3 případy byly též invazivního charakteru, 2 z nich byly molekulárně geneticky neanalyzovatelné a 1 byl negativní. Celkem 42,4 % případů v sérii IC mělo zlom v genu *RET*.

Ve skupině 20 SDC, z nichž 10 bylo vyšetřeno molekulárně geneticky, nebyla zastižena žádná z výše popsaných fúzí. Imunohistochemicky se jednalo o klasické SDC, exprimující CK7 a negativní s S100 proteinem a s markery proti bazální-myoepiteliální vrstvě.

Z hlediska molekulárně genetického pozadí pouze jedna studie z roku 2016 využívající RNA sekvenaci objevila *NCOA4-RET* fúzi ve 2 případech SDC (80). Tyto případy byly klasifikovány jako SDC na podkladě pozitivity AR. Klinicky se jednalo o nádory, které neodpovídaly na chemoradioterapii ani na terapii androgeny, ale oba pacienti profitovali z léčby RET-inhibitory. I přesto že se jedná o sugestivní nález, v kontextu celé studie a zejména díky obrázkové dokumentaci není morfologie 2 případů *NCOA4-RET* translokovaných SDC kompatibilní s diagnózou SDC. Chybí též údaje o vyšetření SOX10, mammaglobin či S100 protein a AR byly jen fokálně pozitivní. Což nás přivádí k hypotéze, že tyto *RET*-translokované nádory nejsou pravými SDC a že, dle našeho názoru, spíše představují hybridní apokrinně/vmezeřenou variantu IC.

Různý molekulární profil IC a SDC podporuje tvrzení, že se jedná o odlišné maligní nádory slinných žláz. Nález nádorově-specifických fúzí *NCOA4-RET* a *TRIM27-RET* v podskupině invazivních karcinomů s fenotypem z vmezeřených duktů a apokrinním je více než podnětný. Přivádí nás k názoru, že spíše než termín „intraduktální karcinom“ navržený WHO klasifikací z roku 2017 by se měl vžít termín „neinvazivní (či invazivní) karcinom z vmezeřených duktů“ pro nádory s S100 protein/SOX10/mammaglobin pozitivitou, negativitou AR a se zachovanou myoepiteliální vrstvou. Tento typ karcinomu z vmezeřených duktů představuje jednu linii diferenciace, která může obsahovat onkocytární, apokrinní či světlobuněčnou komponentu. Nádory charakterizované pozitivitou AR, negativitou na S100 protein/mammaglobin či případně ohraničené *TRIM27-RET* genovou fúzí by měly být pojmenovány „karcinomy z vmezeřených duktů s apokrinními rysy“. Termín SDC by pak měl být rezervovaný pro pokročile invazivní high-grade malignity a měl by být klasifikovaný podle

již dříve stanovených kritérií (81). Genetické alterace postihující SDC zahrnují amplifikaci genu *HER2-neu*, hotspot mutace *PIK3CA* a *HRAS* a mnoho dalších, které nebyly popsané v IC (55).

NCOA4-RET and *TRIM27-RET* Are Characteristic Gene Fusions in Salivary Intraductal Carcinoma, Including Invasive and Metastatic Tumors

Is "Intraductal" Correct?

Alena Skálová, MD, PhD,† Nikola Ptáková, MSc,‡ Thalita Santana, DDS, MSc, PhD,§ Abbas Agaimy, MD, PhD,‖ Stephan Ihrler, MD, PhD,¶ Emmanuelle Uro-Coste, MD, PhD,#** Lester D.R. Thompson, MD,†† Justin A. Bishop, MD, PhD,‡‡ Martina Baněčkova, MD,* Niels J. Rupp, MD,§§ Patrizia Morbini, MD,‖‖ Stefano de Sanctis, MD, PhD,¶¶ Marco Schiavo-Lena, MD,## Tomas Vanecek, PhD,‡ Michal Michal, MD,* and Ilmo Leivo, MD, PhD****

Abstract: Intraductal carcinoma (IC) is the new WHO designation for tumors previously encompassed by "low-grade cribriform cystadenocarcinoma" and "low-grade salivary duct carcinoma." The relationship of IC to salivary duct carcinoma (SDC) is controversial, even though they are considered to be distinct entities. IC is a rare low-grade malignant salivary gland neoplasm with histopathological features reminiscent of atypical ductal hyperplasia or ductal carcinoma in situ of the breast, showing diffuse S100 protein and mammaglobin positivity, while it is partially defined genetically. Recently, *RET* rearrangements including *NCOA4-RET* and *TRIM27-RET* have been described in IC. Here, we genetically characterize the largest cohort of IC to date (33 cases) including 8 cases with focal or widespread invasive growth and 1 case with lymph node metastasis. Thirty-three cases of IC were analyzed by next-generation sequencing (NGS) using the FusionPlex Solid Tumor kit (ArcherDX). Identified gene fusions were confirmed using fluorescence in situ hybridization break-apart and fusion probes and an reverse transcription polymerase chain reaction designed specifically for the detected breakpoints. Ten cases of SDC were analyzed for comparison using NGS panels that detect mutations and fusion transcripts. NGS analysis detected an *NCOA4-RET* fusion transcript in 11 cases of intercalated duct-type IC joining exon 7 or 8 of *NCOA4* gene and exon 12 of the *RET* gene. Eight cases of IC had an invasive growth pattern, including one with widespread invasion and lymph node metastasis. Three invasive ICs harbored an *NCOA4-RET* fusion transcript, while 1 case was negative, and 2 cases were not analyzable. In addition, a novel *TRIM27-RET* fusion transcript between exon 3 of *TRIM27* and exon 12 of *RET* was identified in 2 cases of IC with apocrine features, and one of them displayed invasive growth. Two IC cases with invasive growth harbored novel fusions *TUT1-ETV5* and *KIAA1217-RET*, respectively. A total of 42.4% of the cases in this series of IC harbored fusions involving *RET*. Such fusion transcripts were not detected in any of the 10 SDC cases. We have confirmed *NCOA4-RET* as a predominant fusion in intercalated duct-type IC, including 3 cases with invasive growth pattern. A novel finding in our series was a case of widely invasive intercalated duct-type IC, with a single lymph node metastasis that revealed an *NCOA4-RET* fusion transcript. We also demonstrated that a subset of apocrine ICs harbored a *TRIM27-RET* gene fusion, including one case with invasive growth. In contrast, neither *NCOA4-RET* nor *TRIM27-RET* fusions were detected in any tested SDCs. Thus, the distinct molecular findings in IC and SDC support that the

From the *Department of Pathology, Charles University, Faculty of Medicine in Plzen; †Biopticka Laboratory Ltd; ‡Molecular and Genetic Laboratory, Biopticka Laboratory Ltd, Plzen, Czech Republic; §Department of Oral Pathology, Faculty of Dentistry, University of São Paulo, São Paulo, Brasil; ‖Department of Pathology, University of Erlangen, Erlangen; ¶Dermpath, Muenchen, Germany; #Department of Pathology, Toulouse University Hospital, IUC-Oncopole; **INSERM U1037, Cancer Research Center of Toulouse (CRCT), Toulouse, France; ††Department of Pathology, Southern California Permanente Medical Group, Woodland Hills, CA; ‡‡Department of Pathology, UT Southwestern Medical Center, Dallas, TX; §§Department of Pathology and Molecular Pathology, University Hospital and University of Zurich, Zurich, Switzerland; ‖‖Unit of Pathology, University of Pavia and Foundation I.R.C.C.S Policlinico San Matteo, Pavia, Italy; ¶¶Histopathology Department, Addenbrooke Hospital, Cambridge University Hospitals NHS Trust, Cambridge, UK; ##Department of Pathology, IRCCS San Raffaele Scientific Institute, Milan, Italy; and ***Institute of Biomedicine, Pathology, University of Turku, and Turku University Hospital, Turku, Finland.

Preliminary results of the study were presented as a platform presentation at the 107th Annual Meeting of the USCAP, Vancouver, Canada, March 17–22, 2018.

Conflicts of Interest and Source of Funding: Supported in parts by the grant SVV–2018 No. 260 391 provided by the Ministry of Education Youth and Sports of the Czech Republic (A.S. and M.B.); and by grants from the Finnish Cancer Society and Finska Läkaresällskapet, Helsinki (I.L.). The authors have disclosed that they have no significant relationships with, or financial interest in, any commercial companies pertaining to this article.

Correspondence: Alena Skálová, MD, PhD, Sikl's Department of Pathology, Medical Faculty of Charles University, Faculty Hospital, E. Benese 13, Plzen 305 99, Czech Republic (e-mail: skalova@fnplzen.cz).

tumors are separate malignant salivary tumor entities. The presence of tumor-type–specific *NCOA4-RET* or *TRIM27-RET* translocations in a subset of widely invasive carcinomas with intercalated duct-like immunoprofiles suggests that a recharacterization of IC including its redesignation as "intercalated duct carcinoma, invasive or noninvasive" may be appropriate.

Key Words: salivary gland neoplasms, intraductal carcinoma, intercalated duct carcinoma, apocrine, *NCOA4-RET*, *TRIM27-RET*, *RET*-targeted therapy, gene fusion, cohort studies

(*Am J Surg Pathol* 2019;43:1303–1313)

In the 2017 World Health Organization Classification of Head and Neck Tumours,[1] the tumor entity originally described as "low-grade salivary duct carcinoma"[2] and later called "low-grade cribriform cystadenocarcinoma"[3] was renamed as intraductal carcinoma (IC). IC is a rare low-grade salivary gland malignancy with histomorphologic features reminiscent of atypical ductal hyperplasia or ductal carcinoma in situ of the breast. The tumor is, in typical cases, characterized by intraductal and intracystic proliferation of luminal ductal cells exhibiting solid, cribriform, and papillary patterns. Its in situ intraductal nature is demonstrated by an intact myoepithelial cell layer highlighted by antibodies to p63 protein, calponin, and/or cytokeratin 14. IC typically shows an intercalated duct phenotype demonstrating S100 protein and SOX10 positivity of luminal cells, while a subset of IC shows apocrine morphology further supported by androgen receptor (AR) immunoexpression.[4] Rare lesions show mixed features of the 2 (hybrid types).

Recent studies investigating the molecular genetics of IC showed recurrent rearrangements of the *RET* gene with a predominant *NCOA4-RET* fusion in the intercalated duct-type IC,[5,6] and a *TRIM27-RET* fusion in the apocrine-type IC.[6,7] Recurrent rearrangements involving *RET* have been identified in 47% of cases of low-grade IC with S100 positivity and intercalated duct phenotype.[5,6] *NCOA4-RET* fusion was described in noninvasive IC, and the *RET* gene was identified as an apparent early oncogenic driver.[5,6] Interestingly, rare but well-documented cases of IC with focal or widespread invasive growth have been reported.[4,6] Although previous cases of IC with microinvasion were known,[2,8,9] the first case of S100 protein–positive and AR-negative intercalated duct-type IC with *NCOA4-RET* gene fusion and an invasive component was described recently by Weinreb et al (case 1).[5] In our previous study, we reported invasive growth in one case of IC with apocrine features and *TRIM27-RET* gene fusion (case 3).[6] Thus, there is a growing body of evidence indicating that *RET*-rearranged ICs are not always indolent in situ malignancies, but may be widely invasive.

Moreover, *RET*-rearranged IC cases with hybrid intercalated duct and apocrine features have been reported.[5,7] These findings, in particular, intercalated predominant and pure apocrine carcinomas with widely invasive growth patterns and *RET* rearrangement suggest that the current term "intraductal carcinoma" (WHO 2017)[1] should be replaced by a more appropriate designation. It is the opinion of the authors of this study that the term "intraductal carcinoma" is a misnomer because of cases with widely invasive carcinomas with a background of in situ intraductal low-grade lesions harboring *NCA4-RET* or *TRIM27-RET* gene fusions. To support this hypothesis, we have genetically characterized the largest cohort of IC to date (33 cases), including 8 cases with focal to widespread invasive growth and 1 case with lymph node metastasis. The relationship of IC to salivary duct carcinoma (SDC) has been controversial since the first description of IC.[2,8–13] Ten cases of SDC were analyzed for comparison using next-generation sequencing (NGS) panels that detect mutations and fusion transcripts.

MATERIALS AND METHODS

Among >6200 cases of primary salivary gland tumors, 33 cases of IC were retrieved from the consultation files of the Salivary Gland Tumor Registry, at the Department of Pathology, Faculty of Medicine in Plzen, and Biopticka Laboratory Ltd, Plzen, Czech Republic, and from the consultation files of the coauthors. Twenty-nine cases originally diagnosed as SDC were, for comparison, retrieved from the consultation files of the Salivary Gland Tumor Registry, and 10 of them were analyzed by NGS.

The histopathologic features of all tumors and the immunohistochemical stains, when available, were reviewed by 3 pathologists (A.S., T.S., and M.B.). A diagnosis of IC was confirmed in cases that displayed histologic features consistent with the original description in conjunction with the appropriate immunohistochemical profile, that is, co-expression of S100 protein, cytokeratin CK7, and mammaglobin in the absence of DOG1 staining. Moreover, an intact myoepithelial layer decorated by p63 and/or CK14 and calponin provided evidence of the intraductal component. Tumors were classified further into 2 groups, according to criteria published recently[4]: those that showed an intercalated duct phenotype and those with an apocrine phenotype. This was determined both histologically and immunohistochemically. Thus, a total of 33 IC cases were studied by NGS using ArcherDX Fusion Plex kit.

A diagnosis of SDC was confirmed in cases that displayed histologic features consistent with original description in conjunction with the appropriate immunohistochemical profile, using criteria published recently.[14]

For conventional microscopy, the excised tissues were fixed in formalin, routinely processed, embedded in paraffin (FFPE), cut, and stained with hematoxylin and eosin.

For immunohistochemical analysis, 4-μm-thick sections were cut from paraffin blocks and mounted on positively charged slides (TOMO, Matsunami Glass IND, Japan). Sections were processed on a BenchMark ULTRA (Ventana Medical System, Tucson, AZ), deparaffinized, and then subjected to heat-induced epitope retrieval by

TABLE 1. Antibodies Used for Immunohistochemical Evaluation

Antibody Specificity	Clone	Dilution	Antigen Retrieval/time	Source
S-100 protein	Polyclonal	RTU	CC1/20 min	Ventana
Mammaglobin	304-1A5	RTU	CC1/36 min	DakoCytomation
CK7	OV-TL 12/30	1:200	CC1/36 min	DakoCytomation
p63	4A4	RTU	CC1/64 min	Ventana
SOX-10	Polyclonal	1:100	CC1/64 min	Cell Marque
MIB1	30-9	RTU	CC1/64 min	Ventana
Androgen receptor	SP107	RTU	CC1/64 min	Cell Marque
Calponin	EP798Y	RTU	CC1/36 min	Cell Marque
CK 14	SP53	RTU	CC1/64 min	Cell Marque

CC1 indicates EDTA buffer, pH 8.6; RTU, ready to use.

immersion in a CC1 solution at pH 8.6 at 95°C. All primary antibodies used are summarized in Table 1. The bound antibodies were visualized using the ultraView Universal DAB Detection Kit (Roche) and ultraView Universal Alkaline Phosphatase Red Detection Kit (Roche). The slides were counterstained with Mayer's hematoxylin. Appropriate positive and negative controls were used.

Where available, clinical follow-up was obtained from the patients, their physicians, or from referring pathologists.

Molecular Genetic Study

Sample Preparation for NGS and Reverse Transcription Polymerase Chain Reaction

For NGS and reverse transcription polymerase chain reaction (RT-PCR) analysis, 2 to 3 FFPE sections (10 μm thick) were macrodissected to isolate tumor-rich regions. Samples were extracted for total nucleic acid using Agencourt FormaPure Kit (Beckman Coulter, Brea, CA). The RNA integrity was evaluated using PreSeq RNA QC Assay, as was previously described.[6]

RNA Integrity Assessment and Library Preparation for NGS

Unless otherwise indicated, 250 ng of FFPE RNA was used as input for NGS library construction. To assess RNA quality, the PreSeq RNA QC Assay using iTaq Universal SYBR Green Supermix (Biorad, Hercules, CA) was performed on all samples during library preparation to generate a measure of the integrity of RNA (in the form of a cycle threshold [Ct] value). Library preparation and RNA QC were performed following the Archer FusionPlex Protocol for Illumina (ArcherDX Inc.). The Archer FusionPlex Solid Tumor Kit was used. Final libraries were diluted 1:100,000 and quantified in a 10 μL reaction following the Library Quantification for Illumina Libraries protocol and assuming a 200 bp fragment length (KAPA, Wilmington, MA). The concentration of final libraries was around 200 nM. Threshold representing the minimum molar concentration for which sequencing can be robustly performed was set at 50 nM.

NGS Sequencing and Analysis

Libraries were diluted to 4 nM and sequenced on a NextSeq sequencer (Illumina, San Diego, CA). The optimal number of raw reads per sample was set to 3 million. Library pools were diluted to 1.6 pM library stock with 20% 1.8 pM PhiX and loaded in the NextSeq cartridge.

The fusion and other rearrangement detection algorithm in Archer Analysis relies on the specificity of the gene-specific primers used in the amplification steps in the AMP process. The resulting FASTQ files were analyzed using the Archer Analysis software (version 5.1.7; ArcherDX Inc.).

Fluorescence In Situ Hybridization Analysis of RET Break and TRIM27-RET Fusion

Four-micrometer-thick FFPE sections were placed onto positively charged slides. Hematoxylin and eosin–stained slides were examined for determination of areas for cell counting.

The unstained slides were deparaffinized and incubated in the 1× Target Retrieval Solution Citrate pH 6 (Dako, Glostrup, Denmark) at 95°C for 40 minutes and subsequently cooled for 20 minutes at room temperature in the same solution. The slides were washed in deionized water for 5 minutes and digested in protease solution with Pepsin (0.5 mg/mL) (Sigma Aldrich, St. Louis, MO) in 0.01 M HCl at 37°C for 35 to 60 minutes according to the sample conditions. The slides were then placed into deionized water for 5 minutes, dehydrated in a series of ethanol solution (70%, 85%, and 96% for 2 min each), and air-dried.

For the detection of *RET* rearrangement, factory premixed commercial probe ZytoLight SPEC RET Dual Color Break Apart Probe (ZytoVision GmbH, Bremerhaven, Germany) was used. For the *TRIM27-RET* dual-fusion detection custom-designed SureFISH probe (Agilent Technologies Inc., Santa Clara) with chromosomal regions chr6:28631476-29131075 and chr10:43354893-43849282 was used. Probe mixture for fusion detection was prepared from corresponding probes (each color was delivered in a separated well), deionized water, and LSI Buffer (Vysis/Abbott Molecular) in a 1:1:1:7 ratio, respectively.

An appropriate amount of mixed and premixed probes was applied on specimens, covered with a glass coverslip, and sealed with rubber cement. The slides were incubated in the ThermoBrite instrument (StatSpin/Iris Sample Processing, Westwood, MA) with co-denaturation at 85°C/8 minutes and hybridization at 37°C/16 hours. The rubber-cemented coverslip was then removed, and the slide was placed in posthybridization wash solution (2xSSC/0.3% NP-40) at 72°C/2 minutes. The slide was air-dried in the dark, counterstained with 4′, 6′-diamidino-2-phenylindole DAPI (Vysis/Abbott Molecular), cover slipped, and immediately examined.

Fluorescence In Situ Hybridization Interpretation

The sections were examined with an Olympus BX51 fluorescence microscope (Olympus Corporation, Tokyo, Japan) using a ×100 objective and filter sets

Triple Band Pass (DAPI/SpectrumGreen/SpectrumOrange), Dual Band Pass (SpectrumGreen/SpectrumOrange), and Single Band Pass (SpectrumGreen or SpectrumOrange).

For each probe, 100 randomly selected nonoverlapping tumor cell nuclei were examined for the presence of yellow or green and orange fluorescent signals. As regards break-apart probe, yellow signals were considered negative, and separate orange and green signals were considered as positive; conversely, for fusion probe, yellow signals were considered positive, and separate orange and green signals were considered as negative. Cut-off values for break-apart and fusion probes were set to > 10% and 20% of nuclei with chromosomal breakpoint and fusion signals, respectively (mean+3 SD in normal non-neoplastic control tissues).

RT-PCR Analysis of NCOA4-RET and TRIM27-RET Fusion Transcripts

Two sample of cDNA prepared by standard reverse transcription procedure using Transcriptor First Strand cDNA Synthesis Kit (RNA input 500 ng) (Roche Diagnostics, Mannheim, Germany) was added to the reaction mixture consisting of 12.5 µL of HotStar Taq PCR Master Mix (QIAgen, Hilden, Germany), 10 pmol of each fusion-specific primer (Table 2), and distilled water up to 25 µL. The amplification program comprised denaturation at 95° C for 14 minutes and then 45 cycles of denaturation at 95° C for 1 minute, annealing at a temperature of 55°C for 1 minute and extension at 72°C for 1 minute. The program was completed by incubation at 72°C for 7 minutes.

Successfully amplified PCR products were purified with magnetic particles Agencourt AMPure (Agencourt Bioscience Corporation, A Beckman Coulter Company, Beverly, MA). Products were then bidirectionally sequenced using Big Dye Terminator Sequencing kit (Applied Biosystems, Foster City, CA), purified with magnetic particles Agencourt CleanSEQ (Agencourt Bioscience Corporation), all according to the manufacturer's protocol, and run on an automated sequencer ABI Prism 3130×l (Applied Biosystems) at a constant voltage of 13.2 kV for 11 minutes.

RESULTS

Molecular Genetic Findings

Thirty-three cases of IC were analyzed by NGS using the Anchored Multiplex PCR (AMP) chemistry technique (ArcherDX). An *NCOA4-RET* fusion transcript joining exon 7 or 8 of the *NCOA4* gene and exon 12 of the *RET* gene was detected in 11 cases of intercalated duct or hybrid types of IC. A novel *TRIM27-RET* fusion transcript between exon 3 of *TRIM27* and exon 12 of *RET* was detected in 2 cases with histologic and immunohistochemical features typical of the apocrine variant of IC. Two IC cases with invasion harbored novel fusions *TUT1-ETV5* and *KIAA1217-RET*, respectively. The fusion transcripts were confirmed by RT-PCR and by sequencing. Fluorescence in situ hybridization (FISH) analysis using *RET* break-apart probe showed 2 different patterns. One was deemed "negative" when distance criteria of the break-apart probe were used according to interpretation rules, even if a minor separation of signals was seen (cases 1 to 2, 8, 15 to 19, 26, and 29). The other pattern showed a regular break (classic positive pattern) with separation of signals detected in 3 cases (cases 3, 28, and 31). Confirmation using FISH *TRIM27-RET* fusion probe displayed fusion signals with amplification. Localization of *RET*, *NCOA4*, and *TRIM27* genes to obtain an explanation of the 2 different patterns in FISH break-apart results is shown in the Figure 1.

A total of 42.4% of the analyzed cases harbored an *RET* fusion by NGS. This was less than that in previous reports,[5,6] but almost one-third of our cases were found not analyzable (NA). By RT-PCR, the fusions *NCOA4-RET* and *TRIM27-RET* were confirmed in all NGS-positive cases. The *RET* break-apart probe and the *TRIM27-RET* fusion probe successfully detected rearrangement in both cases with *TRIM27-RET* fusion identified by NGS. Only a narrow separation of the FISH signals for *RET* rearrangement was obtained, as this rearrangement contains an intrachromosomal inversion. Such "false"-negative FISH results were obtained for all *NCOA4-RET* cases. The molecular findings are summarized in Tables 3 and 4.

Ten cases of high-grade salivary carcinomas, originally diagnosed as SDC, were analyzed by NGS using the Fusion Plex Solid Tumor and Comprehensive Thyroid and Lung (CTL) kits for Illumina (ArcherDX). The analysis revealed one case harboring an *ETV6-NTRK3* fusion, and therefore it was reclassified as a high-grade secretory carcinoma. NGS also detected 5 likely pathogenic mutations in 5 SDC cases (*HRAS*: c.182A > G p.Gln61Arg, *HRAS*: c.37G > C p.Gly13Arg, *AKT1*: c.49G > A p.Glu17Lys, *PTEN* c.1003C > T p.Arg335Ter). Homozygous deletion of locus 9p21 (*CDKN2A*) was detected in one case harboring an *HRAS* mutation. Two cases presented rearrangement of the *MYB* gene, while one case was positive for *PLAG1* rearrangement. *MDM2* amplification was found in one case harboring also a *PTEN* mutation. The other SDC cases were negative for *MDM2* amplification and showed no rearrangement in the genes *MYB*, *MYBL1*, *NFIB*, *NTRK1*, *RET*, and *PLAG1*. Neither *NCOA4-RET* nor *TRIM27-RET* fusions were detected in any SDC cases.

TABLE 2. Primers Used for RT-PCR Analysis

Name of Primer	Sequence 5′-3′
NCOA4-RET_7-12_F	CCCTTCCTGGAGAAGAGAGG
NCOA4-RET_7-12_R	GTACCCTGCTCTGCCTTTCA
NCOA4-RET_8-12_F	TACCCAAAAGCAGACCTTGG
NCOA4-RET_8-12_R	CGCCTTCTCCTAGAGTTTTTCC
TRIM27-RET_3-12_F	TGATCGCTCAGCTAGAAGAGAA
TRIM27-RET_3-12_R	CCAAGTTCTTCCGAGGGAAT
TUT1-ETV5_7-8_F	GTACTCGGCCTAGCCTCCAC
TUT1-ETV5_7-8_R	TCTGACATTTGCCGATGGTA
KIA1217-RET_14-9_F	CCAGTGGACAAGGTGGAACT
KIA1217-RET_14-9_R	AGGTGCCATAGCCAGCTTTA

Clinical and Histologic Characteristics of the Study Group

The study series consisted of 33 ICs; 25 neoplasms were pure intraductal in situ lesions, while 8 cases showed apparent

FIGURE 1. A–C, Sanger sequencing analysis of RT-PCR generated fusion transcripts NCOA4-RET (exon joining 7 to 12), NCOA4-RET (exon joining 8 to 12), and TRIM27-RET (exon joining 3 to 12). The arrow shows the fusion position.

invasive growth, in one case with a single metastasis in a periparotideal lymph node. The invasive carcinomas occurred in patients ranging in age from 36 to 64 years (mean: 52.5 y), and noninvasive IC in patients ranging in age from 17 to 81 years (mean: 56 y). The most common anatomic site of involvement was the parotid gland (n = 28), and there was 1 case each in the buccal mucosa, the palate, and the submandibular gland. Detailed clinical and histopathologic findings and follow-up information of 33 patients with IC are summarized in Table 4.

Microscopic and Immunohistochemical Features

Histologically, at low-power magnification, the ICs were well circumscribed and encapsulated in most cases. They were characterized by luminal epithelial proliferations with intercalated duct phenotype arranged mainly in multiple cystic patterns, besides solid and cribriform islands in 24/33 (73%) (Fig. 2A). Intracystic growth often formed micropapillary structures with anastomosing epithelial tufts, with snouts, decapitation secretion, and apocrine features in 6/33 cases (18%) (Fig. 2C). A hybrid intercalated duct and apocrine growth pattern were seen in 4/33 cases (12%). Widespread or focal invasive growth was found in 8 cases. In the cases of invasion, we estimate that the invasive component ranged roughly from 10 to 60% of the total tumor area. While no peritumoral lymphovascular invasion was noted in the IC cases, perineural invasion (Fig. 3A) and metastatic infiltration in a periparotid lymph node were observed in 1 case (Fig. 3B). Invasive areas revealed a compressed fibrotic stroma with desmoplasia. Case 6 was an unusual multinodular invasive low-grade carcinoma of the parotid gland composed of 2 distinctive growth patterns. A large part of the tumor was a low-grade salivary epithelial-myoepithelial carcinoma with apocrine differentiation in both the luminal epithelial and the abluminal myoepithelial cells, and it had a broadly invasive growth pattern. Another section of the same tumor revealed a noninvasive IC, of the intercalated duct type, with intracystic papillary and cribriform features.

TABLE 3. Detailed Molecular Findings of 33 Cases of Salivary Gland Intraductal Carcinomas

No.	Age (y)/Sex	Diagnosis	NGS	Exons Joining	FISH RET ba	FISH TRIM27-RET Fusion	RT-PCR Fusion Specific	FISH ETV6 ba	RT-PCR ETV6-NTRK3
1	38/M	Pure IC intercalated duct type, solid microcystic, rich lymphoid stroma	NCOA4-RET	8-12	Positive*	ND	Positive	Negative	Negative
2	47/M	Pure IC intercalated duct type, solid multicystic	NCOA4-RET	7-12	Positive*	ND	Positive	Negative	Negative
3	54/M	IC with apocrine features, micropapillary, invasive	TRIM27-RET	3-12	Positive	Positive	Positive	Negative	Negative
4	50/M	Pure IC intercalated duct type, solid multicystic	NA	—	NA	ND	Negative	Negative	Negative
5	58/M	Pure IC hybrid intercalated duct and apocrine type, solid microcystic, papillary	NA	—	NA	ND	ND	NA	Negative
6	81/M	Pure IC intercalated duct type, "roman bridges" Invasive component of epithelial-myoepithelial ca	NA	—	Negative	ND	Negative	Negative	Negative
7	50/F	Pure IC intercalated duct type, unicystic	Negative	—	Negative	ND	ND	Negative	Negative
8	74/M	Pure IC intercalated duct type, papillary, multicystic	NCOA4-RET	8-12	Positive*	ND	Positive	Negative	Negative
9	36/F	Pure IC intercalated duct type, few apocrine cells	Negative	—	Negative	ND	ND	Negative	Negative
10	53/F	IC intercalated duct type, stromal invasion, perineural invasion	Negative	—	Negative	ND	ND	Negative	Negative
11	75/F	IC with apocrine features, papillary, thick fibrous capsule	Negative	—	Negative	ND	ND	Negative	Negative
12	69/M	IC with apocrine features, unicystic	Negative	—	ND	ND	ND	ND	Negative
13	42/F	Pure IC intercalated duct type, unicystic	Negative	—	ND	ND	ND	Negative	Negative
14	75/F	Pure IC intercalated duct type, solid, microcystic	Negative	—	Negative	ND	Negative	Negative	Negative
15	61/F	Pure IC intercalated duct type, solid, microcystic	NCOA4-RET	7-12	Positive*	ND	Positive	NA	Negative
16	36/M	Pure IC intercalated duct type, solid, microcystic	NCOA4-RET	8-12	Positive*	ND	Positive	ND	ND
17	50/M	IC with widespread apocrine features, and hybrid intercalated duct pattern	NCOA4-RET	8-12	Positive*	Positive	Positive	ND	ND
18	36/M	IC intercalated duct pattern with widespread stromal invasion, periparotideal lymph node metastasis	NCOA4-RET	8-12	Positive*	ND	Positive	Negative	ND
19	48/M	IC intercalated duct type, solid microcystic	NCOA4-RET	8-12	ND	ND	ND	ND	ND
20	54/M	Pure IC with apocrine features	Negative	—	ND	ND	ND	ND	ND
21	51/M	Pure IC with widespread apocrine features, and hybrid intercalated duct pattern	Negative	—	ND	ND	ND	ND	ND
22	71/F	Pure IC intercalated duct type, solid microcystic	Negative	—	ND	ND	ND	ND	ND
23	64/M	Pure IC intercalated duct type	NA	—	ND	ND	ND	ND	ND
24	70/M	Pure IC intercalated duct type	NA	—	ND	ND	ND	ND	ND
25	17/M	IC intercalated duct type, solid, microcystic	NA	—	ND	ND	ND	ND	ND
26	55/F	IC intercalated duct type, solid, macrocystic, focally invasive	NCOA4-RET	7-12	ND	ND	ND	ND	ND
27	59/M	IC intercalated duct type, solid, macrocystic, focally invasive	NA	—	ND	ND	ND	ND	ND
28	66/M	IC, apocrine variant, intracystic papillary and micropapillary structures predominate, focal intercalated duct type of growth with solid pattern, no invasive growth	TRIM27-RET	3-12	Positive	Positive	Positive	ND	ND
29	52/M	IC, predominantly in situ intercalated duct variant, focally invasive	NCOA4-RET	7-12	ND	ND	Positive	ND	ND
30	64/M	IC, intercalated duct variant, focally invasive	TUT1-ETV5	7-8	ND	ND	NA	ND	ND

TABLE 3. (*continued*)

No.	Age (y)/Sex	Diagnosis	NGS	Exons Joining	FISH RET ba	FISH TRIM27-RET Fusion	RT-PCR Fusion Specific	FISH ETV6 ba	RT-PCR ETV6-NTRK3
31	47/F	IC, hybrid intercalated duct structures predominate, apocrine features, focally invasive	KIAA1217-RET	14-9	Positive	ND	Positive	ND	ND
32	70/F	IC, intercalated duct variant	Negative	—	ND	ND	ND	ND	ND
33	48/F	IC, intercalated duct variant	NCOA4-RET	7-12	ND	ND	Positive	ND	ND

Cases 1 to 17 were published in Skálová et al.[6]

*Cases showed an *RET* FISH signal pattern indicative of an inversion/rearrangement (in one allele a gap between orange and green signals was observed; hovewer, this gap did not reach internal cutoff (≥2 signal diameters apart).

F indicates female; M, male; NA, not analyzable; ND, not done.

On high-power magnification, all cases showed bland cytologic features, with tumor cells ranging from small to medium size. They had indistinct cell borders and round or ovoid nuclei with dark condensed or finely dispersed chromatin and large pale to eosinophilic cytoplasm. None of the cases in this study had an oncocytic morphology, although an oncocytic variant has been described in the literature.[15] Mitoses were inconspicuous. In all 8 IC cases with invasive growth, we have seen compressed sclerotic fibrosis representing apparent desmoplastic reaction around the invasive foci of the tumors (Fig. 3C). These invasive ICs did not have higher MIB1 indices. Proliferative activity in ICs was generally low, with a mean MIB1 index <5% (ranging from 1% to 10%). No difference was seen between invasive and noninvasive ICs.

The tumor islands of IC were surrounded by a layer of myoepithelial cells, as evidenced by the immunohistochemical expression of p63, calponin, and/or CK 14 (all of which were negative in luminal epithelial tumor cells) in a continuous abluminal pattern in 14/33 cases (43%) (Fig. 2B). A partly discontinuous immunostaining for p63 was seen in most cases (Fig. 3D). All IC cases assessed as completely intraductal were examined in total and stained with antibodies to calponin and p63/p40. Thus, hematoxylin and eosin–based information was verified by continuous immunostains corresponding to intact myoepithelial cell layers. In ICs with apocrine and mixed hybrid growth patterns (10/33 cases; 30%), most tumor cells were positive for nuclear AR (Fig. 2D). Diffuse and strong coexpression of S100 protein, mammaglobin, and SOX10 was detected in 24/33 cases (73%). Pure apocrine ICs were positive for AR and negative for S100 protein/SOX10 and mammaglobin in 4 cases, while, in one case, AR was strongly expressed together with S100 protein/SOX10 and mammaglobin.

DISCUSSION

The term "intraductal carcinoma" of the salivary gland was first introduced in 1983 by Chen[10] in a description of a single case arising in the minor salivary gland of the oral cavity. Subsequently, several case reports and small series of the same tumor entity were published with various names, including "low-grade salivary duct carcinoma"[2,8] and "low-grade cribriform cystadenocarcinoma." The latter designation was introduced by the editors of the 2005 WHO Classification of Head and Neck Tumours, although this term had never appeared in the literature before that point.[3] This term referred to cystic and solid structures formed by intraductal epithelial proliferation of cells resembling intercalated duct cells and structures reminiscent of atypical ductal hyperplasia and ductal carcinoma in situ of the breast. In the 2017 WHO Classification of Head and Neck Tumours, this tumor is regarded as an IC.[1] IC has been surrounded by controversy since its description not only because of variable terminologies but primarily because of the uncertain relationship to salivary duct carcinoma.[2,3,8,11] In typical cases, IC is a noninvasive low-grade carcinoma composed of bland neoplastic cells positive for S100 protein, in sharp contrast to those features seen in SDC. SDC is defined by the 2017 WHO classification as an aggressive epithelial malignancy resembling high-grade mammary ductal carcinoma. It is composed of pleomorphic S100 protein-negative and AR-positive neoplastic cells.[16] Therefore, these 2 lesions are generally accepted as distinct and separate entities.[5,6,13,14] However, the literature describes occasional well-documented low-grade ICs with widespread invasive growth.[2,3,5,6] Even more confusing are rare cases of true high-grade SDC reported as purely "in situ lesions."[11] Moreover, IC cases with hybrid intercalated duct and apocrine features,[5,7] oncocytic features,[15] and pure apocrine features with diffuse AR-positive and S100 protein/mammaglobin and/or SOX10-negative immunoprofile[4,6] have been described.

In recent years, many salivary gland low-grade carcinomas have been found to demonstrate characteristic tumor type–specific chromosomal rearrangements, such as *ETV6-NTRK3* and *ETV6-RET,* in secretory carcinoma (also known as mammary analogue secretory carcinoma),[17,18] *EWSR1-ATF1* and *EWSR1-CREM* in hyalinizing clear cell carcinoma of minor salivary glands,[19,20] *CRTC1-MAML2* and *CRTC3-MAML2* in mucoepidermoid carcinoma,[21] *ARID1A-PRKD1* and variant *PRKD1*, *PRKD2*, and *PRKD3* fusions in cribriform adenocarcinoma of minor salivary glands and *PRKD1* somatic mutations in polymorphous adenocarcinoma,[22–24] and *HTN3-MSANTD3* in a subset of acinic cell carcinoma of the salivary gland.[25] The growing list of gene fusion–positive salivary carcinomas

TABLE 4. Clinicopathologic and Molecular Findings in 33 Intraductal Carcinoma Cases

Case No.	Age (y)/Sex	Site	Size (cm)	NGS (Archer)	FISH	RT-PCR	Outcome (mo)
1	38/M	PA	4.0×1.7×1.4	*NCOA4-RET*	*RET*+* *ETV6*−	*NCOA4-RET*+ *ETV6-NTRK3*−	28 NED
2	47/M	PA	1.4	*NCOA4-RET*	*RET*+* *ETV6*−	*NCOA4-RET*+ *ETV6-NTRK3*−	44 NED
3	54/M	PA	2.2×1.2×0.9	*TRIM27-RET*	*RET*+† *ETV6*−	*TRIM27-RET*+ *ETV6-NTRK3*−	16 NED
4	50/M	PA	1.0	NA	*ETV6*−	*ETV6-NTRK3*−	65 NED
5	58/M	PA	1.5×1.0×0.9	NA	NA	*ETV6-NTRK3*−	152 NED
6	81/M	PA	—	NA	*ETV6*−	*ETV6-NTRK3*−	NAv
7	50/F	PA	15	No fusion	*ETV6*−	*ETV6-NTRK3*−	80 NED
8	74/M	PA	1.5	*NCOA4-RET*	*RET*+* *ETV6*−	*NCOA4-RET*+ *ETV6-NTRK3*−	70 NED
9	36/F	Buccal mucosa	0.6	No fusion	*ETV6*−	*ETV6-NTRK3*−	188 NED
10	53/F	PA	2.0×1.0×1.0	No fusion	*ETV6*−	*ETV6-NTRK3*−	188 NED
11	75/F	PA	4.6×4.0×1.7	No fusion	*ETV6*−	*ETV6-NTRK3*−	80 NED
12	69/M	PA	0.9	No fusion	ND	*ETV6-NTRK3*−	68 NED
13	42/F	PA	0.7	No fusion	*ETV6*−	*ETV6-NTRK3*−	68 NED
14	75/F	Hard palate	—	No fusion	*MAML2*−	*ETV6-NTRK3*− *CRTC3-MAML2*− *CTRC1-MAML2*−	NAv
15	61/F	PA	1.5×1.0×1.4	*NCOA4-RET*	ND	*ETV6-NTRK3*−	16 NED
16	36/M	PA	1.0×0.7×0.7	*NCOA4-RET*	*RET*+* *ETV6*− NA	*ETV6-NTRK3*−	16 NED
17	50/M	PA	2.6	*NCOA4-RET*	*RET*+*	*NCOA4-RET*+	20 NED
18	36/M	PA	5×4×4	*NCOA4-RET*	*RET*+* *NTRK3*− *ETV6*−	*NCOA4-RET*+	RT proton; 8 NED
19	48/M	PA	—	*NCOA4-RET*	ND	ND	12 NED
20	54/M	PA	1.5×8×0.5	No fusion	ND	ND	NAv
21	51/M	PA	2	No fusion	ND	ND	NAv
22	71/F	PA	1.8	No fusion	ND	ND	NAv
23	64/M	Subm	—	NA	ND	ND	NAv
24	70/M	PA	1.5	NA	ND	ND	NAv
25	17/M	PA	1.0	NA	ND	ND	96 NED
26	55/F	PA	1.5	*NCOA4-RET*	ND	ND	48NED
27	59/M	PA	1.2	NA	ND	ND	60 NED
28	66/M	PA	—	*TRIM27-RET*	*TRIM27*+ *RET*+†	*TRIM27-RET*+	NAv
29	52/M	PA	2.8	*NCOA4-RET*	*ETV6*− *RET*+*	*NCOA4-RET*+	NAv
30	64/M	PA	1.9	*TUT1-ETV5*	ND	NA	NAv
31	47/F	PA	1.0	*KIAA1217-RET*	*ETV6*− *RET*+†	*KIAA1217-RET*+	NAv
32	70/F	PA	2.5	No fusion	ND	ND	NAv
33	48/F	PA	2.4	*NCOA4-RET*	ND	*NCOA4-RET*+	NAv

*Cases showed an *RET* FISH signal pattern indicative of an inversion/rearrangement.
†Cases 3, 28, and 31 showed a classic break-apart signal pattern.
F indicates female; M, male; NA, not anlyzable; NAv, not available; ND, not done; NED, no evidence of disease; PA, parotid gland; RT proton, radiotherapy in proton center; subm, submandibular gland.

includes IC with an *NCOA4-RET* fusion reported recently.[5,6] In addition, we have described a subset of IC with apocrine morphology harboring a novel *TRIM27-RET* fusion.[6] Interestingly, one study using RNA sequencing has revealed *NCOA4-RET* fusions in 2 cases of salivary gland neoplasms classified as SDC on the basis of expression of AR.[13] Both *NCOA4-RET* translocated neoplasms progressed in spite of undergoing concurrent chemoradiation, combination chemotherapy, and dual androgen deprivation therapy. Both patients, however, benefited from *RET*-targeted therapy.[13] This would be a challenging finding, but the neoplasm described as *NCOA4-RET*-translocated SDC, and depicted in their Figure 3B is morphologically not compatible with SDC.[13] No reference to SOX10, mammaglobin, or S100 protein was made, while their Figure 3B shows only focal AR staining. Therefore, it is not clear whether these *RET*-translocated neoplasms are true SDCs.[13] It is the opinion of the authors that they most likely represented a hybrid apocrine/intercalated variant of IC.

None of the above-cited gene fusions were documented in SDC cases of the previous study[5] or in this current series. In view of the tumor type–specific rearrangements described in salivary neoplasms so far, it is not likely that multiple separate salivary tumor types would have the same *NCOA4-RET* and *RET* rearrangements. Thus, *NCOA4-RET* and *TRIM27-RET* gene

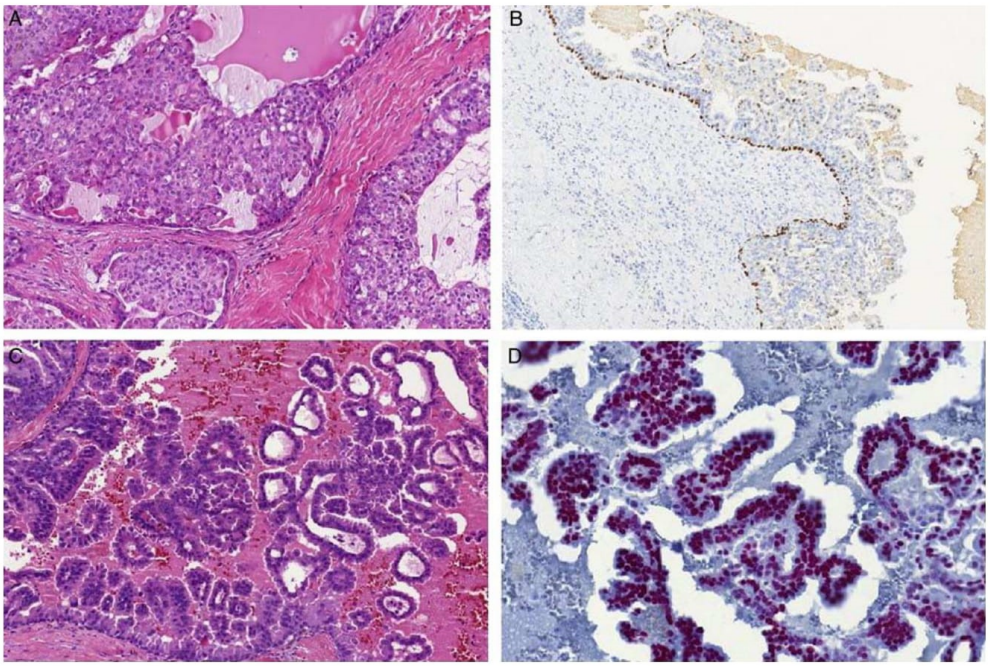

FIGURE 2. IC, intercalated duct variant (A, B), and apocrine variant (C, D). IC is characterized by luminal epithelial proliferations, with intercalated duct phenotype arranged in multiple cystic patterns (A), with the intact myoepithelial abluminal layer decorated by p63 protein in immunohistochemical staining (B). An apocrine variant of IC shows intracystic papillary structures composed of tumor cells exhibiting abundant eosinophilic cytoplasm with apical snouts of decapitation secretion (C) and androgen receptors in immunohistochemical staining (D).

fusions appear to present a rather specific marker of the intercalated duct and apocrine variants of IC, respectively, including cases of widely invasive and metastasizing neoplasms. Therefore, the 2017 WHO Classification term "intraductal carcinoma" is confusing and should be replaced by a more appropriate and accurate one. We propose the designation "intercalated duct carcinoma, noninvasive (or invasive)" for neoplasms formed by intraductal epithelial proliferation composed of cells resembling intercalated duct cells with an S100 protein/SOX10 and mammaglobin-positive and AR-negative immunoprofile, and an intact or focally disrupted abluminal myoepithelial cell layer. Thus, the intercalated duct carcinoma represents a line of differentiation toward intercalated duct features, but, in some cases, ICs may show oncocytic,[15] apocrine, or clear cell features. The neoplasms characterized by apocrine morphology, and an AR-positive and S100 protein/SOX10-negative immunoprofile harboring the *TRIM27-RET* gene fusion, should be designated "intercalated duct carcinoma, with apocrine features." Interestingly, we observed one case of pure intercalated duct IC associated with invasive low-grade epithelial-myoepithelial carcinoma (EMCa). Fittingly, EMCa also recapitulates the intercalated duct phenotype,[26,27] and has been suggested to differentiate in that direction. Moreover, the reported observation of background intercalated duct hyperplasia in some cases of EMCa suggests the possibility of an intercalated duct precursor lesion.[28,29]

In contrast to IC, the well-established term "salivary duct carcinoma" should be reserved for widely invasive high-grade malignancies and should be classified according to previously reported criteria.[14] SDCs have shown a number of genomic alterations including *HER2-neu* gene amplification, and hotspot *PIK3CA* and *HRAS* mutations and many others, not present in ICs.[16,30–32]

A novel finding in our series was a case of widely invasive intercalated duct-type IC, with a single lymph node metastasis that revealed an *NCOA4-RET* fusion transcript. Two IC cases with invasive growth harbored novel fusions *TUT1-ETV5* and *KIAA1217-RET*, respectively. Finally, *NCOA4-RET* and *TRIM27-RET*, *TUT1-ETV5*, and *KIAA1217-RET* were not detected by NGS in any of the 10 SDCs studied as a comparison group. The molecular distinction reported herein between IC and SDC supports the idea that they represent separate malignant salivary tumor

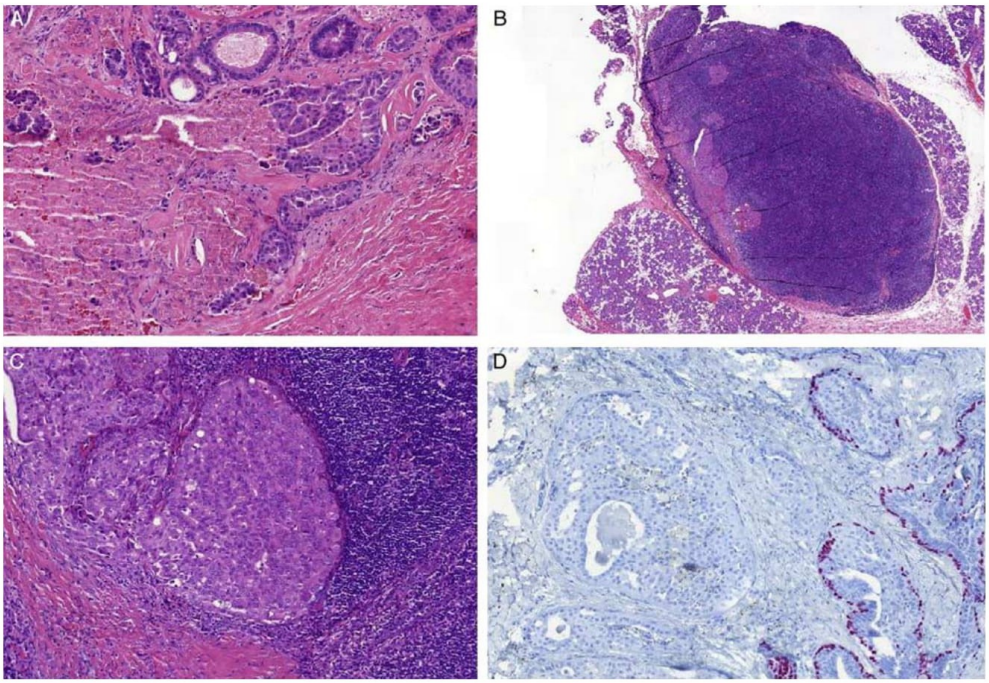

FIGURE 3. Invasive IC (A–D). The invasive growth pattern is seen in IC with perineural infiltration (A) and metastatic invasion in periparotideal lymph node (B, C). The discontinuous myoepithelial layer is seen in immunohistochemical staining with p63 antibody (D).

entities, and should be considered separately in future classifications.

In summary, recurrent rearrangements involving the *RET* gene were identified in a subset of invasive and metastasizing IC, with intercalated duct and apocrine variants resulting in *NCOA4-RET* and *TRIM27-RET* fusions, respectively. Patients with locally invasive, advanced, and metastatic *RET*-rearranged tumors could benefit from targeted therapy using *RET*-inhibitors.[33–36] However, the presence of oncogenic rearrangements cannot be predicted reliably by tumor morphology only. Therefore, we propose that salivary gland cancers should be tested in a screening program for targetable *RET* alterations, if available. Finally, our study indicates that ICs can also manifest significant invasive growth, and, consequently, a designation of these tumors as ICs seems inappropriate by conventional histopathologic rules. The authors suggest that IC should be redesignated as intercalated duct carcinoma, noninvasive or invasive.

ACKNOWLEDGMENTS

The authors thank Prof. Cécile Badual, MD, PhD, Paris, France (case 4), Prof. Jan Laco, MD, PhD, Hradec Králové, Czech Republic (cases 7, 12 to 13), Petr Hrabal, MD, Prague, Czech Republic (case 10), Prof. Nina Zidar, MD, PhD, Ljubljana, Slovenia (case 14), and Vera Fischerova, MD, Ceske Budejovice, Czech Republic (case 18) for submitting their cases, and thus contributing in the study.

REFERENCES

1. Loening T, Leivo I, Simpson RHW, et al. Intraductal carcinoma. In: El-Naggar A, Chan JKC, Grandis JR, Takata T, Slootweg PJ, eds. *World Health Organization (WHO) Classification of Head and Neck Tumours*, 4th ed. Lyon, France: IARC Press; 2017:170–171.
2. Delgado R, Klimstra D, Albores-Saavedra J. Low grade salivary duct carcinoma. A distinctive variant with a low grade histology and a predominant intraductal growth pattern. *Cancer*. 1996;78:958–967.
3. Brandwein-Gensler MS, Gnepp DR. WHO classification of tumours. In: Barnes L, Eveson JW, Reichart P, Sidransky D, eds. *Pathology and Genetics of Head and Neck Tumours*. Lyon: IARC Press; 2005: 233.
4. Weinreb I, Tabanda-Lichauco R, Van der Kwast T, et al. Low-grade intraductal carcinoma of salivary gland: report of 3 cases with marked apocrine differentiation. *Am J Surg Pathol*. 2006;30: 1014–1021.
5. Weinreb I, Bishop JA, Chiosea SI, et al. Recurrent *RET* gene rearrangements in intraductal carcinomas of salivary gland. *Am J Surg Pathol*. 2018;42:442–452.
6. Skálová A, Vanecek T, Uro-Coste E, et al. Molecular profiling of salivary gland intraductal carcinoma revealed a subset of tumors harboring *NCOA4-RET* and novel *TRIM27-RET* fusions: a report of 17 cases. *Am J Surg Pathol*. 2018;42:1445–1455.

7. Lu H, Graham RP, Seethala R, et al. Intraductal carcinoma of salivary glands harboring TRIM27-RET fusion with mixed low grade and apocrine types. *Head Neck Pathol*. 2019. [Epub ahead of print].
8. Brandwein-Gensler M, Hille J, Wang BY, et al. Low-grade salivary duct carcinoma: description of 16 cases. *Am J Surg Pathol*. 2004;28:1040–1044.
9. Bahrami A, Perez-Ordonez B, Dalton JD, et al. An analysis of *PLAG1* and *HMGA2* rearrangements in salivary duct carcinoma and examination of the role of precursor lesions. *Histopathology*. 2013;63:250–262.
10. Chen KT. Intraductal carcinoma of the minor salivary gland. *J Laryngol Otol*. 1983;97:189–191.
11. Simpson RH, Desai S, Di Palma S. Salivary duct carcinoma in situ of the parotid gland. *Histopathology*. 2008;53:416–425.
12. Cheuk W, Miliauskas JR, Chan JK. Intraductal carcinoma of the oral cavity: a case report and a reappraisal of the concept of pure ductal carcinoma in situ in salivary duct carcinoma. *Am J Surg Pathol*. 2004;28:266–270.
13. Wang K, Russell JS, McDermott JD, et al. Profiling of 149 salivary duct carcinomas, carcinoma ex pleomorphic adenomas, and adenocarcinomas, not otherwise specified reveals actionable genomic alterations. *Clin Cancer Res*. 2016;22:6061–6068.
14. Simpson RHW. Salivary duct carcinoma: new developments—morphological variants including pure in situ high grade lesions; proposed molecular classification. *Head Neck Pathol*. 2013;7:S48–S58.
15. Nakaguro M, Urano M, Suzuki H, et al. Low-grade intraductal carcinoma of the salivary gland with prominent oncocytic change: a newly described variant. *Histopathology*. 2018;73:314–320.
16. Nagao T, Licitra L, Loening T, et al. Salivary duct carcinoma. In: El-Naggar A, Chan JKC, Grandis JR, Takata T, Slootweg PJ, eds. *World Health Organization (WHO) Classification of Head and Neck Tumours*, 4th ed. Lyon, France: IARC Press; 2017:173–174.
17. Skálová A, Vanecek T, Sima R, et al. Mammary analogue secretory carcinoma of salivary glands, containing the *ETV6-NTRK3* fusion gene: a hitherto undescribed salivary gland tumor entity. *Am J Surg Pathol*. 2010;34:599–608.
18. Skálová A, Vanecek T, Martinek P, et al. Molecular profiling of mammary analog secretory carcinoma revealed a subset of tumors harboring a novel *ETV6-RET* translocation: report of 10 cases. *Am J Surg Pathol*. 2018;42:234–246.
19. Antonescu CR, Katabi N, Zhang L, et al. *EWSR1-ATF1* fusion is a novel and consistent finding in hyalinizing clear-cell carcinoma of salivary gland. *Genes Chromosomes Cancer*. 2011;50:559–570.
20. Chapman E, Skálová A, Ptakova N, et al. Molecular profiling of hylinizing clear cell carcinoma revealed a subset of tumors harboring a novel *EWSR1-CREM* fusion: report of three cases. *Am J Surg Pathol*. 2018;42:1182–1189.
21. Jee KJ, Persson M, Heikinheimo K, et al. Genomic profiles and *CRTC1-MAML2* fusion distinguish different subtypes of mucoepidermoid carcinoma. *Mod Pathol*. 2013;26:213–222.
22. Skálová A, Sima R, Kaspirkova-Nemcova J, et al. Cribriform adenocarcinoma of minor salivary gland origin principally affecting the tongue: characterization of new entity. *Am J Surg Pathol*. 2011;35:1168–1176.
23. Weinreb I, Zhang L, Tirunagari LM, et al. Novel *PRKD* gene rearrangements and variant fusions in cribriform adenocarcinoma of salivary gland origin. *Genes Chromosomes Cancer*. 2014;53:845–856.
24. Weinreb I, Piscuoglio S, Martelotto LG, et al. Hotspot activating *PRKD1* somatic mutations in polymorphous low-grade adenocarcinomas of the salivary glands. *Nat Genet*. 2014;46:1166–1169.
25. Andreasen S, Varma S, Barasch N, et al. The *HTN3-MSANTD3* fusion gene defines a subset of acinic cell carcinoma of the salivary gland. *Am J Surg Pathol*. 2019;43:489–496.
26. Corio RL, Sciubba JJ, Brannon RB, et al. Epithelial-myoepithelial carcinoma of intercalated duct origin. A clinicopathologic and ultrastructural assessment of sixteen cases. *Oral Surg Oral Med Oral Pathol*. 1982;53:280–287.
27. Luna MA, Ordonez NG, Mackay B, et al. Salivary epithelial myoepithelial carcinomas of intercalated ducts: a clinical, electron microscopic, and immunocytochemical study. *Oral Surg Oral Med Oral Pathol*. 1985;59:482–490.
28. Chetty R. Intercalated duct hyperplasia: possible relationship to epithelial-myoepithelial carcinoma and hybrid tumours of salivary gland. *Histopathology*. 2000;37:260–263.
29. Di Palma S. Epithelial-myoepithelial carcinoma with co-existing multifocal intercalated duct hyperplasia of the parotid gland. *Histopathology*. 1994;25:494–496.
30. Shimura T, Tada Y, Hirai H, et al. Prognostic and histogenetic roles of gene alteration and the expression of key potentially actionable targets in salivary duct carcinomas. *Oncotarget*. 2018;9:1852–1867.
31. Dalin MG, Desrichard A, Katabi N, et al. Comprehensive molecular characterization of salivary duct carcinoma reveals actionable targets and similarity to apocrine breast cancer. *Clin Cancer Res*. 2016;22:4623–4633.
32. Khoo TK, Yu B, Smith JA, et al. Somatic mutations in salivary duct carcinoma and potential therapeutic targets. *Oncotarget*. 2017;8:75893–75903.
33. Roskoski R Jr, Sadeghi-Najad A. Role of RET protein-tyrosine kinase inhibitors in the treatment *RET*-driven thyroid and lung cancers. *Pharmacol Res*. 2018;128:1–17.
34. Drilon A, Hu Zishuo I, Lai GGY, et al. Targeting *RET*-driven cancers: lessons from evolving preclinical and clinical landscapes. *Nat Rev Clin Oncol*. 2018;15:151–167.
35. Li GG, Somwar R, Joseph J, et al. Antitumor activity of RXDX-105 in multiple cancer types with RET rearrangements or mutations. *Clin Cancer Res*. 2017;23:2981–2990.
36. Sabari JK, Siau ED, Drilon A. Targeting RET-rearranged lung cancers with multikinase inhibitors. *Oncoscience*. 2017;4:23–24.

1.11.3 IMUNOHISTOCHEMICKÁ A GENETICKÁ ANALÝZA RESPIRAČNÍCH EPITELIÁLNÍCH ADENOMATOIDNÍCH HAMARTOMŮ A SEROMUCINÓZNÍCH HAMARTOMŮ: JEDNÁ SE O PREKURZOROVÉ LÉZE SINONAZÁLNÍCH LOW-GRADE TUBULOPAPILÁRNÍCH ADENOKARCINOMŮ?

Respirační epiteliální adenomatoidní hamartomy (REAH) a seromucinózní hamartomy (SH) jsou nádorům podobné léze nacházející se v dutině nosní, paranazálních sinusech a v nazofaryngu (82, 83). Patogeneze REAH a SH je stále nejistá. Jsou dávány do souvislosti s neoplastickou proliferací, mechanickým drážděním, zánětem či případně poruchou migrace tkáně v průběhu embryonálního vývoje. Low-grade tubulopapilární adenokarcinomy (LGTA) patří do skupiny non-slivárních a non-intestinálních sinonazálních adenokarcinomů.

Cílem studie bylo prokázat vztah REAH/SH s LGTA ve smyslu REAH/SH jako možného prekurzoru vzniku LGTA. Dále byla provedena molekulárně genetická studie REAH a SH.

Celkem jsme vyšetřili 10 případů REAH a SH imunohistochemicky (IHC) (MUC1, MUC2, MUC4, MUC5AC, MUC6, CK7, CK20, CDX2, SATB2, S100 protein, p63 a SOX10) a molekulárně geneticky (metoda NGS, analýza klonality metodou HUMARA). Imunohistochemické hodnocení proběhlo zvlášť pro komponenty serózní, mucinózní a respirační. Získané údaje byly porovnány s IHC daty 9 případů LGTA vyšetřených stejnými markery.

Serózní komponenta REAH/SH byla pozitivní s markery CK7 (10/10), SOX10 (9/10), MUC1 (8/10) a S100 proteinem (7/10), slabá a fokální pozitivita byla zjištěna s MUC4 (5/10) a p63 (1/10). Respirační komponenta REAH/SH byla pozitivní s MUC1 (10/10) MUC4 (10/10), MUC5AC (10/10) a p63 (9/10). Menší množství případů vykazovalo pozitivitu s CK7 (3/10). Zejména S100 protein a SOX10 zvýraznily tzv. pučení serózních acinů ze stran záhybů respiračního epitelu do stromatu. IHC profil LGTA zahrnoval následující pozitivní markery: CK7 (9/9), MUC4 (8/9), SOX10 (7/9), MUC1 (5/9), S100 (5/9), SATB2 (2/9), a MUC5AC (1/9). Shrneme-li IHC výsledky, dostaneme závěr, že serózní komponenta REAH/SH exprimuje markery CK7, MUC1 a SOX10 shodně s LGTA.

Molekulárně geneticky jsme v 1 případě SH metodou NGS zastihli *EGFR-ZNF267* genovou fúzi a v 1 případě SH byla potvrzena klonalita za použití HUMARA eseje.

REAH a SH jsou sice klasifikovány jako samostatné jednotky, z našeho pohledu však představují morfologicky a imunohistochemicky se prolínající spektrum jedné léze, která může být potenciálními prekurzorem maligních nádorových onemocnění.

Human Pathology (2020) **97**, 94–102

ELSEVIER

Human PATHOLOGY

www.elsevier.com/locate/humpath

Original contribution

Immunohistochemical and genetic analysis of respiratory epithelial adenomatoid hamartomas and seromucinous hamartomas: are they precursor lesions to sinonasal low-grade tubulopapillary adenocarcinomas?☆,☆☆,★

Martina Baněčková MD[a,b,*], Michael Michal MD, PhD[a,b,c], Jan Laco MD, PhD[d], Ilmo Leivo MD, PhD[e], Nikola Ptáková PhD[b], Markéta Horáková MD, PhD[a,b], Michal Michal MD[a,b], Alena Skálová MD, CSc[a,b]

[a]*Department of Pathology, Charles University, Faculty of Medicine in Plzen, Plzen 30605, Czech Republic*
[b]*Bioptic Laboratory, ltd, Plzen 32600, Czech Republic*
[c]*Biomedical Center, Charles University, Faculty of Medicine in Plzen, Plzen 32300, Czech Republic*
[d]*The Fingerland Department of Pathology, Charles University, Faculty of Medicine and University Hospital, Hradec Kralove 50005, Czech Republic*
[e]*Institute of Biomedicine, Pathology, University of Turku, and Turku University Hospital, Turku 50521, Finland*

Received 24 July 2019; revised 11 September 2019; accepted 11 September 2019

Keywords:
Respiratory epithelial adenomatoid hamartoma;
REAH;
Seromucinous hamartoma;
Low-grade tubulopapillary adenocarcinoma;
Sinonasal tract;
Nasal cavity

Summary Respiratory epithelial adenomatoid hamartoma (REAH) and seromucinous hamartoma (SH) are rare tumor-like lesions of the nasal cavity, paranasal sinuses, and nasopharynx. The pathogenesis of REAH/SH is still unclear. Neoplastic proliferation, chronic mechanical irritation, inflammation, or possible embryological tissue misplacement are speculated as possible mechanisms of their development. Low-grade tubulopapillary adenocarcinoma (LGTA) is a rare variant of nonsalivary, nonintestinal type sinonasal adenocarcinoma. The aim of this study was to evaluate the immunohistochemical and genetic profiles of 10 cases of REAH/SH, with serous, mucinous, and respiratory components evaluated separately and to compare these findings with the features of 9 cases of LGTA. All cases of REAH/SH and LGTA were analyzed immunohistochemically with a cocktail of mucin antigens (MUC1, MUC2, MUC4, MUC5AC, MUC6) and with epithelial (CK7, CK20, CDX2, SATB2) and myoepithelial markers (S100 protein, p63, SOX10). The next-generation sequencing assay was performed using FusionPlex Solid Tumor Kit (ArcherDx) in 10 cases of REAH/SH, and the *EGFR-ZNF267* gene fusion was detected in 1 of them. Two female REAH/SH cases were assessed for the presence of clonality. Using the human androgen receptor assay, 1 case was proved to be clonal. The serous component of REAH/SH was positive for CK7/MUC1 and SOX10 similarly to LGTA. Although REAH/SH and

☆ Competing interests: none.
☆☆ Funding/Support: supported in parts by the National Sustainability Program I (NPU I) No. LO1503 and by grant SVV-2019 No. 260391 provided by the Ministry of Education Youth and Sports of the Czech Republic.
★ The study was partially presented at USCAP 2019 in Maryland.
* Corresponding author at: Sikl's Department of Pathology, Medical Faculty of Charles University, Faculty Hospital, E. Benese 13, 305 99 Plzen, Czech Republic.
E-mail address: baneckova.martina@gmail.com (M. Baněčková).

https://doi.org/10.1016/j.humpath.2019.09.018

LGTA are histopathologically and clinically separate entities, the overlap in their morphological and immunohistochemical profiles suggests that REAH/SH might be a precursor lesion of LGTA.

1. Introduction

The sinonasal tract comprises a broad spectrum of reactive and neoplastic lesions [1-3], the classification of which, especially in small biopsy samples with a limited amount of tissue material, can be challenging. Most of the specimens are categorized as recurrent inflammatory polyps in patients with chronic hyperplastic rhinitis, followed by squamous papillomas and squamous cell carcinomas. In contrast, the lesions, such as hamartomas, Schneiderian papillomas, and various types of adenocarcinomas, are uncommon.

Respiratory epithelial adenomatoid hamartoma (REAH) and seromucinous hamartoma (SH) are rare lesions arising in the sinonasal tract. REAH was described for the first time by Wenig and Heffner in 1995 [4], whereas SH was initially described as a case report by Baillie and Batsakis in 1974 [5] and later in a small series by Weinreb at el [6]. Sinonasal hamartomas may present in early life with symptoms of the airway obstruction, or they may be asymptomatic and discovered later in adulthood.

Sinonasal adenocarcinomas (SNACs) are classified as either salivary or nonsalivary adenocarcinomas. Nonsalivary type adenocarcinomas encompass a wide spectrum of intestinal-type adenocarcinoma (ITAC) and non–intestinal-type adenocarcinoma (non-ITAC), of both low-grade (LG) and high-grade (HG) morphologies [1,3,7]. Whereas ITACs occur mostly in men and represent aggressive HG malignancies, LG non-ITACs have an excellent prognosis and no sex predilection. Low-grade tubulopapillary adenocarcinoma (LGTA) has been recognized as a distinctive variant of LG-SNACs. It is, characterized by variable morphologic features, including resemblance to the serous glandular component of SH [3,8-12].

Although REAH and SH are considered different entities, cases presenting histologic features of both REAH and SH have been reported, suggesting they both might be within a spectrum of the same lesion [6]. In recent studies, Ozolek and Hunt demonstrated alterations in tumor suppressor genes with intermediate fractional allelic loss in REAH compared to low rate in chronic sinusitis and high rate in sinonasal adenocarcinomas [13]. Jo et al described possible association of REAH with nonintestinal sinonasal adenocarcinomas in 6/29 cases [14]. Another study by Ambrosini-Spaltro et al showed mitochondrial DNA mutation rate in 5 SH cases [15].

Therefore, there is a growing body of evidence that, rather than hamartomas, REAH/SH may represent a benign neoplasm and carry a potential to become a precursor lesion of LGTA. To support this hypothesis, we have analyzed sinonasal REAH/SH and LGTA cases immunohistochemically and by molecular genetic methods.

2. Materials and methods

Five cases of REAHs, 5 cases of SHs, and 9 cases of LGTAs (n = 9) were retrieved from the consultation files of the authors. The appropriate ethics committee approved this study.

2.1. Histology and immunohistochemistry

For conventional microscopy, tissues were fixed in formalin, routinely processed, embedded in paraffin, cut, and stained with hematoxylin and eosin.

For immunohistochemistry, 2-μm-thick sections were cut from paraffin blocks and mounted on positively charged slides (TOMO, Matsunami Glass IND, Osaka, Japan). Sections were processed on a BenchMark ULTRA (Ventana Medical Systems, Tucson, AZ), deparaffinized, and subjected to heat-induced epitope retrieval by immersion in a CC1 solution (pH 8.6) at 95°C. The primary antibodies used in this study are summarized in Table 1. Visualization was performed using the ultraView Universal DAB Detection Kit (Roche, Arizona, USA) and ultraView Universal Alkaline Phosphatase Red Detection Kit (Roche). The slides were counterstained with Mayer hematoxylin. Appropriate positive and negative controls were used.

The WHO classification criteria for distinguishing REAH and/or SH from LGTA were used by 4 skilled head and neck pathologists (A. S., J. L., I. L., M. M.) [16]. REAHs presented as polypoid structures with respiratory epithelial buddings, with or without small amount of seromucinous glands. SHs

Table 1 Antibodies used for the immunohistochemical study

Antibody	Clone	Dilution	Antigen retrieval/time	Source
CK7	OV-TL 12/30	1:200	CC1/36 min	Dako Cytomation
CK20	Ks20.8	1:100	CC1/36 min	Dako Cytomation
CDX2	EPR2764Y	RTU	CC1/64 min	Cell Marque
SATB 2	polyclonal	1:100	CC2/68 min	Sigma Aldrich
MUC1	H23	RTU	CC1/64 min	Ventana
MUC2	MRQ-18	RTU	CC1/64 min	Cell Marque
MUC4	8G7	1:200	CC1/36 min	Santa Cruz
MUC5AC	MRQ-19	RTU	CC1/36 min	Cell Marque
MUC6	MRQ-20	RTU	CC1/36 min	Cell Marque
S-100 protein	polyclonal	RTU	CC1/20 min	Ventana
SOX 10	polyclonal	1:100	CC1/64 min	Cell Marque
p63	4A4	RTU	CC1/64 min	Ventana

Abbreviations: CC1, EDTA buffer (pH 8.6); RTU, ready to use.

were also bland-looking polypoid tumors composed of seromucinous glands with the predominance of serous component, occasionally admixed with lymphoplasmocytic infiltration and basal membrane thickening. No mitoses, invasion, or atypia was presented in both REAH and SH.

The morphological features of studied LGTAs are consistent with neoplasms described earlier by Skalova et al [9].

2.2. Molecular genetic study

2.2.1. FusionPlex Solid Tumor Kit (AST) (ArcherDx)

FusionPlex Solid Tumor Kit (ArcherDX Inc., Boulder, CO) was used to construct cDNA library for the detection of fusion transcripts in 53 genes (Supplementary file: list of genes). All steps were performed according to the manufacturer's protocol (version LA135.F of the protocol, San Diego-USA), and the library was sequenced on an Illumina platform as described previously [17].

2.2.2. Detection of *EGFR-ZNF267* fusion transcript by polymerase chain reaction and reverse-transcription polymerase chain reaction

RNA was extracted using the RecoverAll Total Nucleic Acid Isolation Kit (Ambion, Austin, TX). cDNA was synthesized using the Transcriptor First Strand cDNA Synthesis Kit (RNA input 500 ng; Roche Diagnostics, Mannheim, Germany). All procedures were performed according to the manufacturer's protocols.

Two microliters of cDNA or 50 ng of total NA was added to the reaction that consisted of 12.5 μL of HotStar Taq PCR Master Mix (QIAgen, Hilden, Germany), 10 pmol of each custom-designed primer in several combinations (Table 1), and distilled water up to 25 μL. The amplification program comprised denaturation at 95°C for 14 minutes and then 45 cycles of denaturation at 95°C for 1 minute, annealing at 60°C for 1 minute, and extension at 72°C for 1 minute. The program was finished by incubation at 72°C for 7 minutes. Successfully amplified polymerase chain reaction (PCR) products were purified with magnetic particles Agencourt AMPure (Agencourt Bioscience Corporation, A Beckman Coulter Company, Beverly, MA, USA). Products were then bidirectionally sequenced using Big Dye Terminator Sequencing kit (Applied Biosystems, Foster City, CA, USA), purified with magnetic particles Agencourt CleanSEQ (Agencourt Bioscience Corporation), all according to manufacturer's protocol, and run on an automated sequencer ABI Prism 3130xl (Applied Biosystems, Foster City, CA, USA) at a constant voltage of 13.2 kV for 11 minutes.

Despite successful product amplification, subsequent sequencing was not successful.

2.2.3. Detection of X chromosome methylation status in the human androgen receptor locus

Clonality analysis using the testing of X chromosome methylation status in the human androgen receptor (HUMARA) locus began by the cleavage of DNA using the methylation-sensitive restriction enzymes (*Hha*I and *Hpa*II).

This was followed by PCR of cleaved and uncleaved DNA which amplifies small tandem repeats HUMARA. A set of primers labeled with fluorescent substance 6-FAM was used. PCR products were then separated using an automatic sequencer ABI Prism 3130 XL. Fragmentation analysis compared the pattern of cleaved and uncleaved samples.

3. Results

3.1. Clinical findings

We collected a series of 10 REAH/SH cases, all of which were from the nasal cavity (Table 2). All REAHs/SHs were polypoid lesions. Five cases were classified as REAH; 2 of them were combined with areas of inflammatory nasal polyp structures. The other 5 cases were SH; 1 case was associated with chronic hyperplastic rhinitis.

Eight of 10 patients were males and 2 were females. There was no age predilection, with the age ranging between 11 and 76 years (mean 49.5). The age of males and females ranged between 11 and 69 years and between 23 and 76 years respectively, with an identical mean value of 49.5 years in both groups.

Nine LGTA cases of the sinonasal mucosa and the epipharynx were studied (Table 2). There was a female predilection—female to male ratio was 2:1. The patients ranged in age from 54 to 91 (mean 69.4) years. The size of the lesions varied from 6 to 70 (mean 69.4) mm. The presenting symptoms included nasal obstruction and chronic hyperplastic rhinitis. Four cases were localized in the nasal cavity, and 1 case each in the epipharynx, paranasal sinus, and the left tonsil. Case 6 showed an aggressive behavior with destruction of the maxilla, and the frontal and ethmoidal sinuses and with invasive growth into the orbit. The tumor in case 7 invaded the palate. Case 9 had to be reexcised 1 month after the first surgical treatment.

3.2. Histological findings

Histologically, REAH cases were characterized by invaginated slit-like spaces lined by respiratory epithelium, which in some fields was detached from the surface, creating small- to medium-sized glands. They were composed of multilayered ciliated respiratory epithelium with numerous mucin-producing goblet cells. The glandular structures were surrounded by a thickened basement membrane (Fig. 1A). Occasional budding of the serous eosinophilic component from the side of a respiratory invagination was seen (Fig. 1B). Cases of SH additionally contained small to large seromucinous acini and ducts lined by a single layer of flattened cuboidal epithelial cells with eosinophilic cytoplasm, sometimes containing luminal secretory material. Entrapped respiratory epithelium similar to REAH was also present in some areas (Fig. 1C). One case of SH was associated with areas of chronic mucosal inflammation, stromal edema, and thickening of the surface epithelial basement membrane (Fig. 1D).

All LGTAs were composed of an admixture of uniform small glandular and tubular structures, lined by cuboidal or

Table 2 Clinical information

No.	Sex	Age	Site	Size (mm)	Symptoms	Diagnosis
REAH						
1	M	60	Nasal cavity	18	NA	SH
2	M	56	Nasal cavity	21	NA	REAH
3	M	63	Nasal cavity	22	NA	REAH in inflammatory nasal polyp
4	M	69	Nasal cavity	20	NA	REAH in inflammatory nasal polyp
5	M	46	Nasal cavity	14	NA	REAH
6	M	11	Nasal cavity	8	NA	SH
7	F	23	Nasal cavity	18	Chronic hyperplastic rhinitis	SH with hyperplastic polyp
8	M	30	Nasal cavity	23	NA	SH
9	F	76	Nasal cavity	20	NA	REAH
10	M	61	Nasal cavity	40	NA	SH
LGTA						
1	M	70	Nasal cavity	25	Nasal obstruction, chronic hyperplastic rhinitis for 5 y, watery secretion from the left nasal cavity, repeated excision of nasal polyps	LGTA first diagnosed in 1995, recurred in 1996, 2003
2	F	76	Nasal cavity	15	Nasal cavity expansion	LGTA
3	F	54	Nasal cavity	25	Nasal obstruction	LGTA
4	F	86	Nasopharynx	10	Symptoms for several months	LGTA
5	F	58	Nasal cavity	21	Nasal obstruction for 2 y	LGTA
6	F	91	Paranasal sinuses	70	Destruction of sinus maxillaris, ethmoidalis and frontalis, partially invading the orbit	LGTA
7	M	74	Left tonsil	30	Palate invasion	LGTA
8	M	72	Nasal cavity	22	Recurrent polyps in nose and sinuses	LGTA
9	F	44	Anterior part of the ethmoid sinus	6	Recurrent nasal inflammation	LGTA

Abbreviation: NA, not available.

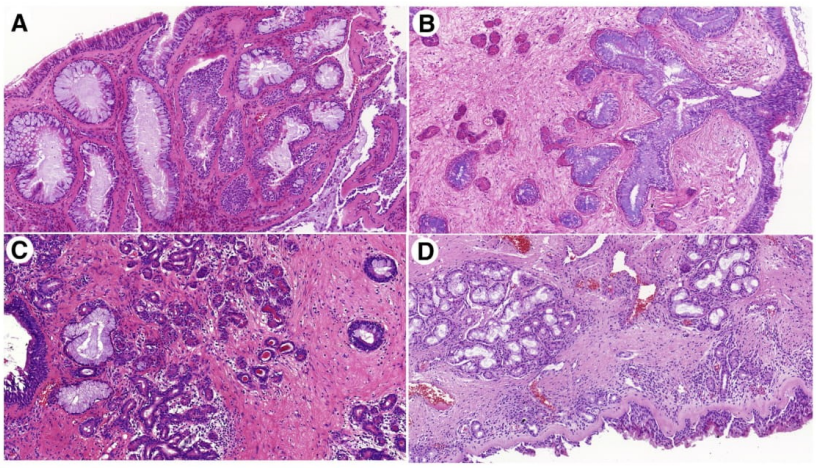

Fig. 1 A, Respiratory epithelial adenomatoid hamartoma is composed of invaginated respiratory epithelium which occasionally detaches from the surface, creating medium-sized glands with multilayered ciliated respiratory epithelium. Occasionally, mucus production may be seen. The glands are surrounded by a thickened basement membrane. B, The eosinophilic serous glands are sprouting from the invaginations of the respiratory epithelium. C, Seromucinous hamartoma with focal respiratory epithelium entrapments. The predominant components are small to large seromucinous acini and tubules, lined by single-layered epithelium, sometimes with eosinophilic secretory material within the lumen. D, Seromucinous hamartoma admixed with structures of hyperplastic polyp and with chronic lymphoplasmacytic infiltrate. There is also a thickening of the basement membrane and stromal edema.

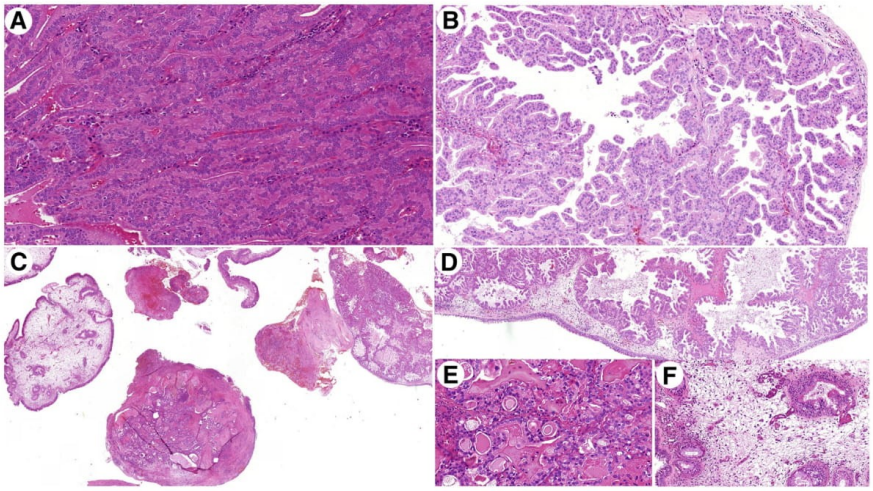

Fig. 2 A-C, Clonality (HUMARA) positive seromucinous hamartoma (case 7) is a fragmented polypoid lesion 18 mm in the largest diameter (A), composed of seromucinous acini (B) with chronic inflammation and thickening of the epithelial basement membrane (C). D-E, *EGFR-ZNF267*–rearranged seromucinous hamartoma (case 10) was a polypoid lesion measuring 40 mm in the largest diameter (D). It consisted of seromucinous glands with occasionally entrapped respiratory epithelial glands (E) and luminal secretory material (F). Glands are focally irregular with intraluminal snouts and spikes of cells and haphazard luminal cell layer stratification with partial loss of the outer myoepithelial layer. F, The larger the gland, the greater structural and occasionally also cytological abnormalities are seen. E and F, The stroma is dense and compact.

columnar epithelium (Fig. 2A). These areas alternated with a papillary growth pattern, composed of haphazardly branching fibrovascular micropapillae covered by bland looking epithelial cells (Fig. 2B). The neoplastic glands were arranged back to back, and there was no or little intervening stroma. Occasional tiny microcysts or intraepithelial mucin vacuoles were also seen (Fig. 2C and E). Four cases of LGTA had overlapping morphological features with REAH/SH despite fragmentation of tissues in most of them (Fig. 2C-F). Case 9 had to be reexcised. The reexcised specimen histologically showed an admixture of LGTA and REAH structures, with the latter being the dominant component. None of the cases showed squamoid morules [18].

3.3. Immunohistochemical findings

The immunohistochemical findings of 10 cases of REAH/SH and 9 cases of LGTA are summarized in Tables 3 and 4, respectively.

The serous component of REAH/SH was positive for CK7 (10/10), SOX10 (9/10), MUC1 (8/10), and S100 (7/10), and weakly and focally positive for MUC4 (5/10) and p63 (1/10). The respiratory component of REAH/SH was positive for MUC1 (10/10), MUC4 (10/10), and MUC5AC (10/10), and showed scattered reactivity with CK7 (3/10) and p63 (9/10). This immunostaining was focally and irregularly confined only to the abluminal myoepithelial layer of

Table 3 The immunohistochemical results of REAH/SH

No.	CK20			CK7			CDX2			SATB2			MUC1			MUC2			MUC4			MUC5AC			MUC6			S100			SOX10			p63		
	S	M	R	S	M	R	S	M	R	S	M	R	S	M	R	S	M	R	S	M	R	S	M	R	S	M	R	S	M	R	S	M	R	S	M	R
1	–	–	–	+	–	–	–	–	–	–	–	–	+	–	+	–	–	–	+W	–	+	–	–	+	–	–	–	–	–	–	+	–	–	–	–	+
2	–	–	–	+	–	–	–	–	–	–	–	–	–	–	+	–	–	–	+W	–	+	–	–	+	–	–	–	–	–	–	+	–	–	–	–	+
3	–	–	–	+	–	+F	–	–	–	–	–	–	+W	–	+	–	–	–	–	–	+	–	–	+	–	–	–	+	–	–	+	–	–	–	–	+
4	–	–	–	+	–	–	–	–	–	–	–	–	+W	–	+W	–	–	–	+W	–	+	–	–	+	–	–	–	+W	–	–	+	–	–	–	–	+
5	–	–	–	+	–	–	–	–	–	–	–	–	+W	–	+W	–	–	–	–	–	+	–	–	+F	–	–	–	+	–	–	+	–	–	–	–	+
6	–	–	–	+	–	+F	–	–	–	–	–	–	+	–	+W	–	–	–	+W	–	+	–	–	+F	–	–	–	+	–	–	+	–	–	–	–	+
7	–	–	–	+	–	–	–	–	–	–	–	–	+	–	+W	–	–	–	–	–	+	–	–	+F	–	–	–	–	–	–	+	–	–	–	–	+
8	–	–	–	+	–	–	–	–	–	–	–	–	+F	–	+	–	–	–	+	–	+	–	–	+	–	–	–	+W	–	–	–	–	–	–	–	–
9	–	–	–	+	–	+F	–	–	–	–	–	–	–	–	+W	–	–	–	–	–	+	–	–	+F	–	–	–	+	–	–	+	–	–	–	–	+
10	–	–	–	+	–	+	–	–	–	–	–	–	+F	–	+	–	–	–	–	–	+	–	–	+F	–	–	–	+	–	–	+	–	–	+	–	+

Abbreviations: F, focal; M, mucinous component; R, respiratory component; S, serous component; W, weak.

Table 4 The immunohistochemical results of LGTA

No	CK20	CK7	CDX2	SATB2	MUC1	MUC2	MUC4	MUC5AC	MUC6	S100	SOX10	p63
1	–	+	–	–	+	–	+F	–	–	+	+	–
2	–	+	–	–	–	–	+F	–	–	–	+	–
3	–	+	–	–	+	–	+F	–	–	+	+	–
4	–	+	–	+	+F	–	+	+F	–	–	–	–
5	–	+	–	–	–	–	+	–	–	–	+	–
6	–	+	–	–	+	–	+F	–	–	–	–	–
7	–	+	–	–	–	–	+F	–	–	+	+	–
8	–	+	–	–	+	–	–	–	–	+	+	–
9/1	–	+	–	+F	–	–	+	–	–	+	+	–
9/2	–	+	–	+F	–	–	+F	–	–	+	+	–

respiratory crypts, whereas other markers were completely negative (Fig. 3). S100 protein/SOX10 highlighted the budding of serous acini from the sides of invaginated respiratory epithelium (Fig. 3A and B) (Table 3).

The immunohistochemical profile of 9 LGTAs (Table 4) encompassed a positivity for CK7 (9/9), MUC4 (8/9), SOX10 (7/9), MUC1 (5/9), S100 (5/9), SATB2 (2/9), and MUC5AC (1/9), whereas CK20, CDX2, MUC2, MUC6, and p63 were negative in all cases (9/9).

The immunohistochemical features of the serous component of REAH/SH are identical to those of LGTA (Tables 3 and 4).

3.4. Molecular findings

The molecular features of REAH/SH are summarized in Table 5.

All REAHs/SHs were analyzed using the FusionPlex Solid Tumor Kit (ArcherDx), and in case 10 (Fig. 4A-C), *EGFR-ZNF267* gene fusion has been found. This fusion was not confirmed by reverse-transcription PCR (RT-PCR).

All female cases of REAH/SH (2/10) were tested by HUMARA. Case 7 (Fig. 4D-F) was SH with areas of hyperplastic polyp and was positive for X chromosome methylation in the HUMARA locus—region q13. The second investigated case (case 9) was REAH without any SH component and was HUMARA negative.

4. Discussion

Benign and malignant lesions of the sinonasal tract are rare, and their differential diagnosis can be challenging,

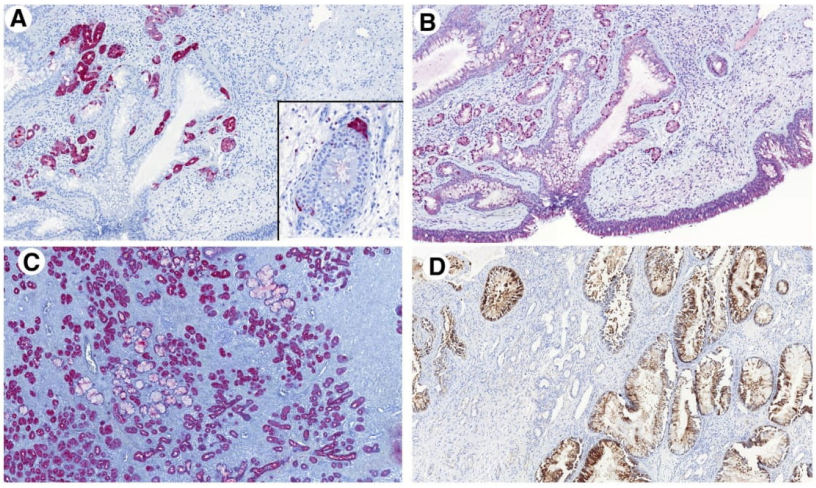

Fig. 3 IHC. A, S100 protein positivity is seen in the serous component of REAH; serous bud sprouting from the invaginated gland layered by respiratory epithelium (inset). B, SOX10—a similar view as in panel A. C, CK7 shows diffuse positivity in serous glands of seromucinous hamartoma, whereas mucinous glands are completely negative. D, MUC4 positivity in REAH; the serous component is negative or weakly positive.

Table 5 Molecular analysis

No.	Diagnosis	Sex	NGS-AST	Illumina (TS 170)	HUMARA
1	SH	M	Neg	NA	
2	REAH	M	Neg	NA	
3	REAH in inflammatory nasal polyp	M	Neg	Neg	
4	REAH in inflammatory nasal polyp	M	Neg	Neg	
5	REAH	M	NA	NA	
6	SH	M	Neg	NA	
7	SH with hyperplastic polyp	F	NA	Neg	Pos
8	SH	M	ND	NA	
9	REAH	F	Neg	Neg	Neg
10	SH	M	Neg	EGFR-ZNF267 [a]	

Abbreviations: NA, not analyzable; ND, not done.
[a] Not confirmed by PCR and RT-PCR.

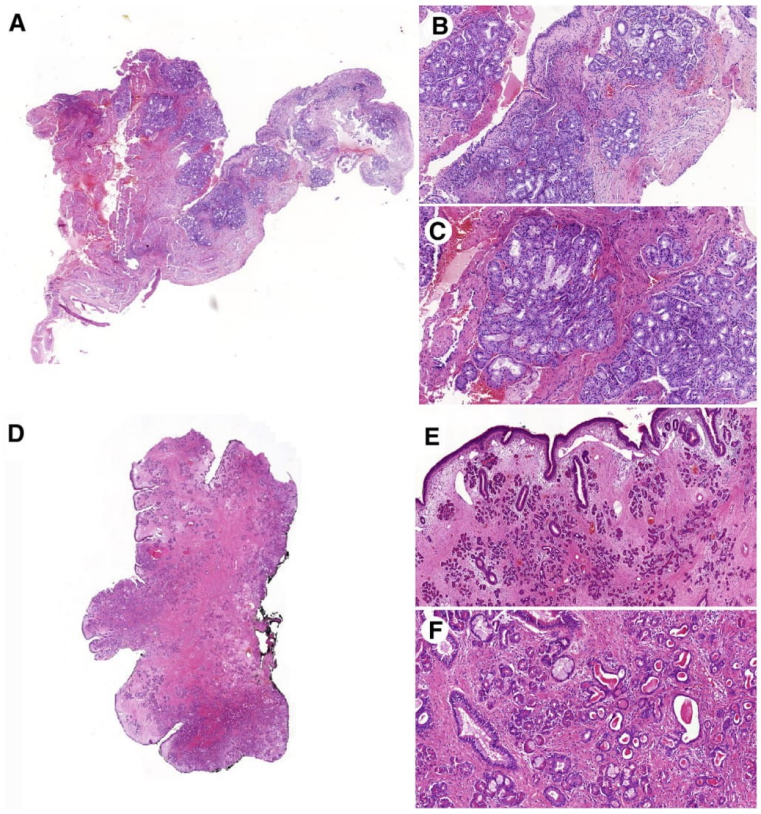

Fig. 4 A, Low-grade tubulopapillary adenocarcinoma is characterized either by tubular and glandular structures or (B) by micropapillary architecture with bland-looking epithelial cells arranged in a back-to-back pattern. C, Low-grade tubulopapillary adenocarcinoma showing micropapillary architecture (C, D), or tubules with mucus accumulation (C, E), and occasional fragments with REAH structures (C, F).

particularly in small biopsy samples. Various hamartomas of epithelial, mesenchymal, or mixed origin may occur in the sinonasal tract [16,19-21]. REAH [4,22-30], SH [5,6,31], and the recently recognized olfactory epithelial hamartomas [32] belong to the pure epithelial group. Chondroosseous hamartoma and respiratory epithelial hamartoma [33,34] belong to the mixed epithelial and mesenchymal group, whereas nasal chondromesenchymal hamartoma [20] represents the pure mesenchymal group. The etiology of many of these lesions including REAH is still the possible association to proinflammatory environment, and chronic rhinosinusitis is speculated. [25].

Mucins (MUC) are high–molecular weight glycoproteins which can be divided into secreted and membrane-related groups. Mucins are broadly included in the surface epithelial structures—mucus membranes with barrier function. Many studies have described mucin expression in different types of carcinomas of variable locations [35-43]. Nevertheless, only a few studies focused on mucins in the sinonasal tract. Whereas the mucin production in chronic sinusitis [38-41], the mucin profile of the signet ring cell carcinoma of the sinonasal tract [42], and the expression of different markers and mucins in the sinonasal adenocarcinomas [44-46] have been well characterized, the expression of mucins in REAH/SH has not been studied so far.

The S100 protein, SOX10, and mucin expression was found in the serous component of REAH/SH and LGTA. These findings further strengthened the connection between both lesions and suggested the origin of LGTA from the seromucinous glands rather than from the respiratory or squamous surface epithelium.

All cases of REAH/SH were analyzed by next-generation sequencing using FusionPlex Solid Tumor Kit (ArcherDx), which revealed *EGFR-ZNF267* gene fusion in SH in case 10. The fusion transcript was not confirmed by RT-PCR, most likely due to lower sensitivity of RT-PCR method (20%) compared to next-generation sequencing (NGS) (5%). The alternative explanation might be a lack of the neoplastic tissue in the paraffin block which was previously used for multiple immunohistochemical and molecular genetic analyses. The false positivity of NGS may not be excluded as well.

The *EGFR-ZNF267* gene fusion has not been published so far, and the confirmation of the *EGFR* break by FISH breakapart probe is suggested in the next step of investigation.

In neoplastic lesions, monoclonality and polyclonality are 2 significant pathways of tumor cells development [47-51]. The monoclonal pathway and the principles HUMARA assay were explained in an earlier study by Boudewijns et al [47]. Briefly, the analysis of the X-chromosome inactivation allows detecting clonality in female patients. It is based on a theory of a random inactivation of a single paternal or maternal X-chromosome in all female cells during embryonal development and its amplification in all daughter cells. One type of the X-chromosome inactivation analysis uses the *HUMARA* gene, whose locus is located on the chromosome X in the region q13. The presence of monoclonality in a tumor is thought to confirm its neoplastic nature. However, nontumorous lesions can be monoclonal as well, as discussed by Skalova et al in a study of 6 cases of sclerosing polycystic adenosis with monoclonal cell populations [51].

The polyclonal pathway is explained as 2 independent events in 2 different cells or group of cells that lead to the polyclonal type of tumorigenesis. [49]. However, this pathway is still under investigation, and the prevailing view remains that most neoplasms are of monoclonal origin [49].

In the present study, 2 cases of REAH/SH were analyzed using HUMARA assay, which demonstrated monoclonality in 1 case of SH (Case 7), further supporting the notion that it is indeed a neoplastic process [13,15].

In conclusion, the present study demonstrated that REAH and SH share many morphological and immunohistochemical features, forming a continuous spectrum. The eosinophilic serous epithelial buds originating in respiratory epithelial invaginations were positive for S100 protein and SOX10, thus having an identical immunoprofile as LGTA, whereas the respiratory component of REAH/SH was completely negative. Moreover, 4 cases of LGTA showed overlapping morphological features with REAH/SH. There was also an immunohistochemical overlap between both these lesions. This is the first study which demonstrated monoclonality in 1 case of SH, further supporting the notion that it is a neoplastic process. Although REAH/SH and LGTA are separate entities, our findings point toward the possibility that SH or the serous component of REAH might be the precursor lesion of LGTA.

Supplementary data

Supplementary data to this article can be found online at https://doi.org/10.1016/j.humpath.2019.09.018.

References

[1] Perez-Ordoñez B. Hamartomas, papillomas and adenocarcinomas of the sinonasal tract and nasopharynx. J Clin Pathol 2009 Dec;62(12):1085-95.
[2] Heffner DK. Classification of human upper respiratory tract tumors. Environ Health Perspect 1990 Apr;85:219-29.
[3] Weinreb I. Low grade glandular lesions of the sinonasal tract: a focused review. Head Neck Pathol 2010 Mar;4(1):77-83.
[4] BM1 Wenig, Heffner DK. Respiratory epithelial adenomatoid hamartomas of the sinonasal tract and nasopharynx: a clinicopathologic study of 31 cases. Ann Otol Rhinol Laryngol 1995 Aug;104(8):639-45.
[5] Baillie EE, Batsakis JG. Glandular (seromucinous) hamartoma of the nasopharynx. Oral Surg Oral Med Oral Pathol 1974 Nov;38(5):760-2.
[6] Weinreb I, Gnepp DR, Laver NM. Seromucinous hamartomas: a clinicopathological study of a sinonasal glandular lesion lacking myoepithelial cells. Histopathology 2009 Jan;54(2):205-13.
[7] Leivo I. Sinonasal adenocarcinoma: update on classification, immunophenotype and molecular features. Head Neck Pathol 2016 Mar;10(1):68-74.
[8] Kleinsasser O. Terminal tubulus adenocarcinoma of the nasal seromucous glands. A specific entity. Arch Otorhinolaryngol 1985;241:183-93.
[9] Skalova A, Cardesa A, Leivo I, et al. Sinonasal tubulopapillary low-grade adenocarcinoma. Histopathological, immunohistochemical and ultrastructural features of poorly recognised entity. Virchows Arch 2003;443:152-8.

[10] Luna MA. Sinonasal tubulopapillary low-grade adenocarcinoma: a specific diagnosis or just another seromucous adenocarcinoma? Adv Anat Pathol 2005 May;12(3):109-15.
[11] Franchi A, Palomba A, Massi D. Low-grade salivary type tubulopapillary adenocarcinoma of the sinonasal tract. Histopathology 2006 Jun;48(7):881-4.
[12] Bansal A, Pradeep KE, Gumparthy KP. An unusual case of low-grade tubulopapillary adenocarcinoma of the sinonasal tract. World J Surg Oncol 2008 May 20;6:54.
[13] Ozolek JA, Hunt JL. Tumor suppressor gene alterations in respiratory epithelial adenomatoid hamartoma (REAH): comparison to sinonasal adenocarcinoma and inflamed sinonasal mucosa. Am J Surg Pathol 2006; 30:1576-80.
[14] Jo VY, Mills SE, Cathro HP. Low-grade sinonasal adenocarcinomas: the association with and distinction from respiratory epithelial adenomatoid hamartomas and other glandular lesions. Am J Surg Pathol 2009 Mar; 33(3):401-8.
[15] Ambrosini-Spaltro A, Morandi L, Spagnolo DV, et al. Nasal seromucinous hamartoma (microglandular adenosis of the nose): a morphological and molecular study of five cases. Virchows Arch 2010;457: 727-34.
[16] Wenig BM, Franchi A, Ro JY. Respiratory epithelial lesions. In: El-Naggar AK, Chan JKC, Grandis JR, Takata T, Slootweg PJ, editors. WHO classification of head and neck tumours. 4th ed. Lyon: IARC Press; 2017. p. 31-2.
[17] Skalova A, Vanecek T, Martinek P, et al. Molecular profiling of mammary analog secretory carcinoma revealed a subset of tumors harboring a novel ETV6-RET translocation: report of 10 cases. Am J Surg Pathol 2018 Feb;42(2):234-46.
[18] Purgina B, Bastaki JM, Duvvuri U, et al. A subset of sinonasal non-intestinal type adenocarcinomas are truly seromucinous adenocarcinomas: a morphologic and immunophenotypic assessment and description of a novel pitfall. Head Neck Pathol 2015 Dec;9(4):436-46.
[19] Wenig BM. Recently described sinonasal tract lesions/neoplasms: considerations for the new world health organization book. Head Neck Pathol 2014 Mar;8(1):33-41.
[20] Graeme-Cook F, Pilch BZ. Hamartomas of the nose and nasopharynx. Head Neck 1992 Jul-Aug;14(4):321-7.
[21] Zarbo RJ, McClatchey KD. Nasopharyngeal hamartoma: report of a case and review of the literature. Laryngoscope 1983 Apr;93(4):494-7.
[22] Nguyen DT, Gauchotte G, Arous F. Respiratory epithelial adenomatoid hamartoma of the nose: an updated review. Am J Rhinol Allergy 2014 Sep-Oct;28(5):187-92.
[23] Lima NB, Jankowski R, Georgel T, Grignon B. Respiratory adenomatoid hamartoma must be suspected on CT-scan enlargement of the olfactory clefts. Rhinology 2006 Dec;44(4):264-9.
[24] Seol JG, Livolsi VA, O'Malley. Respiratory epithelial adenomatoid hamartoma of the bilateral olfactory recesses: a neoplastic mimic? AJNR Am J Neuroradiol 2010 Feb;31(2):277–9.
[25] Al Hawat A, Mouchon E, De Bonnecaze G. Our experience with respiratory epithelial adenomatoid hamartomas of the olfactory cleft. Eur Arch Otorhinolaryngol 2015 Oct;272(10):2867-70.
[26] Vira D, Bhuta S, Wang MB. Respiratory epithelial adenomatoid hamartomas. Laryngoscope 2011 Dec;121(12):2706-9.
[27] Lorentz C, Marie B, Vignaud JM. Respiratory epithelial adenomatoid hamartomas of the olfactory clefts. Eur Arch Otorhinolaryngol 2012 Mar;269(3):847-52.
[28] Roffman E, Baredes S, Mirani N. Respiratory epithelial adenomatoid hamartomas and chondroosseous respiratory epithelial hamartomas of the sinonasal tract: a case series and literature review. Am J Rhinol 2006 Nov-Dec;20(6):586-90.
[29] Gauchotte G, Marie B, Gallet P. Respiratory epithelial adenomatoid hamartoma: a poorly recognized entity with mast cell recruitment and frequently associated with nasal polyposis. Am J Surg Pathol 2013 Nov;37(11):1678-85.
[30] Lee JT, Garg R, Brunworth J, Keschner DB. Sinonasal respiratory epithelial adenomatoid hamartomas: series of 51 cases and literature review. Am J Rhinol Allergy 2013 Jul-Aug;27(4):322-8.
[31] Huang YW, Kuo YJ, Ho CY. Sinonasal seromucinous hamartoma. Eur Arch Otorhinolaryngol 2018 Mar;275(3):743-9.
[32] Kossai M, El Zein S, Wassef M. Olfactory epithelial hamartoma: a new subtype of sinonasal hamartoma. Am J Surg Pathol 2018 Jan;42(1): 9-17.
[33] Fang G, Wang C, Piao Y. Chondro-osseous respiratory epithelial adenomatoid hamartoma of the nasal cavity. Pediatr Int 2016 Mar;58(3): 229-31.
[34] Chatzopoulos K, Stavrakas M, Hytiroglou P. Bizarre stromal cells mimicking malignancy in chondro-osseous respiratory epithelial adenomatoid hamartoma. Pathol Int 2017 May;67(5):276-7.
[35] Sierzega M, Młynarski D, Tomaszewska R. Semiquantitative immunohistochemistry for mucin (MUC1, MUC2, MUC3, MUC4, MUC5AC, and MUC6) profiling of pancreatic ductal cell adenocarcinoma improves diagnostic and prognostic performance. Histopathology 2016 Oct;69(4):582-91.
[36] Nabavinia MS, Gholoobi A, Charbgoo F. Anti-MUC1 aptamer: a potential opportunity for cancer treatment. Med Res Rev 2017 Nov;37(6): 1518-39.
[37] Lau SK, Weiss LM, Chu PG. Differential expression of MUC1, MUC2, and MUC5AC in carcinomas of various sites: an immunohistochemical study. Am J Clin Pathol 2004 Jul;122(1):61-9.
[38] Luo Q, Zhang Z, Liu D, et al. Human neutrophil elastase induces MUC5AC overexpression in chronic rhinosinusitis through tumour necrosis factor-α converting enzyme. Acta Otolaryngol 2016 Jun;136(6):641-8.
[39] Ye Y, Zhao J, Ye J. The role of autophagy in the overexpression of MUC5AC in patients with chronic rhinosinusitis. Int Immunopharmacol 2019 Mar 22;71:169-80.
[40] Viswanathan H, Brownlee IA, Pearson JP, et al. MUC5B secretion is upregulated in sinusitis compared with controls. Am J Rhinol 2006 Sep-Oct;20(5):554-7.
[41] Saieg A, Brown KJ, Pena MT, et al. Proteomic analysis of pediatric sinonasal secretions shows increased MUC5B mucin in CRS. Pediatr Res 2015 Feb;77(2):356-62.
[42] Castillo C, Buob D, Mortuaire G, et al. Signet-ring cell adenocarcinoma of sinonasal tract: an immunohistochemical study of the mucins profile. Arch Pathol Lab Med 2007 Jun;131(6):961-4.
[43] Yamashita MSA, Melo EO. Mucin 2 (MUC2) promoter characterization: an overview. Cell Tissue Res 2018 Dec;374(3):455-63.
[44] Skalova A, Sar A, Laco J. The role of SATB2 as a diagnostic marker of sinonasal intestinal-type adenocarcinoma. Appl Immunohistochem Mol Morphol 2018 Feb;26(2):140-6.
[45] Kennedy MT, Jordan RC, Berean KW. Expression pattern of CK7, CK20, CDX-2, and villin in intestinal-type sinonasal adenocarcinoma. J Clin Pathol 2004 Sep;57(9):932-7.
[46] Taverna C, Cannavicci A, Franchi GA et al. Immunohistochemical profiling of mucins in sinonasal adenocarcinomas. *Pathol Res Pract.* 2019 Jul;215(7):152439.
[47] Boudewijns M, van Dongen JJ, Langerak AW. The human androgen receptor X-chromosome inactivation assay for clonality diagnostics of natural killer cell proliferations. J Mol Diagn 2007 Jul;9(3):337-44.
[48] Allen RC, Zoghbi HY, Moseley AB, et al. Methylation of HpaII and HhaI sites near the polymorphic CAG repeat in the human androgen-receptor gene correlates with X chromosome inactivation. Am J Hum Genet 1992 Dec;51(6):1229-39.
[49] Parsons BL. Many different tumor types have polyclonal tumor origin: evidence and implications. Mutat Res 2008 Sep-Oct;659(3):232-47.
[50] Ammerpohl O, Bens S, Appari M. Androgen receptor function links human sexual dimorphism to DNA methylation. PLoS One 2013 Sep 4;8 (9):e73288.
[51] Skálová A, Gnepp DR, Simpson RH, et al. Clonal nature of sclerosing polycystic adenosis of salivary glands demonstrated by using the polymorphism of the human androgen receptor (HUMARA) locus as a marker. Am J Surg Pathol 2006 Aug;30(8):939-44.

1.11.4 REVIZE SOLITÁRNÍCH FIBRÓZNÍCH TUMORŮ HLAVY A KRKU: ZKUŠENOSTI JEDNÉ INSTITUCE S 20 PŘÍPADY A PŘEHLED LITERATURY

Cílem práce zabývající se solitárními fibrózními tumory (SFT) bylo představit naše zkušenosti s 20 případy těchto vzácných mezenchymálních lézí z oblasti hlavy a krku. Dále jsme diskutovali nejčastější nádory jim podobné, zdokumentovali přesný genetický profil účastnících se fúzních genů a prohledali literární prameny, obsahující molekulárně-genetické a klinicko-patologické informace týkající se SFT.

Všechny vyšetřované případy byly pozitivní v barvení STAT6 a ve všech byla potvrzena *NAB2-STAT6* genová fúze metodou NGS. Molekulárně-geneticky jsme zastihli 3 hlavní fúzní varianty: *NAB2ex2-STAT6int1* (5/20, 25 %), *NAB2ex6-STAT6ex16* (4/20, 20 %), and *NAB2ex4-STAT6ex2* (3/20, 15 %). Nalezené fúzní varianty byly rozděleny do dvou kategorií podle místa zlomu *STAT6* genu (84). Do první kategorie spadaly případy s 5´ fúzí *STAT6* genu neboli *STAT6-full* varianty. Druhou kategorií byly SFT s 3´ fúzí genu *STAT6*, které chybí DNA-vázající doména (DNA-binding domain = DBD), tato skupina byla pojmenovaná *STAT6-ΔDBD*.

Navazující klinické sledování bylo provedené u 16 pacientů. Jeden pacient s morfologicky maligním SFT vyvinul mnohočetné relapsy a metastázy do plic a mozkových plen, tento případ měl aberantní nukleární expresi FLI1 markeru, který doposud v SFT nebyl popsaný. Žádný jiný SFT z naší studie nevykazoval pozitivitu s FLI1 markerem. V další části studie jsme se věnovali revizi literatury. Shromáždili jsme 579 případů SFT z různých lokalit, které popisovaly typ fúze *NAB2-STAT6*. Dvě stě případů SFT reportujících participaci jednotlivých exonů v *NAB2-STAT6* fúzi bylo z oblasti hlavy a krku. V naší studii jsme zjistili, že metastazovaly pouze ty SFT hlavy a krku, v nichž byla zjištěná přítomnost *STAT6-full* varianty.

Diferenciální diagnóza SFT v oblasti hlavy a krku zahrnuje řadu benigních i maligních nádorů včetně meningiomu, epiteloidního hemangioendoteliomu, glomus tumoru, juvenilního angiofibromu, obrovskobuněčného fibroblastomu, sklerózujícího epiteloidního fibrosarkomu, hladkosvalových tumorů, bifenotypického sinonazálního sarkomu či metastázy low-grade endometriálního stromálního sarkomu. Navíc pokud SFT roste infiltrativně a dyskohezivně pouze v jednotlivých buňkách může imitovat metastatický lobulární karcinom prsu. Na druhou stranu, pokud již na diagnózu SFT pomýšlíme, STAT6 imunohistochemické vyšetření je velmi nápomocné a diagnózu případně potvrdíme detekcí *NAB2-STAT6* fúze.

Human Pathology (2020) 99, 1–12

ELSEVIER

Human PATHOLOGY

www.elsevier.com/locate/humpath

Original contribution

Solitary fibrous tumors of the head and neck region revisited: a single-institution study of 20 cases and review of the literature☆,☆☆,☆☆☆

Martina Baněčková MD, PhD[a,b], Petr Martínek PhD[b], Alena Skálová MD, PhD[a,b], Roman Mezencev PhD[c], Ladislav Hadravský MD, PhD[d], Michal Michal MD[a,b], Marián Švajdler MD, PhD[a,b,*]

[a] *Department of Pathology, Charles University, The Faculty of Medicine and Faculty Hospital in Pilsen, Alej Svobody 80, Pilsen, 304 60, Czech Republic*
[b] *Bioptická laboratoř s.r.o., Mikulášske nám. 4, Pilsen, 326 00, Czech Republic*
[c] *School of Biological Sciences, Georgia Institute of Technology, Atlanta, GA, 30332, USA*
[d] *Department of Pathology, First Faculty of Medicine, Charles University, General University Hospital in Prague, Studničkova 2, Prague, 128 00, Czech Republic*

Received 23 January 2020; revised 7 March 2020; accepted 16 March 2020

Available online 23 March 2020

Keywords:
Solitary fibrous tumor;
Hemangiopericytoma;
NAB2-STAT6;
Head and neck

Summary A solitary fibrous tumor (SFT) is a rare, *NAB2-STAT6* fusion gene-associated mesenchymal neoplasm. It most commonly arises in the pleural site, but it can occur at many other sites, and rarely also in the head and neck (H&N) region. STFs may show many growth patterns and therefore can be easily mistaken for other more common H&N spindle cell or epithelial lesions. In this study, we present our experience in the diagnosis of 20 cases of SFT in the H&N region and discuss their most notable mimickers. In all cases, STAT6 expression was found positive by immunohistochemistry, and the *NAB2-STAT6* fusion was confirmed by next-generation sequencing. Three major fusion variants were detected: *NAB2ex2-STAT6int1* (5/20, 25%), *NAB2ex6-STAT6ex16* (4/20, 20%), *and NAB2ex4-*

☆ The preliminary results of the study were presented as a poster presentation during the United States and Canadian Academy of Pathology's 108th Annual Meeting in National Harbor, Maryland, on March 16–21, 2019. The study was supported by the Charles University Research Fund (project number Q39) and by the project Institutional Research Fund of University Hospital Pilsen (Faculty Hospital in Pilsen – FNPl 00669806).

☆☆ Disclosures: The authors have no conflict of interest to disclose.

☆☆☆ Funding: The study was supported by the Charles University Research Fund (project number Q39) and by the Institutional Research Fund of University Hospital Plzen (Faculty Hospital in Plzen- FNPl 00669806.

* Corresponding author. Bioptická laboratoř s.r.o, Mikulášske nám. 4, 326 00, Pilsen, Czech Republic.
E-mail address: svajdler@yahoo.com (M. Švajdler).

https://doi.org/10.1016/j.humpath.2020.03.007

STAT6ex2 (3/20, 15%). Clinical follow-up was available for 16 patients (median follow-up time: 84 months). One patient with a morphologically malignant SFT experienced multiple local recurrences, followed by dissemination into the lungs and meninges. This malignant SFT also displayed an aberrant FLI1 expression, which was not previously reported in SFT cases. We also summarize findings from 200 cases of SFT of the H&N region, which included cases from our study, and from previous studies that reported on the fusion status of the STAT6 gene. The results suggest that metastatic disease developed only in cases with STAT6 variants that included the DNA-binding domain (STAT6-full variants), which contradicts expectations from previous reports and deserves further investigation.

1. Introduction

Solitary fibrous tumors (SFTs), including lesions previously diagnosed as hemangiopericytoma (HPC) or HPC-like lesions, are spindle cell neoplasms that can occur in any region of the body [1]. This entity was first described by Klemperer and Coleman [2] as a neoplasm primarily localized in the pleural region. Approximately 30% of SFTs/HPCs occur in extrathoracic locations, with or without attachment to serosal membranes [3]. These locations include extremities, vulva, thyroid gland, and the head and neck (H&N) region (6%), among others. Within the H&N region, the sinonasal tract and the orbit are the most commonly involved sites, making up 30% and 25% of cases, respectively [4–14].

Macroscopically, SFTs are usually well circumscribed and partially encapsulated white to reddish brown neoplasms.

Microscopically, SFTs reveal miscellaneous phenotypes. Based on their prevailing component, cellular and fibrous types of SFTs are distinguished. The typical SFT architecture is a combination of a hypercellular and hypocellular patterns (the so-called *patternless pattern*), with collagenous stroma and prominent branching, or staghorn-like vessels. Hypercellular areas are composed of round or spindle cells that form storiform, herringbone, fascicular, fibrosarcoma-like, or epithelioid patterns. Tumor cell nuclei are round to oval, with open vesicular chromatin and frequent nuclear pseudoinclusions [15].

There is no correlation between morphology and behavior of SFTs. The criteria of malignancy, which were proposed for extrapleural SFTs [8,13,15], include tumor size (>50 mm), disease dissemination at the time of presentation, infiltrative margins, hypercellularity, nuclear pleomorphism, the presence of sarcomatoid areas (dedifferentiation), necrosis, and mitotic activity (>4/10 high-power fields [HPF]). According to Gold et al. [16], the extrathoracic SFTs with (i) positive surgical margins, (ii) size exceeding 10 cm, and (iii) the malignant histological features described previously are associated with poor clinical outcomes and therefore deserve close surveillance. For meningeal SFTs/HPCs, a three-tiered grading is available based on the updated 2016 World Health Organization classification of CNS tumors, which classifies collagenized tumors with low mitotic activity (SFT pattern) as grade 1 and more cellular tumors with the HPC pattern as grade 2 or 3, depending on the mitotic count (<5 vs. ≥5 per 10 HPF) [15].

2. Materials and methods

Twenty cases of H&N SFTs/HPCs were retrieved from the registry and consultation files at the Department of Pathology, Faculty of Medicine in Pilsen, and Biopticka Laboratory, Ltd, Pilsen, Czech Republic, by using keywords "hemangiopericytoma" and "solitary fibrous tumor." Clinical follow-up was obtained from the patients, their physicians, or from referring pathologists. Representative tissue blocks were selected for immunohistochemical and genetic testing. The study was conducted following the rules set by the Faculty Hospital in Pilsen Ethics Committee. Informed consent was not required.

2.1. Histology and immunohistochemistry

For conventional microscopy, tissues were fixed in formalin, routinely processed, embedded in paraffin, cut on the microtome, and stained with hematoxylin and eosin.

For immunohistochemistry, 4-μm sections were cut from paraffin blocks and mounted on the positively charged slides (TOMO, Matsunami Glass IND, Japan). The sections were processed using the BenchMark ULTRA (Ventana Medical Systems, Tucson, AZ) and deparaffinized, and the epitope retrieval was performed by immersion in CC1 (pH 8.6; Cell Conditioning Solution, Ventana Medical Systems) at 95 °C.

All the primary antibodies used in this study are summarized in Supplementary file 1. Visualization was performed using the ultraView Universal DAB Detection Kit (Ventana, Roche, Tucson, AZ) and ultraView Universal Alkaline Phosphatase Red Detection Kit (Roche). The slides were counterstained with Mayer's hematoxylin. Appropriate positive and negative controls were used.

Table 1 Clinical information and follow-up data.

Case	Age/sex	Site	Symptom length (months)	Treatment	Recurrence	Metastasis	Other tumors	Follow-up	Notes
1	38/F	Ear	NA	E, CHT, RT	Yes	Lung, skull	NA	Alive, with disease, 15 years	Diagnosed in 2003; recurrence in 2004–2009, 2014, and 2018
2	70/F	Face	24	E (positive surgical margins)	No	No	No	NED	NA
3	13/M	Eye + adjacent tissues	1	E (re-excision 2/2017)	No	No	No	NED 2 years	
4	44/M	Intradural space	2	Laminectomy C7+Th1	No	No	No	NED 3 years	January 16, 2018—PET/CT—NED
5	45/F	Eye + adjacent tissues	NA	E	No	No	No	NED 3 years	
6	55/F	Nuchal area	24	E	No	No	No	NED 5 years	
7	41/M	Nuchal area	NA	E	No	No	No	NED 3 years	NA
8	47/F	Nuchal area	NA	NA	NA	NA	NA	NA	NA
9	51/M	Nuchal area	NA	NA	NA	NA	NA	NA	NA
10	61/M	Nuchal area	NA	E	NA	NA	NA	DONR 4 years (December 2009)	NA
11	49/M	Nuchal area	NA	E	No	No	No	NED 9 years	
12	60/F	Oral mucosa	NA	E	No	No	No	NED 9 years	April 2016, abscess in the epiglottis
13	49/F	Eye + adjacent tissues	NA	E	Yes – January 2013	No	No	NED 5 years	
14	64/F	Nuchal area	NA	E	No	No	Adenocarcinoma of the lung (2003)	DONR 4 years (generalized lung carcinoma), April 2018	
15	67/F	Oral mucosa	NA	E	No	No	Squamous carcinoma of the forearm skin (same year)	NED 12 years	
16	44/M	Eye + adjacent tissues	NA	E	No	No	No	NED 15 years	
17	49/F	Sinonasal tract	NA	NA	NA	NA	NA	NA	
18	54/M	Sinonasal tract	7	E, CHT, RT	Yes – 1985, 1987, 1996, 2000	No	No	DOD 20 years (cranial progression), February 2002	Malignant fibrous histiocytoma/SFT
19	43/F	Oral mucosa	NA	E	No	No	No	NED 20 years	
20	77/M	Eye + adjacent tissues	NA	NA	NA	NA	NA	NA	

Abbreviations: E, excision; CHT, chemotherapy; RT, radiotherapy; NA, not available; NED, no evidence of disease; DOD, died of disease; DONR, died of nonrelated reason; SFT, solitary fibrous tumor; CT, computed tomography; PET, positron emission tomography.

Table 2 Histological and molecular biological findings.

Case	Pattern	Epithelioid	Myxoid	Atypia	Mitoses/ 10 HPF	Necrosis	Infiltrative	Size (mm)	Additional features	Differential diagnosis	Genetic fusion	Exons	Group
1	HPC	+/–	–	+	14–15	+	–	20	Cysts		NAB2-STAT6	6–16	STAT6-ΔDBD
2	SFT	–	+	–	1	–	–	11			NAB2-STAT6	2-int1	STAT6-full
3	HPC	–	–	–	0	–	–	12	Reticulated pattern, clear cells, microcysts	Perineurioma, juvenile angiofibroma	NAB2-STAT6	5–17	STAT6-ΔDBD
4	SFT	–	–	–	0	–	–	12			NAB2-STAT6	4–2	STAT6-full
5	HPC	–	–	–	4–5	–	–	10			NAB2-STAT6	2-int1	STAT6-full
6	HPC/SFT	–	+	–	0	–	–	30	Reticulated pattern		NAB2-STAT6	2–1	STAT6-full
7	HPC/SFT	–	–	–	1–2	–	–	NA			NAB2-STAT6	2-int1	STAT6-full
8	HPC/SFT	+	+	–	1	–	–	25		Sclerosing epithelioid fibrosarcoma, epithelioid hemangioendothelioma	NAB2-STAT6	6–16	STAT6-ΔDBD
9	HPC/SFT	–	–	–	1–2	–	–	67			NAB2-STAT6	3–19	STAT6-ΔDBD
10	HPC	–	–	–	29	–	–	15		Paraganglioma	NAB2-STAT6	6–16	STAT6-ΔDBD
11	HPC/SFT	–	–	–	0	–	–	8	Fat forming		NAB2-STAT6	2-int1	STAT6-full
12	HPC/SFT	–	+	–	0–1	–	–	11	Lymphoid infiltration	Meningothelial and fibrous meningioma	NAB2-STAT6	2–5	STAT6-full
13	HPC/SFT	–	–	–	0–1	–	–	50			NAB2-STAT6	2-int1	STAT6-full
14	SFT/GCA	–	+	–	0	–	–	20	Lymphoid infiltration	Sclerosing epithelioid fibrosarcoma	NAB2-STAT6	6–16	STAT6-ΔDBD
15	HPC	–	–	–	0	–	–	28			NAB2-STAT6	6–4	STAT6-full
16	SFT/GCA	–	–	–	0	–	–	19	Reticulated pattern, atypical giant cells	Perineurioma, juvenile angiofibroma	NAB2-STAT6	6–19	STAT6-ΔDBD
17	HPC/SFT	–	+	–	0	–	+	25	Single-cell pattern	Hemangioma, glomus tumor, metastasis of mammary lobular carcinoma	NAB2-STAT6	4–2	STAT6-full
18	HPC/SFT	–	+	–	1–2	–	+	21	Single-cell pattern	Metastasis of mammary lobular carcinoma, glomus tumor	NAB2-STAT6	4–2	STAT6-full
19	HPC	–	+	–	0–1	–	–	19			NAB2-STAT6	4–5	STAT6-full
20	SFT	–	+	–	0	–	–	50	Fascicular growth	Smooth muscle tumors	NAB2-STAT6	2–1	STAT6-full

Abbreviations: SFT, solitary fibrous tumor; HPC, hemangiopericytoma; GCA, giant-cell angiofibroma; HPF, high-power fields.

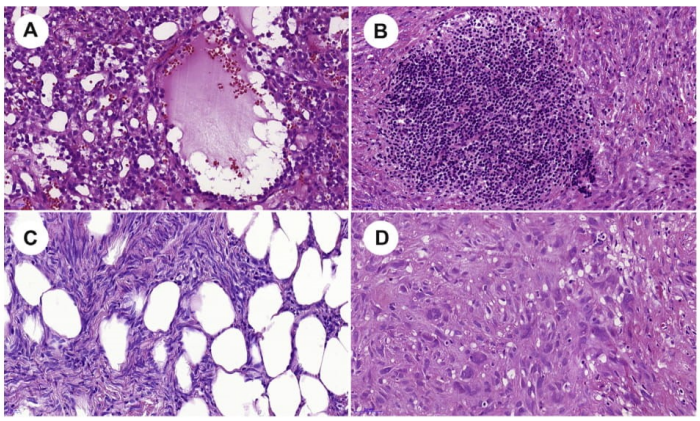

Fig. 1 Head and neck solitary fibrous tumor—histological variants. Cases 1 and 3 showed microcystic or cystic areas (A); cases 12 and 14 showed lymphocytic infiltration in the form of lymphoid nodules (B); fat-forming variant (case 11) (C); 2 cases were characterized by the presence of giant cells (D).

2.2. Detection of *NAB2-STAT6* fusion transcripts by next-generation sequencing

Depending on the sample size, up to 3 formalin-fixed paraffin-embedded sections (10-μm thick) were macrodissected, and the total nucleic acid (NA) was extracted using the Agencourt FormaPure Kit (Beckman Coulter, Brea, CA) with modifications recommended by ArcherDX (ArcherDX Inc., Boulder, CO). The extracted NA was quantified using the Qubit Broad Range RNA Assay Kit (ThermoFisher Scientific, Waltham, MA, USA), and the input amount for each sample library preparation was 250 ng. The PreSeq RNA QC Assay using iTaq Universal SYBR Green Supermix (Bio-Rad, Hercules, CA) was performed to assess sample quality. Samples with the threshold cycle lower than 30 were passed to the target-enrichment step. The Sarcoma kit (ArcherDx Inc, Boulder, CO) containing 143 target gene-specific probes in 26 genes was used, and all steps were performed following the Archer's Fusion Plex Protocol for Illumina. Final libraries were quantified following the Library Quantification for Illumina Libraries protocol (KAPA, Wilmington, MA) assuming a 200-bp fragment length. The samples were multiplexed and spiked with 20% PhiX control and sequenced on a NextSeq 500 (Illumina, San Diego, CA) to achieve at least 1.5 million reads per sample. The analysis of the sequencing results was performed using Archer Analysis software (version 5.1.7; ArcherDX Inc.). Fusion parameters were set to a minimum of 5 valid fusion reads with a minimum of 3 unique start sites within the valid fusion reads.

2.3. Review of the literature

The PubMed database was searched for relevant peer-reviewed reports published in English, using a combination of the following keywords: "solitary fibrous tumor," "hemangiopericytoma," "genetic," and/or "molecular." From more than 200 retrieved articles published in the period from 2013 to August 2019, we selected all relevant studies with at least 5 SFT/HPC cases, for which the *NAB2-STAT6* fusion status was determined by molecular genetic testing. Fourteen articles meeting these criteria were selected, and the genetic data and clinical information were extracted and analyzed together with our data.

3. Results

3.1. Clinical features and follow-up information

We identified 20 patients with SFTs of the extrathoracic H&N region who were included in the study. The cohort consisted of 11 women and 9 men with age at diagnosis ranging from 13 to 77 years (median = 49 years and mean = 51 years). Their clinical information and follow-up are summarized in Table 1. The most frequent sites of occurrence were the nuchal area (7/20, 35%), the orbit (5/20, 25%), and the oral mucosa (3/20, 15%). Two cases occurred in the sinonasal tract (2/20, 10%), and one case each involved the ear, the face, and the intradural space at the level C7−Th1.

The follow-up data were available for 16 cases. The median follow-up time after surgery was 84 months (range = 23 months−240 months). Most patients (18/20)

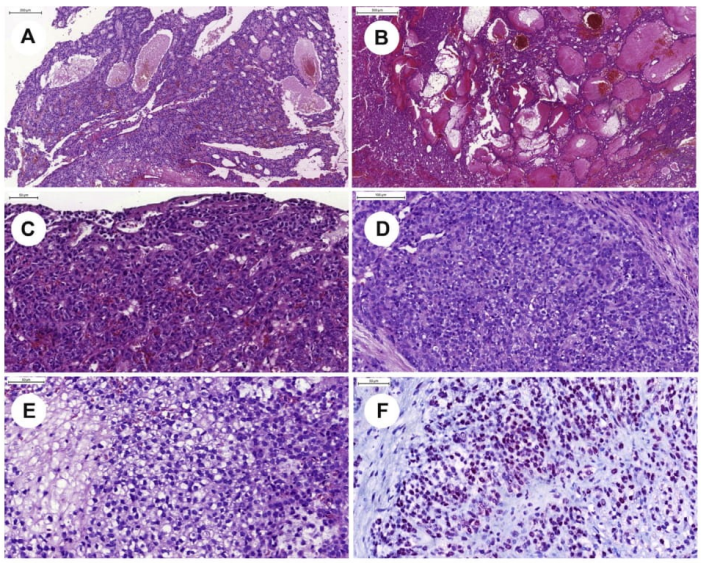

Fig. 2 Case 1 histomorphology. Case 1 showed protean morphology, resembling low-grade adenocarcinoma (A) or metastatic thyroid carcinoma (B), also had a trabecular pattern reminiscent of paraganglioma (C), and focally showed solid epithelioid growth pattern (D) and clear cell differentiation (E). FLI-1 nuclear expression was present (F).

underwent surgical excision only, without adjuvant chemotherapy or radiotherapy.

Locoregional recurrence was recorded in two cases, and one tumor metastasized. Specifically, in case 1, the SFT originated in the left auditory canal and obstructed the whole cavum conchae. The lesion was initially excised in 2003 and diagnosed as HPC. During the following six years, the patient underwent three reoperations of the recurrent tumors, involving various adjacent H&N regions. In 2009 and 2010, the patient received chemotherapy and radiotherapy, but the disease progression occurred between 2010 and 2015, with pulmonary and brain metastases, which were treated by radiotherapy. Subsequent local recurrence in the fossa temporalis was followed by gamma knife therapy. In 2017 and 2018, another local recurrence was diagnosed in the middle ear and auditory channel and subsequently treated by surgical excision. To date (February 2018), the patient is alive with disease.

In case 13, an orbital SFT recurred locally five years after the first surgical treatment in 2013. The tumor was re-excised, and the patient is alive without evidence of the disease.

In case 18, the tumor originated in the sinonasal tract and was originally (in 1982) diagnosed as hemangioendothelioma. The patient had been presenting signs of disease for seven months before the surgical treatment. The tumor recurred in 1985, 1987, 1996, and 2000 and was diagnosed as a recurrent malignant fibrous histiocytoma. This diagnosis was changed to malignant SFT after positive STAT6 staining was detected in our department. The patient underwent chemotherapy and radiotherapy and died two years after the last recurrence owing to cranial progression of the disease.

The median time to the first recurrence was 36 months (range = 12−60 months), and the time to metastasis in a single metastatic case was 7 years after the initial diagnosis.

3.2. Pathological and immunohistochemical findings

The histological findings are summarized in Table 2. Microscopically, 18 cases were classified as benign SFTs, and two cases (cases 1 and 18) were classified as malignant, based on their morphology and clinical behavior.

Morphologically, three cases (cases 2, 4, and 20) showed pure classic SFT phenotype, with alternating hypercellular and hypocellular proliferation, composed of spindle-shaped cells within collagenous stroma and typical staghorn vessels. In six cases (cases 1, 3, 5, 10, 15, and 19), the HPC-like phenotype predominated and was characterized by a high level of cellular proliferation composed of small oval to epithelioid cells with moderate to large nuclei and irregular or discrete nucleoli. Nine cases (cases 6−9, 11−13, 17, and 18) showed a combination of the HPC-like and SFT morphology. Two cases showed prominent

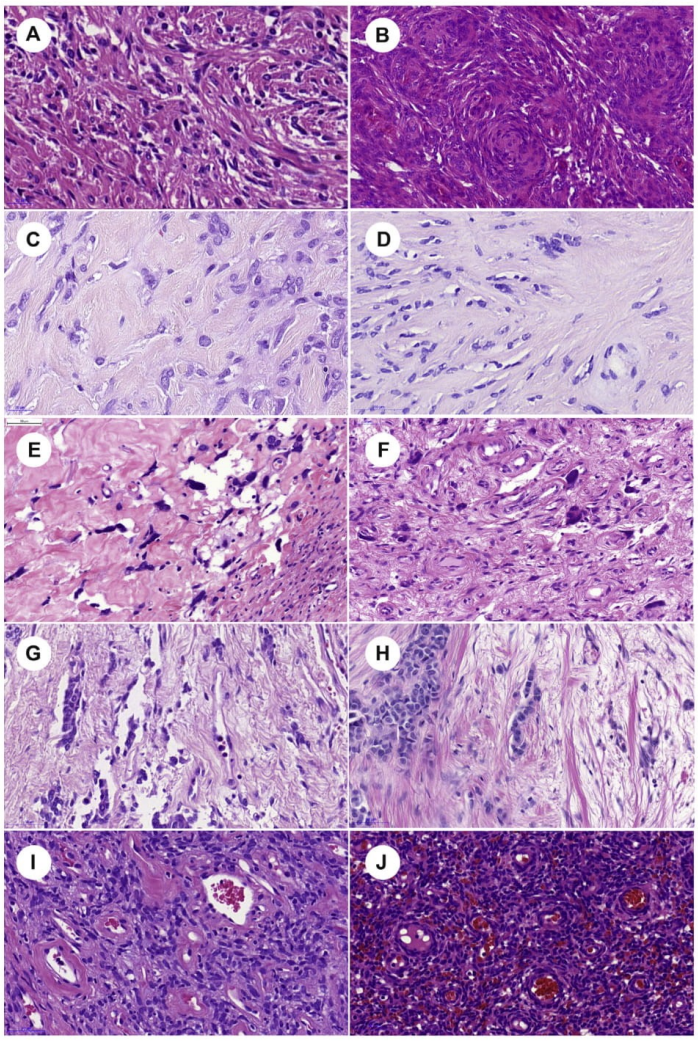

Fig. 3 Differential diagnostic considerations of SFT. Morphologically, SFT may mimic many head and neck benign or malignant neoplasms with spindle cell and epithelioid morphology. SFT (A) may imitate meningothelial and fibrous meningioma (B); SFT (C) resembling sclerosing epithelioid fibrosarcoma (D). Giant-cell angiofibroma, a SFT variant (E), may be indistinguishable from giant-cell fibroblastoma (dermatofibrosarcoma protuberans variant) (F) by histomorphology alone. Distinguishing SFT (G) from metastatic lobular carcinoma (H) maybe a diagnostic challenge; SFT (I) and metastatic low-grade endometrial stromal sarcoma (J) are look-alikes and indistinguishable by H&E alone. H&E, hematoxylin and eosin; SFT, solitary fibrous tumor.

admixture of giant cells (giant cell angiofibroma phenotype). Focal myxoid stromal change and microcystic to macrocystic formations were noted in nine and two cases, respectively (Fig. 1A). Lymphocytic infiltration forming lymphoid nodules was present in two cases (Fig. 1B). Lipomatous differentiation (fat forming variant of SFT) was seen in one case (Fig. 1C), and the multinucleated giant cells were present in two cases (Fig. 1D). Except for cases 1 and 10, which displayed up to 15 and 29 mitotic figures, respectively, mitotic figures were rarely observed

(≤2/10 HPF). Only case 1 showed hemorrhage and necrosis.

All cases (except case 1) were diagnosed as SFTs based only on their morphology. The STAT6 expression (positive in all cases) and the next-generation sequencing were used as supplementary investigative tools.

Case 1 was diagnostically challenging owing to its histological overlapping patterns with other tumors of the H&N region, and it best demonstrates protean histomorphology of the SFTs (Fig. 2A–F). This case was histologically heterogeneous, showing a mixture of adenoid and microcystic patterns resembling sinonasal low-grade adenocarcinoma or metastatic thyroid carcinoma (Fig. 2A and B), featuring a trabecular pattern reminiscent of paraganglioma (Fig. 2C), a solid epithelioid growth pattern (Fig. 2D), and focal clear cell differentiation (Fig. 2E). A wide panel of antibodies was used to rule out epithelial tumors, paraganglioma, vascular lesions, melanoma, and other *small round blue cell tumors*. The tumor was negative for synaptophysin, chromogranin, INSM1, Islet 1, S100, SOX10, cytokeratin cocktail AE1/AE3, OSCAR, GATA3, smooth muscle actin, desmin, NKX 2.2, CD99, CD34, CD31, PROX1, LYVE1, and ERG, but showed a strong BCL2 positivity. Interestingly, FLI-1 nuclear expression was also present (Fig. 2F). Nuclear STAT6 expression confirmed the diagnosis of a SFT, and the genetic analysis showed *NAB2ex6-STAT6ex16* fusion.

3.3. Results of the *NAB2-STAT6* gene fusion testing

NAB2-STAT6 fusion transcripts were detected in all cases (Table 2). The most common fusion break points were *NAB2ex2-STAT6int1,* detected in five cases (25%), and *NAB2ex6-STAT6ex16*, present in four cases (20%). Other detected fusion break points included *NAB2ex4-STAT6ex2* (3/20, 15%), *NAB2ex2-STAT6ex1* (2/20, 10%), and *NAB2ex5-STAT6ex17*, *NAB2ex6*-STAT6ex4, NAB2ex2-*STAT6ex5*, *NAB2ex4-STAT6ex5*, *NAB2ex3-STAT6ex19*, and *NAB6ex-STAT6ex19* (each in one case [1/20, 5%]). Transcript entries used for exon numbering were NM_005967.3 for *NAB2* and NM_001178078.1 for *STAT6*.

In summary, 7 SFTs showed STAT6-ΔDBD fusion variants, and 13 cases had STAT6-full type of fusion [17].

3.4. Review of the literature

Including our study, genetic *NAB2-STAT6* testing was performed in 579 SFT/HPC cases; of which, 263 cases arose in the H&N region [17–30]. The median age at diagnosis was 55 years (mean = 54 years, range = 12–89 years). The male-to-female ratio was 201:210. (Gender was not reported for 168 cases.)

Tumor tissues from cases included in the study cohorts were analyzed by reverse transcription polymerase chain reaction (RT-PCR), long-range genome PCR, multiplex RT-PCR, and whole-exome sequencing methods. The detection rate of the *NAB2-STAT6* genetic fusion varied across studies, ranging from 44% to 100% for all sites and from 0 to 100% for the H&N region (Supplementary file 2).

The most frequent fusion variants detected in all 579 cases were those involving exon 4 of the NAB2 gene: *NAB2ex4-STAT6ex2* (88 cases; 15%), *NAB2ex4-STAT6ex3* (41 cases; 7%), and *NAB2ex4-STAT6ex2/3* (29 cases; 5%), followed by the variants with fusions between exons 5, 6, or 7 of the *NAB2* gene and exons 16 or 17 of the *STAT6* gene (*NAB2ex6-STAT6ex17* – 63 cases, 11%; *NAB2ex6-STAT6ex16* – 34 cases, 6%; and *NAB2ex5/7-STAT6ex16/17* – 60 cases, 10%). The remaining fusion variants were identified as *NAB2ex6-STAT6ex18* (26 cases, 4%), *NAB2ex1-STAT6ex4* (19 cases, 3%), and other (102 cases, 18%). The remaining 117 cases (20%) were not analyzable (Supplementary file 3).

These 579 cases were most commonly diagnosed as typical SFTs (297 cases, 51%), followed by malignant SFTs (94 cases, 16%) and cellular SFTs/HPCs (60 cases, 10%).

Yuzawa et al. classified *NAB2-STAT6* fusions into two categories based on the break points of the STAT6 gene: (i) the 5′ site fusions of the STAT6 gene were labeled as *STAT6-full*, and the 3′ site fusions of the STAT6 gene missing the DNA-binding domain (DBD) were labeled as *STAT6-ΔDBD* [17]. Considering this 2-tiered system, variants from the STAT6-full group were characterized by break points between *NAB2ex1-7-STAT6ex1-6,* and the STAT6-ΔDBD group comprised *NAB2ex3-6-STAT6ex16-20* gene fusions (Supplementary file 3).

Of 579 SFT cases at all sites, 251 (55%) were STAT6-full and 206 (45%) were STAT6-ΔDBD. The remaining 17 (3%) cases were *NAB2-STAT6*, rearranged with no specified fusion type, and 105 (18%) cases were fusion negative. The median age at diagnosis was higher in the STAT6-full group (59.5 years) than in the STAT6-ΔDBD group (46.9 years). The ages at diagnosis ranged from 12 to 89 years in the STAT6-full group and from 12 to 82 years in the STAT6-ΔDBD group. The male-to-female ratio was 201:210. Disease recurrence was detected in 29 cases in the STAT6-full group and in 37 cases in the STAT6-ΔDBD group. Metastatic disease was more common in the STAT6-ΔDBD group (12 cases; cumulative incidence over the follow-up: 5.8%) than in the STAT6-full group (6 cases; cumulative incidence over the follow-up: 2.4%), but this difference was not statistically significant (risk difference CI_{95}: −0.5% to 7.8%; Fisher's exact test two-sided *P*-value: 0.0885).

In the H&N region, the total number of cases was 263. The *NAB2-STAT6* fusion status was available for 200 cases; of which, 72 cases displayed STAT6-full and 128 cases displayed STAT6-ΔDBD fusion variants. The average age at diagnosis was 58 years (range: 30–88 years) in the STAT6-full group and 42 years (range: 13–69 years) in the STAT6-ΔDBD group. The male-to-female ratio was 69:57, and the gender was not reported for 137

cases. Disease recurrence was reported in 15 cases in the STAT6-full group and 19 cases in the STAT6-ΔDBD group. Metastasis developed in 9 H&N SFT cases and only among patients with the STAT6-full variants (cumulative incidence over the follow-up: 12.5%). The difference in the occurrence of metastasis between the STAT6-ΔDBD and STAT6-full groups is statistically significant (risk difference CI_{95}: 5.3−22.4%; Fisher's exact test $P < 0{,}0001$).

4. Discussion

H&N SFT is a rare lesion, which was so far documented in several single-case reports and in a few case series [31,32]. The largest study of H&N SFT published to date included 88 patients from several North American institutions [3]. Previous reports indicated that SFTs can involve any H&N structure, including the sinonasal tract, orbit, buccal space and oral mucosa, thyroid, major salivary glands, soft tissues of the neck, ear and external auditory canal, or palatine tonsils [3,31−38].

The protean morphology of SFT is notorious, and the diagnosis may be challenging for H&N pathologists, especially when dealing with small biopsy specimens. It is particularly difficult to distinguish SFTs from a full spectrum of possible benign and malignant mesenchymal neoplasms (Fig. 3A−J).

Differential diagnosis of H&N SFT includes meningothelial or fibrous meningioma, epithelioid hemangioendothelioma (EHE), glomus tumor, juvenile angiofibroma, paraganglioma, giant-cell fibroblastoma (GCF), sclerosing epithelioid fibrosarcoma (SEF), smooth muscle tumors, biphenotypic sinonasal sarcoma (BSNS), and metastatic low-grade endometrial sarcoma, among others. SFT growing infiltratively in a single-cell pattern may also mimic a metastatic mammary lobular carcinoma.

Meningiomas, especially of meningothelial or fibrous type, can be potentially confused with meningeal SFTs, and it may be difficult to differentiate them from SFTs based on the morphology alone (Fig. 3A and B) [20]. Consequently, the recommended approach to distinguish between SFTs and meningiomas involves IHC detection of STAT6 expression, followed by the detection of ALDH1 and CD34 expression in the STAT6-negative cases [15]. However, in our experience, virtually all cases of the SFT are positive for nuclear STAT6 expression by immunohistochemical. In contrast, meningiomas show no positivity for STAT6 and display variable positivity for epithelial membrane antigen, progesterone receptors, somatostatin receptors 2A, claudin 1, and MUC4 [39−42].

EHE is a malignant vascular neoplasm, characterized by the presence of cords and nests of epithelioid eosinophilic endothelial cells, some of which may show intracytoplasmic lumina, growing within the myxoid or hyaline matrix [43]. EHE is immunohistochemically positive for endothelial cell markers such as FLI1, CD31, or CD34 and displays nuclear expression of CAMTA1 or TFE3 [44,45].

Nasopharyngeal angiofibroma (NAF) is a locally aggressive fibrovascular neoplasm, affecting mostly adolescent boys [46]. Histologically, NAFs are composed of vascular and stromal components, with vessels of various calibers and shapes and bipolar or stellate fibroblastic cells, showing nuclear androgen receptor and beta-catenin positivity in the majority of cases [47].

Paraganglioma is an uncommon neural crest−derived neuroendocrine neoplasm, composed of chief cells arranged in nests (*zellballen*), surrounded by sustentacular spindle-shaped cells and delicate capillary and reticulin fiber network. The chief cells are positive for neuroendocrine markers and have a variable expression of S100 protein. Sustentacular cells exhibit S100 protein and GFAP positivity [48].

SEF [49] is most commonly localized in the deep soft tissue of the lower extremities, and its occurrence in the H&N region is extremely rare [50] (Fig. 3C and D). SEF is composed of small epithelioid cells arranged in nests, cords, and small acini surrounded by a densely sclerotic matrix. A subset of SEF appears to be genetically related to low-grade fibromyxoid sarcoma, and both tumors share diagnostically useful immunopositivity for MUC4 [51,52]. SEF lacks STAT6 and may be genetically characterized by *EWSR1-CREB3L1* or *FUS-CREB3L2* rearrangements [52].

BSNS is a low-grade spindle cell sarcoma with myogenic and neural differentiation. Typically, the cells of BSNS are arranged in intersecting fascicles, but herringbone and hemangiopericytomatous patterns resembling SFTs are also frequently found [53,54]. Immunohistochemically, BSNS is characterized by positivity for S100 and actin as well as a focal and weak positivity for CD34, desmin, myogenin, and MyoD1. Genetically, the BSNS is characterized by *PAX3-MAML3* or alternate (*PAX3-FOXO1, PAX3-NCOA1*) gene fusions [55−57].

GCF, which is a locally aggressive pediatric variant of dermatofibrosarcoma protuberans, rarely occurs in the H&N region. GCF is very similar to giant-cell angiofibroma (SFT variant, Fig. 3E and F) [58,59]. Importantly, both these lesions share CD34 immunoexpression, and therefore, STAT6 immunohistochemistry is necessary to distinguish between the GCF and giant-cell angiofibroma/SFT.

Breast cancers can, albeit rarely, metastasize to the H&N region, which brings additional challenges to the differential diagnosis [60]. Of note, one of our SFT cases (female patient, case 17) with an infiltrating single-file linear growth pattern resembled metastasis of lobular carcinoma of the breast (Fig. 3G and H). Correct diagnosis in these cases is contingent on the evaluation of clinical history and immunohistochemical studies.

Finally, metastatic low-grade endometrial stromal sarcoma (LG ESS) should also be included in the differential

diagnosis of the H&N SFT (Fig. 3I and J). LG ESS is typically diffusely positive for CD10, WT1, estrogen receptors (α isoform), and progesterone receptors. Moreover, CD99, calretinin, α-inhibin, or Melan-A may be positive when sex cord-stromal differentiation is present. Genetically, approximately 50% LG ESSs harbor *JAZF1-SUZ12* fusion [61–63].

The *NAB2-STAT6* fusion is a hallmark of SFT [18–20,26,64,65], and the positive nuclear STAT6 expression, which results from this fusion, is the most important immunohistochemical marker of the SFT/HPC.

Tai et al. [66] confirmed that NAB2ex4–STAT6ex2/4 (STAT6-full) variants were strongly associated with the intrathoracic SFTs; however, they did not find any correlation between *NAB2-STAT6* fusion variants and prognosis of the SFTs. SFTs with aggressive histology tended to occur in the STAT6-ΔDBD group in case series reported by Yazawa et al. [17], but no correlation was found between fusion types and prognosis. Barthelmess et al. [22] showed that NAB2ex6-STAT6ex16/17 fusion variants occurred more frequently in typical HPCs from the deep soft tissue with a more aggressive histology and clinical behavior. Likewise, another study also reported a highly aggressive phenotype and a poor outcome of the SFT cases with STAT6-ΔDBD rearrangements [25,67]. In contrast with these findings, analysis of our data, combined with data extracted from the literature, identified metastatic disease occurrence only in the STAT6-full group of the H&N SFT. This is an intriguing finding that warrants further investigation in prospective cohorts of H&N SFTs.

In conclusion, we present a single-center experience with H&N SFT and discuss its differential diagnosis. Based on the review of data presented in the literature, *NAB2-STAT6* fusion variants may show association with metastatic potential of SFT in the H&N, but this observation needs confirmation in future studies.

Appendix A. Supplementary data

Supplementary data to this article can be found online at https://doi.org/10.1016/j.humpath.2020.03.007.

Acknowledgments

The authors thank Dr. Roger M. Wartell for his helpful comments and proofreading this article.

References

[1] Gengler C, Guillou L. Solitary fibrous tumour and haemangiopericytoma: evolution of a concept. Histopathology 2006;48:63–74.
[2] Klemperer P, Coleman BR. Primary neoplasms of the pleura. A report of five cases. Am J Ind Med 1992;22:1–31.
[3] Smith SC, Gooding WE, Elkins M, Patel RM, Harms PW, McDaniel AS, et al. Solitary fibrous tumors of the head and neck: a multi-institutional clinicopathologic study. Am J Surg Pathol 2017;41:1642–56.
[4] Taccagni G, Sambade C, Nesland J, Terreni MR, Sobrinho-Simoes M. Solitary fibrous tumour of the thyroid: clinicopathological, immunohistochemical and ultrastructural study of three cases. Virchows Arch A Pathol Anat Histopathol 1993;422:491–7.
[5] Tanahashi J, Kashima K, Daa T, Kondoh Y, Suzuki M, Kerakawauchi H, et al. Solitary fibrous tumor of the thyroid gland: report of two cases and review of the literature. Pathol Int 2006;56:471–7.
[6] Westra WH, Gerald WL, Rosai J. Solitary fibrous tumor. Consistent CD34 immunoreactivity and occurrence in the orbit. Am J Surg Pathol 1994;18:992–8.
[7] Hanau CA, Miettinen M. Solitary fibrous tumor: histological and immunohistochemical spectrum of benign and malignant variants presenting at different sites. Hum Pathol 1995;26:440–9.
[8] Hasegawa T, Matsuno Y, Shimoda T, Hasegawa F, Sano T, Hirohashi S. Extrathoracic solitary fibrous tumors: their histological variability and potentially aggressive behavior. Hum Pathol 1999;30:1464–73.
[9] Chan JK. Solitary fibrous tumour–everywhere, and a diagnosis in vogue. Histopathology 1997;31:568–76.
[10] Nielsen GP, O'Connell JX, Dickersin GR, Rosenberg AE. Solitary fibrous tumor of soft tissue: a report of 15 cases, including 5 malignant examples with light microscopic, immunohistochemical, and ultrastructural data. Mod Pathol 1997;10:1028–37.
[11] Brunnemann RB, Ro JY, Ordonez NG, Mooney J, El-Naggar AK, Ayala AG. Extrapleural solitary fibrous tumor: a clinicopathologic study of 24 cases. Mod Pathol 1999;12:1034–42.
[12] Goldsmith JD, van de Rijn M, Syed N. Orbital hemangiopericytoma and solitary fibrous tumor: a morphologic continuum. Int J Surg Pathol 2001;9:295–302.
[13] Vallat-Decouvelaere AV, Dry SM, Fletcher CD. Atypical and malignant solitary fibrous tumors in extrathoracic locations: evidence of their comparability to intra-thoracic tumors. Am J Surg Pathol 1998;22:1501–11.
[14] Croxatto JO, Font RL. Hemangiopericytoma of the orbit: a clinicopathologic study of 30 cases. Hum Pathol 1982;13:210–8.
[15] Giannini C, Rushing EJ, Hainfellner JA, Bouvier C, Figarella-Branger G, von Deimling A. Solitary fibrous tumour/haemangiopericytoma. In: Louis DN, Ohgaki H, Wiestler OD, Cavenee WK, editors. WHO classification of tumours of the central nervous system (revised 4th edition) 2016. Lyon: IARC; 2016. p. 249–54.
[16] Gold JS, Antonescu CR, Hajdu C, Ferrone CR, Hussain M, Lewis JJ, et al. Clinicopathologic correlates of solitary fibrous tumors. Cancer 2002;94:1057–68.
[17] Yuzawa S, Nishihara H, Wang L, Tsuda M, Kimura T, Tanino M, et al. Analysis of NAB2-STAT6 gene fusion in 17 cases of meningeal solitary fibrous tumor/hemangiopericytoma: review of the literature. Am J Surg Pathol 2016;40:1031–40.
[18] Chmielecki J, Crago AM, Rosenberg M, O'Connor R, Walker SR, Ambrogio L, et al. Whole-exome sequencing identifies a recurrent NAB2-STAT6 fusion in solitary fibrous tumors. Nat Genet 2013;45:131–2.
[19] Robinson DR, Wu YM, Kalyana-Sundaram S, Cao X, Lonigro RJ, Sung YS, et al. Identification of recurrent NAB2-STAT6 gene fusions in solitary fibrous tumor by integrative sequencing. Nat Genet 2013;45:180–5.
[20] Schweizer L, Koelsche C, Sahm F, Piro RM, Capper D, Reuss DE, et al. Meningeal hemangiopericytoma and solitary fibrous tumors carry the NAB2-STAT6 fusion and can be diagnosed by nuclear expression of STAT6 protein. Acta Neuropathol 2013;125:651–8.
[21] Mohajeri A, Tayebwa J, Collin A, Nilsson J, Magnusson L, von Steyern FV, et al. Comprehensive genetic analysis identifies a pathognomonic NAB2/STAT6 fusion gene, nonrandom secondary genomic imbalances, and a characteristic gene expression profile in

solitary fibrous tumor. Genes Chromosomes Cancer 2013;52: 873–86.
[22] Barthelmess S, Geddert H, Boltze C, Moskalev EA, Bieg M, Sirbu H, et al. Solitary fibrous tumors/hemangiopericytomas with different variants of the NAB2-STAT6 gene fusion are characterized by specific histomorphology and distinct clinicopathological features. Am J Pathol 2014;184:1209–18.
[23] Vogels RJ, Vlenterie M, Versleijen-Jonkers YM, Ruijter E, Bekers EM, Verdijk MA, et al. Solitary fibrous tumor - clinicopathologic, immunohistochemical and molecular analysis of 28 cases. Diagn Pathol 2014;9:224.
[24] Yamada Y, Kohashi K, Bekki H, Ishii T, Iura K, Maekawa A, et al. Malignant solitary fibrous tumor with high-grade nuclear atypia: an alternate entity for the undetermined tumor group. Pathol Res Pract 2015;211:117–24.
[25] Akaike K, Kurisaki-Arakawa A, Hara K, Suehara Y, Takagi T, Mitani K, et al. Distinct clinicopathological features of NAB2-STAT6 fusion gene variants in solitary fibrous tumor with emphasis on the acquisition of highly malignant potential. Hum Pathol 2015;46: 347–56.
[26] Dagrada GP, Spagnuolo RD, Mauro V, Tamborini E, Cesana L, Gronchi A, et al. Solitary fibrous tumors: loss of chimeric protein expression and genomic instability mark dedifferentiation. Mod Pathol 2015;28:1074–83.
[27] Kao YC, Lin PC, Yen SL, Huang SC, Tsai JW, Li CF, et al. Clinicopathological and genetic heterogeneity of the head and neck solitary fibrous tumours: a comparative histological, immunohistochemical and molecular study of 36 cases. Histopathology 2016;68:492–501.
[28] Huang SC, Li CF, Kao YC, Chuang IC, Tai HC, Tsai JW, et al. The clinicopathological significance of NAB2-STAT6 gene fusions in 52 cases of intrathoracic solitary fibrous tumors. Cancer Med 2016;5: 159–68.
[29] Chuang IC, Liao KC, Huang HY, Kao YC, Li CF, Huang SC, et al. NAB2-STAT6 gene fusion and STAT6 immunoexpression in extrathoracic solitary fibrous tumors: the association between fusion variants and locations. Pathol Int 2016;66:288–96.
[30] Fritchie K, Jensch K, Moskalev EA, Caron A, Jenkins S, Link M, et al. The impact of histopathology and NAB2-STAT6 fusion subtype in classification and grading of meningeal solitary fibrous tumor/-hemangiopericytoma. Acta Neuropathol 2019;137:307–19.
[31] Thompson LDR, Lau SK. Sinonasal tract solitary fibrous tumor: a clinicopathologic study of six cases with a comprehensive review of the literature. Head Neck Pathol 2018;12:471–80.
[32] Agaimy A, Barthelmess S, Geddert H, Boltze C, Moskalev EA, Koch M, et al. Phenotypical and molecular distinctness of sinonasal haemangiopericytoma compared to solitary fibrous tumour of the sinonasal tract. Histopathology 2014;65:667–73.
[33] Okui T, Ibaragi S, Kawai H, Sasaki A. Solitary fibrous tumor arising in the buccal space. Case Rep Med 2019;2019:9459837.
[34] Bauer JL, Miklos AZ, Thompson LD. Parotid gland solitary fibrous tumor: a case report and clinicopathologic review of 22 cases from the literature. Head Neck Pathol 2012;6:21–31.
[35] de Carvalho AD, Abrahao-Machado LF, Viana CR, de Castro Capuzzo R, Mamere AE. Malignant fat-forming solitary fibrous tumor (lipomatous hemangiopericytoma) in the neck: imaging and histopathological findings of a case. J Radiol Case Rep 2013;7:1–7.
[36] Alves Filho W, Mahmoud RR, Ramos DM, Araujo-Filho VJ, Lima PP, Cernea CR, et al. Malignant solitary fibrous tumor of the thyroid: a case-report and review of the literature. Arq Bras Endocrinol Metabol 2014;58:402–6.
[37] Kanazawa T, Kodama K, Nokubi M, Gotsu K, Shinnabe A, Hasegawa M, et al. A case of solitary fibrous tumor arising from the palatine tonsil. Ear Nose Throat J 2015;94:117–20.
[38] Lee CK, Lee HJ. Is a solitary fibrous tumor in the external auditory canal benign? J Audiol Otol 2016;20:120–2.
[39] Matsuyama A, Jotatsu M, Uchihashi K, Tsuda Y, Shiba E, Haratake J, et al. MUC4 expression in meningiomas: under-recognized immunophenotype particularly in meningothelial and angiomatous subtypes. Histopathology 2019;74:276–83.
[40] Barresi V, Alafaci C, Salpietro F, Tuccari G. Sstr2A immunohistochemical expression in human meningiomas: is there a correlation with the histological grade, proliferation or microvessel density? Oncol Rep 2008;20:485–92.
[41] Boulagnon-Rombi C, Fleury C, Fichel C, Lefour S, Marchal Bressenot A, Gauchotte G. Immunohistochemical approach to the differential diagnosis of meningiomas and their mimics. J Neuropathol Exp Neurol 2017;76:289–98.
[42] Hahn HP, Bundock EA, Hornick JL. Immunohistochemical staining for claudin-1 can help distinguish meningiomas from histologic mimics. Am J Clin Pathol 2006;125:203–8.
[43] Weiss SW, Enzinger FM. Epithelioid hemangioendothelioma: a vascular tumor often mistaken for a carcinoma. Cancer 1982;50: 970–81.
[44] Gill R, O'Donnell RJ, Horvai A. Utility of immunohistochemistry for endothelial markers in distinguishing epithelioid hemangioendothelioma from carcinoma metastatic to bone. Arch Pathol Lab Med 2009;133:967–72.
[45] Doyle LA, Fletcher CD, Hornick JL. Nuclear expression of CAMTA1 distinguishes epithelioid hemangioendothelioma from histologic mimics. Am J Surg Pathol 2016;40:94–102.
[46] Boghani Z, Husain Q, Kanumuri VV, Khan MN, Sangvhi S, Liu JK, et al. Juvenile nasopharyngeal angiofibroma: a systematic review and comparison of endoscopic, endoscopic-assisted, and open resection in 1047 cases. Laryngoscope 2013;123:859–69.
[47] Hwang HC, Mills SE, Patterson K, Gown AM. Expression of androgen receptors in nasopharyngeal angiofibroma: an immunohistochemical study of 24 cases. Mod Pathol 1998;11:1122–6.
[48] Brandner SD, Soffer D, Stratakis CA, Yousry T. In: Paraganglioma Louis DN, Ohgaki H, Wiestler OD, Cavenee WK, editors. WHO classification of tumours of the central nervous system (revised 4th edition). Lyon: IARC Press; 2016. p. 164–7.
[49] Meis-Kindblom JM, Kindblom LG, Enzinger FM. Sclerosing epithelioid fibrosarcoma. A variant of fibrosarcoma simulating carcinoma. Am J Surg Pathol 1995;19:979–93.
[50] Folk GS, Williams SB, Foss RB, Fanburg-Smith JC. Oral and maxillofacial sclerosing epithelioid fibrosarcoma: report of five cases. Head Neck Pathol 2007;1:13–20.
[51] Doyle LA, Wang WL, Dal Cin P, Lopez-Terrada D, Mertens F, Lazar AJ, et al. MUC4 is a sensitive and extremely useful marker for sclerosing epithelioid fibrosarcoma: association with FUS gene rearrangement. Am J Surg Pathol 2012;36:1444–51.
[52] Prieto-Granada C, Zhang L, Chen HW, Sung YS, Agaram NP, Jungbluth AA, et al. A genetic dichotomy between pure sclerosing epithelioid fibrosarcoma (SEF) and hybrid SEF/low-grade fibromyxoid sarcoma: a pathologic and molecular study of 18 cases. Genes Chromosomes Cancer 2015;54:28–38.
[53] Andreasen S, Bishop JA, Hellquist H, Hunt J, Kiss K, Rinaldo A, et al. Biphenotypic sinonasal sarcoma: demographics, clinicopathological characteristics, molecular features, and prognosis of a recently described entity. Virchows Arch 2018;473:615–26.
[54] Lewis JT, Oliveira AM, Nascimento AG, Schembri-Wismayer D, Moore EA, Olsen KD, et al. Low-grade sinonasal sarcoma with neural and myogenic features: a clinicopathologic analysis of 28 cases. Am J Surg Pathol 2012;36:517–25.
[55] Wang X, Bledsoe KL, Graham RP, Asmann YW, Viswanatha DS, Lewis JE, et al. Recurrent PAX3-MAML3 fusion in biphenotypic sinonasal sarcoma. Nat Genet 2014;46:666–8.
[56] Huang SC, Ghossein RA, Bishop JA, Zhang L, Chen TC, Huang HY, et al. Novel PAX3-NCOA1 fusions in biphenotypic sinonasal sarcoma with focal rhabdomyoblastic differentiation. Am J Surg Pathol 2016;40:51–9.

[57] Fritchie KJ, Jin L, Wang X, Graham RP, Torbenson MS, Lewis JE, et al. Fusion gene profile of biphenotypic sinonasal sarcoma: an analysis of 44 cases. Histopathology 2016;69:930−6.
[58] Shmookler BM, Enzinger FM, Weiss SW. Giant cell fibroblastoma. A juvenile form of dermatofibrosarcoma protuberans. Cancer 1989;64: 2154−61.
[59] Jha P, Moosavi C, Fanburg-Smith JC. Giant cell fibroblastoma: an update and addition of 86 new cases from the Armed Forces Institute of Pathology, in honor of Dr. Franz M. Enzinger. Ann Diagn Pathol 2007;11:81−8.
[60] Gondim DD, Chernock R, El-Mofty S, Lewis Jr JS. The great mimicker: metastatic breast carcinoma to the head and neck with emphasis on unusual clinical and pathologic features. Head Neck Pathol 2017;11:306−13.
[61] Norris HJ, Taylor HB. Mesenchymal tumors of the uterus. I. A clinical and pathological study of 53 endometrial stromal tumors. Cancer 1966;19:755−66.
[62] Thiel FC, Halmen S. Low-grade endometrial stromal sarcoma - a review. Oncol Res Treat 2018;41:687−92.
[63] Chiang S, Ali R, Melnyk N, McAlpine JN, Huntsman DG, Gilks CB, et al. Frequency of known gene rearrangements in endometrial stromal tumors. Am J Surg Pathol 2011;35:1364−72.
[64] Koelsche C, Schweizer L, Renner M, Warth A, Jones DT, Sahm F, et al. Nuclear relocation of STAT6 reliably predicts NAB2-STAT6 fusion for the diagnosis of solitary fibrous tumour. Histopathology 2014;65:613−22.
[65] Doyle LA, Vivero M, Fletcher CD, Mertens F, Hornick JL. Nuclear expression of STAT6 distinguishes solitary fibrous tumor from histologic mimics. Mod Pathol 2014;27:390−5.
[66] Tai HC, Chuang IC, Chen TC, Li CF, Huang SC, Kao YC, et al. NAB2-STAT6 fusion types account for clinicopathological variations in solitary fibrous tumors. Mod Pathol 2015;28:1324−35.
[67] Nakada S, Minato H, Nojima T. Clinicopathological differences between variants of the NAB2-STAT6 fusion gene in solitary fibrous tumors of the meninges and extra-central nervous system. Brain Tumor Pathol 2016;33:169−74.

1.11.5 SATB2 JE ČASTO EXPRIMOVANÝ V OSIFIKUJÍCÍCH PERIFERNÍCH ORÁLNÍCH FIBROMECH V OBLASTI DÁSNĚ, ALE NE V REAKTIVNÍCH FIBROMATÓZNÍCH LÉZÍCH JINÝCH ČÁSTÍ DUTINY ÚSTNÍ

Periferní orální fibromy (POF) dásňové oblasti jsou malé benigní léze, které pravděpodobně vznikají na podkladě dlouhodobého lokálního fyzického či chemického dráždění. Klinicky jsou to bezbolestné a pomalu rostoucí uzlíky obvykle menší než 2 cm. Přítomnost centrálně uložené pletivové kosti je charakteristickým rysem osifikující varianty POF.

V přiložené studii jsme si dali za cíl prozkoumat expresi SATB2, osteoblastického transkripčního faktoru v souboru 28 gingiválních POF, z nichž 10 bylo osifikujících. Získané výsledky jsme porovnali s dalšími 28 lézemi z jiných než gingiválních oblastí dutiny ústní. Hlavní otázka, která byla v průběhu studie řešena, se týkala kontroverzního tématu, proč některé gingivální léze osifikují a jiné nikoliv.

Elanagai a spol. studovali expresi osteopontinu v normální gingivální tkáni a v různých typech fokálních reaktivních lézí včetně osifikujícího POF. Zjišťovali, zda se osteopontin může uplatnit ve vývoji kostní komponenty lézí (73). Popsali jeho expresi ve všech případech osifikujících POF a přišli s tvrzením, že POF vzniká ze stromálních buněk exprimujících osteopontin, nebo-li z osteoblastů odvozených z periodontálního ligamenta (73).

Výsledkem našeho studia bylo 10 případů osifikujících POF a 8 případů neosifikujícího POF gingivální oblasti se silnou až středně silnou expresí SATB2. Silná reaktivita se SATB2 byla pozorována pouze v 1 případě non-gingiválního POF. Výsledky jasně ukazují konzistentní expresi osteoblastického markeru SATB2 v osifikujících a většině neosifikujících POF gingivální oblasti a chybění tohoto markeru v reaktivních lézích z jiných oblastí dutiny ústní než gingivální. Toto tvrzení je dále ve shodě s navrhovaným původem gingiválních POF v periodontálních ligamentech.

SATB2 je pozitivní v řadě benigních a maligních nádorů hlavy a krku včetně osteosarkomu, osteoblastomu, obrovskobuněčného tumoru, fibrózní dysplázie a epiteliálních nádorů jako sinonazální adenokarcinom intestinálního typu ITAC. Nedávno byla exprese SATB2 popsaná ve fosfaturickém mezenchymálním tumoru včetně oblasti hlavy a krku (85). Naše studie tak nově přidává na seznam orofaciálních lézí pozitivních se SATB2 další lézi, a to osifikující variantu POF. Exprese SATB2 v jakékoliv polypoidní intraorální lézi by měla být proto zvažována obezřetně, abychom se vyhnuli nadhodnocení léze jako maligní.

Annals of Diagnostic Pathology 46 (2020) 151510

Contents lists available at ScienceDirect

Annals of Diagnostic Pathology

journal homepage: www.elsevier.com/locate/anndiagpath

Original Contribution

SATB2 is frequently expressed in ossifying and non-ossifying peripheral oral fibroma of the gingival region but not in reactive fibromatous lesions from other intraoral sites

Martina Baněčková[a,b,c], Abbas Agaimy[c,*]

[a] Department of Pathology, Charles University, Faculty of Medicine in Plzen, Czech Republic
[b] Bioptic Laboratory, ltd, Plzen, Czech Republic
[c] Institute of Pathology, University Hospital, Erlangen, Germany.

ARTICLE INFO

Keywords:
Peripheral oral fibroma
Ossifying fibroma
Non-ossifying fibroma
Oral cavity
Jaw tumors
SATB2
Fibrous epulis

ABSTRACT

Ossifying and non-ossifying peripheral oral fibromas (POF) of the gingival and alveolar mucosa are localized, cellular, small fibrous nodular lesions likely resulting from diverse external/ internal physical and chemical irritation or injuries. A central nidus of metaplastic woven bone characterizes and defines the ossifying variant. The inherent tendency of these lesions to ossify remains elusive. We herein analyze SATB2 expression as osteoblastic transcription and differentiation factor in 28 gingival POFs (10 of them ossifying) and compare them to 28 fibrous lesions from different non-gingival intraoral sites. Strong to moderate diffuse nuclear SATB2 immunoreactivity was detected in all ossifying (10/10; 100%) and in 8/18 (44%) non-ossifying gingival POFs, but in only 1/28 (3%) non-gingival oral reactive nodular fibrous lesions. This study illustrates for the first-time consistent expression of the osteoblastic marker SATB2 in ossifying and most of non-ossifying POFs of the gingival area but lack of this marker in reactive fibrous lesions from other oral cavity sites. This finding is in line with the proposed origin of gingival POFs from periodontal ligaments and may explain the frequent ossification observed in them. It is mandatory to consider this finding when assessing biopsies from SATB2-positive oral cavity neoplasms to avoid misinterpretation.

1. Introduction

Peripheral oral fibroma (POF) is a benign localized lesion that originates from the gingival and alveolar oral mucosa and presents clinically as a painless, slowly growing, pedunculated or sessile firm nodule, usually < 2 cm in size. Histologically, POF is characterized by fibrous tissue that entraps variable numbers of fibroblastic cells. Presence of a well-defined island of metaplastic woven bone defines the ossifying (versus non-ossifying) variant [1,2]. Several descriptive names have been used for ossifying POF: peripheral cementifying fibroma, peripheral fibroma with cementogenesis, peripheral fibroma with osteogenesis, peripheral fibroma with calcification, calcified or ossified fibrous epulis, and calcified fibroblastic granuloma [1]. Both variants are considered reactive [3,4].

Women in their 2nd decade of life are mainly affected. Recurrence rates approach 20%. comparable but almost never ossifying fibrous lesions (traumatic fibromas and fibroepithelial polyps) may occur at any oral site including the tongue, lips, mouth floor, palate, and others, likely resulting from traumatization or chronic irritation.

The special AT-rich sequence-binding protein 2 (SATB2) encodes a nuclear matrix DNA-binding multifunctional transcriptional regulator protein [5] involved in osteoblast lineage commitment [6-8], craniofacial skeleton, and bone and neuronal evolution [9,10]. *SATB2* gene inactivation caused by diverse molecular mechanisms results in so-called SATB2-associated syndrome [11], a condition characterized by neurodevelopmental and behavioral disabilities, palatal clefts, dental anomalies, skeletal anomalies and, rarely, involvement and impairment of other organ systems [7,12].

In surgical pathology practice, SATB2 has been increasingly used as a context-specific marker of osteoblastic differentiation and as a marker of colorectal cancer [13]. In the head and neck, SATB2 represents a valuable adjunct for intestinal-type sinonasal adenocarcinoma and in uncommon mesenchymal neoplasms including variants of craniofacial osteosarcomas and phosphaturic mesenchymal tumors [14,15]. Expression of SATB2 in POF has not been studied before. We herein analyzed 56 fibromatous lesions from the oral cavity for expression of

* Corresponding author at: Pathologisches Institut, Universitätsklinikum Erlangen, Krankenhausstrasse 8-10, 91054 Erlangen, Germany.
E-mail address: abbas.agaimy@uk-erlangen.de (A. Agaimy).

https://doi.org/10.1016/j.anndiagpath.2020.151510

SATB2 and correlated topographic and morphological findings with the immunohistochemical SATB2 expression.

2. Materials and methods

All cases have been identified in the routine surgical pathology files of the Institute of Pathology, University Hospital of Erlangen, Germany. Tissue samples have been fixed in formalin overnight and embedded routinely for histological evaluation. Immunohistochemistry (IHC) was performed on 3-µm sections cut from paraffin blocks using a fully automated system ("Benchmark XT System," Ventana Medical Systems Inc., 1910 Innovation Park Drive, Tucson, Arizona, USA). The Anti-SATB2 antibody was retrieved from Abcam (clone EPNCIR130A, dilution, 1:200).

2.1. Immunohistochemical scoring

Only nuclear staining was considered positive. The extent of SATB2 expression was scored as 0 = negative, 1+: 1–25% of cells, 2+: 26–50%, 3+: 51–75% and 4+ if > 75% of cells stained positive. The "intensity score" – was defined as negative (no staining), 1 + (weak positivity), 2 + (moderate positivity) and 3+ (strong positivity).

The results of the extent and intensity scores were then multiplied to obtain a final score of 0–12 for each lesion (Table 1).

3. Results

There were 56 lesions from 53 patients available for analysis. Three patients (case 10 and 11 in Table 1; and cases, 13 and 14, 16 and 17 in Table 2) underwent surgical excision of two lesions during same operation. The female to male ratio was 1.2: 1. Cases were distributed over a wide age range (15–82 years). The average age was 52 years (56 and 51 years for males and females, respectively). Twenty-eight lesions were gingival (14 in the maxilla, 13 in the mandible & one in unspecified gingival site). Ten (35%) of the gingival lesions were ossifying. The non-gingival reactive fibrous oral cavity lesions (28) were located in tongue [8], palate [8], mouth angle & lip [7], buccal mucosa [3] and unspecified non-gingival oral cavity [2].

3.1. Ossifying peripheral oral fibroma (n = 10)

Table 1 (Cases 1 to 10) shows the clinical and histological characteristics of the ten patients with ossifying POF. Affected were 6 women (60%) and 4 (40%) men; the average age was 51.1 years. 5 cases were localized in maxilla and 5 in the mandible. The lesion size ranged from 0.5–1.8 cm (mean, 0.9 cm).

Microscopically all were well-defined polypoid fibroepithelial growths (Fig. 1A). They showed low to moderate cellularity in the form of fibroblast-like spindled or fusiform cells without significant atypia (Fig. 1B, C). This fibroblastic component was admixed with a chronic inflammatory infiltrate composed of fibroblasts, histiocytes, lymphocytes and plasma cells, occasionally forming granuloma-like aggregates. A few neutrophils were seen. The background stroma of all lesions was fibroblastic with prominent collagenous material that varies from few collagen fibrils to large areas with hyalinization or sclerosis. Dense and mature collagen was seen predominantly in cases with a moderate inflammatory component. Variable stromal edema and prominent vascularization were seen in most cases as well as occasional myxoid changes (Fig. 1C). Bone formation was present in all cases and varied from a few psammomatous microcalcifications to well defined partially anastomosing trabeculae of lamellar and woven bone characteristically forming a well-defined central nidus-like bony island (Fig. 1D). The covering mucosa was frequently hyper-/parakeratotic. None of the lesions had evidence of intra-osseous component or features of peripheral odontogenic fibroma, peripheral giant cell granuloma or other specific entity.

SATB2 immunohistochemical staining showed very strong and diffuse nuclear positivity in all cases, both in the bony component and the fibrous tissue surrounding bone structures (Fig. 1E, F). The total SATB2 score was in the range of "6 to 12". All cases were marked as score "3" for SATB2 intensity.

Table 1
Clinicopathological features of ossifying and non-ossifying gingival peripheral oral fibromas (n = 28).

No	Age/sex	Site	Size (cm)	Type	Cellularity	SATB2%	SATB2 intensity	Total score
1	52/F	Maxilla right (Region 13)	0,8 × 0,4	Ossifying	High	4+	3	12
2	71/F	Maxilla	1,8 × 1,0	Ossifying	High	4+	3	12
3	60/F	Maxilla left (Region 24)	0,5 × 0,4	Ossifying	High	4+	3	12
4	35/F	Maxilla left (Region 25)	0,6 × 0,6	Ossifying	High	4+	3	12
5	20/M	Mandible right (Region 44)	0,8 × 0,5	Ossifying	High	4+	3	12
6	63/F	Maxilla left (Region 23/24)	0,8 × 0,5	Ossifying	Moderate	3+	3	9
7	29/F	Mandible (Region 31)	0,6 × 0,6	Ossifying	High	3+	3	9
8	40/M	Mandible middle (Regions 31–41)	1,2 × 0,6	Ossifying	High	2+	3	6
9	74/M	Mandible left	1,0 × 0,3	Ossifying	Moderate	2+	3	6
10*	67/M	Mandible right (Region 45)	1,0 × 0,5	Ossifying	Moderate	2+	3	6
11*	67/M	Maxilla right (Region 13)	0,5 × 0,4	Non-ossifying	Moderate	1+	1	1
12	25/F	Maxilla left (Regions 23/24)	0,9 × 0,6	Non-ossifying	High	3+	3	9
13	15/F	Mandible right (Regions 41,42)	0,6 × 0,5	Non-ossifying	High	2+	3	6
14	53/F	Gingiva not specified	0,6 × 0,4	Non-ossifying	High	2+	2	4
15	68/F	Mandible left (Regions 32/33)	0,6 × 0,5	Non-ossifying	Moderate	2+	2	4
16	72/F	Mandible right (Region 46)	1,5 × 0,5	Non-ossifying	High	2+	2	4
17	20/F	Mandible right (Regions 41,42)	0,8 × 0,4	Non-ossifying	High	2+	2	4
18	42/F	Mandible left (Region 36)	0,8 × 0,4	Non-ossifying	High	1+	3	3
19	65/M	Palate/maxilla left (Region 26)	0,5 × 0,5	Non-ossifying	Moderate	1+	1	1
20	69/M	Maxilla and Mandible (Regions 48, 37, 17–18)	1,0 × 0,5	Non-ossifying	Moderate	1+	1	1
21	65/F	Maxilla middle (Regions 11/21)	0,7 × 0,4	Non-ossifying	Low	1+	1	1
22	32/F	Palate/Maxilla right (Regions 14/15)	1,1 × 07	Non-ossifying	Low	1+	1	1
23	56/F	Maxilla	0,8 × 0,6	Non-ossifying	Low	1+	2	2
24	73/M	Maxilla	0,9 × 0,5	Non-ossifying	Moderate	0	0	0
25	55/M	Maxilla	2,5 × 2,2	Non-ossifying	Low	0	0	0
26	30/M	Mandible right (Region 48)	0,9 × 0,5	Non-ossifying	Low	0	0	0
27	43/F	Mandible left (Region 38)	0,4 × 0,4	Non-ossifying	Low	0	0	0
28	40/M	Maxilla right (Region 12)	0,5 × 0,3	Non-ossifying	Low	0	0	0

* This patient had two separate lesions removed at same time.

Table 2
Clinicopathological features of non-gingival fibrous oral lesions (n = 28).

No	Age/sex	Site	Size (cm)	Type	Cellularity	SATB2%	SATB2 intensity	Total score
1	82/F	Palate	0,3 × 0,3	Non-ossifying	Moderate	1+	1	1
2	77 M	Top of the tongue	0,5 × 0,4	Non-ossifying	Moderate	1+	1	1
3	36/M	Left tongue margin	1,0 × 0,5	Non-ossifying	Moderate	1+	1	1
4	48/M	Oral cavity unspecified	0,4 × 0,4	Non-ossifying	Moderate	1+	1	1
5	61/M	Tongue	0,3 × 0,3	Non-ossifying	Moderate	1+	1	1
6	76/M	Left tongue	0,9 × 0,4	Non-ossifying	Moderate	1+	1	1
7	72/F	Hard palate	1,2 × 0,7	Non-ossifying	Low	1+	1	1
8	55/M	Top of the tongue	0,4 × 0,3	Non-ossifying	Low	1+	1	1
9	66/M	Left 1/3 of the tongue	1,2 × 0,7	Non-ossifying	Low	1+	1	1
10	25/F	Tongue	0,4 × 0,3	Non-ossifying	Low	1+	1	1
11	48/M	Tongue	0,3 × 0,3	Non-ossifying	Low	1+	2	2
12	39/F	Oral cavity unspecified	1,4 × 1,5	Non-ossifying	Moderate	0	0	0
13*	44/F	Right mouth angle	0,6 × 0,5	Non-ossifying	Moderate	0	0	0
14*	44/F	Left mouth angle	0,7 × 0,5	Non-ossifying	Moderate	0	0	0
15	60/F	Right buccal mucosa	0,7 × 0,7	Non-ossifying	Moderate	0	0	0
16**	55/M	Right palate	0,8 × 0,3	Non-ossifying	Low	0	0	0
17**	55/M	Right palate	1,0 × 0,3	Non-ossifying	Low	0	0	0
18	65/M	Lower lip	0,6 × 0,5	Non-ossifying	Low	0	0	0
19	77/F	Right mouth angle	0,5 × 0,4	Non-ossifying	Low	0	0	0
20	70/F	Palate	2,0 × 1,5	Non-ossifying	Low	0	0	0
21	47/M	Lower lip	0,7 × 0,6	Non-ossifying	Moderate	0	0	0
22	44/M	Right buccal mucosa	0,6 × 0,5	Non-ossifying	Low	0	0	0
23	65/M	Soft palate	0,5 × 0,3	Non-ossifying	Low	0	0	0
24	51/F	Palate	0,4 × 0,3	Non-ossifying	Moderate	0	0	0
25	50/M	Mouth angle	1,1 × 0,7	Non-ossifying	Low	0	0	0
26	44/F	Right palate	0,3 × 0,2	Non-ossifying	Low	0	0	0
27	48/F	Right mouth angle	0,5 × 0,3	Non-ossifying	Low	0	0	0
28	59/F	Right buccal mucosa	1,1 × 0,6	Non-ossifying	Low	0	0	0

* & ** these two patients had two separate lesions removed at the same time.

3.2. Non-ossifying gingival peripheral oral fibroma (n = 18)

Affected were 11 women (61%) and 7 (39%) men; the average age was 49.4 years (range, 15–73 years). Ten cases were localized in maxilla, 7 in the mandible and one case in gingiva not specified. The lesion size ranged from 0.4–2.5 cm (mean, 0.9 cm).

Histologically, non-ossifying gingival POFs were identical to their ossifying counterparts, but they lacked a bony component. SATB2 immunohistochemistry showed very strong to moderate nuclear positivity in 8 (44%) cases (Fig. 1F). Five cases revealed weak SATB2 expression and another 5 were negative. The total SATB2 score was in the range of "0 to 9".

3.3. Fibrous lesions from other non-gingival oral sites (traumatic fibromas & fibroepithelial polyps; n = 28)

Table 2 shows the clinical and histological features of the non-gingival oral fibrous lesions (traumatic fibromas/ fibroepithelial polyps). Affected were 13 women (46%) and 15 (54%) men; the average age was 55.8 years (range 25–82 years). Eight cases were localized in the tongue, 7 cases in palate, 7 cases in the lip and mouth angle and 5 cases in the buccal mucosa and oral cavity not specified. The lesion size ranged from 0.3–2.0 cm (mean, 0.7 cm).

Histologically, these lesions showed polypoid localized fibrous nodules composed of coarse collagen fibers entrapping interspersed fibroblastic stromal cells and small vessels (Fig. 2A, B). The covering mucosa was frequently hyper-/parakeratotic (Fig. 2A). No bone formation or psammomatous calcified bodies were seen. SATB2 immunohistochemical staining showed moderate nuclear positivity in one case from the tongue (3%); 10 cases showed weak SATB2 expression and 17 cases were negative. The total SATB2 score was in the range of "0 to 2" (Fig. 2 C, D).

3.4. Correlation of SATB2 expression in POF with site and histological type

Overall, strong to moderate diffuse SATB2 immunoreactivity was detected in 10/10 (100%) ossifying, 8/18 (44%) non-ossifying gingival POF, and 1/28 (3%) non-gingival oral fibromas.

4. Discussion

Ossifying and non-ossifying POF of the gingival and alveolar mucosa are very similar lesions except for the presence of a mature metaplastic bony island/ component in the ossifying variant [1,2,16,17]. On the other hand, the non-ossifying variant is essentially comparable to other nodular fibrous oral lesions in the spectrum of traumatic fibroma and fibroepithelial polyps, both being composed of paucicellular to moderately cellular fibrous connective tissue covered by squamous mucosa with frequently variable hyper-/parakeratotic changes. Clinical appearance/site is the major distinguishing feature of the gingival (fibrous epulis-like) POF versus similar nodular fibrous lesions from other oral cavity sites. It is generally accepted that these lesions, irrespective of their name and location, are induced by persistent mechanical injury and other type of irritation [3,4,18,19]. The main questions, why some gingival lesions ossify while others do not, and why the non-gingival fibrous counterparts never ossify, remain a subject of controversy. Elanagai et al. studied the expression of osteopontin in the normal gingival tissue and in different types of focal reactive lesions of the gingiva including ossifying POF to explore its potential role in the development of the bony component [20]. They found osteopontin expression in all cases of ossifying POF and suggested, that POF arises from osteopontin expressing stromal cells – osteoblasts derived from the periodontal ligament. However, the exact nature of the ossifying POF and its relationship to the non-ossifying variant remained speculative, some authors adopted the notion that these two lesions possibly represent different entities due to their different histological features including the presence of a bony component in the ossifying type [20].

In the present study, we analyzed for the first time the two types of gingival POF for expression of the osteoblastic differentiation marker SATB2 in a trial to explain their inherent tendency to ossify and form a mature bone and to address histogenesis and relationship between the ossifying and the non-ossifying variant. Our study included as a control

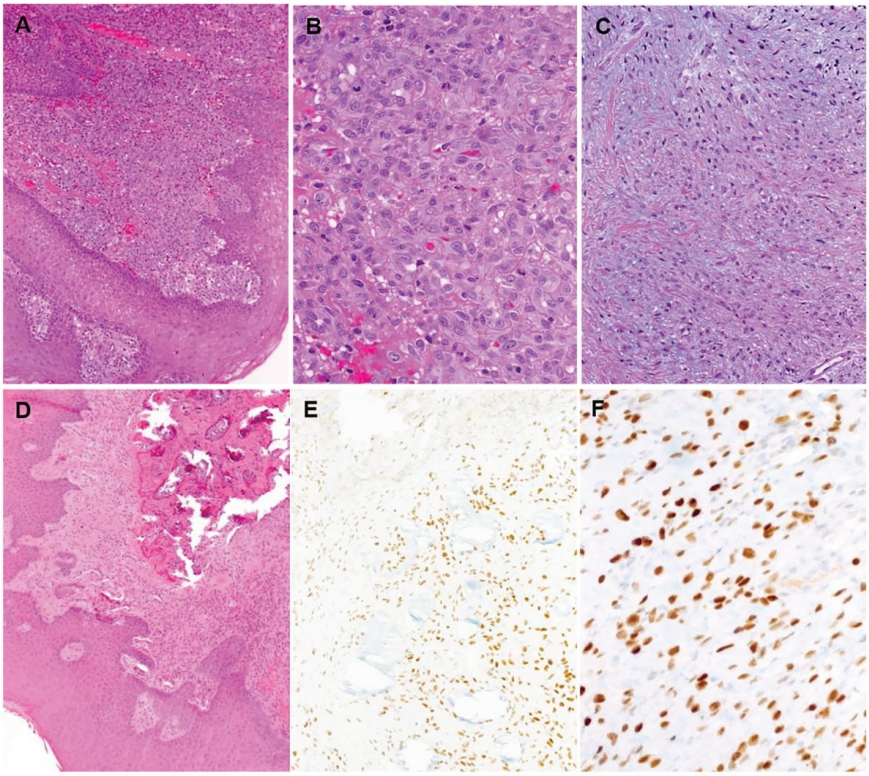

Fig. 1. Ossifying and non-ossifying gingival peripheral oral fibroma presents as a small polypoid lesion covered by hyperplastic mucosa (A) and composed of an admixture of stromal and inflammatory cells (B: higher magnification of cellular stromal area). The stroma varies from sparsely fibrous (B) to fibromyxoid (C). The bony component is frequently represented by a well-defined nidus-like bone island (D). Strong and diffuse SATB2 expression is seen in the peri- and intertrabecular fibroblastic cells in ossifying lesions (E) and diffusely in stromal cells in non-ossifying POF (F).

group histologically comparable localized reactive nodular fibrous lesions from different sites of the oral cavity and the lips in the spectrum of fibroepithelial polyps and traumatic fibromas.

All of ossifying and almost half of the non-ossifying gingival lesions were strongly to moderately SATB2 positive. SATB2 is a transcription regulator that directly binds osteoblast-associated genes to promote or repress their expression. On the other side; SATB2 influences the activity of transcriptional complexes and indirectly manages the expression of genes that are important in osteoblast maturation and differentiation [3-12]. Frequent SATB2 expression in POF reported in this study has not been described before. It indicates osteoblastic differentiation of stromal component that is similar to and in line with the reported osteopontin expression in reactive lesions of the gingiva [21,22].

The etiology of gingival POF is still enigmatic. Iatrogenic and traumatic factors such as tartar and chewing forces have been implicated. Moreover, POF has been suggested to develop as a consequence of periodontal ligament hyperplasia. Considering the etiology of these lesions, another possible factor of POF development suggests the irritation of the tissues surrounding the tooth and bone, which might stimulate osteoblastic proliferation as a result of *SATB2* gene expression in the stromal cells of the periodontal ligaments. Lack of (no more than weak or focal) expression of SATB2 in non-gingival fibrous oral lesions contrasts with that in gingival counterparts and is in line with the hypothesis that gingival lesions do originate from the periodontal fibrous ligament which likely is composed of mesenchymal cells primed to differentiate along the osteoblastic lineage. On the other hand, other fibrous oral lesions represent localized increase in fibrous tissue of the subepithelial stroma which is not related to the periodontal ligaments or associated with underlying bone tissue. The lower frequency of SATB2 expression in non-ossifying gingival POF (44%) is in contrast with the uniform reactivity of SATB2 in all of the gingival ossifying lesions. This suggests that ossifying lesions are likely more advanced or are associated with higher osteoblastic activation sufficient to produce mature bone.

SATB2 is positive in numerous malignant and benign head and neck lesions such as osteosarcoma, osteoblastoma, giant cell tumor, fibrous dysplasia and in epithelial neoplasms such as sinonasal intestinal-type adenocarcinoma [8,23]. More recently, SATB2 expression was reported to be consistently present in phosphaturic mesenchymal tumors including head and neck cases, some of them may closely resemble central giant cell granuloma [15]. Our current study adds to the list of SATB2 expressing orofacial lesions and should be included in the differential diagnosis, especially when expecting any osteogenic process or osteoblastic neoplasm on biopsy. As it is sometimes tricky and challenging to identify and reliably assess crushed resection margins of fibroblastic osteosarcoma and giant cell granuloma of maxillofacial bones, SATB2 expression in any polypoid intraoral lesions or biopsies

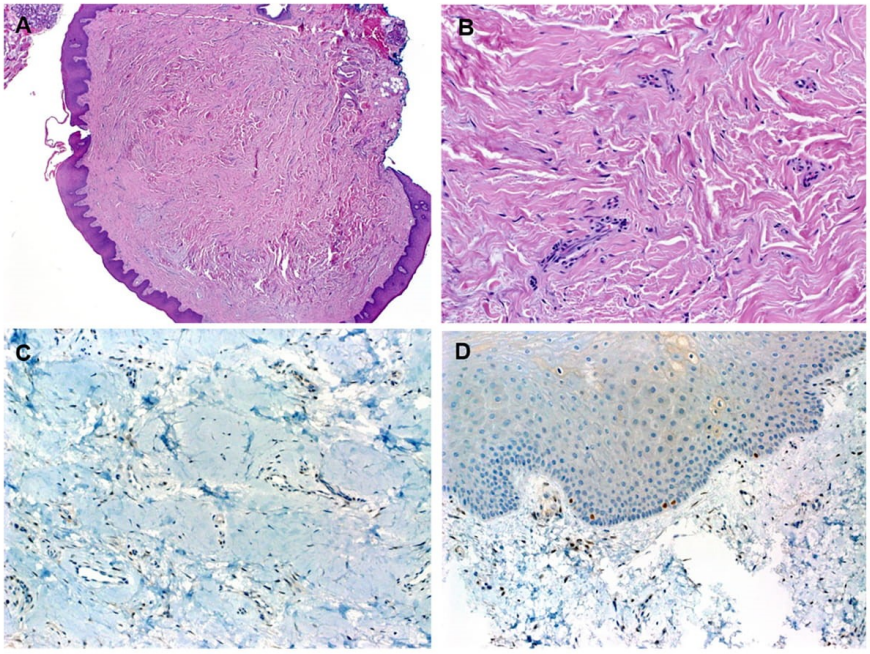

Fig. 2. A: Non-gingival reactive fibrous nodular lesions from different sites of the oral cavity present as polypoid collagenized paucicellular fibrous tissue covered by hyperplastic squamous mucosa. **B**: coarse collagen fibers admixed with a few cells and vessels. **C**: SATB2 is either negative (**C**) or only weakly and focally expressed (**D**) in the non-gingival fibrous oral lesions. Single SATB2-positive cells are seen in the basal mucosa.

should be approached with caution to avoid over-interpretation as meaningful neoplasm or positive margins.

In summary, this study highlights consistent expression of SATB2 in ossifying and most of non-ossifying peripheral oral fibroma of the gingival region of the maxilla and mandible in line with an origin from periodontal ligament/fibrous tissue and explaining the inherent tendency of these lesions to form bone. The question, why a subset of these lesions does not ossify despite SATB2 expression remains enigmatic.

References

[1] Buchner A, Hansen LS. The histomorphologic spectrum of peripheral ossifying fibroma. Oral Surg Oral Med Oral Pathol 1987;63(4):452–61.
[2] Bhaskar SN, Jacoway JR. Peripheral fibroma and peripheral fibroma with calcification: report of 376 cases. J Am Dent Assoc 1966;73(6):1312–20.
[3] Buchner A, Shnaiderman A, et al. Relative frequency of localized reactive hyperplastic lesions of the gingiva: a retrospective study of 1675 cases from Israel. J Oral Pathol Med 2010;39(8):631–8. Sep.
[4] Maturana-Ramírez A, Adorno-Farías D. A retrospective analysis of reactive hyperplastic lesions of the oral cavity: study of 1149 cases diagnosed between 2000 and 2011, Chile. Acta Odontol Latinoam 2015;28(2):103–7.
[5] FitzPatrick DR, Carr IM. Identification of SATB2 as the cleft palate gene on 2q32-q33. Hum Mol Genet 2003 Oct 1;12(19):2491–501.
[6] Sheehan-Rooney K, Palinkasova B, et al. A cross-species analysis of Satb2 expression suggests deep conservation across vertebrate lineages. Developmental dynamics: an official publication of the American Association of Anatomists 2010;239(12):3481–91.
[7] Zhao Xiaoying, Qu Zhihu, et al. The role of SATB2 in skeletogenesis and human disease. Cytokine Growth Factor Rev 2014;25(1):35–44. Feb.
[8] Conner JR, Hornick JL. SATB2 is a novel marker of osteoblastic differentiation in bone and soft tissue tumours. Histopathology 2013;63(1):36–49. Jul.
[9] Magnusson K, de Wit M, Brennan DJ, et al. Satb2 in combination with cytokeratin 20 identifies over 95% of all colorectal carcinomas. Am J Surg Pathol 2011;35:937–48.
[10] Eberhard J, Gaber A, Wangefjord S, et al. A cohort study of the prognostic and treatment predictive value of SATB2 expression in colorectal cancer. Br J Cancer 2012;106:931–8.
[11] Zarate YA, Fish JL. SATB2-associated syndrome: mechanisms, phenotype, and practical recommendations. Am J Med Genet A 2017 Feb;173(2):327–37.
[12] Zarate YA, Kalsner L. Genotype and phenotype in 12 additional individuals with SATB2-associated syndrome. Clin Genet 2017;92(4):423–9. Oct.
[13] Ordóñez NG. SATB2 is a novel marker of osteoblastic differentiation and colorectal adenocarcinoma. Adv Anat Pathol 2014 Jan;21(1):63–7.
[14] Skalova A, Sar A, Laco J, et al. The role of SATB2 as a diagnostic marker of sinonasal intestinal-type adenocarcinoma. Appl Immunohistochem Mol Morphol 2018 Feb;26(2):140–6.
[15] Agaimy A, Michal M, Chiosea S, et al. Phosphaturic mesenchymal tumors: clinicopathologic, immunohistochemical and molecular analysis of 22 cases expanding their morphologic and immunophenotypic spectrum. Am J Surg Pathol 2017;41(10):1371–80. Oct.
[16] García de Marcos JA, García de Marcos MJ, et al. Peripheral ossifying fibroma: a clinical and immunohistochemical study of four cases. J Oral Sci 2010;52:95–9.
[17] Childers ELB, Morton I, et al. Giant peripheral ossifying fibroma: a case report and clinicopathologic review of 10 cases from the literature. Head Neck Pathol 2013;7(4):356–60.
[18] Chang JY, Kessler HP, et al. Localized juvenile spongiotic gingival hyperplasia. Oral Surg Oral Med Oral Pathol Oral Radiol Endod 2008;106(3):411–8.
[19] Damasceno LS, da Silva Gonçalves F, et al. Stromal myofibroblasts in focal reactive overgrowths of the gingiva. Braz Oral Res 2012;26(4):373–7. Jul-Aug.
[20] Elanagai R, Veeravarmal V, Nirmal RM. Osteopontin expression in reactive lesions of gingiva. J Appl Oral Sci 2015;23(1):26–32. Jan-Feb.
[21] Cantor H. The role of Eta-1/osteopontin in the pathogenesis of immunological disorders. Ann N Y Acad Sci 1995;760:143–50.
[22] Elanagai R, Veeravarmal V, et al. Osteopontin expression in reactive lesions of gingiva. J Appl Oral Sci 2015;23(1):26–32.
[23] Skalova A, Sar A. The role of SATB2 as a diagnostic marker of sinonasal intestinal-type adenocarcinoma. Appl Immunohistochem Mol Morphol 2018 Feb;26(2):140–6.

ZÁVĚR

Doktorská dizertační práce uzavírá postgraduální studium z oboru patologie MUDr. Baněčkové Martiny. Výsledkem tříletého studia je 5 prvoautorských prací, které se týkají nádorů hlavy a krku. Dále se autorka podílela jako spoluautor na 9 dalších publikacích. Výsledky všech studií představených v doktorské dizertační práci byly publikovány v zahraničních odborných časopisech s faktorem impaktu (IF).

REFERENCE

1. Bray F, Ferlay J, Soerjomataram I, et al. Global cancer statistics 2018: GLOBOCAN estimates of incidence and mortality worldwide for 36 cancers in 185 countries. *CA Cancer J Clin.* 2018;68:394-424.
2. Gatta G, Botta L, Sanchez MJ, et al. Prognoses and improvement for head and neck cancers diagnosed in Europe in early 2000s: The EUROCARE-5 population-based study. *Eur J Cancer.* 2015;51:2130-2143.
3. Gupta B, Johnson NW, Kumar N. Global Epidemiology of Head and Neck Cancers: A Continuing Challenge. *Oncology.* 2016;91:13-23.
4. International Agency for Research. Global Cancer Observatory [online]. c2019. Dostupné z: https://gco.iarc.fr/. Available.
5. Pindborg J, Kramer, I., Torloni, H. Histological typing of odontogenic tumours, jaw cysts, and allied lesions. *International Histological Classification of Tumours, No 5 Geneva: World Health Organization.* 1971.
6. Barnes L EJ, Reichart P, Sidransky D, eds. Pathology and Genetics of Head and Neck Tumours. Kleihues P, Sobin LH, series eds. *World Health Organization Classification of Tumours.* 2005;Lyon, France: IARC Press, .
7. El-Naggar AK CJ, Grandis JR, Takata T, Slootweg PJ, eds. . WHO Classification of Head and Neck Tumours, 4th ed. Lyon: IARC Press. 2017.
8. Brierley J, Gospodarowicz MK, Wittekind C. *TNM classification of malignant tumours*. Chichester, West Sussex, UK ; Hoboken, NJ: John Wiley & Sons, Inc.; 2017.
9. Thompson LDR, Franchi A. New tumor entities in the 4th edition of the World Health Organization classification of head and neck tumors: Nasal cavity, paranasal sinuses and skull base. *Virchows Arch.* 2018;472:315-330.
10. Stelow EB, Bishop JA. Update from the 4th Edition of the World Health Organization Classification of Head and Neck Tumours: Tumors of the Nasal Cavity, Paranasal Sinuses and Skull Base. *Head Neck Pathol.* 2017;11:3-15.
11. Bishop JA, Ogawa T, Stelow EB, et al. Human papillomavirus-related carcinoma with adenoid cystic-like features: a peculiar variant of head and neck cancer restricted to the sinonasal tract. *Am J Surg Pathol.* 2013;37:836-844.
12. Bishop JA, Antonescu CR, Westra WH. SMARCB1 (INI-1)-deficient carcinomas of the sinonasal tract. *Am J Surg Pathol.* 2014;38:1282-1289.
13. Agaimy A, Koch M, Lell M, et al. SMARCB1(INI1)-deficient sinonasal basaloid carcinoma: a novel member of the expanding family of SMARCB1-deficient neoplasms. *Am J Surg Pathol.* 2014;38:1274-1281.
14. Zur KB, Brandwein M, Wang B, et al. Primary description of a new entity, renal cell-like carcinoma of the nasal cavity: van Meegeren in the house of Vermeer. *Arch Otolaryngol Head Neck Surg.* 2002;128:441-447.
15. French CA BJ, Lewis JS Jr, Müller S,WestraWH. Tumours of the nasal cavity, paranasal sinuses and skull base: carcinomas: NUT carcinoma. In: El-Naggar AK, Chan JKC, Grandis JR, Takata T, Slootweg PJ (eds) WHO classification of head and neck tumours. *IARC, Lyon.* 2017:20-21.
16. Lewis JE OA. Tumours of the nasal cavity, paranasal sinuses and skull base: malignant soft tissue Tumours: biphenotypic sinonasal sarcoma. In: El-Naggar AK, Chan JKC, Grandis JR, Takata T, Slootweg PJ (eds) WHO classification of head and neck tumours. *IARC, Lyon.* 2017:40–41.
17. Seethala RR, Stenman G. Update from the 4th Edition of the World Health Organization Classification of Head and Neck Tumours: Tumors of the Salivary Gland. *Head Neck Pathol.* 2017;11:55-67.
18. Skalova A, Vanecek T, Sima R, et al. Mammary analogue secretory carcinoma of salivary glands, containing the ETV6-NTRK3 fusion gene: a hitherto undescribed salivary gland tumor entity. *Am J Surg Pathol.* 2010;34:599-608.

19. Seethala R GD, Skalova A, Slater L, Williams MD. Sclerosing polycystic adenosis. . *In: El-Naggar AK, Chan JKC, Grandis JR, Takata T, Slootweg PJ (eds) WHO classification of head and neck tumours.* 2017:195.
20. Chiosea S SR, Williams MD. Intercalated duct hyperplasia. *In: El-Naggar AK, Chan JKC, Grandis JR, Takata T, Slootweg PJ (eds) WHO classification of head and neck tumours.* 2017:197.
21. Loening T LI, Simpson RHW, et al. Intraductal carcinoma. *In: El-Naggar A, Chan JKC, Grandis JR, Takata T, Slootweg PJ, eds World Health Organization (WHO) Classification of Head and Neck Tumours.* 2017;4th ed. Lyon, France: IARC Press:170–171.
22. Skálová A, Bell D, Bishop JA, et al. Secretory carcinoma. *In: El-Naggar A, Chan JKC, Grandis JR, Takata T, Slootweg PJ, eds World Health Organization (WHO) Classification of Head and Neck Tumours, 4th ed Lyon, France: IARC Press.* 2017:177-178.
23. Dogan S, Wang L, Ptashkin RN, et al. Mammary analog secretory carcinoma of the thyroid gland: A primary thyroid adenocarcinoma harboring ETV6-NTRK3 fusion. *Mod Pathol.* 2016;29:985-995.
24. Reynolds S, Shaheen M, Olson G, et al. A Case of Primary Mammary Analog Secretory Carcinoma (MASC) of the Thyroid Masquerading as Papillary Thyroid Carcinoma: Potentially More than a One Off. *Head Neck Pathol.* 2016;10:405-413.
25. Bishop JA, Taube JM, Su A, et al. Secretory Carcinoma of the Skin Harboring ETV6 Gene Fusions: A Cutaneous Analogue to Secretory Carcinomas of the Breast and Salivary Glands. *Am J Surg Pathol.* 2017;41:62-66.
26. Lurquin E, Jorissen M, Debiec-Rychter M, et al. Mammary analogue secretory carcinoma of the sinus ethmoidalis. *Histopathology.* 2015;67:749-751.
27. Ramos J, Mahmud W, Ocampo FA, et al. Primary Mammary-Analogue Secretory Carcinoma of the Lung: A Rare Entity With an Unusual Location. *Int J Surg Pathol.* 2020:1066896920914975.
28. Nguyen JK, Bridge JA, Joshi C, et al. Primary Mammary Analog Secretory Carcinoma (MASC) of the Vulva With ETV6-NTRK3 Fusion: A Case Report. *Int J Gynecol Pathol.* 2019;38:283-287.
29. Knezevich SR, Garnett MJ, Pysher TJ, et al. ETV6-NTRK3 gene fusions and trisomy 11 establish a histogenetic link between mesoblastic nephroma and congenital fibrosarcoma. *Cancer Res.* 1998;58:5046-5048.
30. De Braekeleer E, Douet-Guilbert N, Morel F, et al. ETV6 fusion genes in hematological malignancies: a review. *Leuk Res.* 2012;36:945-961.
31. Alassiri AH, Ali RH, Shen Y, et al. ETV6-NTRK3 Is Expressed in a Subset of ALK-Negative Inflammatory Myofibroblastic Tumors. *Am J Surg Pathol.* 2016;40:1051-1061.
32. Brenca M, Rossi S, Polano M, et al. Transcriptome sequencing identifies ETV6-NTRK3 as a gene fusion involved in GIST. *J Pathol.* 2016;238:543-549.
33. Seethala RR, Chiosea SI, Liu CZ, et al. Clinical and Morphologic Features of ETV6-NTRK3 Translocated Papillary Thyroid Carcinoma in an Adult Population Without Radiation Exposure. *Am J Surg Pathol.* 2017;41:446-457.
34. Ito Y, Ishibashi K, Masaki A, et al. Mammary analogue secretory carcinoma of salivary glands: a clinicopathologic and molecular study including 2 cases harboring ETV6-X fusion. *Am J Surg Pathol.* 2015;39:602-610.
35. Skalova A, Vanecek T, Simpson RH, et al. Mammary Analogue Secretory Carcinoma of Salivary Glands: Molecular Analysis of 25 ETV6 Gene Rearranged Tumors With Lack of Detection of Classical ETV6-NTRK3 Fusion Transcript by Standard RT-PCR: Report of 4 Cases Harboring ETV6-X Gene Fusion. *Am J Surg Pathol.* 2016;40:3-13.
36. Skalova A, Vanecek T, Martinek P, et al. Molecular Profiling of Mammary Analog Secretory Carcinoma Revealed a Subset of Tumors Harboring a Novel ETV6-RET Translocation: Report of 10 Cases. *Am J Surg Pathol.* 2018;42:234-246.
37. Rooper LM, Karantanos T, Ning Y, et al. Salivary Secretory Carcinoma With a Novel ETV6-MET Fusion: Expanding the Molecular Spectrum of a Recently Described Entity. *Am J Surg Pathol.* 2018;42:1121-1126.

38. Guilmette J, Dias-Santagata D, Nose V, et al. Novel gene fusions in secretory carcinoma of the salivary glands: enlarging the ETV6 family. *Hum Pathol.* 2019;83:50-58.
39. Kastnerova L, Luzar B, Goto K, et al. Secretory Carcinoma of the Skin: Report of 6 Cases, Including a Case With a Novel NFIX-PKN1 Translocation. *Am J Surg Pathol.* 2019;43:1092-1098.
40. Sasaki E, Masago K, Fujita S, et al. Salivary Secretory Carcinoma Harboring a Novel ALK Fusion: Expanding the Molecular Characterization of Carcinomas Beyond the ETV6 Gene. *Am J Surg Pathol.* 2020;44:962-969.
41. Skalova A, Banečkova M, Thompson LDR, et al. Expanding the Molecular Spectrum of Secretory Carcinoma of Salivary Glands with a Novel VIM-RET Fusion. . *Am J Surg Pathol (Accepted for publication).* 2020.
42. Skalova A, Vanecek T, Majewska H, et al. Mammary analogue secretory carcinoma of salivary glands with high-grade transformation: report of 3 cases with the ETV6-NTRK3 gene fusion and analysis of TP53, beta-catenin, EGFR, and CCND1 genes. *Am J Surg Pathol.* 2014;38:23-33.
43. Chi HT, Ly BT, Kano Y, et al. ETV6-NTRK3 as a therapeutic target of small molecule inhibitor PKC412. *Biochem Biophys Res Commun.* 2012;429:87-92.
44. Tognon CE, Somasiri AM, Evdokimova VE, et al. ETV6-NTRK3-mediated breast epithelial cell transformation is blocked by targeting the IGF1R signaling pathway. *Cancer Res.* 2011;71:1060-1070.
45. Sabari JK, Siau ED, Drilon A. Targeting RET-rearranged lung cancers with multikinase inhibitors. *Oncoscience.* 2017;4:23-24.
46. Drilon A, Cappuzzo F, Ou SI, et al. Targeting MET in Lung Cancer: Will Expectations Finally Be MET? *J Thorac Oncol.* 2017;12:15-26.
47. Mano H. ALKoma: a cancer subtype with a shared target. *Cancer Discov.* 2012;2:495-502.
48. Delgado R, Klimstra D, Albores-Saavedra J. Low grade salivary duct carcinoma. A distinctive variant with a low grade histology and a predominant intraductal growth pattern. *Cancer.* 1996;78:958-967.
49. Brandwein-Gensler MS GD. Low-grade cribriform cystadenocarcinoma. *In: Barnes L, Eveson JW, Reichart P, Sidransky D, eds Pathology and Genetics of Head and Neck Tumours.* 2005;Lyon: IARC Press.
50. Skalova A, Vanecek T, Uro-Coste E, et al. Molecular Profiling of Salivary Gland Intraductal Carcinoma Revealed a Subset of Tumors Harboring NCOA4-RET and Novel TRIM27-RET Fusions: A Report of 17 cases. *Am J Surg Pathol.* 2018;42:1445-1455.
51. Skalova A, Ptakova N, Santana T, et al. NCOA4-RET and TRIM27-RET Are Characteristic Gene Fusions in Salivary Intraductal Carcinoma, Including Invasive and Metastatic Tumors: Is "Intraductal" Correct? *Am J Surg Pathol.* 2019;43:1303-1313.
52. Weinreb I, Bishop JA, Chiosea SI, et al. Recurrent RET Gene Rearrangements in Intraductal Carcinomas of Salivary Gland. *Am J Surg Pathol.* 2018;42:442-452.
53. Weinreb I, Tabanda-Lichauco R, Van der Kwast T, et al. Low-grade intraductal carcinoma of salivary gland: report of 3 cases with marked apocrine differentiation. *Am J Surg Pathol.* 2006;30:1014-1021.
54. Stevens TM, Kovalovsky AO, Velosa C, et al. Mammary analog secretory carcinoma, low-grade salivary duct carcinoma, and mimickers: a comparative study. *Mod Pathol.* 2015;28:1084-1100.
55. Santana T, Pavel A, Martinek P, et al. Biomarker immunoprofile and molecular characteristics in salivary duct carcinoma: clinicopathological and prognostic implications. *Hum Pathol.* 2019;93:37-47.
56. Wenig BM, Franchi A, Ro JY. Respiratory epithelial adenomatoid hamartoma. *In: El-Naggar A, Chan JKC, Grandis JR, Takata T, Slootweg PJ, eds World Health Organization (WHO) Classification of Head and Neck Tumours, 4th ed Lyon, France: IARC Press.* 2017:31-32.
57. Ro JY, Franchi A. Seromucinous hamartoma.

In: El-Naggar A, Chan JKC, Grandis JR, Takata T, Slootweg PJ, eds World Health Organization (WHO) Classification of Head and Neck Tumours, 4th ed Lyon, France: IARC Press. 2017:32.

58. Weinreb I, Gnepp DR, Laver NM, et al. Seromucinous hamartomas: a clinicopathological study of a sinonasal glandular lesion lacking myoepithelial cells. *Histopathology.* 2009;54:205-213.
59. Ozolek JA, Hunt JL. Tumor suppressor gene alterations in respiratory epithelial adenomatoid hamartoma (REAH): comparison to sinonasal adenocarcinoma and inflamed sinonasal mucosa. *Am J Surg Pathol.* 2006;30:1576-1580.
60. Ozolek JA, Barnes EL, Hunt JL. Basal/myoepithelial cells in chronic sinusitis, respiratory epithelial adenomatoid hamartoma, inverted papilloma, and intestinal-type and nonintestinal-type sinonasal adenocarcinoma: an immunohistochemical study. *Arch Pathol Lab Med.* 2007;131:530-537.
61. Jo VY, Mills SE, Cathro HP, et al. Low-grade sinonasal adenocarcinomas: the association with and distinction from respiratory epithelial adenomatoid hamartomas and other glandular lesions. *Am J Surg Pathol.* 2009;33:401-408.
62. Ambrosini-Spaltro A, Morandi L, Spagnolo DV, et al. Nasal seromucinous hamartoma (microglandular adenosis of the nose): a morphological and molecular study of five cases. *Virchows Arch.* 2010;457:727-734.
63. Flucke U, Thompson LD, Wenig BM. Solitary fibrous tumor. *In: El-Naggar A, Chan JKC, Grandis JR, Takata T, Slootweg PJ, eds World Health Organization (WHO) Classification of Head and Neck Tumours, 4th ed Lyon, France: IARC Press.* 2017:45.
64. Klemperer P, Coleman BR. Primary neoplasms of the pleura. A report of five cases. *Am J Ind Med.* 1992;22:1-31.
65. Demicco EG, Harms PW, Patel RM, et al. Extensive survey of STAT6 expression in a large series of mesenchymal tumors. *Am J Clin Pathol.* 2015;143:672-682.
66. Chmielecki J, Crago AM, Rosenberg M, et al. Whole-exome sequencing identifies a recurrent NAB2-STAT6 fusion in solitary fibrous tumors. *Nat Genet.* 2013;45:131-132.
67. Mohajeri A, Tayebwa J, Collin A, et al. Comprehensive genetic analysis identifies a pathognomonic NAB2/STAT6 fusion gene, nonrandom secondary genomic imbalances, and a characteristic gene expression profile in solitary fibrous tumor. *Genes Chromosomes Cancer.* 2013;52:873-886.
68. Robinson DR, Wu YM, Kalyana-Sundaram S, et al. Identification of recurrent NAB2-STAT6 gene fusions in solitary fibrous tumor by integrative sequencing. *Nat Genet.* 2013;45:180-185.
69. Schweizer L, Koelsche C, Sahm F, et al. Meningeal hemangiopericytoma and solitary fibrous tumors carry the NAB2-STAT6 fusion and can be diagnosed by nuclear expression of STAT6 protein. *Acta Neuropathol.* 2013;125:651-658.
70. Gold JS, Antonescu CR, Hajdu C, et al. Clinicopathologic correlates of solitary fibrous tumors. *Cancer.* 2002;94:1057-1068.
71. Maturana-Ramirez A, Adorno-Farias D, Reyes-Rojas M, et al. A retrospective analysis of reactive hyperplastic lesions of the oral cavity: study of 1149 cases diagnosed between 2000 and 2011, Chile. *Acta Odontol Latinoam.* 2015;28:103-107.
72. Buchner A, Shnaiderman-Shapiro A, Vered M. Relative frequency of localized reactive hyperplastic lesions of the gingiva: a retrospective study of 1675 cases from Israel. *J Oral Pathol Med.* 2010;39:631-638.
73. Elanagai R, Veeravarmal V, Nirmal RM. Osteopontin expression in reactive lesions of gingiva. *J Appl Oral Sci.* 2015;23:26-32.
74. Andreasen S, Skalova A, Agaimy A, et al. ETV6 Gene Rearrangements Characterize a Morphologically Distinct Subset of Sinonasal Low-grade Non-intestinal-type Adenocarcinoma: A Novel Translocation-associated Carcinoma Restricted to the Sinonasal Tract. *Am J Surg Pathol.* 2017;41:1552-1560.
75. Li GG, Somwar R, Joseph J, et al. Antitumor Activity of RXDX-105 in Multiple Cancer Types with RET Rearrangements or Mutations. *Clin Cancer Res.* 2017;23:2981-2990.
76. Subbiah V, Gainor JF, Rahal R, et al. Precision Targeted Therapy with BLU-667 for RET-Driven Cancers. *Cancer Discov.* 2018;8:836-849.
77. Stenman G, Andersson MK, Andren Y. New tricks from an old oncogene: gene fusion and copy number alterations of MYB in human cancer. *Cell Cycle.* 2010;9:2986-2995.

78. Rossi ED, Wong LQ, Bizzarro T, et al. The impact of FNAC in the management of salivary gland lesions: Institutional experiences leading to a risk-based classification scheme. *Cancer Cytopathol.* 2016;124:388-396.
79. Liu H, Ljungren C, Lin F, et al. Analysis of histologic follow-up and risk of malignancy for salivary gland neoplasm of uncertain malignant potential proposed by the Milan System for Reporting Salivary Gland Cytopathology. *Cancer Cytopathol.* 2018;126:490-497.
80. Wang K, Russell JS, McDermott JD, et al. Profiling of 149 Salivary Duct Carcinomas, Carcinoma Ex Pleomorphic Adenomas, and Adenocarcinomas, Not Otherwise Specified Reveals Actionable Genomic Alterations. *Clin Cancer Res.* 2016;22:6061-6068.
81. Simpson RH. Salivary duct carcinoma: new developments--morphological variants including pure in situ high grade lesions; proposed molecular classification. *Head Neck Pathol.* 2013;7 Suppl 1:S48-58.
82. Wenig BM, Heffner DK. Respiratory epithelial adenomatoid hamartomas of the sinonasal tract and nasopharynx: a clinicopathologic study of 31 cases. *Ann Otol Rhinol Laryngol.* 1995;104:639-645.
83. Baillie EE, Batsakis JG. Glandular (seromucinous) hamartoma of the nasopharynx. *Oral Surg Oral Med Oral Pathol.* 1974;38:760-762.
84. Yuzawa S, Nishihara H, Wang L, et al. Analysis of NAB2-STAT6 Gene Fusion in 17 Cases of Meningeal Solitary Fibrous Tumor/Hemangiopericytoma: Review of the Literature. *Am J Surg Pathol.* 2016;40:1031-1040.
85. Agaimy A, Michal M, Chiosea S, et al. Phosphaturic Mesenchymal Tumors: Clinicopathologic, Immunohistochemical and Molecular Analysis of 22 Cases Expanding their Morphologic and Immunophenotypic Spectrum. *Am J Surg Pathol.* 2017;41:1371-1380.

PUBLIKACE

1.12 PUBLIKACE AUTORKY SE VZTAHEM K TÉMATU DIZERTAČNÍ PRÁCE

1. Skalova A, Vanecek T, Simpson RHW, Laco J, Majewska H, **Baneckova M**, Steiner P, Michal M. Mammary Analogue Secretory Carcinoma of Salivary Glands. Molecular Analysis of 25 *ETV6* Gene Rearranged Tumors With Lack of Detection of Classical *ETV6-NTRK3* Fusion Transcript by Standard RT-PCR: Report of 4 Cases Harboring *ETV6-X* Gene Fusion. *Am J Surg Pathol.* 2016; 40:3–13. **IF - 5,363**

2. Skalova A, Vanecek T, Martinek P, Weinreb I, Stevens TM, Simpson RHW, Hyrcza M, Rupp NJ, **Baneckova M**, Michal M Jr, Slouka D, Svoboda T, Metelkova A, Etebarian A, Pavelka J, Potts SJ, Christiansen J, Steiner P, Michal M. Molecular Profiling of Mammary Analog Secretory Carcinoma Revealed a Subset of Tumors Harboring a Novel *ETV6-RET* Translocation: Report of 10 Cases. *Am J Surg Pathol*. 2018 Feb;42(2):234-246. **IF - 6,155**

3. **Baneckova M**, Agaimy A, Andreasen S, Vanecek T, Steiner P, Slouka D, Svoboda T, Miesbauerova M, Michal M Jr, Skálová A. Mammary Analog Secretory Carcinoma of the Nasal Cavity: Characterization of 2 Cases and Their Distinction From Other Low-grade Sinonasal Adenocarcinomas. *Am J Surg Pathol*. 2018 Mar 14. **IF - 6,155**

4. Skálová A, Vanecek T, Uro-Coste E, Bishop JA, Weinreb I, Thompson LDR, de Sanctis S, Schiavo-Lena M, Laco J, Badoual C, Santana Conceiçao T, Ptáková N, **Baněčkova M**, Miesbauerová M, Michal M. Molecular Profiling of Salivary Gland Intraductal Carcinoma Revealed a Subset of Tumors Harboring *NCOA4-RET* and Novel *TRIM27-RET* Fusions: A Report of 17 cases. *Am J Surg Pathol*. 2018 Nov;42(11):1445-1455. **IF - 6,155**

5. Haller F, Skálová A, Ihrler S, Märkl B, Bieg M, Moskalev EA, Erber R, Blank S, Winkelmann C, Hebele S, **Baněčková M**, Wiemann S, Müller S, Zenk J, Eils R, Iro H, Hartmann A, Agaimy A. Nuclear NR4A3 Immunostaining is a Specific and Sensitive Novel Marker for Acinic Cell Carcinoma of the Salivary Glands. *Am J Surg Pathol*. 2019 Sep;43(9):1264-1272. **IF - 6,155**

6. Miesbauerová M, Tommola S, Šteiner P, **Baněčková M**, Skálová A, Kholová I. Cytopathological features of secretory carcinoma of salivary glands and ancillary techniques in its diagnostics: impact of new Milan system for reporting salivary gland cytopathology. *APMIS*. 2019 2019 Jul; 127(7):491-502. **IF - 2,406**

7. Skálová A, Ptáková N, Santana T, Agaimy A, Ihrler S, Uro-Coste E., Thompson LDR, Bishop JA, **Baněčkova M,** Rupp NJ, Morbini P, de Sanctis S, Schiavo-Lena M, Vanecek T, Michal M, Leivo I. *NCOA4-RET* and *TRIM27-RET* are Characteristic Gene Fusions in Salivary Intraductal Carcinoma, Including Invasive and Metastatic Tumors. Is "Intraductal" Correct? *Am J Surg Pathol.* 2019 Oct;43(10):1303-1313. **IF - 6,155**

8. Santana T, Pavel A, Martinek P, Steiner P, Grossmann P, **Baněčková M**, Skálová A. Biomarker immunoprofile and molecular characteristics in salivary duct carcinoma:

clinicopathological and prognostic implications. *Hum Pathol.* 2019 Aug 19;93:37-47. **IF - 2,830**

9. **Baněčková M**, Michal M, Laco J, Leivo I, Ptáková N, Horáková M, Michal M, Skálová A. Immunohistochemical and genetic analysis of respiratory epithelial Adenomatoid Hamartomas and Seromucinous Hamartomas: are they precursor lesions to Sinonasal low-grade Tubulopapillary adenocarcinomas? *Hum Pathol*. 2020 Mar; 97:94-102. **IF - 2,830**

10. **Baněčková M**, Martínek P, Skálová A, Mezencev R, Hadravský L, Michal M, Švajdler M. Solitary fibrous tumors of the head and neck region revisited: a single-institution study of 20 cases and review of the literature. *Hum Pathol*. 2020 Mar 23;99:1-12. **IF - 2,830**

11. **Baněčková** M, Agaimy A. SATB2 is frequently expressed in ossifying and non-ossifying peripheral oral fibroma of the gingival region but not in reactive fibromatous lesions from other intraoral sites. *Ann Diagn Pathol.* 2020 Apr 2;46:151510. **IF - 1,620**

12. Skalova A, **Banečkova M**, Thompson LDR, Ptáková N, Stevens TM, Brcic L, Hyrcza M, Michal M Jr, Simpson RHW, Santana T, Michal M, Vaněček T, Leivo I. Expanding the Molecular Spectrum of Secretory Carcinoma of Salivary Glands with a Novel *VIM-RET* Fusion. *Am J Surg Pathol.* 2020 přijato k publikaci. **IF - 6,155**

13. **Baněčková M**, Uro-Coste E, Ptáková N, Šteiner P, Stanowska O, Benincasa G, Colella G, Vondrák J Jr, Michal M, Leivo I, Skálová A. What is hiding behind S100 protein and SOX10 positive oncocytomas? Oncocytic pleomorphic adenoma and myoepithelioma with novel gene fusions in a subset of cases. *Hum Pathol*. 2020 přijato k publikaci**IF - 2,830**

1.13 PUBLIKACE AUTORKY BEZ VZTAHU K TÉMATU DIZERTAČNÍ PRÁCE

1. Slouka D, Honnerova M, Hosek P, Gal B, Trcka O, Kostlivy T, Landsmanova J, Havel D, **Baneckova M**, Kucera R. Improved prediction of CPAP failure using T90, age and gender. *J Appl Biomed* 17:81, 2019. **IF - 1,680**

2. Gál B, Kubec V, Kostlivý T, **Baněčková M**, Slouka D. Syndrom spánkové apnoe. In: Slouka D et al. eds Otorinolaryngologie. Praha: Galén Press; 2018: 239-260.

3. Gál B, Kubec V, Kostlivý T, **Baněčková M**, Slouka D. Sleep apnea syndroma. In: Slouka D et al. eds Otorhinolaryngology. Praha: Galén Press; 2018: 239-260.

1.14 PREZENTACE NA VĚDECKÝCH KONFERENCÍCH

1) **Studentská vědecká konference, 17. května 2017, Šafránkův pavilon, Plzeň –** Sekreční karcinom slinných žláz, karcinom potenciálně léčitelný tyrosin-kinázovými inhibitory, se může maskovat: „zamaskovaný MASC“. **Baněčková M,** Miesbauerová M, Skálová A.
   První cena v pregraduální sekci.

2) **Studentská vědecká konference, 30. května 2018, Modrá posluchárna, Biomedicínské centrum, Plzeň –** Sekreční karcinom mamárního typu nosní dutiny: Popis 2 případů. **Baněčková M**, Miesbauerová M, Skálová A.

3) **Studentská vědecká konference, 21. května 2019, Modrá posluchárna, Biomedicínské centrum, Plzeň** – Solitární fibrózní tumor hlavy a krku: klinicko-patologická a genetická studie 20 případů. **Baněčková M,** Martínek P, Skálová A, Švajdler M, Michal M.

4) **Pannonský kongres patologů, 16. – 19. května 2018, Mikulov –** Case report v sekci Seminář hlavy a krku. **Baněčková M**, Skálová A.

5) **25. Sjezd českých a slovenských patologů, 15. – 16. listopadu 2018, Mikulov** – Solitární fibrózní tumor. **Baněčková M**, Švajdler M, Martínek P, Skálová A, Michal M.

6) **108th Annual Meeting of the United States & Canadian Academy of Pathology, 16th February – 21st March 2019, Gaylord National Resort & Convention Center, National Harbor, MD, USA**
   Poster: Immunohistochemical Analysis of Respiratory Epithelial Adenomatoid Hamartomas/Seromucinous Hamartomas and Low-grade Tubulopapillary Adenocarcinomas: Related or Not? **Baněčková M**, Skálová A, Michal M, Laco J, Michal M.
   Poster: Solitary Fibrous Tumors of The Head and Neck Region Revisited: Study of 20 Cases. **Baněčková M**, Martínek P, Skálová A, Švajdler M, Michal M.
   Poster: Salivary Secretory Carcinoma with a Novel *VIM-RET* and Dual *ETV6-NTRK3/MYB-SMR3B* Fusions: NGS Based Molecular Profiling of 49 Cases Revealed an Expanding Molecular Spectrum of a Recently Described Entity. Skalova A, Vanecek T, Ptakova N, Brcic L, Hyrcza M, Santana T, Simpson R, Michael M, **Baneckova M,** Michal M.

7) **Letní bioptický seminář SD IAP, 28. června 2019**, **Senec, Slovensko –** Případová studie: Sekreční karcinom s duální fúzí *ETV6-NTRK3 a MYB-SMR3B.* **Baněčková M**, Ptáková N, Skálová A.

8) **Konference České kooperativní skupiny pro nádory hlavy a krku, 11. – 12. 10. 2019, Tábor**

Přednáška: Vliv tkáňové fixace na velikost chirurgických okrajů. **Baněčková M,** Skálová A.
Přednáška: Co se skrývá za S100 protein pozitivními onkocytomy slinných. **Baněčková M,** Martínek P, Ptáková N, Súkeníková A, Horáková M, Michal M, Skálová A.

9) **109th Annual Meeting of the United States & Canadian Academy of Pathology, 29th February – 5th March, Los Angeles Convention Center – Los Angeles, CA, USA:**
Platform presentation Head and Neck section: What Hides Behind S100 protein/SOX10 Positive Oncocytomas of the Salivary Glands? **Baněčková M**, Martínek P, Ptáková N, Šteiner P, Stanowska O, Súkeníková A, Horáková M, Michal M, Leivo I, Skálová A.
*NASHNP **Vincent Hyams award** for the best platform presentation in Head and Neck Pathology, by a pathologist in training*
Poster: Molecular Profiling of Salivary Oncocytic Mucoepidermoid Carcinomas Helps to Resolve Diagnostic Dilemma with Low-Grade Oncocytic Lesions. Stanowska SO, Agaimy A, Ardighieri l, Steiner P, Nicolai P, Durzyńska M, Majewska H, Prochorec-Sobieszek M, Bakula-Zalewska E, **Baneckova M,** Michal M, Skalova A.
Poster: Novel Rearrangements in Salivary Gland Tumors Detected by Next Generation Sequencing Assay: Series of 104 Fusion Positive Cases. Skalova A, Vanecek T, Martinek P, Ptakova N, Agaimy A, Laco J, Brcic L, **Baneckova M,** Koshyk O.
Poster: Report of 20 Cases of Seromucinous Hamartomas and Respiratory Epithelial Adenomatoid Hamartomas with Dysplastic and Malignant Features. **Baněčková M**, Vaněček T, Laco J, Hyrcza M, Ihrler S, Rupp JN, Petersson F, Koshyk O, Spagnolo VD, Sanjiv J, Schlageter M, Shelekhova VK., Skálová A, Michal M.

DOPLŇKOVÝ MATERIÁL

1.15 Výčet nádorů sinonazálního traktu dle WHO 2017 (7) – tabulka č. 1

Karcinomy
Keratinizující dlaždicobuněčný karcinom
Nekeratinizující dlaždicobuněčný karcinom
Vřetenobuněčný (sarkomatoidní) dlaždicobuněčný karcinom
Lymfoepiteliání karcinom
Sinonazální nediferencovaný karcinom
NUT karcinom
Neuroendokrinní karcinom
Adenokarcinom
Adenokarcinom intestinálního typu
Adenokarcinom ne-intestinálního typu
Teratokarcinosarkom
Sinonazální papilomy
Sinonazální papilomy, invertovaný typ
Sinonazální papilomy, onkocytární typ
Sinonazální papilomy, exofytický typ
Respirační epiteliální léze
Respirační epiteliální adenomatoidní hamartom
Seromucinózní hamartom
Nádory slinných žláz
Plemorfní adenom
Maligní měkkotkáňové nádory
Fibrosarkom
Nediferencovany pleomorfní sarkom
Leiomyosarkom
Rhabdomyosarkom
Angiosarkom
Maligní tumor z pochvy periferního nervu
Bifenotypický sinonazální sarkom
Synoviální sarkom
Hraniční / low-grade maligní měkkotkáňové tumory
Desmoidní fibromatóza
Sinonazální glomangiopericytom
Solitární fibrózní tumor
Epitelioidní hemangioendoteliom
Benigní měkkotkáňové tumory
Leiomyom
Hemangiom
Schwannom
Neurofibrom
Ostatní nádory
Meningiom
Sinonazální ameloblastom
Chondromezenchymální hamartomy
Hematolymfoidní nádory
Extranodální NK/T-buněčné lymfomy
Extraoseální plazmocytom
Neuroektodermální / melanocytické tumory

Ewing sarkom / primitivní neuroektodermální tumory
Olfaktorický neuroblastom
Mukozální melanom

1.16 Výčet nádoru slinných žláz dle WHO 2017 (7) – tabulka č. 2

Maligní nádory
Mukoepidermoidní karcinom
Adenoidně cystický karcinom
Acinický karcinom
Polymorfní adenokarcinom
Světlobuněčný karcinom
Karcinom z bazálních buněk
Intraduktální karcinom
Adenokarcinom, NOS
Salivární duktální karcinom
Myoepiteliální karcinom
Epiteliálně-myoepiteliální karcinom
Karcinom ex pleomorfní adenom
Sekreční karcinom
Sebaceózní adenokarcinom
Karcinosarkom
Špatně diferencovaný karcinom
Lymfoepiteliální karcinom
Dlaždicobuněčný karcinom
Onkocytární karcinom
Sialoblastom
Benigní nádory
Pleomorfní adenom
Myoepiteliom
Adenom z bazálních buněk
Warthinův tumor
Onkocytom
Lymfadenom
Cystadenom
Sialadenoma papilliferum
Duktální papilom
Sebaceózní adenom
Kanalikulární adenom a ostatní duktální adenomy
Non-neoplastické epiteliální léze
Sklerózující polycystická adenóza
Nodulární onkocytární hyperplázie
Lymfoepiteliální sialoadenitida
Hyperplázie z vmezeřených duktů
Benigní měkkotkáňové léze
Hemangiom
Lipom/sialolipom
Nodulární fasciitida
Hematolymfoidní nádory
Extranodální lymfom z plášťové zóny slizniční lymfatické tkáně (MALT lymfom)

1.17 Molekulárně genetické alterace nádorů slinných žláz – tabulka č. 3

Tumor	Chromozomální změna	Geny
Sklerózující polycystická adenóza		inaktivace X-chromozomu
		PTEN ztráta funkce
		PIK3CA a *PIK3R1* mutace
Pleomorfní adenom	8q12 translokace	*PLAG1* fúze
	12q13-15 translokace	*HMGA2* fúze
Karcinom ex pleomorfní adenom	8q12 translokace	*PLAG1* fúze
	12q13-15 translokace	*HMGA2* fúze
	12q15 amplifikace	*MDM2, TP53* mutace
Epiteliálně-myoepiteliální karcinom		*HRAS* mutace
		TP53, FBXW7, SMARB1 (INI1) delece
Tubulotrabekulární adenom z bazálních buněk		*CTTNB1* mutace
Membranózní adenom z bazálních buněk	16q12-13 delece	*CYLD* LOH/mutace
Mukoepidermoidní karcinom	t(11;19)(q21;13)	*CRTC1-MAML2*
	t(11;15)(q21;26)	*CRTC3-MAML2*
	9p21.3	*CDKN2A* delece
Salivární duktální karcinom	17q21.1	TP53, *HRAS/NRAS, cyclin D1/CDK* mutace
		ERBB2, *EGFR, BRAF* amplifikace
		PIK3CA, PTEN, RICTOR, AKT1, AKT3 mutace
	Xq12	*AR* copy gain
	9p21	*CDKN2A* homozygotní delece
		MDM2 amplifikace
Adenoidně cystický karcinom	t(6;9)(q22-23;p23-24)	*MYB-NFIB*
	t(8;9)(q13.1;p23-22.3)	*MYBL1-NFIB*
		MYC overexprese
Sekreční karcinom	t(12;15)(p13;q25)	*ETV6-NTRK3*
	t(6;12)	*ETV6-RET*
	t(12;7)(q13;q31)	*ETV6-MET*
		ETV6-NTRK3 s *ETV6-MAML3*
		VIM-RET
		ETV6-NTRK3 s *MYB-SMR3B*
	t(5;2)	*CTNNA1-ALK*
Světlobuněčný karcinom	t(12;22)(q21;q12)	*EWSR1-ATF1*
Polymorfní adenokarcinom a kribriformní adenokarcinom		*PRKD1* mutace
	t(1;14)(p36.11;q12)	*ARID1A-PRKD1*
	t(X;14)(p11.4;q12)	*DDX3X-PRKD1*
	19q13.32	*PRKD2* rearanže
	2p21	*PRKD3* rearanže
Intraduktální karcinom	t(10;10)(q11.22;q11.21)	*NCOA4-RET*
	t(10;6)(p22.5;q11.21)	*TRIM27-RET*
		TUT1-ETV5, KIAA1217-RET
		HRAS, TP53, PIK3CA, SPEN, ATM mutace
Acinický karcinom	t(4;9)(q13;q31)	*HTN3-MSANTD3*

1.18 Molekulárně genetické alterace nádorů sinonazálního traktu – tabulka č. 4

Tumor	**Chromozomální změna**	**Geny**
Chondromezenchymální hamartom		*DICER1* mutace
NUT karcinom	t(15;19)(q14;p13.1)	*NUTM1-BRD4*
	t(15;9)(q14;p34.2)	*NUTM1-BRD3*
	t(15;8)(q14;11.23)	*NUT-NSD3 (WHSC1L1)*
Bifenotypický sinonazální sarkom		*PAX3-MAML3*
		PAX3-FOXO1
		PAX3-NCOA1
Adenokarcinomy intestinálního a ne-intestinálního typu		*TP53, KRAS, BRAF, EGFR* mutace
		CDKN2A alterace
Synoviální sarkom	t(X;18)(p11;q11)	*SYT-SSX*
Desmoidní fibromatóza		*CTNNB1, APC* mutace
Sinonazální glomangiopericytom		*CTNNB1* mutace
Solitární fibrózní tumor	t(12;12)(q13.3;13)	*NAB2-STAT6*
Epithelioidní hemangioendoteliom	t(1;3)(p36;q25)	*WWTR1-CAMTA1*
	t(11;X)(q13;p11.22)	*YAP1-TFE3*
Seromucinózní hamartom		částečná alelická ztráta
		inaktivace X-chromozomu
Nově diskutovaná jednotka		
SMARCB1 (INI1) deficientní karcinom		*SMARCB1* homozygotní/ heterozygotní delece

1.19 Diferenciální diagnóza SFT – tabulka č. 5

NÁDOR	IMUNOHISTOCHEMIE	GENETIKA
PRIMÁRNÍ NÁDORY:		
Meningoteliální/Fibrózní meningiom	pozitivní – EMA, somatostatin receptor 2A negativní – STAT6, CD34, ALDH1	mutace *NF2, AKT1* Delece *9p21 (CDKN2A) a další*
Epitelioidní hemangioendoteliom	pozitivní – ERG, CD31, CD34, CAMTA1, TFE3 (malá část) negativní – STAT6	*WWTR1-CAMTA1, YAP1-TFE3 (malá část)*
Nasofaryngeální (juvenilní) angiofibrom	pozitivní – β-catenin, AR, SMA negativní – STAT6	Mutace v *β-catenin* genu
Paragangliom	pozitivní – S100 protein (sustentakulární buňky), chromogranin, synaptophysin negativní – STAT6, CD34	mutace: *VHL, RET, NF1, SHDA-SDHB, TREM127, MAX*
Sklerózující epitelioidní fibrosarkom	pozitivní – MUC4 (80%), EMA negativní – STAT6, CD34	*EWSR1-CREBL1, FUS-CREB3L2, YAP-KMT2A*
Biphenotypicky sinonazální sarkom	pozitivní – S100 protein, SMA, malá část - desmin, myoegenin, MyoD1 negativní – STAT6	*PAX3-MAML3, PAX3-FOXO1, PAX3-NCOA1*
Glomus tumor	pozitivní – SMA, h-caldesmon negativní – STAT6	*MIR143-NOTCH*, *BRAF V600E*
Protuberujícíc dermatofibrosarkom/Obrovskobuněčný fibroblastom	pozitivní – CD34 negativní – STAT6	*COL1A1-PDGFB*
Dediferencovaný liposarkom	pozitivní – MDM2, CDK4, může být i STAT6	*MDM2* a *CDK4* amplifikace
Synoviální sarkom	pozitivní –cytokeratiny, EMA, TLE1, SYT, SSX negativní – STAT6	*SYT-SSX*
Nodulární fasciitida	Pozitivní – SMA Negativní – STAT6	Fúze genu *USP6* s mnoha různými partnery
Nediferencovaný pleomorfní sarkom	vzácně STAT6 pozitivní spíše cytoplazmaticky	Komplexní molekulární aberace
SEKUNDÁRNÍ NÁDORY:		
Hladkosvalové tumory	pozitivní – SMA, desmin negativní – STAT6	
Lobulární karcinom prsu	pozitivní – cytokeratiny, GATA3, Mammaglobin, GCDFP-15 negativní – STAT6	
LG a HG endometriální stromální sarkom	pozitivní – variabilní CD10, ER, PR, část je BCOR pozitivní (může být i u SFT) negativní – STAT6	LG: *JAZF1-SUZ12, PHF1-JAZF1, EPC1-PHF1, MEAF6-PHF1* HG: *YWHAE-NUTM2A/B, rearanže BCOR genu*